



Summary of the searches for squarks and gluinos using $\sqrt{s} = 8$ TeV pp collisions with the ATLAS experiment at the LHC

The ATLAS Collaboration

Abstract

A summary is presented of ATLAS searches for gluinos and first- and second-generation squarks in final states containing jets and missing transverse momentum, with or without leptons or b -jets, in the $\sqrt{s} = 8$ TeV data set collected at the Large Hadron Collider in 2012. This paper reports the results of new interpretations and statistical combinations of previously published analyses, as well as a new analysis. Since no significant excess of events over the Standard Model expectation is observed, the data are used to set limits in a variety of models. In all the considered simplified models that assume R-parity conservation, the limit on the gluino mass exceeds 1150 GeV at 95% confidence level, for an LSP mass smaller than 100 GeV. Furthermore, exclusion limits are set for left-handed squarks in a phenomenological MSSM model, a minimal Supergravity/Constrained MSSM model, R-parity-violation scenarios, a minimal gauge-mediated supersymmetry breaking model, a natural gauge mediation model, a non-universal Higgs mass model with gaugino mediation and a minimal model of universal extra dimensions.

Contents

1	Introduction	4
2	SUSY models	5
2.1	Phenomenological models	6
2.1.1	A phenomenological MSSM model	6
2.1.2	Minimal Supergravity/Constrained MSSM and bilinear R-parity-violation models	7
2.1.3	Minimal gauge-mediated supersymmetry breaking model	7
2.1.4	Natural gauge mediation model	8
2.1.5	Non-universal Higgs mass models with gaugino mediation	8
2.1.6	Minimal Universal Extra Dimensions model	9
2.2	Simplified models	9
2.2.1	Direct decays of squarks and gluinos	11
2.2.2	One-step decays of squarks and gluinos	12
2.2.3	Two-step decays of squarks and gluinos	13
2.2.4	Gluino decays via third-generation squarks	13
3	The ATLAS detector and data sample	16
4	Monte Carlo simulated samples	16
5	Object reconstruction and identification	18
6	Analysis strategy	20
7	Experimental signatures	21
7.1	Final states with high- p_T jets, missing transverse momentum and no electrons or muons	25
7.2	Final states with high- p_T jets, missing transverse momentum and at least one electron or muon	27
7.3	Final states with high- p_T jets, missing transverse momentum and at least one hadronically decaying tau lepton	28
7.4	Final states with many b -jets and missing transverse momentum	30
8	Systematic uncertainties	30
9	Results for the new signal regions	31
10	Combination strategy	34
11	Limits in SUSY models	37
11.1	Limits in phenomenological models	37
11.1.1	A phenomenological MSSM model	37
11.1.2	Minimal Supergravity/Constrained MSSM and bilinear R-parity-violation models	37
11.1.3	Minimal gauge-mediated supersymmetry breaking model	39
11.1.4	Natural gauge mediation model	39
11.1.5	Non-universal Higgs mass model with gaugino mediation	41
11.1.6	Minimal Universal Extra Dimension model	41
11.2	Limits in Simplified Models	43

11.2.1	Direct decays of squarks and gluinos	43
11.2.2	One-step decays of squarks and gluinos	47
11.2.3	Two-step decays of squarks and gluinos	47
11.2.4	Gluino decays via third-generation squarks	53
12	Conclusions	59
A	Extension of the $\tilde{g} \rightarrow t\bar{t}\tilde{\chi}_1^0$ simplified model to include decays with off-shell top quarks	61
B	Summary of selection criteria	63
C	0-lepton Razor analysis details	71
C.1	The Razor variables	71
C.2	Signal regions	72
C.3	Control and validation regions for SM background processes	75

1. Introduction

Supersymmetry (SUSY) [1–9] is a generalization of space-time symmetries that predicts new bosonic partners for the fermions and new fermionic partners for the bosons of the Standard Model (SM). If R-parity is conserved [10–13], SUSY particles (called sparticles) are produced in pairs and the lightest supersymmetric particle (LSP) is stable. The scalar partners of the left- and right-handed quarks, the squarks (\tilde{q}_L and \tilde{q}_R which mix to form two mass eigenstates \tilde{q}_1 and \tilde{q}_2 , ordered by increasing mass), and the fermionic partners of the gluons, gluinos (\tilde{g}), could be produced in strong interaction processes at the Large Hadron Collider (LHC) [14] and decay via cascades ending with a stable LSP. The rest of the cascade would yield final states with multiple jets and possibly leptons arising from the decay of sleptons ($\tilde{\ell}$), the superpartners of leptons, or W , Z and Higgs (h) bosons originating from the decays of charginos ($\tilde{\chi}^\pm$) or neutralinos ($\tilde{\chi}^0$), where the charginos and neutralinos are the mass eigenstates formed from the linear superpositions of the superpartners of the charged and neutral electroweak and Higgs bosons. In the Minimal Supersymmetric extension of the Standard Model (MSSM) [10–13, 15], there are four charginos, $\tilde{\chi}_1^\pm$ and $\tilde{\chi}_2^\pm$, and four neutralinos, $\tilde{\chi}_i^0$ ($i = 1$ to 4, ordered by increasing mass); unless stated otherwise, this is assumed in the following. In a large variety of models, the LSP is the lightest neutralino ($\tilde{\chi}_1^0$), which interacts weakly and is a possible candidate for dark matter [16]. Undetected $\tilde{\chi}_1^0$ LSPs would result in substantial missing transverse momentum (E_T^{miss} , with magnitude E_T^{miss}). Significant E_T^{miss} can also arise in R-parity-violating (RPV) scenarios in which the LSP decays to final states containing neutrinos or in scenarios where neutrinos are present in the cascade decay chains of the produced SUSY particles. Significant mass splitting between the top squark (stop) mass eigenstates \tilde{t}_1 and \tilde{t}_2 is possible due to the large top Yukawa coupling.¹ Because of the SM weak isospin symmetry the mass of the left-handed bottom squark (sbottom, \tilde{b}_L) is tied to the mass of the left-handed stop (\tilde{t}_L), and as a consequence the lightest sbottom (\tilde{b}_1) and stop (\tilde{t}_1) could be produced via the strong interaction with relatively large cross-sections at the LHC, either through direct pair production or in the decay of pair-produced gluinos.

The ATLAS experiment [17] performed several searches for supersymmetric particles in Run 1. No statistically significant excesses of events compared to the predictions of the Standard Model were observed. Therefore the results were expressed as model-independent limits on the production cross-sections of new particles and limits in the parameter space of supersymmetric or simplified models.

The large cross-sections of squark and gluino production in strong interaction processes offer sensitivity to a broad range of SUSY models. This paper provides a summary of the results from inclusive searches for gluinos and first- and second-generation squarks performed by ATLAS, using data from proton–proton (pp) collisions at a centre-of-mass energy of 8 TeV collected during Run 1 of the LHC. The results for direct production of third-generation squarks are reported elsewhere [18]. In addition to summarizing already published searches for squarks and gluinos, this paper presents new signal regions, new interpretations and statistical combinations of those searches, as well as an additional search using the Razor variable set [19], thus improving the sensitivity to supersymmetric models. In order to differentiate strongly produced SUSY events from the SM background, the searches typically require high E_T^{miss} due to the presence of the LSP and possibly neutrinos, several high- p_T jets and large deposited transverse energy. They are further classified according to the presence of leptons and b -jets. A first class of searches applies a veto on leptons [20–22], a second considers final states containing electrons and muons [23–25], and a third requires tau leptons in the final state [26]. A fourth class of searches concentrates on final states containing multiple b -jets [27].

¹ The masses of the \tilde{t}_1 and \tilde{t}_2 are the eigenvalues of the stop mass matrix. The stop mass matrix involves the top quark Yukawa coupling in the off-diagonal elements, which typically induces a large mass splitting.

The paper is organized as follows. Section 2 summarizes the SUSY signals in the strong production of gluinos and light-flavour squarks. Section 3 describes the ATLAS experiment and the data sample used, and section 4 the Monte Carlo (MC) simulation samples used for background and signal modelling. The physics object reconstruction and identification are presented in section 5. A description of the analysis strategy is given in section 6, and the experimental signatures are presented in section 7. A summary of systematic uncertainties is presented in section 8. Results obtained using the new signal regions with selections similar to those used in previous publications as well as the new analysis using the Razor variable set are reported in section 9. The strategy used for the combination of the results from different analyses is discussed in section 10. Limits in phenomenological and simplified models are presented in section 11. Section 12 is devoted to a summary and conclusions.

2. SUSY models

Since no superpartners of any of the SM particles have been observed, SUSY, if realized in nature, must be a broken symmetry with a mechanism for breaking the symmetry taking place at a higher energy scale. It is difficult to construct a realistic model of spontaneously broken low-energy supersymmetry where the SUSY breaking arises solely as a consequence of the interactions of the particles of the MSSM [28–30]. Therefore, it is often assumed that the SUSY breaking originates in a “hidden” sector, and its effects are transmitted to the MSSM by some unknown mechanism. Various such mechanisms have been proposed, such as gravity-mediated SUSY breaking (SUGRA) [31–36], gauge-mediated SUSY breaking (GMSB) [37–42] and anomaly-mediated SUSY breaking (AMSB) [43, 44]. As a result, these models consider only a small part of the parameter space of the more general MSSM. In such SUSY models, the particle spectrum is typically specified by fixing parameters at the high scale. In order to translate this set of parameters into physically meaningful quantities that describe physics near the electroweak scale, it is necessary to evolve them using their renormalization group equations.

Another approach to constraining SUSY at the electroweak scale is to use simplified models [45, 46] which are based on an effective Lagrangian that only describes a small set of kinematically accessible particles, interactions, production cross-sections and branching ratios. The simplest case corresponds to considering one specific SUSY production process with a fixed decay chain.

Several classes of phenomenological and simplified models, as well as a minimal Universal Extra Dimensions (mUED) scenario [47, 48], covering different combinations of physics objects in the final state, are considered in this paper. Unless otherwise specified, R-parity is assumed to be conserved and the lightest neutralino, $\tilde{\chi}_1^0$, is taken to be the LSP. The phenomenological models include a scenario for the phenomenological MSSM (pMSSM) [49–51], minimal Supergravity/Constrained MSSM (mSUGRA/CMSSM) [31–36], bilinear R-parity violation (bRPV) [52], a minimal gauge-mediated supersymmetry breaking model (mGMSB) [37–42], natural gauge mediation (nGM) [53], and a non-universal Higgs mass model with gaugino mediation (NUHMG) [54]. The simplified models presented here include the pair production of gluinos or first- and second-generation squarks with various hypotheses for their decay chains (direct, one-step or two-step decay), as well as gluino decays via real or virtual third-generation squarks. Direct decays are those where the considered SUSY particles decay directly into SM particles and the LSP, e.g., $\tilde{q} \rightarrow q\tilde{\chi}_1^0$. One-step (two-step) decays refer to the cases where the decays occur via one (two) intermediate on-shell SUSY particle(s), e.g., $\tilde{q} \rightarrow q\tilde{\chi}_1^\pm \rightarrow qW\tilde{\chi}_1^0$ ($\tilde{q} \rightarrow q\tilde{\chi}_1^\pm \rightarrow qW\tilde{\chi}_2^0 \rightarrow qWZ\tilde{\chi}_1^0$). In gluino decays via third-generation squarks, gluinos undergo a one-step decay to a stop or sbottom such as $\tilde{g} \rightarrow t\tilde{t} \rightarrow t\tilde{\chi}_1^0$, or decay directly to final states containing top or bottom quarks, for example $\tilde{g} \rightarrow t\tilde{\chi}_1^0$

if the stop is off-shell. In these simplified models, all supersymmetric particles which do not directly enter the production and decay chain are effectively decoupled, i.e. with masses set above a few TeV. The list of models considered is not comprehensive, and the searches presented here are sensitive to a larger class of decay patterns, mass combinations and hierarchies.

2.1. Phenomenological models

2.1.1. A phenomenological MSSM model

In the pMSSM scenario, no specific theoretical assumption is introduced at the scale of Grand Unification Theories (GUT), or associated with a SUSY breaking mechanism. A short list of experimentally motivated considerations is used to reduce the 120 parameters of the MSSM to 19 real, weak-scale parameters:

- R-parity is exactly conserved,
- there are no new sources of CP violation beyond that already present in the quark mixing matrix,
- Minimal Flavour Violation [55] is imposed at the electro weak scale,
- the first two generations of squarks and sleptons with the same quantum numbers are mass-degenerate, and their Yukawa couplings are too small to affect sparticle production or precision observables.

The remaining 19 independent parameters are: 10 squark and slepton masses, the gaugino masses (M_1 , M_2 , M_3 , associated with the $U(1)_Y$, $SU(2)_L$, $SU(3)_C$ gauge groups, respectively), the higgsino mass parameter (μ), the ratio ($\tan\beta$) of the vacuum expectation values of the two Higgs fields, the mass of the pseudoscalar Higgs boson (m_A), and the trilinear couplings for the third generation (A_b , A_t and A_τ) [49].

In the pMSSM model considered here only the left-handed squarks of the first two generations, the two lightest neutralinos $\tilde{\chi}_2^0$ and $\tilde{\chi}_1^0$, and the lightest chargino $\tilde{\chi}_1^\pm$ are assumed to be within kinematic reach. Three gluino masses are considered, $m_{\tilde{g}} = 1.6, 2.2$ and 3.0 TeV, while the masses of all other SUSY particles are kinematically decoupled with masses set to 5 TeV. The parameter $\tan\beta$ is set to 4. The model is further specified by four parameters: $m_{\tilde{q}_L}$, μ , and M_1 and M_2 , from which $m_{\tilde{\chi}_1^0}$, $m_{\tilde{\chi}_2^0}$ and $m_{\tilde{\chi}_1^\pm}$ can be calculated. Either M_1 is fixed to 60 GeV and M_2 is varied independently, or M_1 is varied and M_2 is set to $(M_1 + m_{\tilde{q}_L})/2$.

Left-handed squarks can be pair produced only via t -channel gluino exchange. They can undergo a direct $\tilde{q}_L \rightarrow q\tilde{\chi}_1^0$ decay, or one-step decays: $\tilde{q}_L \rightarrow q + \tilde{\chi}_2^0 \rightarrow q + Z/h + \tilde{\chi}_1^0$ or $\tilde{q}_L \rightarrow q + \tilde{\chi}_1^\pm \rightarrow q + W^\pm + \tilde{\chi}_1^0$. Here the lightest Higgs boson h is assumed to have the SM decay branching fractions, and its mass is set to 125 GeV. The $\tilde{\chi}_1^\pm$ always decays to W^\pm and $\tilde{\chi}_1^0$ (figure 1). The branching fraction to a left-handed squark via the one-step decay with $\tilde{\chi}_2^0$ ($\tilde{\chi}_1^\pm$) is $\sim 30\%$ (65%). The branching fraction of the $\tilde{\chi}_2^0 \rightarrow h\tilde{\chi}_1^0$ decay is between 70% and 90% depending on $m_{\tilde{q}_L}$.

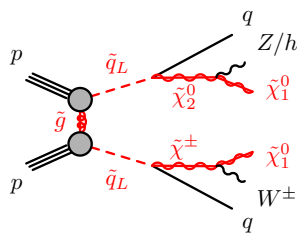


Figure 1: Example of a one-step decay topology of the left-handed squark in the phenomenological MSSM.

2.1.2. Minimal Supergravity/Constrained MSSM and bilinear R-parity-violation models

The mSUGRA/CMSSM model is specified by five parameters: a universal scalar mass (m_0), a universal gaugino mass ($m_{1/2}$), a universal trilinear scalar coupling (A_0), all defined at the grand unification scale, $\tan\beta$, and the sign of the higgsino mass parameter (μ). The dependence of the SUSY particle mass spectrum on these five parameters is such that all masses increase with increasing $m_{1/2}$, while squark and slepton masses also depend on m_0 . In the mSUGRA/CMSSM model studied here the values $\tan\beta = 30$, $A_0 = -2m_0$ and $\mu > 0$ are chosen, such that the lightest scalar Higgs boson mass is approximately 125 GeV in a large fraction of the $(m_0, m_{1/2})$ parameter space studied.

The bRPV scenario uses the same parameters as the mSUGRA/CMSSM model, but R-parity violation is allowed through the bilinear terms² $\epsilon_i L_i H_2$, whose coupling parameters are determined by a fit to neutrino oscillation data [56] under the tree-level dominance scenario [57]. In this scenario, the $\tilde{\chi}_1^0$ LSP decays promptly to $W\mu$, $W\tau$, $Z\nu_\tau$ or $h\nu_\tau$ (where the $W/Z/h$ boson can either be on- or off-shell) with branching fractions which are weakly dependent on m_0 and $m_{1/2}$ and are typically on the order of 20–40%, 20–40%, 20–30% and 0–20%, respectively.

2.1.3. Minimal gauge-mediated supersymmetry breaking model

In gauge-mediated SUSY breaking models, the LSP is a very light gravitino (\tilde{G}). The mGMSB model is described by six parameters: the SUSY-breaking mass scale felt by the low-energy sector (Λ), the mass of the SUSY breaking messengers (M_{mess}), the number of SU(5) messenger fields (N_5), $\tan\beta$, μ and the gravitino coupling scale factor (C_{grav}) which determines the lifetime of the next-to-lightest SUSY particle (NLSP). Four parameters are fixed to the values previously used in refs. [58–60]: $M_{\text{mess}} = 250$ TeV, $N_5 = 3$, $\mu > 0$ and $C_{\text{grav}} = 1$. With this choice of parameters the production of squark and/or gluino pairs is expected to dominate over other SUSY processes at the LHC. These SUSY particles decay into the NLSP, which subsequently decays to the LSP. The experimental signatures are largely determined by the nature of the NLSP: this can be either the lightest stau ($\tilde{\tau}$), a selectron or a smuon ($\tilde{\ell}$), the lightest neutralino ($\tilde{\chi}_1^0$), or a sneutrino ($\tilde{\nu}$), leading to final states usually containing tau leptons, light leptons ($\ell = e, \mu$), photons, or neutrinos, respectively.

² In this notation, L_i indicates a lepton SU(2)-doublet superfield, the Higgs SU(2)-doublet superfield H_2 contains the Higgs field that couples to up-type quarks, and the ϵ_i parameters have dimension of mass.

2.1.4. Natural gauge mediation model

In the nGM scenario, which assumes general gauge mediation [61, 62], the phenomenology depends on the nature of the NLSP [63, 64]. Various models assume that the mass hierarchies of squarks and sleptons are generated by the same physics responsible for breaking SUSY (for example refs. [65, 66]). Typically in these models the third generation of squarks and sleptons is lighter than the other two, and together with the fact that sleptons only acquire small masses through hypercharge interactions in gauge mediation, this leads to a stau NLSP. In the model considered here, it is also assumed that the gluino is the only light coloured sparticle. All squark and slepton mass parameters are set to 2.5 TeV except the lightest stau mass, $m_{\tilde{\tau}}$, which is assumed to be smaller. The parameters M_1 and M_2 are also set to 2.5 TeV, while all trilinear coupling terms are set to zero. The value of μ is set to 400 GeV to ensure that strong production dominates in the parameter space studied. This leaves the gluino mass M_3 and the stau mass $m_{\tilde{\tau}}$ as the only free parameters. The chosen value of the μ parameter sets the masses of the $\tilde{\chi}_1^\pm$, $\tilde{\chi}_1^0$ and $\tilde{\chi}_2^0$, which are almost mass-degenerate. The only light sparticles in the model are the stau, a light gluino, higgsino-dominated charginos and neutralinos, and a very light gravitino LSP. Therefore, the strong production process allowed in this model is gluino-pair production followed by the three possible decay chains: $\tilde{g} \rightarrow g\tilde{\chi}_{1,2}^0 \rightarrow g\tilde{\tau}\tau \rightarrow g\tau\tau\tilde{G}$, $\tilde{g} \rightarrow q\bar{q}\tilde{\chi}_{1,2}^0 \rightarrow q\bar{q}\tilde{\tau}\tau \rightarrow q\bar{q}\tau\tau\tilde{G}$ and $\tilde{g} \rightarrow qq\tilde{\chi}_1^\pm \rightarrow qq\nu_\tau\tilde{\tau} \rightarrow qq\nu_\tau\tau\tilde{G}$ (figure 2), where the final-state quarks are almost exclusively top or bottom quarks. A range of signals with varying gluino and stau masses is studied. The lightest Higgs boson mass is specifically set to 125 GeV.

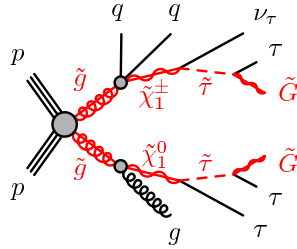


Figure 2: Example of a gluino-pair production followed by the two possible decay chains within the nGM scenario.

2.1.5. Non-universal Higgs mass models with gaugino mediation

The NUHMG model is specified with parameters $m_0 = 0$, $\tan\beta = 10$, $\mu > 0$, $m_{H_2}^2 = 0$, and A_0 chosen to maximize the mass of the lightest Higgs boson. The ranges of the two remaining free parameters of the model, $m_{1/2}$ and $m_{H_1}^2$, are chosen such that the NSLP is a tau sneutrino with properties satisfying Big Bang nucleosynthesis constraints [54]. The squared mass terms of the two Higgs doublets, $m_{H_1}^2$ and $m_{H_2}^2$, are defined at the unification scale. This model is characterized by significant cross-sections for \tilde{q} and \tilde{g} production. The gluino decays mainly to a light quark/squark pair $q\bar{q}$ ($\approx 50\%$), but also to $t\bar{t}$ ($\approx 30\%$) or $b\bar{b}$ ($\approx 20\%$), while the squark multi-step decays typically involve charginos, neutralinos and/or sleptons.

2.1.6. Minimal Universal Extra Dimensions model

The mUED model is the minimal extension of the SM with one additional universal spatial dimension. In this non-SUSY model, the Kaluza–Klein (KK) quark excitation’s decay chain to the lightest KK particle, the KK photon, gives a signature very similar to the supersymmetric decay chain of a squark to the lightest neutralino. The properties of the model depend on two parameters: the compactification radius R_c and the cut-off scale Λ . This cut-off is interpreted as the scale at which some new physics underlying the effective non-renormalizable UED framework becomes relevant. The Higgs boson mass is fixed to 125 GeV.

2.2. Simplified models

The details of the simplified models considered are given below and summarized in tables 1–3.

Diagram	Production	Parameters	Mass relation	Branching ratio	Result
fig. 3(a)	$\tilde{q}\tilde{q}$	$m_{\tilde{q}}, m_{\tilde{\chi}_1^0}$	$m_{\tilde{q}} > m_{\tilde{\chi}_1^0}$	$\text{BR}(\tilde{q} \rightarrow q\tilde{\chi}_1^0) = 1$	fig. 18
fig. 3(b)	$\tilde{g}\tilde{q}$	$m_{\tilde{q}}, m_{\tilde{\chi}_1^0}$	$m_{\tilde{q}} = 0.96 m_{\tilde{g}} > m_{\tilde{\chi}_1^0}$	$\text{BR}(\tilde{q} \rightarrow q\tilde{\chi}_1^0) = 1$ $\text{BR}(\tilde{g} \rightarrow \tilde{q}q) = 1$	fig. 20(a)
		$m_{\tilde{q}}, m_{\tilde{g}}$	$m_{\tilde{\chi}_1^0} = (0, 395, 695) \text{ GeV}$	If $m(\tilde{g}) > m(\tilde{q})$: $\text{BR}(\tilde{q} \rightarrow q\tilde{\chi}_1^0) = 1, \text{BR}(\tilde{g} \rightarrow \tilde{q}q) = 1$ If $m(\tilde{q}) > m(\tilde{g})$: $\text{BR}(\tilde{g} \rightarrow q\tilde{\chi}_1^0) = 1, \text{BR}(\tilde{q} \rightarrow \tilde{g}q) = 1$	fig. 20(b)
fig. 3(c)	$\tilde{g}\tilde{g}$	$m_{\tilde{g}}, m_{\tilde{\chi}_1^0}$	$m_{\tilde{g}} > m_{\tilde{\chi}_1^0}$	$\text{BR}(\tilde{g} \rightarrow q\tilde{\chi}_1^0) = 1$	fig. 19
fig. 3(d)	$\tilde{g}\tilde{g}$	$m_{\tilde{g}}$	$m_{\tilde{\chi}_1^0} = 0$	$\text{BR}(\tilde{g} \rightarrow g\tilde{\chi}_1^0) = 1$	fig. 21(a)
		$m_{\tilde{\chi}_1^0}$	$m_{\tilde{g}} = 850 \text{ GeV}$		fig. 21(b)

Table 1: Simplified models of squark and gluino production with direct decays to $\tilde{\chi}_1^0$. For each model the diagram of the decay topology, the model parameters and assumptions about mass relations and branching ratios are listed. The last column refers to the experimental results presented in section 11.2. Horizontal dashed lines separate different mass or branching ratio assumptions within a model.

Diagram	Production	Parameters	Mass relation	Branching ratio	Result
fig. 4(a)	$\tilde{q}\tilde{q}$	$m_{\tilde{q}}, m_{\tilde{\chi}_1^0}$	$m_{\tilde{\chi}_1^\pm} = (m_{\tilde{q}} + m_{\tilde{\chi}_1^0})/2$	$\text{BR}(\tilde{q} \rightarrow qW\tilde{\chi}_1^0) = 1$	fig. 22(a)
		$m_{\tilde{q}}$ $x = \Delta m(\tilde{\chi}_1^\pm, \tilde{\chi}_1^0)/\Delta m(\tilde{q}, \tilde{\chi}_1^0)$	$m_{\tilde{\chi}_1^0} = 60 \text{ GeV}$		fig. 22(b)
fig. 4(b)	$\tilde{g}\tilde{g}$	$m_{\tilde{g}}, m_{\tilde{\chi}_1^0}$	$m_{\tilde{\chi}_1^\pm} = (m_{\tilde{g}} + m_{\tilde{\chi}_1^0})/2$	$\text{BR}(\tilde{g} \rightarrow qqW\tilde{\chi}_1^0) = 1$	fig. 23(a)
		$m_{\tilde{g}}$ $x = \Delta m(\tilde{\chi}_1^\pm, \tilde{\chi}_1^0)/\Delta m(\tilde{g}, \tilde{\chi}_1^0)$	$m_{\tilde{\chi}_1^0} = 60 \text{ GeV}$		fig. 23(b)
fig. 5(a)	$\tilde{q}\tilde{q}$	$m_{\tilde{q}}, m_{\tilde{\chi}_1^0}$	$m_{\tilde{\chi}_1^\pm, \tilde{\chi}_2^0} = (m_{\tilde{q}} + m_{\tilde{\chi}_1^0})/2$ $m_{\tilde{\ell}, \tilde{\nu}} = (m_{\tilde{\chi}_1^\pm, \tilde{\chi}_2^0} + m_{\tilde{\chi}_1^0})/2$	$\text{BR}(\tilde{q} \rightarrow q(\ell\nu/\ell\ell)\tilde{\chi}_1^0) = 1$ $\ell \equiv (e, \mu)$	fig. 26
				$\text{BR}(\tilde{q} \rightarrow q(\tau\nu/\tau\tau/\nu\nu)\tilde{\chi}_1^0) = 1$ $\ell \equiv \tau$	fig. 28
fig. 5(b)	$\tilde{q}\tilde{q}$	$m_{\tilde{q}}, m_{\tilde{\chi}_1^0}$	$m_{\tilde{\chi}_1^\pm} = (m_{\tilde{q}} + m_{\tilde{\chi}_1^0})/2$ $m_{\tilde{\chi}_2^0} = (m_{\tilde{\chi}_1^\pm} + m_{\tilde{\chi}_1^0})/2$	$\text{BR}(\tilde{q} \rightarrow qWZ\tilde{\chi}_1^0) = 1$	fig. 24
fig. 5(c)	$\tilde{g}\tilde{g}$	$m_{\tilde{g}}, m_{\tilde{\chi}_1^0}$	$m_{\tilde{\chi}_1^\pm, \tilde{\chi}_2^0} = (m_{\tilde{g}} + m_{\tilde{\chi}_1^0})/2$ $m_{\tilde{\ell}, \tilde{\nu}} = (m_{\tilde{\chi}_1^\pm, \tilde{\chi}_2^0} + m_{\tilde{\chi}_1^0})/2$	$\text{BR}(\tilde{g} \rightarrow qq(\ell\nu/\ell\ell)\tilde{\chi}_1^0) = 1$ $\ell \equiv (e, \mu)$	fig. 27
				$\text{BR}(\tilde{g} \rightarrow qq(\tau\nu/\tau\tau/\nu\nu)\tilde{\chi}_1^0) = 1$ $\ell \equiv \tau$	fig. 29
fig. 5(d)	$\tilde{g}\tilde{g}$	$m_{\tilde{g}}, m_{\tilde{\chi}_1^0}$	$m_{\tilde{\chi}_1^\pm} = (m_{\tilde{g}} + m_{\tilde{\chi}_1^0})/2$ $m_{\tilde{\chi}_2^0} = (m_{\tilde{\chi}_1^\pm} + m_{\tilde{\chi}_1^0})/2$	$\text{BR}(\tilde{g} \rightarrow qqWZ\tilde{\chi}_1^0) = 1$	fig. 25

Table 2: Simplified models of squark and gluino production with one- and two-step decays to $\tilde{\chi}_1^0$. For each model the diagram of the decay topology, the model parameters and assumptions about mass relations and branching ratios are listed. The last column refers to the experimental results presented in section 11.2. Horizontal dashed lines separate different mass or branching ratio assumptions within a model.

Diagram	Parameters	Mass relation	Branching ratio	Result
fig. 6(a)	$m_{\tilde{g}}, m_{\tilde{t}_1}$	$m_{\tilde{g}} > m_{\tilde{t}_1} + m_t$ $m_{\tilde{\chi}_1^0} = 60 \text{ GeV}$	$\text{BR}(\tilde{g} \rightarrow \tilde{t}_1 t) = 1$ $\text{BR}(\tilde{t}_1 \rightarrow t\tilde{\chi}_1^0) = 1$	fig. 31
fig. 6(b)	$m_{\tilde{g}}, m_{\tilde{t}_1}$	$m_{\tilde{g}} > m_{\tilde{t}_1} + m_t$ $m_{\tilde{\chi}_1^\pm} = 2m_{\tilde{\chi}_1^0}$ $m_{\tilde{\chi}_1^0} = 60 \text{ GeV}$	$\text{BR}(\tilde{g} \rightarrow \tilde{t}_1 t) = 1$ $\text{BR}(\tilde{t}_1 \rightarrow b\tilde{\chi}_1^\pm) = 1$ $\text{BR}(\tilde{\chi}_1^\pm \rightarrow W^*\tilde{\chi}_1^0) = 1$	fig. 32
fig. 6(c)	$m_{\tilde{g}}, m_{\tilde{t}_1}$	$m_{\tilde{g}} > m_{\tilde{t}_1} + m_t$ $m_{\tilde{\chi}_1^0} = m_{\tilde{t}_1} - 20 \text{ GeV}$	$\text{BR}(\tilde{g} \rightarrow \tilde{t}_1 t) = 1$ $\text{BR}(\tilde{t}_1 \rightarrow c\tilde{\chi}_1^0) = 1$	fig. 33
fig. 6(d)	$m_{\tilde{g}}, m_{\tilde{t}_1}$	$m_{\tilde{g}} > m_{\tilde{t}_1} + m_t$	$\text{BR}(\tilde{g} \rightarrow \tilde{t}_1 t) = 1$ $\text{BR}(\tilde{t}_1 \rightarrow sb) = 1$	fig. 34
fig. 7	$m_{\tilde{g}}, m_{\tilde{b}_1}$	$m_{\tilde{g}} > m_{\tilde{b}_1} + m_b$ $m_{\tilde{\chi}_1^0} = 60 \text{ GeV}$	$\text{BR}(\tilde{g} \rightarrow \tilde{b}_1 b) = 1$ $\text{BR}(\tilde{b}_1 \rightarrow b\tilde{\chi}_1^0) = 1$	fig. 35
fig. 8(a)	$m_{\tilde{g}}, m_{\tilde{\chi}_1^0}$	$m_{\tilde{g}} \ll m_{\tilde{t}_1}$	If $m_{\tilde{g}} > 2m_t + m_{\tilde{\chi}_1^0}$: $\text{BR}(\tilde{g} \rightarrow t\tilde{\chi}_1^0) = 1$ If $m_{\tilde{g}} < 2m_t + m_{\tilde{\chi}_1^0}$: $\text{BR}(\tilde{g} \rightarrow tWb\tilde{\chi}_1^0) + \text{BR}(\tilde{g} \rightarrow WbWb\tilde{\chi}_1^0) = 1$	fig. 30
fig. 8(b)	$m_{\tilde{g}}, m_{\tilde{\chi}_1^0}$	$2m_b + m_{\tilde{\chi}_1^0} < m_{\tilde{g}} \ll m_{\tilde{b}_1}$	$\text{BR}(\tilde{g} \rightarrow b\tilde{b}\tilde{\chi}_1^0) = 1$	fig. 36
fig. 8(c)	$m_{\tilde{g}}, m_{\tilde{\chi}_1^0}$	$m_b + m_t + m_{\tilde{\chi}_1^\pm} < m_{\tilde{g}} \ll m_{\tilde{t}_1}, m_{\tilde{b}_1}$ $m_{\tilde{\chi}_1^\pm} = m_{\tilde{\chi}_1^0} + 2 \text{ GeV}$	$\text{BR}(\tilde{g} \rightarrow t\tilde{b}\tilde{\chi}_1^\pm) = 1$ $\text{BR}(\tilde{\chi}_1^\pm \rightarrow \tilde{\chi}_1^0 f f') = 1$	fig. 37

Table 3: Simplified models of gluino pair production with decays via third-generation squarks. For each model the diagram of the decay topology, the model parameters and assumptions about mass relations and branching ratios are listed. The last column refers to the experimental results presented in section 11.2. Horizontal dashed lines separate different mass or branching ratio assumptions within a model.

2.2.1. Direct decays of squarks and gluinos

Simplified models with direct decay of the pair-produced strongly interacting supersymmetric particles assume the production of gluino pairs with decoupled squarks, light-flavour squark pairs with decoupled gluinos, or light-flavour squarks and gluinos; all other superpartners except the lightest neutralino are decoupled. This assumption forces squarks or gluinos to decay directly to quarks or gluons and the lightest neutralino, as shown in figure 3. In the case of squark–gluino production, the masses of the light-flavour squarks are set to 0.96 times the mass of the gluino as suggested in refs. [67, 68], and gluinos can decay via on-shell squarks as $\tilde{g} \rightarrow \tilde{q}q \rightarrow qq\tilde{\chi}_1^0$. For models with decoupled gluinos two scenarios have been considered: a scenario with eight mass-degenerate light-flavour squarks (\tilde{q}_L and \tilde{q}_R , with $\tilde{q} = \tilde{u}, \tilde{d}, \tilde{s}, \tilde{c}$), or a scenario with only one accessible light-flavour squark [69]. Changing the number of light-flavoured squarks affects only the cross-section but not the kinematics of the events. The free parameters in these models are $m_{\tilde{q}}$ or $m_{\tilde{g}}$, and $m_{\tilde{\chi}_1^0}$.

An additional set of simplified models with direct decay of pair-produced gluinos assumes that all squarks

and sleptons are much heavier than the gluino, which remains relatively light and decays promptly into a gluon and a neutralino [70], as shown in figure 3(d). The free parameters in these models are $m_{\tilde{g}}$ and $m_{\tilde{\chi}_1^0}$.

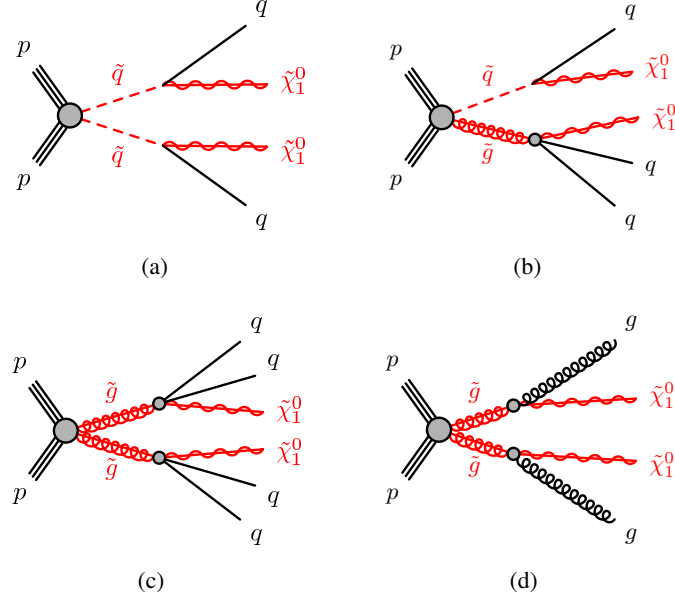


Figure 3: The decay topologies of (a) squark-pair production, (b) squark–gluino production or (c,d) gluino-pair production, in the simplified models with direct decays.

2.2.2. One-step decays of squarks and gluinos

Simplified models with one-step decays of the pair-produced squarks or gluinos assume that these particles decay via the $\tilde{\chi}_1^\pm$ into a W boson and the $\tilde{\chi}_1^0$, as shown in figure 4. The free parameters in these models are $m_{\tilde{q}}$ or $m_{\tilde{g}}$, and either $m_{\tilde{\chi}_1^\pm}$ with a fixed $m_{\tilde{\chi}_1^0} = 60$ GeV or $m_{\tilde{\chi}_1^0}$ with $m_{\tilde{\chi}_1^\pm} = (m_{\tilde{g}/\tilde{q}} + m_{\tilde{\chi}_1^0})/2$.

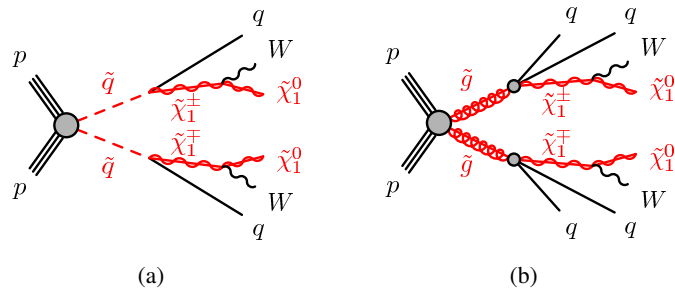


Figure 4: The decay topologies of (a) squark- or (b) gluino-pair production, in the simplified models with one-step decays.

2.2.3. Two-step decays of squarks and gluinos

Two categories of simplified models with two-step decays of squarks and gluinos are considered: models with and without sleptons.

In the two-step models with sleptons the pair-produced squarks or gluinos decay with equal probability to either the lightest chargino or the next-to-lightest neutralino ($\tilde{\chi}_2^0$). These subsequently decay via left-handed sleptons (or sneutrinos) which then further decay into a lepton (or neutrino) and the lightest neutralino. In these models, the free parameters are the mass of the initially produced particle and the mass of the lightest neutralino. The masses of the intermediate charginos or neutralinos are equal and set to be $m_{\tilde{\chi}_1^\pm, \tilde{\chi}_2^0} = (m_{\tilde{q}/\tilde{q}^*} + m_{\tilde{\chi}_1^0})/2$, while the slepton and sneutrino masses are set to be $m_{\tilde{\ell}, \tilde{\nu}} = (m_{\tilde{\chi}_1^\pm/\tilde{\chi}_2^0} + m_{\tilde{\chi}_1^0})/2$. All three slepton flavours are mass-degenerate in this model. A separate model in which the slepton is exclusively a $\tilde{\tau}$ is also considered.

In the second category, two-step models without sleptons, the initial supersymmetric particle decays via the lightest chargino, which itself decays into a W boson and the next-to-lightest neutralino. The latter finally decays into a Z boson and the lightest neutralino. The lightest chargino mass is fixed at $m_{\tilde{\chi}_1^\pm} = (m_{\tilde{q}/\tilde{q}^*} + m_{\tilde{\chi}_1^0})/2$ and the next-to-lightest neutralino mass is set to be $m_{\tilde{\chi}_2^0} = (m_{\tilde{\chi}_1^\pm} + m_{\tilde{\chi}_1^0})/2$.

These two categories of simplified models with two-step decays of squarks and gluinos are illustrated in figure 5.

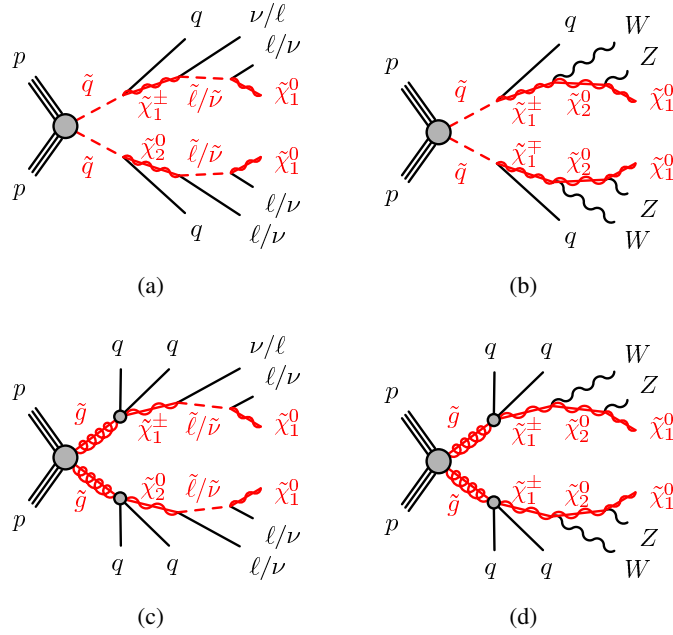


Figure 5: Examples of decay topologies of (a, b) squark- or (c, d) gluino-pair production, in the simplified models with two-step decays with (left) or without (right) sleptons.

2.2.4. Gluino decays via third-generation squarks

Two classes of simplified models with gluino decays via third-generation squarks are considered. In the first, the lightest stop or sbottom is lighter than the gluino, such that \tilde{t}_1 or \tilde{b}_1 are produced via gluino-pair

production followed by $\tilde{g} \rightarrow \tilde{t}_1 t$ or $\tilde{g} \rightarrow \tilde{b}_1 b$ decays. Gluino–stop models within this class assume that the \tilde{t}_1 is the lightest squark while all other squarks are heavier than the gluino, and $m_{\tilde{g}} > m_{\tilde{t}_1} + m_t$ such that the branching ratio for $\tilde{g} \rightarrow \tilde{t}_1 t$ decays is 100%. Top squarks are assumed to decay via either $\tilde{t}_1 \rightarrow t\tilde{\chi}_1^0$, $\tilde{t}_1 \rightarrow b\tilde{\chi}_1^\pm$, $\tilde{t}_1 \rightarrow c\tilde{\chi}_1^0$, or via $\tilde{t}_1 \rightarrow sb$ with R-parity and baryon number violation, as illustrated in figure 6. For the model with the $\tilde{t}_1 \rightarrow b\tilde{\chi}_1^\pm$ decay, the chargino mass is assumed to be twice the mass of the neutralino, and the chargino decays into a neutralino and a W boson. In the model with the $\tilde{t}_1 \rightarrow c\tilde{\chi}_1^0$ decay, which proceeds via a loop and is most relevant when the $\tilde{t}_1 \rightarrow bW\tilde{\chi}_1^0$ decay is kinematically forbidden, the mass gap between the \tilde{t}_1 and the lightest neutralino is fixed to 20 GeV. Using gluino–pair production to probe this decay is particularly interesting because it is complementary to the direct pair production of \tilde{t}_1 , which is more difficult to extract from the background for this specific decay mode [21]. Gluino–sbottom models within this class assume that the \tilde{b}_1 is the lightest squark, all other squarks are heavier than the gluino, and $m_{\tilde{g}} > m_{\tilde{b}_1} + m_b$ such that the branching ratio for $\tilde{g} \rightarrow \tilde{b}_1 b$ decays is 100%. The bottom squarks are assumed to decay exclusively via $\tilde{b}_1 \rightarrow b\tilde{\chi}_1^0$ (figure 7).

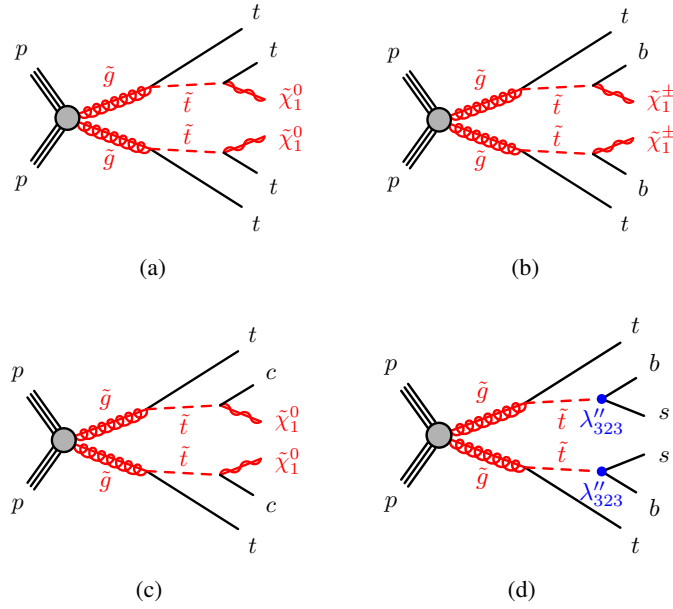


Figure 6: Decay topologies in the gluino–stop simplified models with the top squark decays: (a) $\tilde{t}_1 \rightarrow t\tilde{\chi}_1^0$, (b) $\tilde{t}_1 \rightarrow b\tilde{\chi}_1^\pm$, (c) $\tilde{t}_1 \rightarrow c\tilde{\chi}_1^0$ and (d) $\tilde{t}_1 \rightarrow sb$ with R-parity and baryon number violation, with a strength determined by the parameter λ''_{323} .

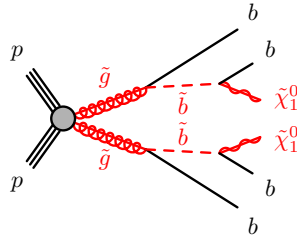


Figure 7: The decay topology in the gluino–sbottom simplified models, with the bottom squark decay $\tilde{b}_1 \rightarrow b\tilde{\chi}_1^0$.

In the second class of simplified models with gluino decays via top or bottom squarks, all sparticles apart from the gluino and the neutralino have masses well above the TeV scale such that the \tilde{t}_1 or the \tilde{b}_1 are only produced off-shell via prompt decay of the gluinos and have little impact on the kinematics of the final state. For the gluino–off-shell–stop model illustrated in figure 8(a), the \tilde{t}_1 is assumed to be the lightest squark, but $m_{\tilde{g}} < m_{\tilde{t}_1}$. A three-body decay $\tilde{g} \rightarrow t\bar{t}\tilde{\chi}_1^0$ via an off-shell stop is assumed for the gluino with a branching ratio of 100%. For the configuration $m_{\tilde{g}} < 2m_t + m_{\tilde{\chi}_1^0}$, decays of the gluino involve an off-shell top quark, e.g. the four-body decay $\tilde{g} \rightarrow tWb\tilde{\chi}_1^0$. Only four- and five-body decays of this type are considered, because for higher multiplicities the gluinos do not decay promptly. For the gluino–off-shell–sbottom model shown in figure 8(b), the \tilde{b}_1 is assumed to be the lightest squark but with $m_{\tilde{g}} < m_{\tilde{b}_1}$. A three-body decay $\tilde{g} \rightarrow b\bar{b}\tilde{\chi}_1^0$ via an off-shell sbottom is assumed for the gluino with a branching ratio of 100%. In the gluino–off-shell–stop/sbottom model illustrated in figure 8(c), the \tilde{b}_1 and \tilde{t}_1 are the lightest squarks, with $m_{\tilde{g}} < m_{\tilde{b}_1, \tilde{t}_1}$. Pair production of gluinos is the only process taken into account, with gluinos decaying via off-shell stops or sbottoms, and a branching ratio of 100% assumed for $\tilde{t}_1 \rightarrow b + \tilde{\chi}_1^\pm$ and $\tilde{b}_1 \rightarrow t + \tilde{\chi}_1^\pm$ decays. The mass difference between charginos and neutralinos is set to 2 GeV, such that the fermions produced in $\tilde{\chi}_1^\pm \rightarrow \tilde{\chi}_1^0 + ff'$ decays do not contribute to the event selection, and gluino decays result in effective three-body decays $b\bar{t}\tilde{\chi}_1^0$.

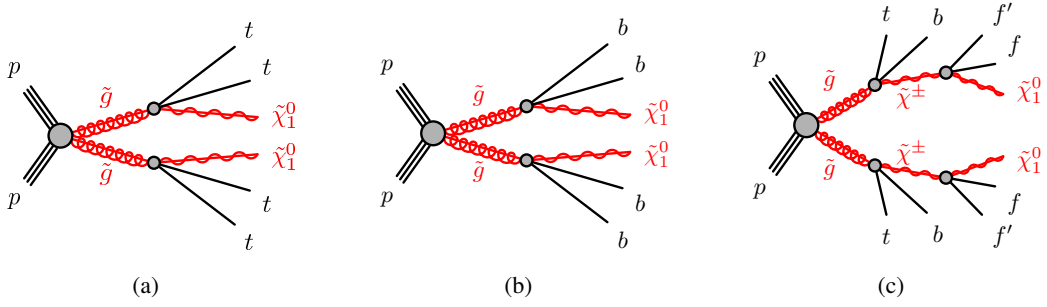


Figure 8: The decay topologies in the (a) gluino–off-shell–stop, (b) gluino–off-shell–sbottom and (c) gluino–off-shell–stop/sbottom simplified models.

3. The ATLAS detector and data sample

The ATLAS detector [17] is a multi-purpose particle physics detector with a forward-backward symmetric cylindrical geometry and nearly 4π coverage in solid angle.³ The inner tracking detector (ID) consists of pixel and silicon microstrip detectors covering the pseudorapidity region $|\eta| < 2.5$, surrounded by a transition radiation tracker (TRT) which enhances electron identification in the region $|\eta| < 2.0$. The ID is surrounded by a thin superconducting solenoid providing an axial 2 T magnetic field and by a fine-granularity lead/liquid-argon (LAr) electromagnetic calorimeter covering $|\eta| < 3.2$. A steel/scintillator-tile calorimeter provides hadronic coverage in the central pseudorapidity range ($|\eta| < 1.7$). The endcap and forward regions ($1.5 < |\eta| < 4.9$) of the hadronic calorimeter are made of LAr active layers with either copper or tungsten as the absorber material. An extensive muon spectrometer with an air-core toroid magnet system surrounds the calorimeters. Three layers of high-precision tracking chambers provide coverage in the range $|\eta| < 2.7$, while dedicated fast chambers allow triggering in the region $|\eta| < 2.4$. The ATLAS trigger system [71] consists of three levels; the first level (L1) is a hardware-based system, while the second and third levels are software-based systems and are together called the High Level Trigger (HLT).

The data used in these searches were collected from March to December 2012 with the LHC operating at a centre-of-mass energy of 8 TeV. After the application of beam, detector and data quality requirements, the total integrated luminosity ranges from 20.1 to 20.3 fb⁻¹, depending on the triggers used for the event selection, with a relative uncertainty of $\pm 2.8\%$. The uncertainty is derived following the methodology detailed in ref. [72]. During the data-taking period, the peak instantaneous luminosity per LHC fill was typically 7×10^{33} cm⁻² s⁻¹, while the average number of pp interactions per LHC bunch crossing ranged from approximately 6 to 40, with a mean value of 21. In order to maximize the efficiency of selecting the various final states used by the analyses included in this paper, different triggers or combinations of triggers were used: E_T^{miss} triggers, multi-jet triggers, combined E_T^{miss} +jet, lepton+ E_T^{miss} or lepton+jet+ E_T^{miss} triggers, single-lepton or dilepton triggers. Details of the trigger selections used in the published ATLAS searches included in this paper are not discussed here and can be found in the corresponding publications [20–27].

4. Monte Carlo simulated samples

The simulated event samples for the SM backgrounds are summarized in table 4, together with the choices of Monte Carlo generator, cross-section calculation, set of tunable parameters (tune) used for the underlying event and parton distribution functions (PDFs). The POWHEG-BOX+PYTHIA $t\bar{t}$ sample is used for all analyses except for the analysis that requires high jet multiplicities (at least seven to at least ten jets) and large missing transverse momentum [22], which uses the SHERPA $t\bar{t}$ sample. The SHERPA Drell–Yan samples have a lepton filter requiring $p_T^{\ell_1(\ell_2)} > 9$ (5) GeV and $|\eta^{\ell_1(\ell_2)}| < 2.8$. This filter prevents its use in analyses requiring the presence of soft leptons in the final state. Such analyses instead use ALPGEN samples with a lepton p_T threshold at 5 GeV. When using the baseline POWHEG-BOX+PYTHIA top quark pair production sample, in some of the analyses events are reweighted in bins of $p_T(t\bar{t})$ to match the top

³ ATLAS uses a right-handed coordinate system with its origin at the nominal interaction point in the centre of the detector. The positive x -axis is defined by the direction from the interaction point to the centre of the LHC ring, with the positive y -axis pointing upwards, while the beam direction defines the z -axis. Cylindrical coordinates (r, ϕ) are used in the transverse plane, ϕ being the azimuthal angle around the z -axis. The pseudorapidity η is defined in terms of the polar angle θ by $\eta = -\ln \tan(\theta/2)$.

quark pair differential cross-section measured in ATLAS data [73, 74]. The exact usage of MC simulated samples together with the additional samples used to assess modelling uncertainties are detailed in the corresponding publication of each analysis.

Process	Generator	Cross-section order in α_s	Tune	PDF set
$W(\rightarrow \ell\nu)+\text{jets}$	SHERPA 1.4.1 [75]	NNLO [76]	SHERPA default	CT10 [77]
$Z/\gamma^*(\rightarrow \ell\ell)+\text{jets}$	SHERPA 1.4.1	NNLO [76]	SHERPA default	CT10
Drell–Yan ($8 < m_{\ell\ell} < 40$ GeV)	SHERPA 1.4.1	NNLO [78]	SHERPA default	CT10
$Z/\gamma^*(\rightarrow \ell\ell) + \text{jets}$ ($10 < m_{\ell\ell} < 60$ GeV)	ALPGEN 2.14 [79] + HERWIG 6.520 [82, 83] + JIMMY [84]	NNLO [78]	AUET2 [80]	CTEQ6L1 [81]
$\gamma+\text{jets}$	SHERPA 1.4.1	LO	SHERPA default	CT10
$t\bar{t}$	POWHEG-Box 1.0 [85–87] + PYTHIA 6.426 [90]	NNLO+NNLL [88, 89]	PERUGIA2011C [91, 92]	CT10
$t\bar{t}$	SHERPA 1.4.1	NNLO+NNLL	SHERPA default	CT10
Single top				
t -channel	ACERMC 3.8 [93] + PYTHIA 6.426	NNLO+NNLL [94]	AUET2B [95]	CTEQ6L1
s -channel, Wt	MC@NLO 4.03 [96, 97] + HERWIG 6.520	NNLO+NNLL [98, 99]	AUET2B	CT10
$t\bar{t} + W/Z$ boson	MADGRAPH 5 1.3.28 [100] + PYTHIA 6.426	NLO [101–103]	AUET2B	CTEQ6L1
Dibosons $WW, WZ, ZZ,$ $W\gamma$ and $Z\gamma$	SHERPA 1.4.1	NLO [104, 105]	SHERPA default	CT10

Table 4: The Standard Model background Monte Carlo simulation samples used in this paper. The generators, the order in α_s of cross-section calculations used for yield normalization (leading order (LO), next-to-leading order (NLO), next-to-next-to-leading order (NNLO), next-to-next-to-leading logarithm (NNLL)), tunes used for the underlying event and PDF sets are shown. For the $\gamma+\text{jets}$ process the LO cross-section is taken directly from the MC generator.

Signal samples for the pMSSM, mSUGRA, mGMSB, nGM and mUED models, as well as the samples for the simplified models of gluino-mediated top squark production (for $m_{\tilde{g}} - m_{\tilde{\chi}_1^0} > 2m_t$) are generated with HERWIG++ 2.5.2 [106]. Samples for all the other simplified models are generated with up to one extra parton in the matrix element using MADGRAPH 5 1.3.33 interfaced to PYTHIA 6.426. The MLM matching scheme [107] is applied with a scale parameter that is set to a quarter of the mass of the lightest sparticle in the hard-scattering matrix element, with a maximum value of 500 GeV. The signal samples used for the bRPV and NUHMG models are generated with PYTHIA 6.426.

For the gluino–off-shell–stop model in the region $m_{\tilde{g}} - m_{\tilde{\chi}_1^0} < 2m_t$, the production of gluino pairs is generated with MADGRAPH 5 1.3.33. The events are subsequently combined with separately generated gluino decays $\tilde{g} \rightarrow f\bar{f}'f''\bar{f}'''\bar{b}\bar{b}\tilde{\chi}_1^0$ based on the full matrix element amplitude (also using MADGRAPH), preserving spin-dependent distributions. A summary of the studies related to event generation in this model can be found in appendix A. Potential effects of the gluino lifetime (displaced decays, hadronization), which are strongly model dependent, have been neglected.

The ATLAS underlying-event tune AUET2B [80] is used for MADGRAPH 5 and PYTHIA 6 samples while the UE-EE-3C tune [108] is used for HERWIG++ samples. The parton distribution functions from CTEQ6L1

[81] are used for all signal samples.

For all except the mUED sample, the signal cross-sections are calculated to next-to-leading order in the strong coupling constant, including the resummation of soft gluon emission at next-to-leading-logarithmic accuracy (NLO+NLL) [109–113]. In each case the nominal cross-section and its uncertainty are taken from an ensemble of cross-section predictions using different PDF sets and factorization and renormalization scales, as described in ref. [114]. For the mUED model, the cross-section is taken at leading order from HERWIG++. For the mSUGRA/CMSSM and NUHMG samples, SUSY-HIT [115] and SDECAY 1.3b [116], interfaced to the SOFTSUSY 3.1.6 spectrum generator [117], are used to calculate the sparticle mass spectra and decay tables, and to ensure consistent electroweak symmetry breaking.

The decays of tau leptons are simulated directly in the generators in the case of event samples produced with SHERPA, HERWIG++ 2.5.2 and PYTHIA 8.165, while in all other cases TAUOLA 2.4 [118, 119] is used.

Standard Model background samples are passed through either the full ATLAS detector simulation [120] based on GEANT4 [121], or through a fast simulation using a parameterization of the performance of the ATLAS electromagnetic and hadronic calorimeters [122] and GEANT4 elsewhere; the latter applies to $W/Z/\gamma$ +jets samples with boson $p_T < 280$ GeV and POWHEG-BOX+PYTHIA $t\bar{t}$ samples. All SUSY signal samples are passed through the fast simulation, with the exception of the mSUGRA/CMSSM model samples which are produced with the GEANT4 simulation. The fast simulation of SUSY signal events was validated against full GEANT4 simulation for several signal models. Differing pile-up (multiple pp interactions in the same or neighbouring bunch-crossings) conditions as a function of the instantaneous luminosity are taken into account by overlaying simulated minimum-bias events (simulated using PYTHIA 8 with the MSTW2008LO PDF set [123] and the A2 tune [95]) onto the hard-scattering process and reweighting events according to the distribution of the mean number of interactions observed in data.

5. Object reconstruction and identification

This paper summarizes different analyses which are combined to improve the sensitivity to a variety of possible topologies originating from the production and decay of squarks and gluinos. Although different event selections are used among these analyses, they share common definitions of the reconstructed objects. Analysis-specific exceptions to these definitions are detailed in the corresponding publication of each analysis.

The reconstructed primary vertex of the event is required to be consistent with the beamspot envelope and to have at least five associated tracks with $p_T > 400$ MeV. When more than one such vertex is found, the vertex with the largest $\sum p_T^2$ of the associated tracks is chosen.

Jet candidates are reconstructed using the anti- k_r jet clustering algorithm [124, 125] with a radius parameter of 0.4. The inputs to this algorithm are topological clusters [126, 127] of calorimeter cells seeded by those with energy significantly above the measured noise (topoclusters). The local cluster weighting (LCW) calibration method [127, 128] is used to classify topoclusters as being either of electromagnetic or hadronic origin, and based on this classification it applies energy corrections derived from MC simulations and measurements in data. The jets are corrected for energy from pile-up using the method suggested in ref. [129]: a contribution equal to the product of the jet area and the median energy density of the event is subtracted from the jet energy [130]. Further corrections, referred to as the jet energy scale (JES) corrections, are derived from MC simulation and data and used to calibrate on average the energies of jets to the scale of their constituent particles [127, 131]. Only jet candidates with $p_T > 20$ GeV

and $|\eta| < 4.5$ after all corrections are retained. To remove events with jets from detector noise and non-collision backgrounds, events are rejected if they include jets failing to satisfy the “loose” quality criteria described in ref. [127].

A neural-network-based algorithm [132] is used to identify jets containing a b -hadron (b -jets). It uses as inputs the output weights of several algorithms exploiting the impact parameter of the inner detector tracks, secondary vertex reconstruction and the topology of b - and c -hadron decays inside the jet. The algorithm used has an efficiency of 70% for tagging b -jets, determined with simulated $t\bar{t}$ events [133]. For this efficiency, the algorithm provides a rejection factor of approximately 140 for light-quark and gluon jets, and of approximately 5 for charm jets [134]. Candidate b -jets are required to have $p_T > 40$ GeV and $|\eta| < 2.5$.

Electrons are reconstructed from energy clusters in the electromagnetic calorimeter matched to tracks in the inner detector [135] and are required to have $p_T > 10$ GeV and $|\eta| < 2.47$. The preselected electron candidates are required to pass a variant of the “medium” selection [135], which was modified in 2012 to reduce the impact of pile-up.

Photon candidates, which in the analyses presented are used only for the measurement of the missing transverse momentum, are required to have $p_T > 10$ GeV and $|\eta| < 1.37$ or $1.52 < |\eta| < 2.47$, to satisfy photon shower shape and electron rejection criteria [136], and to be isolated.

Muon candidates are formed by combining information from the muon spectrometer and inner tracking detectors [137]. The preselected muon candidates are required to have $p_T > 10$ GeV and $|\eta| < 2.4$ or 2.5, depending on the analysis.

Reconstruction of hadronically decaying tau leptons starts from jets with $p_T > 10$ GeV [138], and an η - and p_T -dependent energy calibration to the tau energy scale for hadronic decays is applied [139]. Tau lepton candidates must have one or three associated track(s) with a charge sum of ± 1 , and satisfy $p_T > 20$ GeV and $|\eta| < 2.5$. The “loose” and “medium” working points [138] are used and correspond to efficiencies of approximately 70% and 60%, independent of p_T , with rejection factors of 10 and 20 against jets misidentified as tau candidates, respectively.

After these selections, ambiguities between candidate jets with $|\eta| < 2.8$ and leptons (electrons and muons) are resolved as follows. First, any such jet candidate lying within a distance $\Delta R = \sqrt{(\Delta\eta)^2 + (\Delta\phi)^2} = 0.2$ of a preselected electron is discarded; then any lepton candidate within a distance $\Delta R = 0.4$ of any surviving jet candidate is discarded. In analyses requiring the presence of one lepton (electron or muon) in the final state, electrons are also required to be well separated from muon candidates with $\Delta R(e, \mu) > 0.01$. If two preselected electrons are found within an angular distance $\Delta R(e, e) = 0.05$ of each other, only the electron with the higher p_T is kept. Finally, in the analyses that require the presence of at least one or two opposite-sign leptons in the final state, any event containing a preselected electron in the transition region between the barrel and endcap electromagnetic calorimeters, $1.37 < |\eta| < 1.52$, is rejected.

The measurement of the missing transverse momentum vector is based on the transverse momenta of all electron, photon, jet and muon candidates, and all calorimeter energy clusters not associated with such objects [140]. Fully calibrated electrons and photons with $p_T > 10$ GeV and jets with $p_T > 20$ GeV are used. Energy deposits not associated with these objects are also taken into account in the E_T^{miss} calculation using an energy-flow algorithm that considers calorimeter energy deposits as well as ID tracks [141]. In the E_T^{miss} measurement tau leptons are not distinguished from jets and it has been checked that this does not introduce a bias in any kinematic variables used in the analyses.

Corrections derived from data control samples are applied to account for differences between data and simulation for the lepton trigger and reconstruction efficiencies, momentum/energy scale and resolution, and for the efficiency and mis-tag rate for tagging jets originating from b -quarks.

6. Analysis strategy

A search for squarks and gluinos under various decay mode assumptions necessitates many different event selections targeting the wide range of experimental signatures. This section summarizes the common analysis strategy and statistical techniques that are employed in all searches included in this paper. Signal regions (SRs) are defined using the Monte Carlo simulation of the signal processes and the SM backgrounds, and are optimized to maximize the expected significance for each model considered. To estimate the SM backgrounds in a consistent and robust fashion, corresponding control regions (CRs) are defined for each of the signal regions. They are chosen to be non-overlapping with the SR selections in order to provide independent data samples enriched in particular background sources. The CR selections are optimized to have negligible SUSY signal contamination for the models under investigation, while minimizing as much as possible the systematic uncertainties arising from the extrapolation of the CR event yields to the expectations in the SR. Cross-checks of the background estimates are performed using several validation regions (VRs) selected with requirements such that these regions do not overlap with the CR and SR selections, again with a low probability of signal contamination.

Several classes of profile likelihood fits that utilize the observed numbers of events in the various regions are employed in the analyses [142]. In some analyses, the shape of a final discriminating variable in the SRs is also used. A background-only fit is used to determine the compatibility of the observed event yield in each SR with the corresponding SM background expectation. This fit uses as constraints only the observed event yields or the shape of the discriminating variable distributions from the CRs associated with the SR, but not the SR itself. It is assumed that signal events from physics beyond the Standard Model (BSM) do not contribute to these yields. The numbers of observed and predicted events in each of these CRs are described using Poisson probability density functions. The systematic uncertainties and the MC statistical uncertainties on the expected values are included in the fit as nuisance parameters which are constrained by Gaussian distributions with widths corresponding to the sizes of the uncertainties considered and Poisson distributions, respectively. Correlations of a given nuisance parameter across the various regions, between the various backgrounds, and possibly the signal, are taken into account. The product of the various probability density functions forms the likelihood, which the fit maximizes by adjusting the inputs to the fit and the nuisance parameters. The inputs to the fit for each of the SRs are the number of events observed in each of the CRs, and the corresponding number of events expected from simulation, the extrapolation factors obtained from the simulation which relate the number of predicted SM background events in their associated CR to that predicted in the SR, and the number of events predicted by the simulation in each region for the other background processes. The background fit results are cross-checked in validation regions. The data in the validation regions are not used to constrain the fits; they are only used to compare the results of the fits to statistically independent observations.

A model-independent fit is used to set upper limits on the number of BSM signal events in each SR. This fit proceeds in the same way as the background-only fit, except that the number of events observed in the SR is added as an input to the fit, and the BSM signal strength, constrained to be non-negative, is added as a free parameter. The observed and expected upper limits at 95% confidence level (CL) on the number of events from BSM phenomena for each signal region (S_{obs}^{95} and S_{exp}^{95}) are derived using the CL_S prescription

[143], neglecting any possible signal contamination in the control regions; an uncertainty on S_{exp}^{95} is also computed from the $\pm 1\sigma$ uncertainty on the expectation. These limits, when normalized by the integrated luminosity of the data sample, may be interpreted as upper limits on the visible cross-section of BSM physics ($\langle \epsilon\sigma \rangle_{\text{obs}}^{95}$), where the visible cross-section is defined as the product of production cross-section, acceptance and efficiency. The model-independent fit is also used to compute the one-sided p -value (p_0) of the background-only hypothesis which quantifies the statistical significance of an excess.

Model-dependent fits are used to set exclusion limits on the signal cross-sections for specific SUSY models. Such a fit proceeds in the same way as the model-independent fit, except that signal contamination in the CRs is taken into account as well as the yield in the signal region and, in some analyses, the model shape information. Correlations between signal and background systematic uncertainties are taken into account where appropriate. The systematic uncertainties on the signal expectations originating from detector effects and the theoretical uncertainties on the signal acceptance are included in the fit. The impact of the theoretical uncertainties on the signal cross-section is shown on the limit plots obtained (section 11). Numbers quoted in the text are evaluated from the observed exclusion limit based on the nominal signal cross-section minus its 1σ theoretical uncertainty.

Background-only and model-independent fit results are presented in this paper only for new analyses or signal regions which are not available in earlier ATLAS publications. In the context of this publication, model-dependent exclusion fits for various simplified and phenomenological models are combined to include results from different searches for each model individually, in order to maximize the expected exclusion reach for each model. Where possible a full statistical combination of non-overlapping searches is applied, as explained in section 10.

7. Experimental signatures

This paper summarizes and combines the results of several individual inclusive squark and gluino analyses previously published by the ATLAS experiment. Each of these searches uses one or more sets of signal regions targeting specific experimental signatures which originate from different squark or gluino decay modes and mass hierarchies. Several extensions to the previously published searches in the form of additional signal regions are also included, along with one new analysis channel. The full list of searches and their signal regions used in this paper is presented in table 5, together with the corresponding references. The details of the signal region selections for all searches listed in table 5 can be found in appendix B. The details of the control and validation region selections, together with the strategies used for the estimation of the background processes, can be found in the corresponding publications. The new analysis and extended signal regions, which are also presented in table 5, are discussed in more detail in the subsequent subsections. Each signal region is referred to with an acronym, listed in table 5, indicating the analysis origin, so for example the ‘2jl’ region from the 0-lepton + 2–6 jets + $E_{\text{T}}^{\text{miss}}$ analysis is referred to as ‘0L_2jl’. The correspondence between the searches and the various models probed is provided in table 6 and a summary of the limits in simplified models presented in the respective papers is given in table 7. The 0-lepton + 2–6 jets + $E_{\text{T}}^{\text{miss}}$ and 1-lepton (soft+hard) + jets + $E_{\text{T}}^{\text{miss}}$ statistical combination, referred to as (0+1)-lepton combination, is used to probe the models for which both analyses have comparable sensitivity.

Short analysis name and corresponding reference	Acronym	Signal region name
Monojet [21] 0-lepton + 2–6 jets + E_T^{miss} [20] 0-lepton + 4–5 jets + E_T^{miss} (★) 0-lepton + 7–10 jets + E_T^{miss} [22] 0-lepton Razor (●)	MONOJ OL OL MULTJ OLRaz	M1, M2, M3 2jl, 2jm, 2jt, 2jW, 3j, 4jW, 4jl-, 4jl, 4jm, 4jt, 5j, 6jl, 6jm, 6jt, 6jt+ 4jt+, 5jt 8j50, 9j50, 10j50 (multi-jet+flavour stream), 7j80, 8j80, (multi-jet+flavour stream), 8j50, 9j50, 10j50 (multi-jet+ M_j^Σ stream) SR _{loose} , SR _{tight}
1-lepton (soft+hard) + jets + E_T^{miss} [23] 1-lepton (hard) + 7 jets + E_T^{miss} (★) 2-leptons (soft) + jets + E_T^{miss} [23] 2-leptons (hard) + jets + E_T^{miss} [23] 2-leptons off-Z [24] Same-sign dileptons or 3-leptons + jets + E_T^{miss} [25]	1L(S,H) 1L(H) 2L(S) 2LRaz 2L-offZ SS/3L	3-jet/5-jet/3-jet inclusive (soft lepton), 3-jet/5-jet/6-jet (hard lepton) 7-jet 2-jet (soft dimuon) \leq 2-jet/3-jet SR-2j-bveto, SR-2j-btag, SR-4j-bveto, SR-4j-btag, SR-loose SR3b, SR0b, SR1b, SR3Llow, SR3Lhigh
Taus + jets + E_T^{miss} [26]	TAU	1 τ (Loose, Tight), 2 τ (Inclusive, GMSB, nGM, bRPV), $\tau + l$ (GMSB, nGM, bRPV, mSUGRA)
0/1-lepton + 3b-jets + E_T^{miss} [27]	0/1L3B	SR-0l-4j-A, SR-0l-4j-B, SR-0l-4j-C, SR-0l-7j-A, SR-0l-7j-B, SR-0l-7j-C, SR-1l-6j-A, SR-1l-6j-B, SR-1l-6j-C

Table 5: List of analysis names referring to the experimental signatures addressed, with references to the appropriate publications; their acronyms; and all signal region names. The new analysis is denoted with (●), while the extended signal regions are denoted with (★). The details of the signal region selections for all searches listed in the table can be found in appendix B.

Model	(0+1)-lepton combination	MONOJ	0L	MULTJ	0LRaz	IL(SH)	1L(H)	2L(S)	2LRaz	2L-offZ	SS/3L	TAU	0/IL3B
pMSSM			✓										
mSUGRA/CMSSM	✓			✓			✓				✓	✓	✓
mSUGRA/CMSSM with bRPV			✓	✓		✓	✓				✓	✓	
mGMSB											✓	✓	
mGM			✓			✓						✓	
NUHMG	✓												
mUED			✓			✓		✓	✓		✓		
$\tilde{g}\tilde{g}$ production, $\tilde{q} \rightarrow q\tilde{\chi}_1^0$		✓			✓								
$\tilde{g}\tilde{g}$ production, $\tilde{g} \rightarrow q\tilde{q}\tilde{\chi}_1^0$			✓										
$\tilde{g}\tilde{g}$ production, $\tilde{q} \rightarrow q\tilde{\chi}_1^0, \tilde{g} \rightarrow q\tilde{q}\tilde{\chi}_1^0$			✓										
$\tilde{g}\tilde{g}$ production, $\tilde{g} \rightarrow \tilde{g}\tilde{\chi}_1^0$			✓										
$\tilde{g}\tilde{g}$ production, $\tilde{q} \rightarrow qW\tilde{\chi}_1^0$													
$\tilde{g}\tilde{g}$ production, $\tilde{g} \rightarrow q\tilde{q}W\tilde{\chi}_1^0$				✓							✓		
$\tilde{g}\tilde{g}$ production, $\tilde{q} \rightarrow q(\ell\ell/\ell\nu/\nu\nu)\tilde{\chi}_1^0$									✓	✓	✓		
$\tilde{g}\tilde{g}$ production, $\tilde{g} \rightarrow q\tilde{q}(\ell\ell/\ell\nu/\nu\nu)\tilde{\chi}_1^0$									✓	✓	✓		
$\tilde{g}\tilde{g}$ production, $\tilde{q} \rightarrow q(\tau\tau/\tau\nu/\nu\nu)\tilde{\chi}_1^0$												✓	
$\tilde{g}\tilde{g}$ production, $\tilde{g} \rightarrow q\tilde{q}(\tau\tau/\tau\nu/\nu\nu)\tilde{\chi}_1^0$												✓	
$\tilde{g}\tilde{g}$ production, $\tilde{g} \rightarrow qWZ\tilde{\chi}_1^0$			✓								✓		
$\tilde{g}\tilde{g}$ production, $\tilde{g} \rightarrow q\tilde{q}WZ\tilde{\chi}_1^0$				✓							✓		
$\tilde{g}\tilde{g}$ production, $\tilde{g} \rightarrow \tilde{t}\tilde{\chi}_1^0$ (off-shell stop)				✓		✓					✓		✓
$\tilde{g}\tilde{g}$ production, $\tilde{g} \rightarrow \tilde{t}_1 t, \tilde{t}_1 \rightarrow t\tilde{\chi}_1^0$				✓							✓		✓
$\tilde{g}\tilde{g}$ production, $\tilde{g} \rightarrow \tilde{t}_1 t, \tilde{t}_1 \rightarrow b\tilde{\chi}_1^+$											✓		✓
$\tilde{g}\tilde{g}$ production, $\tilde{g} \rightarrow \tilde{t}_1 t, \tilde{t}_1 \rightarrow c\tilde{\chi}_1^0$											✓		✓
$\tilde{g}\tilde{g}$ production, $\tilde{g} \rightarrow \tilde{t}_1 t, \tilde{t}_1 \rightarrow b_s$				✓							✓		
$\tilde{g}\tilde{g}$ production, $\tilde{g} \rightarrow t\tilde{b}\tilde{\chi}_1^0$													✓
$\tilde{g}\tilde{g}$ production, $\tilde{g} \rightarrow b\tilde{b}\tilde{\chi}_1^0$ (off-shell sbottom)		✓											✓
$\tilde{g}\tilde{g}$ production, $\tilde{g} \rightarrow \tilde{b}_1 b, \tilde{b}_1 \rightarrow t\tilde{\chi}_1^0$													✓

Table 6: Searches used to probe each of the phenomenological models described in section 2.1 and simplified models described in section 2.2.

Analysis acronym	Process	95% CL limit	Assumptions
0L [20]	$\tilde{g}\tilde{g}, \tilde{g} \rightarrow g\tilde{\chi}_1^0, \tilde{g} \rightarrow qq\tilde{\chi}_1^0$ $\tilde{q}\tilde{q}, \tilde{q} \rightarrow q\tilde{\chi}_1^0$ $\tilde{q}\tilde{q}, \tilde{q} \rightarrow q\tilde{\chi}_1^0$ $\tilde{g}\tilde{g}, \tilde{g} \rightarrow qqW\tilde{\chi}_1^0$ $\tilde{q}\tilde{q}, \tilde{q} \rightarrow qW\tilde{\chi}_1^0$ $\tilde{g}\tilde{g}, \tilde{g} \rightarrow \tilde{t}_1 t, \tilde{t}_1 \rightarrow c\tilde{\chi}_1^0$	$m_{\tilde{g}} > 1330$ GeV $m_{\tilde{q}} > 850$ GeV $m_{\tilde{q}} > 440$ GeV $m_{\tilde{g}} > 1100$ GeV $m_{\tilde{q}} > 700$ GeV $m_{\tilde{g}} > 1100$ GeV	$m_{\tilde{\chi}_1^0} = 0$ GeV $m_{\tilde{\chi}_1^0} = 0$ GeV, mass degenerate \tilde{q} $m_{\tilde{\chi}_1^0} = 0$ GeV, single flavour \tilde{q} $m_{\tilde{\chi}_1^0} = 0$ GeV $m_{\tilde{\chi}_1^0} = 0$ GeV $m_{\tilde{\tau}_1} = 400$ GeV, $m_{\tilde{\chi}_1^0} = m_{\tilde{\tau}_1} - 20$ GeV
MULTJ [22]	$\tilde{g}\tilde{g}, \tilde{g} \rightarrow i\tilde{u}\tilde{\chi}_1^0$ $\tilde{g}\tilde{g}, \tilde{g} \rightarrow qqW\tilde{\chi}_1^0$ $\tilde{g}\tilde{g}, \tilde{g} \rightarrow qqWZ\tilde{\chi}_1^0$	$m_{\tilde{g}} > 1100$ GeV $m_{\tilde{g}} > 1000$ GeV $m_{\tilde{g}} > 1100$ GeV	$m_{\tilde{\chi}_1^0} < 350$ GeV $m_{\tilde{\chi}_1^0} < 200$ GeV $m_{\tilde{\chi}_1^0} < 300$ GeV
1L(S,H), 2L(S), 2LRaz [23]	$\tilde{g}\tilde{g}, \tilde{g} \rightarrow qqW\tilde{\chi}_1^0$ $\tilde{q}\tilde{q}, \tilde{q} \rightarrow qW\tilde{\chi}_1^0$ $\tilde{g}\tilde{g}, \tilde{g} \rightarrow qq\ell\nu\tilde{\chi}_1^0$ $\tilde{q}\tilde{q}, \tilde{q} \rightarrow q\ell\nu\tilde{\chi}_1^0$ $\tilde{g}\tilde{g}, \tilde{g} \rightarrow \tilde{t}_1 t, \tilde{t}_1 \rightarrow c\tilde{\chi}_1^0$ $\tilde{g}\tilde{g}, \tilde{g} \rightarrow qqWZ\tilde{\chi}_1^0$	$m_{\tilde{g}} > 1200$ GeV $m_{\tilde{q}} > 700$ GeV $m_{\tilde{g}} > 1320$ GeV $m_{\tilde{q}} > 840$ GeV $m_{\tilde{g}} > 1200$ GeV $m_{\tilde{g}} > 1140$ GeV	$x = \Delta m(\chi_1^\pm, \tilde{\chi}_1^0)/\Delta m(\tilde{g}, \tilde{\chi}_1^0) = 1/2, m_{\tilde{\chi}_1^0} = 60$ GeV $x = \Delta m(\chi_1^\pm, \tilde{\chi}_1^0)/\Delta m(\tilde{q}, \tilde{\chi}_1^0) = 1/2, m_{\tilde{\chi}_1^0} < 200$ GeV $m_{\tilde{\chi}_1^0} = 100$ GeV $m_{\tilde{\chi}_1^0} = 40$ GeV $m_{\tilde{\tau}_1} = 200$ GeV, $m_{\tilde{\chi}_1^0} = m_{\tilde{\tau}_1} - 20$ GeV $m_{\tilde{\chi}_1^0} < 200$ GeV
2L-offZ [24]	$\tilde{g}\tilde{g}, \tilde{g} \rightarrow qq(\ell\ell/\ell\nu/\nu\nu)\tilde{\chi}_1^0$ $\tilde{q}\tilde{q}, \tilde{q} \rightarrow q(\ell\ell/\ell\nu/\nu\nu)\tilde{\chi}_1^0$	$m_{\tilde{g}} > 1170$ GeV $m_{\tilde{q}} > 780$ GeV	$m_{\tilde{\chi}_1^0} = 50$ GeV $m_{\tilde{\chi}_1^0} = 50$ GeV
SS/3L [25]	$\tilde{g}\tilde{g}, \tilde{g} \rightarrow i\tilde{u}\tilde{\chi}_1^0$ $\tilde{g}\tilde{g}, \tilde{g} \rightarrow \tilde{t}_1 t, \tilde{t}_1 \rightarrow sb$ $\tilde{g}\tilde{g}, \tilde{g} \rightarrow qqW\tilde{\chi}_1^0$ $\tilde{g}\tilde{g}, \tilde{g} \rightarrow qqWZ\tilde{\chi}_1^0$ $\tilde{q}\tilde{q}, \tilde{q} \rightarrow qWZ\tilde{\chi}_1^0$ $\tilde{g}\tilde{g}, \tilde{g} \rightarrow qq(\ell\ell/\ell\nu/\nu\nu)\tilde{\chi}_1^0$ $\tilde{q}\tilde{q}, \tilde{q} \rightarrow q(\ell\ell/\ell\nu/\nu\nu)\tilde{\chi}_1^0$	$m_{\tilde{g}} > 950$ GeV $m_{\tilde{g}} > 850$ GeV $m_{\tilde{g}} > 860$ GeV $m_{\tilde{g}} > 1040$ GeV $m_{\tilde{q}} > 670$ GeV $m_{\tilde{g}} > 1200$ GeV $m_{\tilde{q}} > 780$ GeV	$m_{\tilde{\chi}_1^0} < 400$ GeV $m_{\tilde{\chi}_1^0} < 520$ GeV $m_{\tilde{\chi}_1^0} < 300$ GeV $m_{\tilde{\chi}_1^0} < 660$ GeV $m_{\tilde{\chi}_1^0} < 460$ GeV
TAU[26]	$\tilde{g}\tilde{g}, \tilde{g} \rightarrow qq(\tau\tau/\tau\nu/\nu\nu)\tilde{\chi}_1^0$	$m_{\tilde{g}} > 1090$ GeV	nGM model, $\tilde{\tau}$ is NLSP
0/1L3B [27]	$\tilde{g}\tilde{g}, \tilde{g} \rightarrow i\tilde{u}\tilde{\chi}_1^0$	$m_{\tilde{g}} > 1340$ GeV	$m_{\tilde{\chi}_1^0} < 400$ GeV

Table 7: The 95% CL exclusion limits obtained in published ATLAS searches listed in table 5 for the indicated processes and related assumptions. A dedicated search for $\tilde{c}\tilde{c}$ pair production [144] excludes charm squark masses up to 490 GeV for $m_{\tilde{\chi}_1^0} < 200$ GeV (95% CL).

7.1. Final states with high- p_T jets, missing transverse momentum and no electrons or muons

Several searches to address final states without electrons or muons, containing high- p_T jets and missing transverse momentum, have been performed in ATLAS. These searches are split according to the jet multiplicity into three categories: searches with at least one, two to six and seven to ten jets. They are presented in table 5 as Monojet, 0-lepton + 2–6 jets + E_T^{miss} (extended with two additional signal regions) and 0-lepton + 7–10 jets + E_T^{miss} , respectively. Events with reconstructed electrons or muons are vetoed in these searches. A new search using kinematic variables, known as Razor variables [19], which provide longitudinal and transverse information about each event (listed as 0-lepton Razor in table 5), has also been performed and is included in the results presented in this paper.

The monojet (MONOJ) analysis, originally designed to search for direct production of top squarks (\tilde{t}), each decaying into a charm quark and a neutralino ($\tilde{\chi}_1^0$) [21], targets final states characterized by at least one high- p_T jet (with $p_T > 150$ GeV and $|\eta| < 2.8$) and large missing transverse momentum. Signal regions have been specifically optimized for models with a very small mass difference (≤ 20 GeV) between the top squark and the neutralino. The event selection makes use of the presence of initial-state radiation (ISR) jets to identify signal events, and the squark-pair system is boosted, leading to large E_T^{miss} . Three signal regions which are based only on different selection criteria related to the jet p_T and E_T^{miss} have been used to bring additional sensitivity to models with very small mass differences between SUSY particles. These signal regions do not impose any criteria to specifically select events originating from the top squarks and as such they can be used to select events in which squarks are produced in pairs and decay directly via $\tilde{q} \rightarrow q\tilde{\chi}_1^0$ with a small $\tilde{q}-\tilde{\chi}_1^0$ mass difference.

The 0-lepton + 2–6 jets + E_T^{miss} (0L) search [20] targets final states where each initial squark yields one jet and E_T^{miss} and each initial gluino yields two jets and E_T^{miss} . Additional decay modes can include the production of charginos via $\tilde{q} \rightarrow q\tilde{\chi}_1^\pm$ and $\tilde{g} \rightarrow q\tilde{q}\tilde{\chi}_1^\pm$, where the subsequent decay of these charginos to a W boson and $\tilde{\chi}_1^0$ can lead to final states with larger jet multiplicity. The search strategy is optimized for various squark and gluino masses, for a range of models. Fifteen inclusive signal regions are characterized by increasing the minimum jet-multiplicity from two to six (for jets with $p_T > 40$ GeV and $|\eta| < 2.8$), and are based on different selection criteria on the effective mass $m_{\text{eff}}^{\text{incl}}$, defined as the scalar sum of E_T^{miss} and the p_T of the jets; the ratio of $E_T^{\text{miss}}/m_{\text{eff}}^{N_j}$, where $m_{\text{eff}}^{N_j}$ is m_{eff} constructed from only the leading N_j jets; and the minimum azimuthal angle between jets and E_T^{miss} . Two of the signal regions are designed to improve sensitivity to models with the cascade \tilde{q} or \tilde{g} decay via $\tilde{\chi}_1^\pm$ to W and $\tilde{\chi}_1^0$, in cases where the $\tilde{\chi}_1^\pm$ is nearly degenerate in mass with the \tilde{q} or \tilde{g} . These signal regions place additional requirements on the invariant masses $m(W_{\text{cand}})$ of the candidate W bosons reconstructed from a single high-mass jet, or from a pair of jets.

Following the same analysis strategy, two additional signal regions are included in this paper, which are optimized to increase the sensitivity of the 0L search for left-handed squarks within the pMSSM model described in section 2. These two signal regions target the two one-step decays of \tilde{q}_L , $\tilde{q}_L \rightarrow q\tilde{\chi}_1^\pm \rightarrow qW^\pm\tilde{\chi}_1^0$ and $\tilde{q}_L \rightarrow q\tilde{\chi}_2^0 \rightarrow q(Z/h)\tilde{\chi}_1^0$ and are obtained by optimizing on two variables, $E_T^{\text{miss}}/m_{\text{eff}}^{N_j}$ and $m_{\text{eff}}^{\text{incl}}$, in the channels with at least four or at least five jets. All other selection criteria are exactly the same as for the corresponding channels described in the original publication. The two new signal regions, named 4jt+ and 5jt following the naming convention from ref. [20], are summarized in table 8.

Signal region name	0L_4jt+	0L_5jt
Number of jets \geq	4	5
$E_T^{\text{miss}}/m_{\text{eff}}^{N_j} \geq$	0.30	0.15
$m_{\text{eff}}^{\text{incl}} [\text{GeV}] \geq$	2200	1900

Table 8: Additional 0L signal regions optimized to increase the sensitivity of the search for left-handed squarks within the pMSSM.

A high jet multiplicity is expected from the decays of gluino pairs via a top squark, or via squarks involving the production of $\tilde{\chi}^\pm$ and $\tilde{\chi}_2^0$ in their decay chain, and is the main topology targeted by the 0-lepton + 7–10 jets + E_T^{miss} (MULTJ) analysis [22]. The sensitivity of the search is enhanced by the subdivision into two categories. First, in the multi-jet+flavour stream, an event classification based on the number of jets ($p_T > 50$ GeV and $|\eta| < 2$) and number of b -jets ($p_T > 40$ GeV and $|\eta| < 2.5$) gives enhanced sensitivity to models which predict either more or fewer b -jets than the SM background. In the second category (multi-jet+ M_J^Σ stream), which targets models with large numbers of objects in the final state, the jets reconstructed with the jet radius parameter $R = 0.4$ are reclustered into large composite jets using the anti- k_r algorithm with $R = 1.0$. The event variable M_J^Σ is computed as the sum of the masses of the composite jets: $M_J^\Sigma \equiv \sum_j m_j^{R=1.0}$, where the composite jets satisfy $p_T^{R=1.0} > 100$ GeV and $|\eta^{R=1.0}| < 1.5$. In total, nineteen signal regions are defined, based on different selection criteria on the total number of jets, number of b -jets, $E_T^{\text{miss}}/\sqrt{H_T}$ (where H_T is the scalar sum of the p_T of all jets) and on the event variable M_J^Σ .

The Razor variable set is designed to group together visible final-state particles associated with heavy produced sparticles, and in doing so contains information about the mass scale of those sparticles. The events are selected using a combination of E_T^{miss} triggers which are fully efficient for the event selections considered in this search. The new 0-lepton Razor (OLRaz) analysis presented here selects events with at least two high- p_T jets and E_T^{miss} . The baseline object selection and event cleaning, as well as the choice of MC generators for SM background processes and the approach for calculating systematic uncertainties exactly follow those of the 0L search [20]. Two signal regions are identified by optimizing criteria on the Razor variables to give the best expected sensitivity in the model with squark pair production followed by the direct decay of the squarks. One signal region, SR_{loose}, targets models with small mass splittings which typically have softer visible objects, while the other signal region, SR_{tight}, is designed to target models with high squark masses which typically contain harder visible objects. Appendix C describes in detail the construction of the event variables, optimization strategy for these signal regions and corresponding control and validation regions, explicitly showing the distributions of the variables used for the selection, and the impact of the selection on the expected SM background and signal yields. An overview of the selection criteria for the two signal regions used in this search is given in table 9.

	0LRaz_SR_{loose}	0LRaz_SR_{tight}
E_T^{miss} [GeV] >	160	
$p_T^{\text{jet}_{1,2}}$ [GeV] >	150	200
$\Delta\phi(\text{jet}_{1,2}, E_T^{\text{miss}})$ >	0.4	1.4
R >	0.5	0.6
M'_R [GeV] >	700	900

Table 9: Overview of the selection criteria for the two signal regions used by the 0LRaz analysis. The 0LRaz_SR_{tight} targets high masses of the heavy produced sparticle, and the 0LRaz_SR_{loose} targets small mass splittings between the heavy produced sparticle and the LSP. Details of the construction of Razor variables M'_R and R can be found in appendix C.1.

7.2. Final states with high- p_T jets, missing transverse momentum and at least one electron or muon

Three types of searches addressing decays of squarks and gluinos in events containing electrons or muons, jets and missing transverse momentum are summarized here: searches with at least one isolated lepton, which have been extended with an additional signal region with high jet multiplicity, a search with two same-flavour opposite-sign leptons inconsistent with Z boson decay (off- Z search), and searches in final states with a same-sign lepton pair or at least three leptons.

The 1-lepton (soft+hard)/2-leptons + jets + E_T^{miss} (1L(S,H), 2L(S), 2LRaz) searches [23] require the presence of at least one isolated lepton (electron or muon) in the decay chains of strongly produced squarks or gluinos. Different categories of events are defined in order to cover a broad parameter space: first the events are separated by different requirements on the transverse momentum of the leptons, either using an electron or muon with $p_T > 25$ GeV in the hard lepton selection, or an electron (muon) with $p_T > 7$ (6) GeV in the soft lepton selection. Each of these selections is further subdivided into a single-lepton and a dilepton search channel. The soft and hard lepton channels are designed to be complementary, and are more sensitive to supersymmetric spectra with small or large mass splittings, respectively, while the different lepton multiplicities cover different production and decay modes. To enhance the sensitivity to gluino or squark production, high and low jet multiplicity signal regions, respectively, are defined. The single-lepton channels (1L(S,H)) use a statistically independent set of events, compared to the 0L search, allowing the statistical combination of the two searches in the models for which it is relevant. The hard dilepton channel (2LRaz) targets gluino and first- and second-generation squark production, as well as mUED searches. This channel uses a Razor variable set and is not designed to search for signal events in which a real Z boson is present. In all search channels except the soft dimuon channel (2L(S)), two separate selections are performed for each jet multiplicity: one single-bin signal region optimized for discovery reach, which is also used to place limits on the visible cross-section, and one signal region which is binned in an appropriate variable in order to exploit the expected shape of the distribution of signal events when placing model-dependent limits.

An additional signal region with one hard lepton (electron or muon), high jet multiplicity and E_T^{miss} , referred to as 1L(H)_7-jet in table 5, is considered in this paper. The selection is based on looser missing transverse momentum selection criteria compared to the value used in ref. [23] together with the requirement for high jet multiplicity, which is suggested in refs. [145, 146] in the search for natural SUSY. The 1L(H)_7-jet signal region selection follows the concepts of the 1L(H) analysis [23], only modifying the criteria for the signal, validation and control regions to take into account a selection of events with at

least seven jets in the final state. Due to these changes, a re-evaluation of the systematic uncertainties, in particular of the theoretical uncertainties on the background, is also performed. The selection criteria are summarized in table 10.

The 2-leptons off-Z (2L-offZ) search [24] targets events where the final state same-flavour opposite-sign leptons originate from the decay $\tilde{\chi}_2^0 \rightarrow \ell^+ \ell^- \tilde{\chi}_1^0$, where $\tilde{\chi}_2^0$ is produced in the decays of squarks and gluinos, e.g. $\tilde{q} \rightarrow q \tilde{\chi}_2^0$ and $\tilde{g} \rightarrow qq \tilde{\chi}_2^0$. Compared to the decay $Z \rightarrow \ell^+ \ell^-$, which leads to a peak in the $m_{\ell\ell}$ distribution around the Z boson mass, the decay $\tilde{\chi}_2^0 \rightarrow \ell^+ \ell^- \tilde{\chi}_1^0$ leads to a rising distribution in $m_{\ell\ell}$ that terminates at an endpoint (“edge”) [147] because events with larger $m_{\ell\ell}$ values are kinematically forbidden. Four signal regions are defined by requirements on jet multiplicity, b -tagged jet multiplicity and E_T^{miss} . The selection criteria are optimized for the simplified models of pair-produced squarks or gluinos followed by their two-step decays with sleptons, described in section 2.2.2. The signal regions with a b -jet veto provide the best sensitivity in the two-step simplified models considered here, since the signal b -jet content is lower than that of the dominant $t\bar{t}$ background. Signal regions with a requirement of at least one b -tagged jet target other signal models not explicitly considered here, such as those with bottom squarks that are lighter than the other squark flavours. One signal region with similar requirements to those used by the CMS experiment in a comparable search [148] which reported an excess of events above the SM background with a significance of 2.6 standard deviations, is also used for comparison purposes. No evidence for an excess is observed in this region.

Another leptonic search channel [25] is used for an analysis of final states with multiple jets, and either two leptons of the same electric charge or at least three leptons (SS/3L). The motivation for searches using these final states is that pair-produced gluinos have the same probability to decay to pairs of leptons with the same charge as with opposite charge. Squark production (directly in pairs or through $\tilde{g}\tilde{g}$ or $\tilde{g}\tilde{q}$ production with subsequent $\tilde{g} \rightarrow q\tilde{q}$ decay) can also lead to same-sign lepton or three-lepton signatures when the squarks decay in cascades involving top quarks, charginos, neutralinos or sleptons. Requiring a pair of leptons with the same electric charge largely suppresses the background coming from the SM processes, giving a very clean and powerful signature to search for new physics processes. It also allows the use of relatively loose kinematic requirements on E_T^{miss} , increasing the sensitivity to scenarios with small mass differences between SUSY particles or with R-parity violation. Five statistically independent signal regions are defined: two signal regions requiring same-sign leptons and b -jets (optimized for gluino decays via top squarks), a complementary signal region requiring a b -jet veto (optimized for the gluino decays via first- and second-generation squarks), and two signal regions requiring three leptons (designed for scenarios characterized by multi-step decays).

7.3. Final states with high- p_T jets, missing transverse momentum and at least one hadronically decaying tau lepton

A search for squarks and gluinos in events with large missing transverse momentum, jets and at least one hadronically decaying tau lepton [26] is motivated by naturalness arguments [149, 150], and by the assumption that light sleptons could play a role in the co-annihilation with neutralinos in the early universe [151]. In particular, models with light tau sleptons are consistent with dark-matter searches [152]. Four distinct topologies are studied in order to optimize the tau + jets + E_T^{miss} (TAU) search for various models: one hadronically decaying tau (1τ) or two or more hadronically decaying taus (2τ) in the final state with no additional light leptons (e/μ) and one or more tau leptons with exactly one lepton (one electron ($\tau + e$) or muon ($\tau + \mu$)). The different topologies (1τ , 2τ and $\tau + \ell$, where ℓ is electron or muon) have been optimized separately, and, where relevant, are statistically combined to increase the analysis sensitivity.

	1L(H)_7-jet	1L(H)_WR_7-jet	1L(H)_TR_7-jet	1L(H)_VR_7-jet E_T^{miss}	1L(H)_VR_7-jet m_T
N_{lep}			== 1		
$p_T^{l_1}$ [GeV]			> 25 (20)		
$p_T^{l_2}$ [GeV]			< 10		
N_{jet}			≥ 7		
p_T^{jet} [GeV]			> 80, 25, 25, 25, 25, 25, 25		
$N_{b\text{-tag}}$	-	== 0	≥ 1	-	-
E_T^{miss} [GeV]	> 180	$\in [100, 180]$	$\in [100, 180]$	$\in [180, 500]$	$\in [100, 180]$
m_T [GeV]	> 120	$\in [40, 80]$	$\in [40, 120]$	$\in [60, 120]$	$\in [120, 320]$
$m_{\text{eff}}^{\text{incl}}$ [GeV]			> 750		

Table 10: Overview of the selection criteria for the 1L(H) + 7 jets + E_T^{miss} analysis, for the signal region (1L(H)_7-jet), W +jets and semileptonic $t\bar{t}$ control regions (1L(H)_WR_7-jet and 1L(H)_TR_7-jet respectively) and two validation regions used to cross-check the background estimates (1L(H)_VR_7-jet E_T^{miss} and 1L(H)_VR_7-jet m_T). The p_T selections for leptons are given for electrons (muons).

The same signal regions are used for additional model interpretations, not presented in ref. [26]. These are simplified models of squark- or gluino-pair production where the squark or gluino undergoes a two-step cascade decay via sleptons, as shown in figures 5(a) and 5(c), where the sleptons are assumed to be exclusively staus, since the first two generations of sleptons and sneutrinos are kinematically decoupled.

7.4. Final states with many b -jets and missing transverse momentum

A search requiring at least three b -jets [27] is one of the most sensitive searches to various SUSY models favoured by naturalness arguments, where top or bottom quarks are produced in the gluino decay chains. The search is carried out in statistically independent zero- and one-lepton channels (0/1L3B) which are combined to maximize the sensitivity. Three sets of signal regions, two for the zero-lepton channel and one for the one-lepton channel, are defined to enhance the sensitivity to the various models considered. They are characterized by having relatively hard E_T^{miss} requirements and at least four, six or seven jets, amongst which at least three are required to be b -jets. Signal regions with zero leptons and at least four jets target SUSY models with sbottoms in the decay chain, while the one-lepton and the zero-lepton signal regions with at least six or seven jets aim to probe SUSY models where top-quark-enriched final states are expected.

8. Systematic uncertainties

Systematic uncertainties on background estimates in all searches included in this paper arise from the use of transfer factors which relate observations in the control regions to background expectations in the signal regions, and from the MC modelling of minor backgrounds. Since CRs are designed to be kinematically as close as possible to the SRs, many sources of systematic uncertainty largely cancel. In searches which include leptons in the final state, systematic uncertainties also impact the estimation of jets misidentified as leptons or of non-prompt leptons. The full details of all sources of systematic uncertainty and their impact on background predictions for each search included in this paper can be found in the corresponding original publication. Only the dominant uncertainties on the background estimations, common to all searches, are mentioned here.

Since at least one high- p_T jet and significant missing transverse momentum are present in all searches summarized in this paper, the primary common sources of systematic uncertainty for the SM backgrounds estimated with transfer factors derived from MC simulation are the JES and the jet energy resolution (JER). The theoretical modelling of background processes and the limited number of data events in the CRs and in the MC simulation are also typically important.

The JES uncertainty is estimated from a combination of simulation, test beam data and in-situ measurements [127, 153], and depends on the p_T and η of the jet. Additional contributions accounting for the jet-flavour composition, the calorimeter response to different jet flavours, pile-up and b -jet calibration uncertainties are also taken into account. Uncertainties on the JER are obtained with an in-situ measurement [154] of the jet transverse momentum balance in dijet events. Uncertainties in jet measurements are propagated to the E_T^{miss} , and additional subdominant uncertainties on E_T^{miss} arising from the contribution from energy deposits not associated with reconstructed objects are also included. In signal regions designed for searches based on large jet multiplicities these uncertainties can be as large as 30% of the estimated background yield in the SRs.

Searches requiring the presence of tau leptons in the final state are subject to additional systematic uncertainties from the tau energy scale [139] and the tau lepton identification [138]. The uncertainties from the jet and tau energy scales are the largest experimental uncertainties in these searches, being as large as 13% and 8% of the estimated background yield respectively, and are treated as uncorrelated, since the calibration methods differ.

In searches that require the presence of b -jets in the final state, the uncertainty associated with flavour-tagging efficiencies is evaluated by varying the p_T - and flavour-dependent correction factors applied to each jet in the simulation within a range that reflects the systematic uncertainty on the measured tagging efficiencies and mistag rates. This uncertainty varies between 10% and 16% in the different SRs requiring at least three b -jets in the final state.

Uncertainties arising from the theoretical modelling of background processes are typically evaluated by comparing the estimates to those obtained with different MC generators. The uncertainty due to the factorization and renormalization scales is computed by varying these scales up and down by a factor of two with respect to the nominal setting. Uncertainties from PDFs are computed following the PDF4LHC recommendations [155]. These uncertainties vary across the different searches and in some signal regions are the dominant source of systematic uncertainties.

The same sources of experimental uncertainty apply to the signal acceptance. Several theoretical uncertainties on the acceptance for the various signal models are taken into account. These uncertainties are estimated using the MADGRAPH5+PYTHIA6 samples by varying the following parameters up and down by a factor of two: the MADGRAPH scale used to determine the event-by-event renormalization and factorization scale, the parameters used to determine the scales for initial- and final-state QCD radiation and the parameters used for jet matching. The uncertainty on the modelling of initial-state radiation plays an important role in simplified models with small mass differences in the decay cascade, and is as large as 20–30% in such regions. For all models, except the mUED model, the NLO+NLL cross-section uncertainty is taken from an envelope of cross-section predictions using different PDF sets and factorization and renormalization scales, as described in ref. [114]. The mUED model cross-sections are based on a calculation at LO in QCD, and the events are generated with a leading-order MC event generator. No theoretical uncertainties on the acceptance are considered for this case.

The overall background uncertainties for the two new signal regions defined in the 0LRaz search are estimated to be 6% in the 0LRaz_SR_{loose} signal region and 9% in the 0LRaz_SR_{tight} signal region. These uncertainties are dominated by the modelling of the Z +jets process and by the uncertainties on diboson production due to renormalization and factorization scales and PDF uncertainties for which a conservative uniform 50% uncertainty is applied. In the additional signal region for the 1-lepton (hard) + jets + E_T^{miss} analysis, 1L(H)_7-jet, the overall background uncertainty is estimated to be 35%, and it is dominated by the modelling of the $t\bar{t}$ process in the events with high jet multiplicity. The estimated background uncertainties in the two additional signal regions for the 0-lepton + 2–6 jets + E_T^{miss} analysis, 0L_4jt+ and 0L_5jt, are consistent with the uncertainties obtained for the two closest signal regions (4jt and 5j) from the original publication [20].

9. Results for the new signal regions

The number of events observed in the data and expected from SM processes are shown for all new signal regions in tables 11, 12 and 13. Table 11 summarizes the results for the two additional signal regions

for the 0L analysis. Table 12 displays the equivalent results for the two signal regions of the new 0LRaz analysis, and those for the additional region of the 1L(H) analysis are shown in table 13. All results are determined using the background-only fit. The pre-fit background expectations are also shown in the tables, for comparison purposes. The prediction of the W/Z +jets background processes by the simulation prior to the fit is found to be overestimated in the phase space of interest and is consequently decreased by the fit. This is consistent with the behaviour observed in previous publications probing a similar phase space [20]. In all new signal regions presented in this paper the number of events observed is consistent with the post-fit SM expectations. The observed and expected upper limits at 95% CL on the number of BSM events (S_{obs}^{95} and S_{exp}^{95}), together with the upper limits on the visible cross-section of BSM physics ($\langle\epsilon\sigma\rangle_{\text{obs}}^{95}$) and the p -value for the background-only hypothesis, are also presented in the tables 11–13. The confidence levels are calculated with the CL_S prescription [143]. For an observed number of events lower than expected, the p -value is truncated at 0.5.

Signal region	0L_4jt+	0L_5jt
Expected background events before the fit		
$t\bar{t}$ (+ V) + single top	0.37	2.9
W +jets	0.75	4.5
Z/γ^* +jets	2.1	4.8
Diboson	–	0.32
Fitted background events		
$t\bar{t}$ (+ V) + single top	0.39 ± 0.32	3.0 ± 1.8
W +jets	0.55 ± 0.33	2.0 ± 1.5
Z/γ^* +jets	$0.10^{+0.17}_{-0.10}$	1.7 ± 0.9
Diboson	–	0.32 ± 0.16
Multi-jet	–	$0.58^{+0.73}_{-0.58}$
Total background	1.04 ± 0.43	7.6 ± 1.9
Observed events	0	8
$\langle\epsilon\sigma\rangle_{\text{obs}}^{95}$ [fb]	0.17	0.40
S_{obs}^{95}	3.4	8.2
S_{exp}^{95}	$3.5^{+1.3}_{-0.5}$	$7.5^{+3.1}_{-2.0}$
$p(s = 0)$	0.50	0.35

Table 11: The background expectations before the fit and the background fit results for the new 0L signal regions. Negligible contributions are marked as ‘–’. The uncertainties shown combine the statistical uncertainties on the event samples with the systematic uncertainties. Also shown are the 95% CL upper limits on the visible cross-section ($\langle\epsilon\sigma\rangle_{\text{obs}}^{95}$) and on the number of signal events (S_{obs}^{95}). The expected upper limit on the number of signal events (S_{exp}^{95}) is calculated from the expected number of background events after fit, with uncertainties indicating the $\pm 1\sigma$ deviations from the expectation. The p -value ($p(s = 0)$) is also presented in the table.

Signal region	0LRaz_SR_{loose}	0LRaz_SR_{tight}
Expected background events before the fit		
$t\bar{t}$	138	1.8
Single top	23.9	1.6
$t\bar{t} + V$	4.7	0.2
W+jets	794	49
Z+jets	762	58
Diboson	112	10
Fitted background events		
$t\bar{t}$	117 ± 22	1.7 ± 0.5
Single top	24.9 ± 2.6	1.8 ± 0.3
$t\bar{t} + V$	3.7 ± 1.0	0.20 ± 0.07
W+jets	454 ± 40	27.0 ± 3.0
Z+jets	618 ± 76	45 ± 6
Diboson	94 ± 49	10 ± 5
Multi-jet	14 ± 13	2.4 ± 2.4
Total background	1326 ± 84	88 ± 8
Observed events	1322	74
$\langle \epsilon\sigma \rangle_{\text{obs}}^{95}$ [fb]	6.17	0.83
S_{obs}^{95}	125.3	16.8
S_{exp}^{95}	$135.1^{+64.8}_{-42.2}$	$24.3^{+9.9}_{-6.9}$
$p(s = 0)$	0.49	0.50

Table 12: The background expectations before the fit and the background fit results for the 0LRaz analysis. Negligible contributions are marked as ‘-’. The uncertainties shown combine the statistical uncertainties on the event samples with the systematic uncertainties. Also shown are the 95% CL upper limits on the visible cross-section ($\langle \epsilon\sigma \rangle_{\text{obs}}^{95}$) and on the number of signal events (S_{obs}^{95}). The expected upper limit on the number of signal events (S_{exp}^{95}) is calculated from the expected number of background events after fit, with uncertainties indicating the $\pm 1\sigma$ deviations from the expectation. The p -value ($p(s = 0)$) is also presented in the table.

Signal region	1L(H)_7-jet
Expected background events before the fit	
$t\bar{t}$	81
Single top	3.4
$t\bar{t} + V$	2.8
W+jets	11
Z+jets	0.59
Diboson	2.7
Fitted background events	
$t\bar{t}$	56 ± 27
Single top	3.4 ± 2.2
$t\bar{t} + V$	2.8 ± 1.0
W+jets	8 ± 4
Z+jets	0.59 ± 0.17
Diboson	2.7 ± 1.5
Multi-jet	2.4 ± 2.3
Total background	76 ± 27
Observed events	68
$\langle \epsilon\sigma \rangle_{\text{obs}}^{95} [\text{fb}]$	2.06
S_{obs}^{95}	41.9
S_{exp}^{95}	45^{+12}_{-10}
$p(s = 0)$	0.5

Table 13: The background expectations before the fit and the background fit results for the new 1L(H) signal region. An overview of the selection criteria for the signal, validation and control regions used in this analysis is given in table 10. The uncertainties shown combine the statistical uncertainties on the event samples with the systematic uncertainties. Also shown are the 95% CL upper limits on the visible cross-section ($\langle \epsilon\sigma \rangle_{\text{obs}}^{95}$) and on the number of signal events (S_{obs}^{95}). The expected upper limit on the number of signal events (S_{exp}^{95}) is calculated from the expected number of background events after fit, with uncertainties indicating the $\pm 1\sigma$ deviations from the expectation. The p -value ($p(s = 0)$) is also presented in the table.

10. Combination strategy

Statistical combinations of the analyses, as listed in table 6, are performed in order to increase the exclusion reach in several SUSY models in which at least two analyses designed to be statistically independent in their signal and control region definitions provide comparable sensitivities. The conditions are satisfied for a combination of the 1L(S,H) and 0L searches. These analyses search for squarks and gluinos in final states containing jets and missing transverse momentum, either with at least one isolated electron or muon (1L(S,H)), or applying an explicit veto on events containing electrons or muons (0L). They are statistically independent due to a veto on any electron or muon with $p_{\text{T}} > 10$ GeV in the case of the 0L search, and requiring an electron or muon with $p_{\text{T}}(e/\mu) > 25$ GeV (hard single-lepton) or $p_{\text{T}}(e/\mu) > 7/6$ GeV (soft single-lepton) in the case of the 1L(S,H) search. It has been checked explicitly that the difference in lepton- p_{T} thresholds in the 0L and soft single-lepton analyses does not result in events selected by both analyses. The control regions used to estimate contributions from W+jets and top backgrounds used by the 0L search have been slightly modified with respect to the original regions [20] such that events

which are selected by the respective control regions in the 1L(S,H) analyses are vetoed. This modification ensures complete statistical independence of the three analyses, which can therefore be combined where relevant.

The statistical combination is obtained from the individual likelihoods of the analyses involved. In the case of the 0L analysis the likelihood for the signal region that provides the best expected CL_S value for the signal model considered, and its corresponding control regions, is chosen. The choice of this signal region can vary as a function of sparticle masses. For the 1L(S,H) analyses, all the available signal regions are statistically independent and hence a single likelihood that describes all of them serves as input for the combination procedure. Some of the systematic uncertainties can be correlated when building the combined likelihood. The correlated uncertainties in the combination procedure are the luminosity uncertainty, the uncertainty on the SUSY cross-sections, b -tagging uncertainties, and the jet energy resolution and E_T^{miss} -related uncertainties. Other systematic uncertainties, such as theoretical uncertainties, are not correlated, e.g. the uncertainties due to different Monte Carlo generators used in the analyses considered. The jet energy scale uncertainty, which is subdominant, is not correlated due to the use of different prescriptions in the analyses involved. The combination of the analyses was carefully validated by ensuring that the combined likelihood did not lead to artificial correlations between fit parameters or major changes in post-fit values of nuisance parameters with respect to the individual analysis fits discussed in refs. [20, 23].

Figures 9 and 10 show the result of the combination of the 1L(S,H) and 0L analyses for both squark-pair and gluino-pair production for the one-step decays of squarks and gluinos described in section 2.2.2. The limits obtained improve the results of the separate analyses, reaching higher $\tilde{\chi}_1^0$ mass and approximately 50 GeV higher squark or gluino mass for massless neutralinos. The combined limit also approaches the diagonal $m(\tilde{\chi}_1^0) = m(\tilde{q}, \tilde{g})$ closer than the individual analyses.

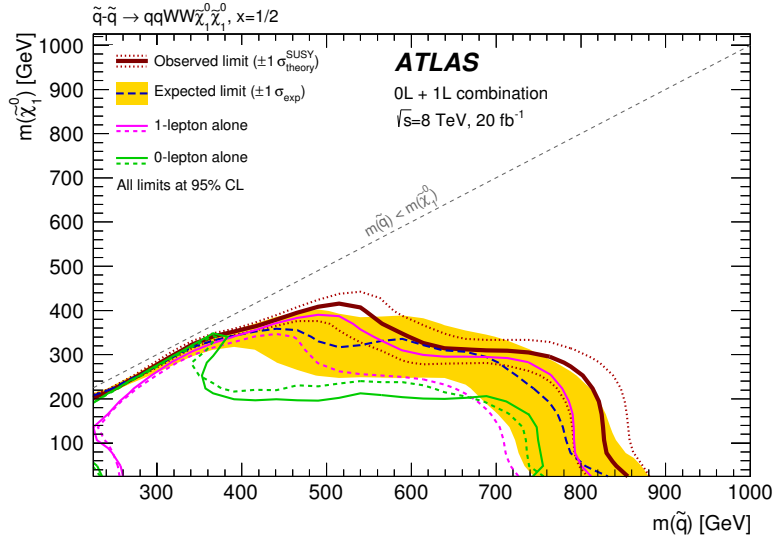


Figure 9: Observed and expected exclusion limits for simplified models of squark-pair production with one-step decays via the $\tilde{\chi}_1^\pm$ into a W boson and the $\tilde{\chi}_1^0$. The mass of the $\tilde{\chi}_1^\pm$ is chosen to be between the $m_{\tilde{q}}$ and $m_{\tilde{\chi}_1^0}$ and is determined by $x = (m_{\tilde{\chi}_1^\pm} - m_{\tilde{\chi}_1^0}) / (m_{\tilde{q}} - m_{\tilde{\chi}_1^0}) = 1/2$. Squark and neutralino masses in the area below the observed limit are excluded at 95% CL. The yellow band includes all experimental uncertainties; the red dotted lines indicate the theory uncertainty on the cross-section. The individual limits from the 0L and the 1L(S,H) analyses are overlaid in green and magenta, respectively.

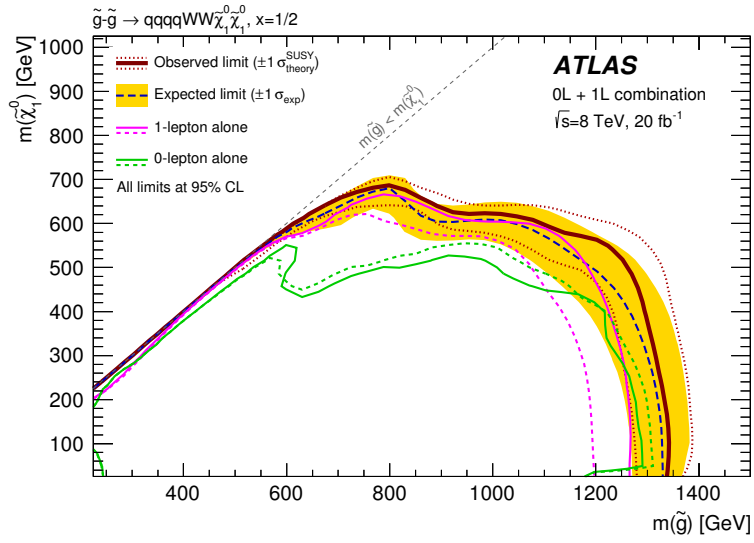


Figure 10: Observed and expected exclusion limits for simplified models of gluino-pair production with decays via the $\tilde{\chi}_1^\pm$ into a W boson and the $\tilde{\chi}_1^0$. The mass of the $\tilde{\chi}_1^\pm$ is chosen to be between the $m_{\tilde{g}}$ and $m_{\tilde{\chi}_1^0}$ and is determined by $x = (m_{\tilde{\chi}_1^\pm} - m_{\tilde{\chi}_1^0}) / (m_{\tilde{g}} - m_{\tilde{\chi}_1^0}) = 1/2$. Gluino and neutralino masses in the area below the observed limit are excluded at 95% CL. The yellow band includes all experimental uncertainties; the red dotted lines indicate the theory uncertainty on the cross-section. The individual limits from the 0L and the 1L(S,H) analyses are overlaid in green and magenta, respectively.

11. Limits in SUSY models

This section summarizes the exclusion limits placed in the various phenomenological and simplified models described in section 2 (there is a one-to-one correspondence between the subsections of section 2 and this section). The analyses and corresponding signal regions are referred to by their acronyms defined in table 5. An overview of all searches used to probe the phenomenological models described in section 2.1 and the simplified models described in section 2.2 is given in table 6. A limit obtained from the statistical combination of 1L(S,H) and 0L analyses is presented for models for which both analyses have comparable sensitivity and is used as a single contribution to the final combined limit. The final combined observed and expected 95% CL exclusion limits are obtained from the signal regions belonging to the contributing analyses that provide the best expected CL_S value. Expected limits from the individual analyses which contribute to the final combined limits are also presented for comparison. The $\pm 1\sigma_{\text{theory}}^{\text{SUSY}}$ lines around the observed limits in the figures are obtained by changing the signal cross-section by one standard deviation ($\pm 1\sigma$), as described in section 8. All mass limits on supersymmetric particles quoted later in this section are derived from the $-1\sigma_{\text{theory}}^{\text{SUSY}}$ line.

11.1. Limits in phenomenological models

This section summarizes the exclusion limits placed on the phenomenological models described in section 2.1.

11.1.1. A phenomenological MSSM model

The measurements are interpreted in a phenomenological MSSM model, which possesses three parameters: $m_{\tilde{q}_L}$, M_1 and M_2 , where M_1 and M_2 are the masses associated with the bino and wino fields. For the exclusion limits in figure 11 either M_1 is fixed to 60 GeV and M_2 is varied independently, or M_1 is varied and M_2 is set to $M_2 = (M_1 + m_{\tilde{q}_L})/2$. The figures show limits in the $(m_{\tilde{q}}, m_{\tilde{\chi}_1^\pm, \tilde{\chi}_2^0})$ and $(m_{\tilde{q}}, m_{\tilde{\chi}_1^0})$ planes, for various gluino masses, as obtained from the 0L analysis with the additional 0L_4jt+ and 0L_5jt signal regions optimized specifically for this model. As expected, for the relatively light gluino mass of 1600 GeV, a large range of squark masses (up to 1500 GeV) and $\tilde{\chi}_1^\pm/\tilde{\chi}_2^0$ masses (up to 1150 GeV) can be excluded. The exclusion reach decreases with increasing gluino mass.

11.1.2. Minimal Supergravity/Constrained MSSM and bilinear R-parity-violation models

The exclusion limits in the $(m_0, m_{1/2})$ mSUGRA/CMSSM plane with $\tan\beta = 30$, $A_0 = -2m_0$ and $\mu > 0$ are shown in figure 12. In the parameter space region with m_0 values smaller than about 1800 GeV the best sensitivity is obtained with the (0+1)-lepton combination, which slightly improves the individual limit obtained by the 0L_3jt signal region from the 0L search. For high m_0 values, final states with four top quarks dominate, and consequently the best sensitivity is provided by the 0/1L3B search. This search excludes gluino masses smaller than 1280 GeV.

The exclusion limits for the RPV model, which uses the same parameters as the mSUGRA/CMSSM but allows for bilinear R-parity-violating terms in the superpotential resulting in an unstable LSP, are shown in the $(m_0, m_{1/2})$ plane in figure 13. The best sensitivity is provided by the TAU and the SS/3L searches.

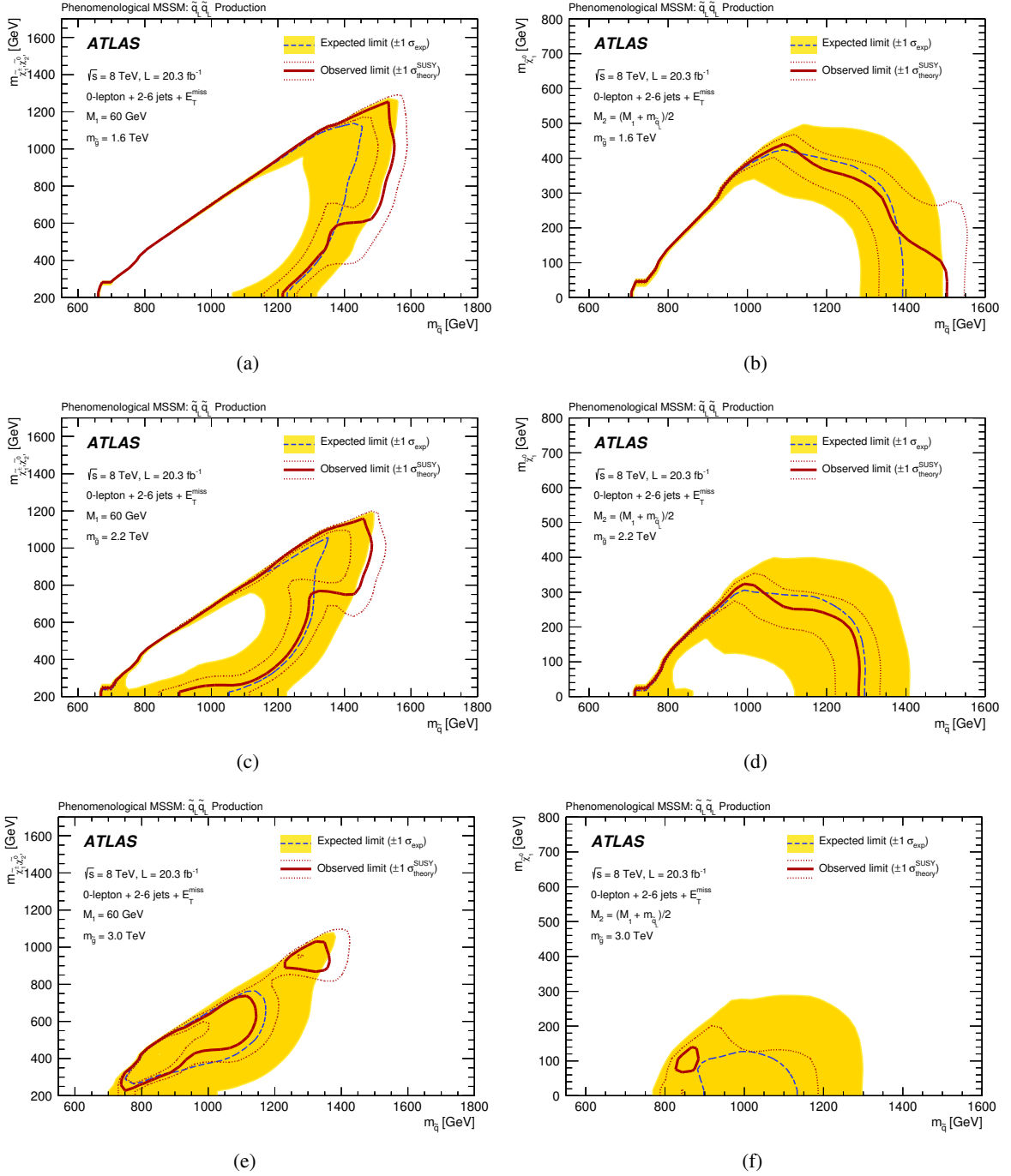


Figure 11: 95% CL exclusion limits in the pMSSM considered in the search for left-handed squarks, with mass parameters M_1 and M_2 , which are associated with the bino and wino masses, respectively. The limits are obtained from the 0L analysis with the additional 0L_4jt+ and 0L_5jt signal regions optimized specifically for this model. The parameter set considered here has either (a, c, e) $M_1 = 60$ GeV and M_2 varying or (b, d, f) $M_2 = (M_1 + m_{\tilde{q}_1})/2$ and M_1 varying. For each M_1, M_2 combination three gluino masses are considered, $m_{\tilde{g}} = 1600, 2200, 3000$ GeV. Gluino pair production is not included. The solid red line and the dashed blue line show respectively the combined observed and expected 95% CL exclusion limits.

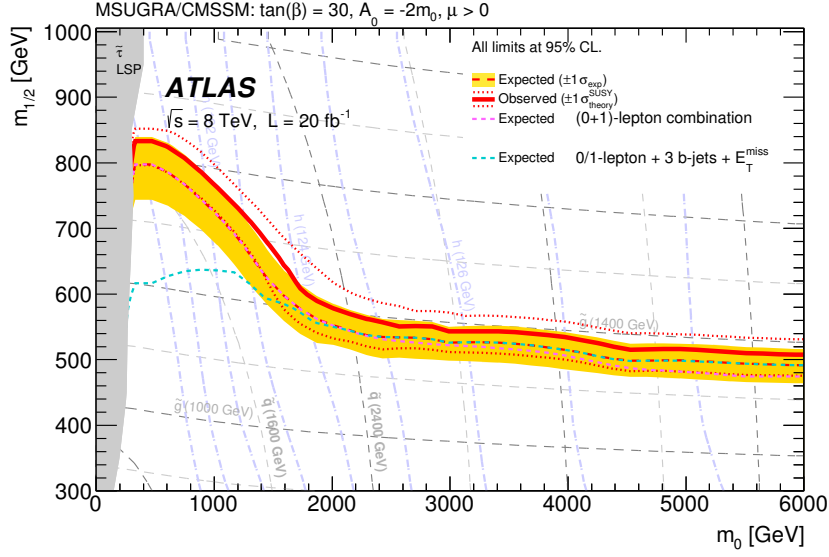


Figure 12: Exclusion limits in the $(m_0, m_{1/2})$ plane for the mSUGRA/CMSSM model. The solid red line and the dashed red line show respectively the combined observed and expected 95% CL exclusion limits. Expected limits from the individual analyses which contribute to the final combined limits are also shown for comparison.

For m_0 values smaller than approximately 750 GeV the sensitivity is dominated by the TAU search which excludes $m_{1/2}$ values up to 680 GeV using the combination of all final states considered in the search. At high m_0 values the best sensitivity is provided by the SS/3L_SR3b signal region from the SS/3L search, which excludes values of $m_{1/2}$ between 200 GeV and 490 GeV. For m_0 values below 2200 GeV, signal models with $m_{1/2} < 200$ GeV are not considered because the lepton acceptance is significantly reduced due to the increased LSP lifetime in that region.

11.1.3. Minimal gauge-mediated supersymmetry breaking model

The observed and expected limits for the mGMSB scenario are shown in figure 14, in the plane defined by the SUSY breaking scale Λ and the $\tan\beta$ value. The region of small Λ and large $\tan\beta$ just above the exclusion limit is excluded theoretically since it leads to tachyonic states. The SS/3L search provides the best sensitivity for this model and excludes values of Λ up to about 75 TeV.

11.1.4. Natural gauge mediation model

The limits obtained for the nGM scenario are shown in figure 15 in the $(m_{\tilde{\tau}}, m_{\tilde{g}})$ plane. The best limits are obtained by the 1L(S,H) and TAU searches, resulting in an exclusion of gluino masses below approximately 1100 GeV independent of the $\tilde{\tau}$ mass.

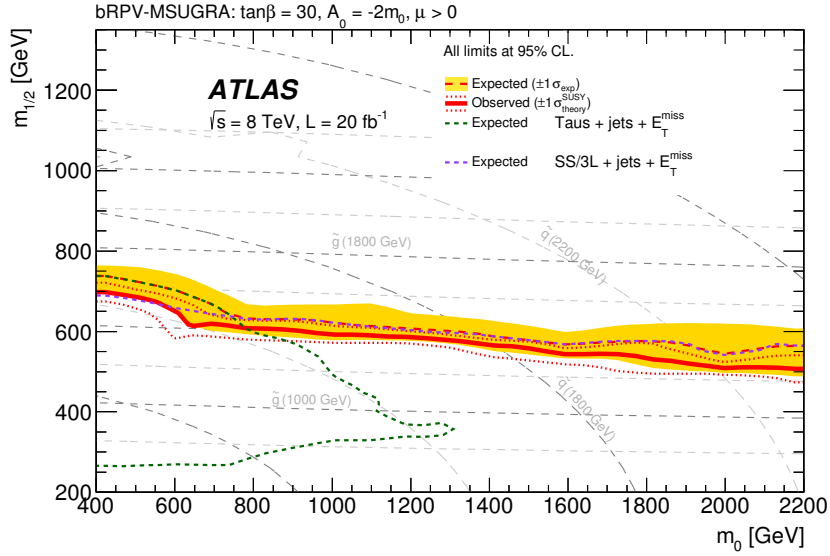


Figure 13: Exclusion limits in the $(m_0, m_{1/2})$ plane for the bRPV model. The solid red line and the dashed red line show respectively the combined observed and expected 95% CL exclusion limits. Expected limits from the individual analyses which contribute to the final combined limits are also shown for comparison.

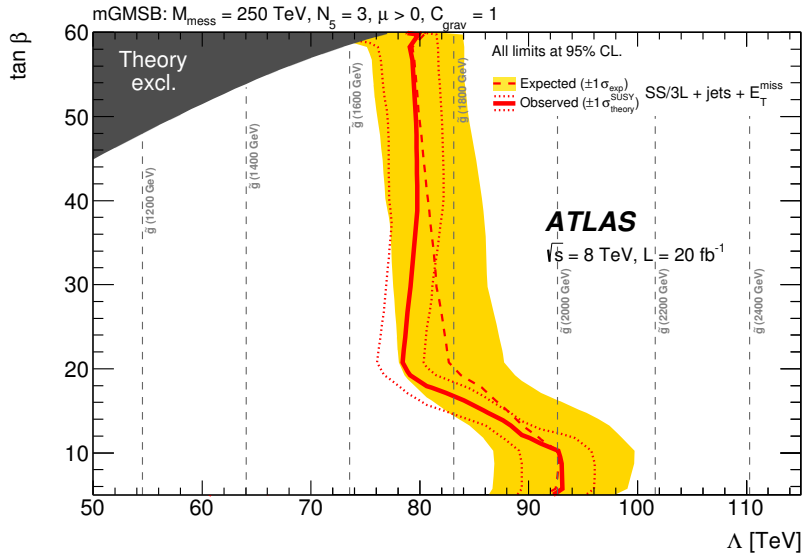


Figure 14: Exclusion limits in the $(\Lambda, \tan\beta)$ plane for the mGMSB model. The solid red line and the dashed red line show respectively the combined observed and expected 95% CL exclusion limits. The region of small Λ and large $\tan\beta$ just above the exclusion limit is excluded theoretically since it leads to tachyonic states.

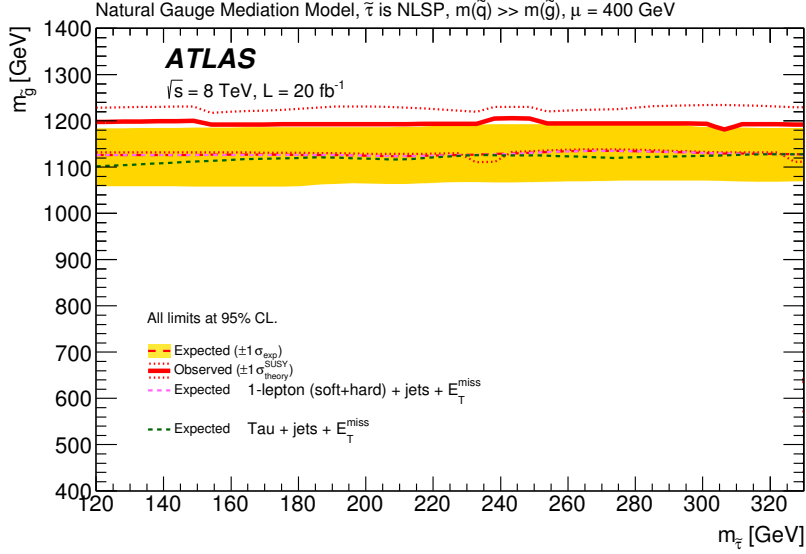


Figure 15: Exclusion limits in the $(m_{\tilde{\tau}}, m_{\tilde{g}})$ plane for the nGM model. The solid red line and the dashed red line show respectively the combined observed and expected 95% CL exclusion limits. Expected limits from the individual analyses which contribute to the final combined limits are also shown for comparison.

11.1.5. Non-universal Higgs mass model with gaugino mediation

The exclusion limits in the context of a NUHMG model with parameters $m_0 = 0$, $\tan\beta = 10$, $\mu > 0$ and $m_{H_2}^2 = 0$ are shown in the $(m_{H_1}^2, m_{1/2})$ plane in figure 16. They are provided by the (0+1)-lepton combination. A band in the $(m_{H_1}^2, m_{1/2})$ plane can be excluded, extending up to the ranges $2000 \times 10^3 \text{ GeV}^2 < m_{H_1}^2 < 5400 \times 10^3 \text{ GeV}^2$ and $450 \text{ GeV} < m_{1/2} < 620 \text{ GeV}$.

11.1.6. Minimal Universal Extra Dimension model

Finally, the limits obtained for the mUED scenario are shown in figure 17 in the $(1/R_c, \Lambda R_c)$ plane. The 2L(S), 2LRaz and SS/3L searches provide competitive sensitivities for this model in which the mass spectrum is naturally degenerate and the decay chain of the Kaluza–Klein (KK) quark excitation to the lightest KK particle, the KK photon, gives a signature very similar to the supersymmetric decay chain of a squark via cascades involving top quarks, charginos, neutralinos or sleptons, which can subsequently produce many leptons. In the region where the cut-off scale times radius (ΛR_c) is smaller than 13, the combined exclusion is dominated by the 2L(S) and 2LRaz searches which are combined based on the best expected CL_S value, while in the remaining regions of the parameter space the final exclusion is dominated by the SS/3L_SR3Lhigh and SS/3L_SR0b signal regions from the SS/3L search. Values of $1/R_c$ below 850 GeV are excluded.

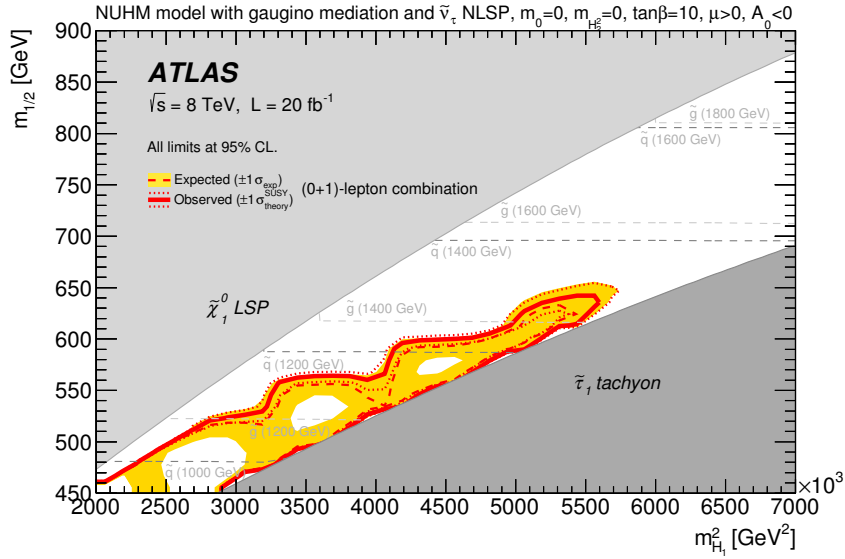


Figure 16: Exclusion limits in the $(m_{H_1}^2, m_{1/2})$ plane for the NUHMG model. The solid red line and the dashed red line show respectively the combined observed and expected 95% CL exclusion limits.

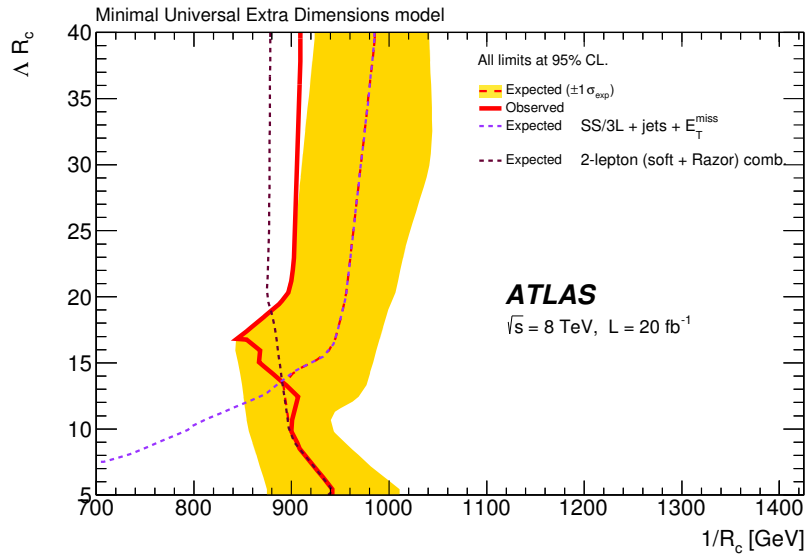


Figure 17: Exclusion limits in the $(1/R_c, \Delta R_c)$ plane for the mUED model. The solid red line and the dashed red line show respectively the combined observed and expected 95% CL exclusion limits. Expected limits from the individual analyses which contribute to the final combined limits are also shown for comparison.

11.2. Limits in Simplified Models

11.2.1. Direct decays of squarks and gluinos

This section summarizes the exclusion limits in simplified models with direct decays of gluinos and squarks of the first and second generation described in section 2.2.1. Here and in sections 11.2.2 and 11.2.3, unless otherwise stated, the eight light-flavoured squarks are always assumed to be mass-degenerate.

Figure 18 shows the exclusion limits in simplified models with squark-pair production and subsequent direct squark decays to a quark and the lightest neutralino. The expected limits from the three most sensitive searches (0L, MONOJ and 0LRaz) are presented individually along with the combined expected and observed exclusion limits. The 0L and 0LRaz analyses yield in general higher expected mass limits, but the MONOJ search provides the best sensitivity close to the diagonal line, in the region of parameter space where the mass difference between the squark and the lightest neutralino is small. From the observed limits, neutralino masses below about 280 GeV can be excluded for squark masses up to 800 GeV, and for a neutralino mass of 100 GeV squark masses are excluded below 850 GeV. In a scenario with only one light-flavour squark produced, which affects only the cross-section but not the kinematics of the events, a lower limit on the squark mass of 440 GeV is obtained with the 0L search [20].

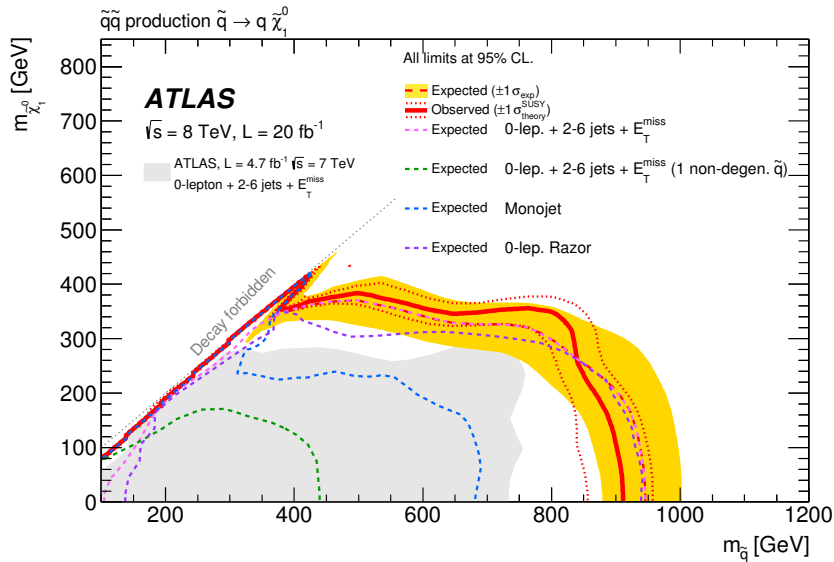


Figure 18: Exclusion limits in the mass plane of the lightest neutralino and first- and second-generation squarks assuming squark-pair production and direct decays $\tilde{q} \rightarrow q\tilde{\chi}_1^0$. The solid red line and the dashed red line show respectively the combined observed and expected 95% CL exclusion limits. Expected limits from the individual analyses which contribute to the final combined limits are also shown for comparison. A previous result from ATLAS [156] using 7 TeV proton–proton collisions is represented by the shaded (grey) area. A limit obtained with the 0L search [20] in a scenario with only one light-flavour squark produced is also presented for completeness.

Another example of a direct decay is shown in figure 19, taken from ref. [20], where gluino-pair production with the subsequent decay $\tilde{g} \rightarrow qq\tilde{\chi}_1^0$ is considered. Due to the higher production cross-sections compared to the squark-pair production, higher mass limits can be obtained. For gluino masses up to about 1000 GeV, neutralino masses can be excluded below about 500 GeV or close to the kinematic limit near the diagonal. For small neutralino masses the observed limit is as large as 1330 GeV.

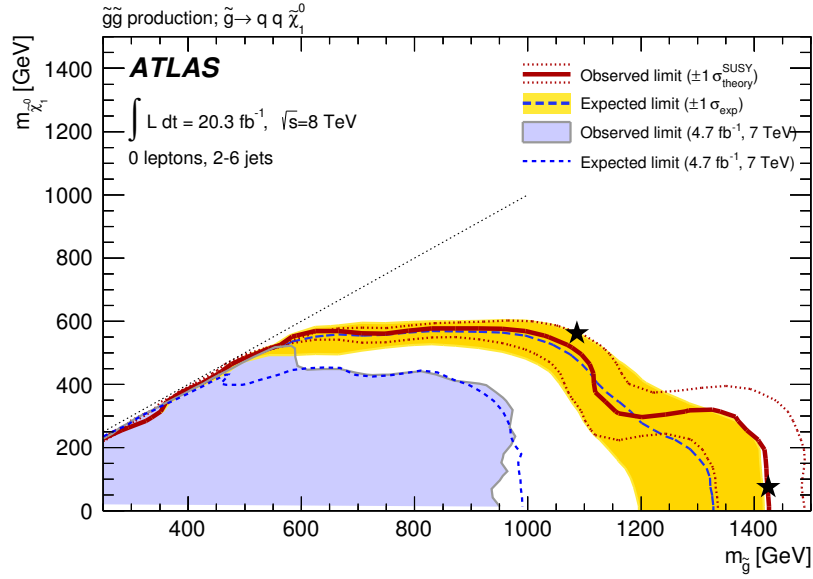
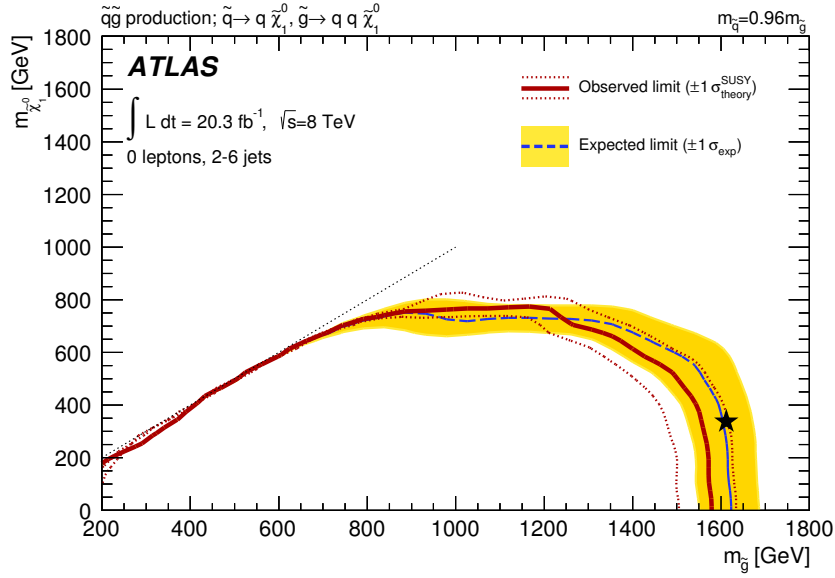


Figure 19: Exclusion limits in the mass plane of the lightest neutralino and the gluino for gluino-pair production with direct decay $\tilde{g} \rightarrow qq\tilde{\chi}_1^0$ taken from the 0L search [20]. The solid red line and the dashed blue line show respectively the observed and expected 95% CL exclusion limits. The star symbols indicates two benchmark models which are investigated in more detail in the publication. A previous result from ATLAS [156] using 7 TeV proton–proton collisions is represented by the shaded (light blue) area.

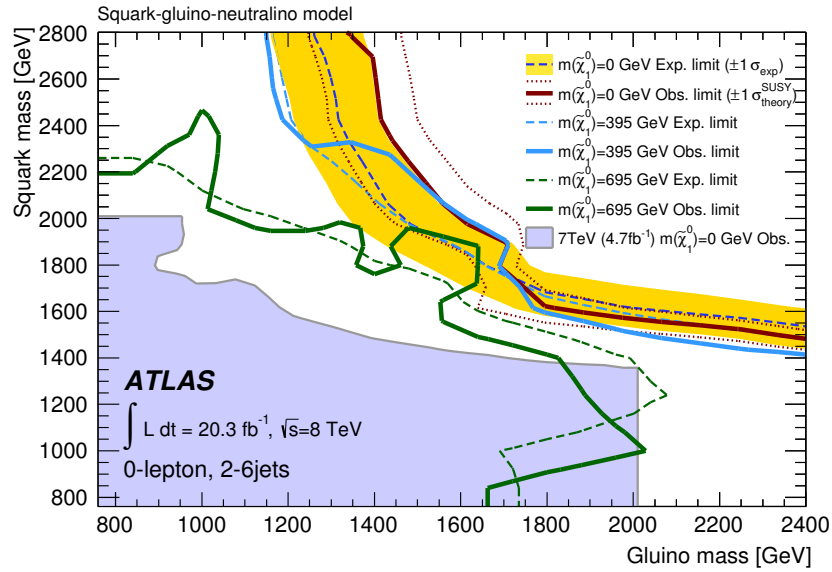
A simplified model of $\tilde{q}\tilde{q}$ strong production with the direct decays of squarks $\tilde{q} \rightarrow q\tilde{\chi}_1^0$ and gluinos $\tilde{g} \rightarrow qq\tilde{\chi}_1^0$ is considered in figure 20, taken from ref. [20], for the 0L analysis. The squark mass is fixed at $0.96m_{\tilde{g}}$ in figure 20(a), and gluinos can decay via on-shell squarks as $\tilde{g} \rightarrow \tilde{q}q \rightarrow qq\tilde{\chi}_1^0$. The exclusion limit for the neutralino mass is very close to the kinematic limit near the diagonal line and reaches 700 GeV for gluino masses up to 1200 GeV. For a massless neutralino, gluino masses below 1500 GeV are excluded.

Figure 20(b) expresses the mass limits in the $(m_{\tilde{g}}, m_{\tilde{q}})$ plane in the model with combined production of squark pairs, gluino pairs, and of squark–gluino pairs, for different assumptions on the neutralino mass: $m_{\tilde{\chi}_1^0} = 0$ GeV, 395 GeV or 695 GeV. Depending on the mass hierarchy, the $\tilde{g} \rightarrow \tilde{q}q$ and $\tilde{q} \rightarrow \tilde{g}q$ one-step decays are taken into account. The masses of all other supersymmetric particles are set outside the kinematic reach. A lower limit of 1650 GeV for equal squark and gluino mass is found for the scenario with a massless $\tilde{\chi}_1^0$.

Figure 21 shows the cross-section times branching ratio limits for gluino-pair production with direct gluino decays to a gluon and the lightest neutralino based on the 0L search. For a massless neutralino (figure 21(a)), gluino masses below 1250 GeV can be excluded. The result can also be used to obtain lower mass limits on $\tilde{\chi}_1^0$, e.g. 550 GeV for a gluino mass of 850 GeV (figure 21(b)). The cross-section exclusion for the $\tilde{g} \rightarrow g\tilde{\chi}_1^0$ model is very similar to that for the $\tilde{q} \rightarrow q\tilde{\chi}_1^0$ as would be expected if there is not much difference between quark- and gluon-initiated jets.

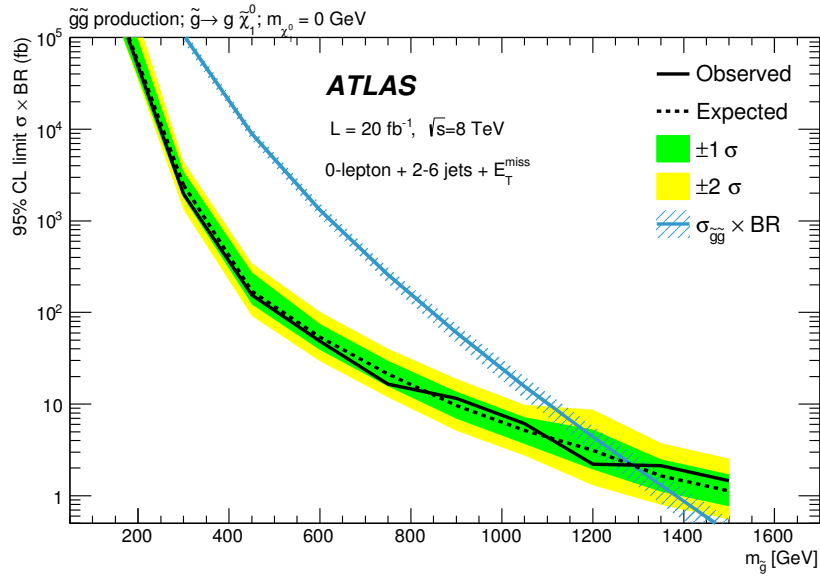


(a)

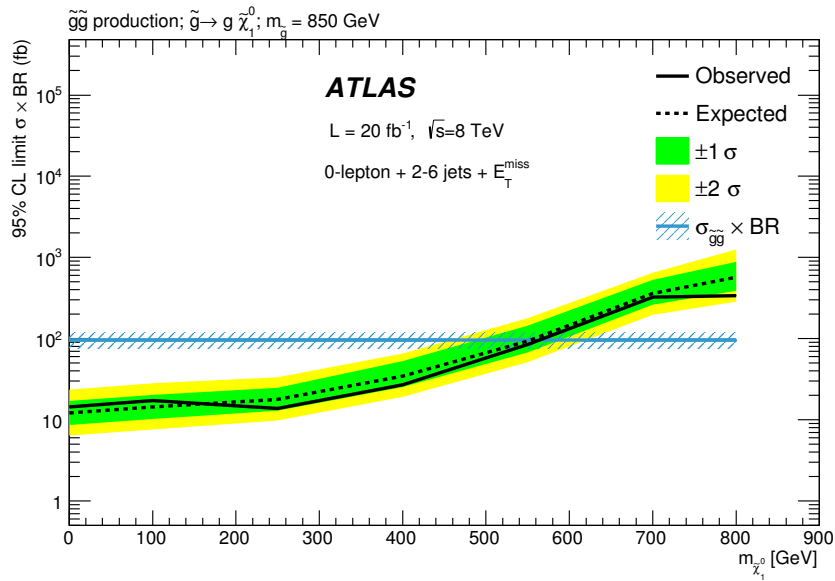


(b)

Figure 20: Exclusion limits on the production of a first- or second-generation squark and a gluino with direct decays of both particles, taken from the 0L search [20]. The solid red line and the dashed blue line show respectively the observed and expected 95% CL exclusion limits. The squark mass is fixed at $0.96 m_{\tilde{g}}$ in (a) and allowed to vary freely in (b) with three assumptions on the neutralino mass of 0, 395 GeV or 695 GeV. The black star indicates a benchmark model as discussed in ref. [20]. Previous results for a massless neutralino from ATLAS at 7 TeV [156] are represented by the shaded (light blue) area. The 7 TeV results are valid for squark or gluino masses below 2000 GeV, the mass range studied for that analysis.



(a)



(b)

Figure 21: Limits at 95% CL on the production cross-section times branching ratio for gluino-pair production with direct decay of gluino to gluon and the lightest neutralino for (a) a massless neutralino as a function of the gluino mass, and (b) as a function of the $\tilde{\chi}_1^0$ mass for a fixed gluino mass of $m_{\tilde{g}} = 850$ GeV. The solid black line shows the observed limit and the dashed line the expected limit. The solid medium dark (blue) line indicates the theoretical cross-section times branching ratio. The hatched (blue) bands around the theoretical $\sigma \cdot \text{BR}$ curves denote the scale and PDF uncertainties.

11.2.2. One-step decays of squarks and gluinos

This section presents the limits in simplified models with one-step decays of squarks and gluinos described in section 2.2.2.

Figure 22 shows the exclusion limits for squark-pair production where the squark decays via an intermediate chargino (one step) to a quark, W boson and neutralino. For the model presented in figure 22(a) the chargino mass is fixed at $m_{\tilde{\chi}_1^\pm} = (m_{\tilde{q}} + m_{\tilde{\chi}_1^0})/2$ and the result is shown in the $(m_{\tilde{q}}, m_{\tilde{\chi}_1^0})$ plane. The best sensitivity is obtained by the (0+1)-lepton combination. Neutralino masses up to 370 GeV are excluded. For a neutralino mass of 100 GeV, squark masses are excluded below 790 GeV. Figure 22(b) shows the exclusion limits in the $(m_{\tilde{q}}, x)$ plane, where x is defined as $x = \Delta m(\tilde{\chi}_1^\pm, \tilde{\chi}_1^0)/\Delta m(\tilde{q}, \tilde{\chi}_1^0)$, in models in which the neutralino mass is fixed at 60 GeV. Squark masses are excluded up to 830 GeV for the most favourable x values. The 1L(S,H) search yields stronger limits than the 0L analysis for most of the parameter space of both types of models.

The results of the searches for gluino-pair production with a one-step decay via an intermediate chargino into $qqW\tilde{\chi}_1^0$ are shown in figure 23. Figure 23(a) shows the limit for a chargino mass fixed at $m_{\tilde{\chi}_1^\pm} = (m_{\tilde{g}} + m_{\tilde{\chi}_1^0})/2$, where the (0+1)-lepton combination provides the best sensitivity. For a neutralino mass of 100 GeV, gluino masses below 1270 GeV are excluded. Neutralino masses are excluded below 480 GeV for gluino masses up to 1200 GeV. Fixing the neutralino mass at 60 GeV (figure 23(b)), one obtains limits on the variable $x = \Delta m(\tilde{\chi}_1^\pm, \tilde{\chi}_1^0)/\Delta m(\tilde{g}, \tilde{\chi}_1^0)$. Nearly the whole range $0 < x < 1$ is excluded for gluino masses below 1100 GeV.

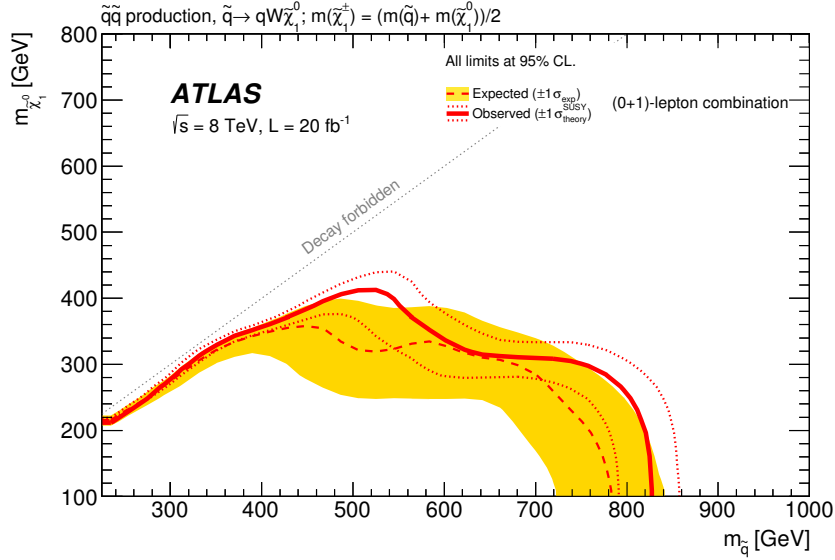
11.2.3. Two-step decays of squarks and gluinos

This section presents the limits in simplified models with two-step decays of squarks and gluinos described in section 2.2.3.

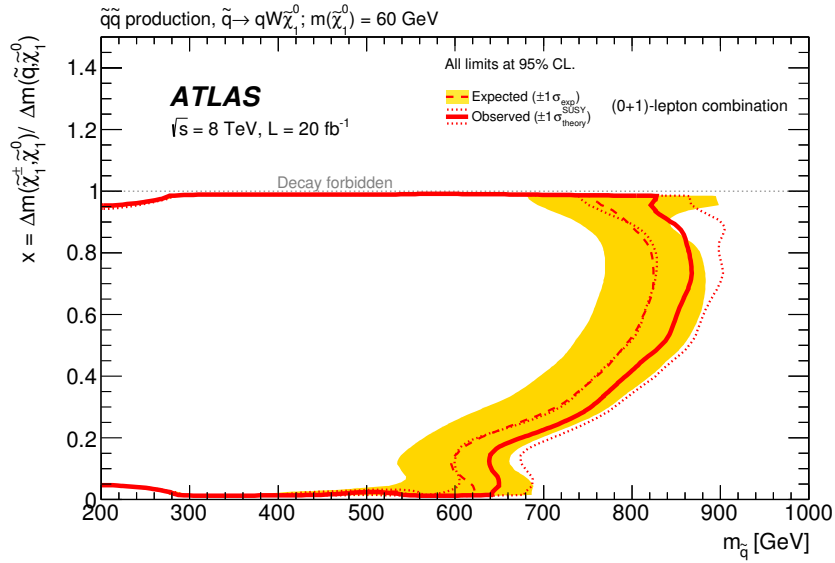
Exclusion limits for squark-pair production with a subsequent two-step squark decay via a chargino and neutralino to $qWZ\tilde{\chi}_1^0$ are shown in figure 24. Results are obtained with two searches, the 0L and the SS/3L searches. The 0L search is mainly sensitive in the low-mass region of $240 \text{ GeV} < m_{\tilde{q}} < 300 \text{ GeV}$, whereas the SS/3L search is most sensitive for squark masses between 450 and 650 GeV, where $\tilde{\chi}_1^0$ masses below 250 GeV are excluded.

Exclusion limits in a simplified model of gluino-pair production with a subsequent two-step gluino decay via a chargino and neutralino to $qqWZ\tilde{\chi}_1^0$ are shown in figure 25. The results are obtained with the (0+1)-lepton combination, MULTJ, and the SS/3L searches. The (0+1)-lepton combination provides the highest $\tilde{\chi}_1^0$ mass limits at low gluino masses. For the intermediate range around $m_{\tilde{g}} \approx 900 \text{ GeV}$ the SS/3L search is most sensitive, while for high gluino masses the best limits are obtained by the MULTJ analysis. For gluino masses below 500 GeV, $\tilde{\chi}_1^0$ masses are excluded up to the kinematic limit indicated by the diagonal line, and in the range $500 \text{ GeV} < m_{\tilde{g}} < 1000 \text{ GeV}$ lower limits on $\tilde{\chi}_1^0$ masses are set around 400 GeV. For $m_{\tilde{\chi}_1^0} = 100 \text{ GeV}$, gluino masses are excluded below 1150 GeV.

Another example of a simplified model with squark-pair production is considered in figure 26, where squarks decay through a two-step process via a chargino or neutralino and a slepton into final states with jets, leptons and missing transverse momentum. Figure 26 shows the exclusion limits in the $(m_{\tilde{q}}, m_{\tilde{\chi}_1^0})$ plane, for which the best results are obtained by the 2LRaz and the SS/3L searches. Masses for the

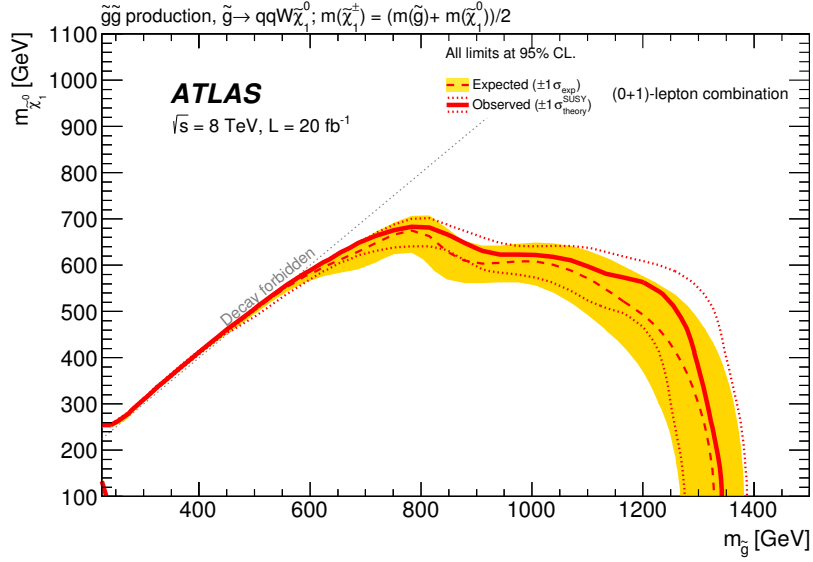


(a)

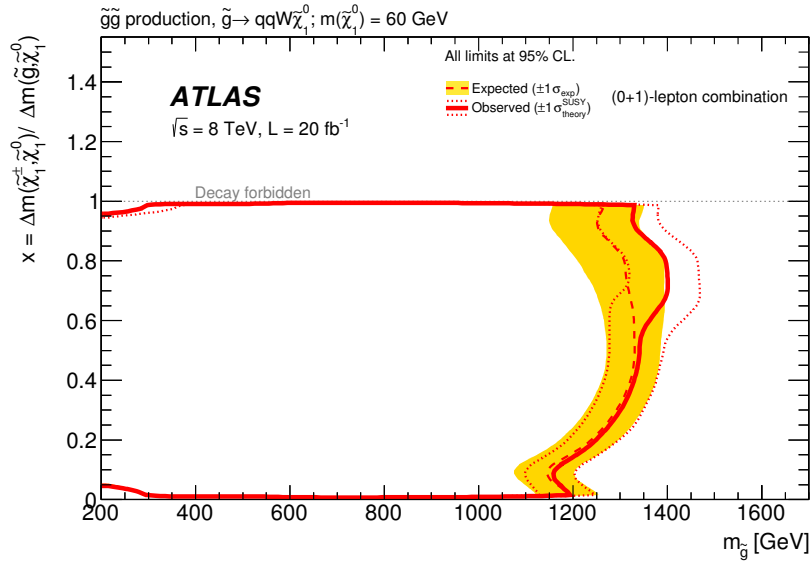


(b)

Figure 22: Exclusion limits for squark-pair production with a one-step decay via an intermediate chargino into $qW\tilde{\chi}_1^0$. Figure (a) shows the limits in the $(m_{\tilde{q}}, m_{\tilde{\chi}_1^0})$ plane for a chargino mass fixed at $m_{\tilde{\chi}_1^\pm} = (m_{\tilde{q}} + m_{\tilde{\chi}_1^0})/2$. Alternatively (b), the neutralino mass is fixed at 60 GeV and exclusion limits are given for $x = \Delta m(\tilde{\chi}_1^\pm, \tilde{\chi}_1^0)/\Delta m(\tilde{q}, \tilde{\chi}_1^0)$ as function of the squark mass. The solid red line and the dashed red line show respectively the combined observed and expected 95% CL exclusion limits.



(a)



(b)

Figure 23: Exclusion limits for gluino-pair production with a one-step decay via an intermediate chargino into $qqW\tilde{\chi}_1^0$. Figure (a) shows the limits in the $(m_{\tilde{g}}, m_{\tilde{\chi}_1^\pm})$ plane for a chargino mass fixed at $m_{\tilde{\chi}_1^\pm} = (m_{\tilde{g}} + m_{\tilde{\chi}_1^0})/2$. Alternatively (b), the neutralino mass is fixed at 60 GeV and exclusion limits are given for $x = \Delta m(\tilde{\chi}_1^\pm, \tilde{\chi}_1^0)/\Delta m(\tilde{g}, \tilde{\chi}_1^0)$ as function of the gluino mass. The solid red line and the dashed red line show respectively the combined observed and expected 95% CL exclusion limits.

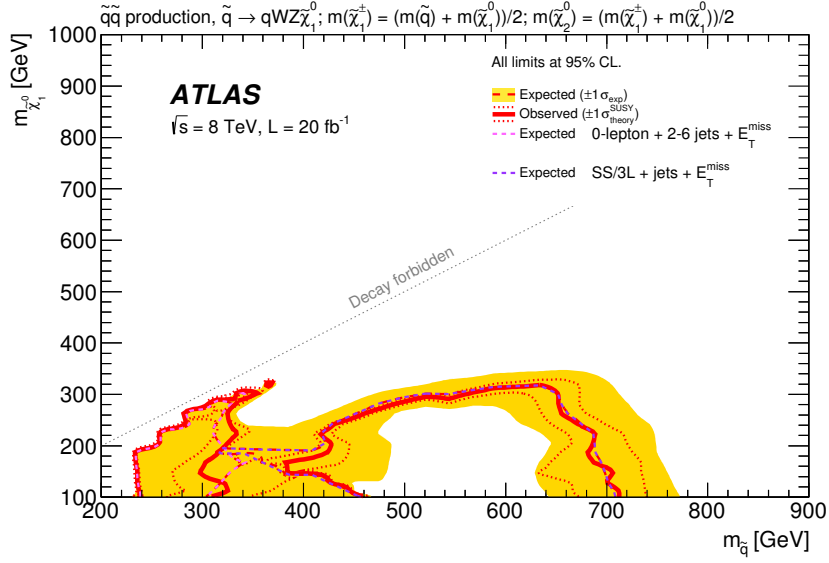


Figure 24: Exclusion limits in the $(m_{\tilde{q}}, m_{\tilde{\chi}_1^0})$ plane for a simplified model of first- and second-generation squark-pair production with two-step decay into $qqWWZZ\tilde{\chi}_1^0\tilde{\chi}_1^0$ and missing transverse momentum. The solid red line and the dashed red line show respectively the combined observed and expected 95% CL exclusion limits. Expected limits from the individual analyses which contribute to the final combined limits are also shown for comparison.

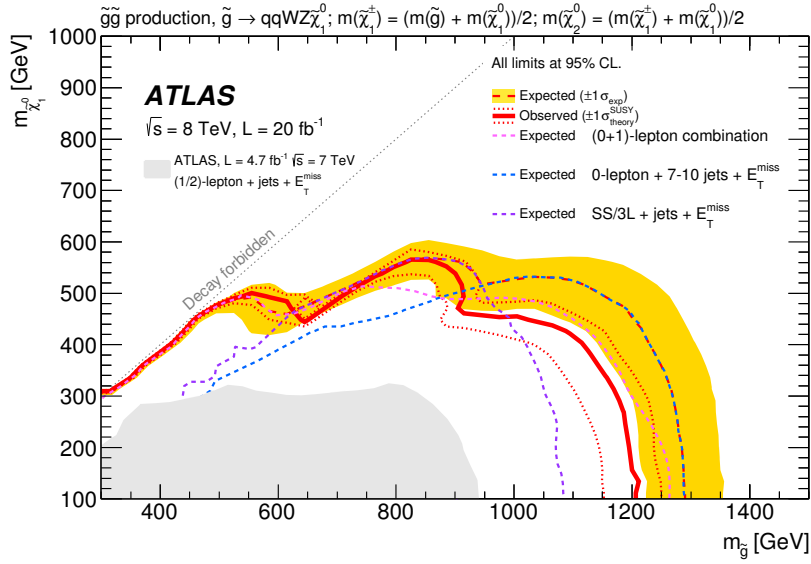


Figure 25: Exclusion limits in the $(m_{\tilde{g}}, m_{\tilde{\chi}_1^0})$ plane for a simplified model of gluino-pair production with two-step decay into $qqq'q'WWZZ\tilde{\chi}_1^0\tilde{\chi}_1^0$ and missing transverse momentum. The solid red line and the dashed red line show respectively the combined observed and expected 95% CL exclusion limits. Expected limits from the individual analyses which contribute to the final combined limits are also shown for comparison. A previous result from ATLAS [60] using 7 TeV proton-proton collisions is represented by the shaded (grey) area.

lightest neutralino can be excluded nearly up to the kinematic limit (diagonal line) for squark masses below 630 GeV. For $\tilde{\chi}_1^0$ masses below 100 GeV, squark masses can be excluded below 820 GeV.

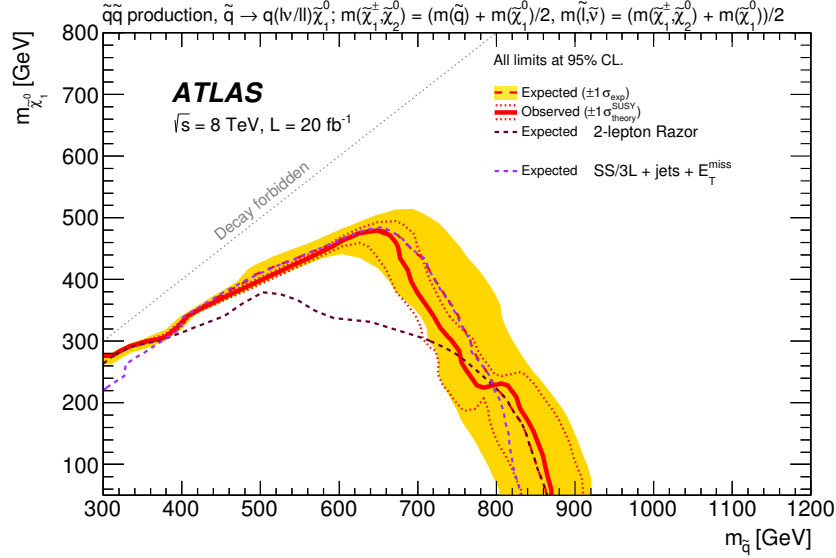


Figure 26: Exclusion limits in the $(m_{\tilde{q}}, m_{\tilde{\chi}_1^0})$ plane for a simplified model of squark-pair production with two-step decay into jets, leptons and missing transverse momentum via sleptons. The solid red line and the dashed red line show respectively the combined observed and expected 95% CL exclusion limits. Expected limits from the individual analyses which contribute to the final combined limits are also shown for comparison.

Similarly, a simplified model with gluino-pair production is considered in figure 27, where gluinos decay through a two-step process via a chargino or neutralino and sleptons into final states with jets, leptons and missing transverse momentum. Figure 27 shows the exclusion limits in the $(m_{\tilde{g}}, m_{\tilde{\chi}_1^0})$ plane. The combined 1L(S,H)+2LRaz searches based on the best expected CL_S value and the SS/3L search provide the best sensitivities for this model. Masses for the lightest neutralino can be excluded nearly up to the kinematic limit (diagonal line) for gluino masses below 600 GeV. For $\tilde{\chi}_1^0$ masses below 100 GeV, gluino masses can be excluded below 1320 GeV.

A further example of a simplified model of squark-pair production and decay through a two-step process is shown in figure 28, where squarks decay via charginos or neutralinos and staus. The exclusion limits obtained by the TAU search are indicated in the $(m_{\tilde{q}}, m_{\tilde{\chi}_1^0})$ plane. For light $\tilde{\chi}_1^0$ masses around 50 GeV, squark masses below 850 GeV are excluded; and for light squark masses of 300 GeV, neutralino masses below 170 GeV are excluded.

A simplified model of gluino-pair production and decay through a two-step process is shown in figure 29, where gluinos decay via charginos or neutralinos and staus. The exclusion limits obtained by the TAU search are indicated in the $(m_{\tilde{g}}, m_{\tilde{\chi}_1^0})$ plane. For light $\tilde{\chi}_1^0$ masses around 100 GeV, gluino masses below 1220 GeV are excluded; and for light gluino masses of 400 GeV, neutralino masses below 280 GeV are excluded.

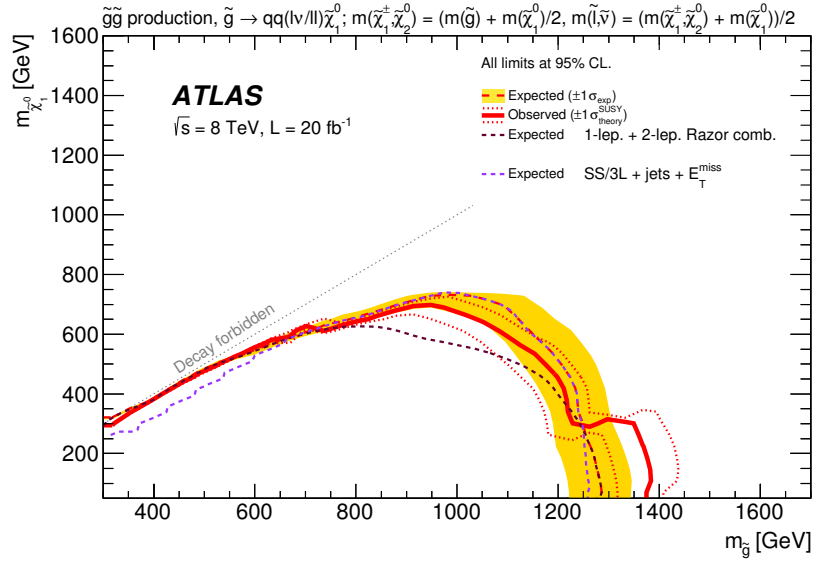


Figure 27: Exclusion limits in the $(m_{\tilde{g}}, m_{\chi_1^0})$ plane for a simplified model of gluino-pair production with two-step decay into jets, leptons and missing transverse momentum via sleptons. The solid red line and the dashed red line show respectively the combined observed and expected 95% CL exclusion limits. Expected limits from the individual analyses which contribute to the final combined limits are also shown for comparison.

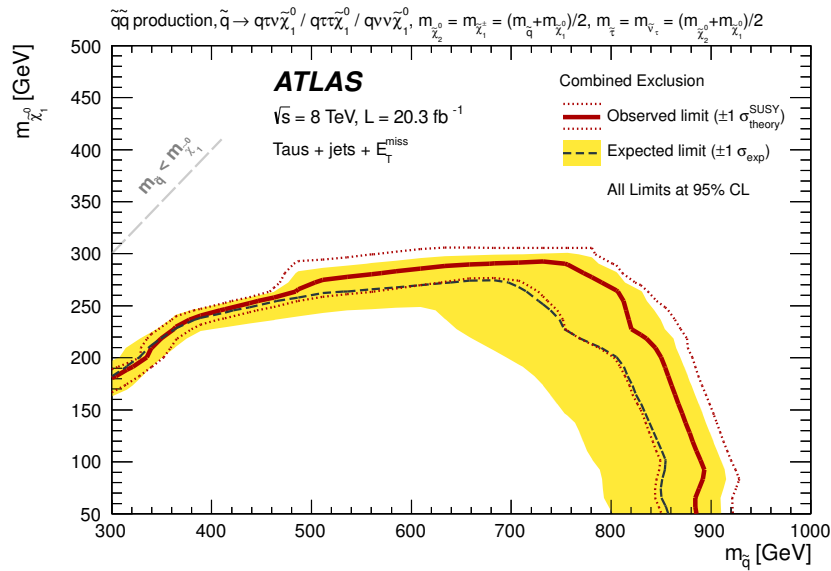


Figure 28: 95% CL exclusion limits in the $(m_{\tilde{g}}, m_{\chi_1^0})$ plane for a simplified model of squark-pair production with two-step decay via staus. The solid red line and the dashed black line show respectively the observed and expected 95% CL exclusion limits.

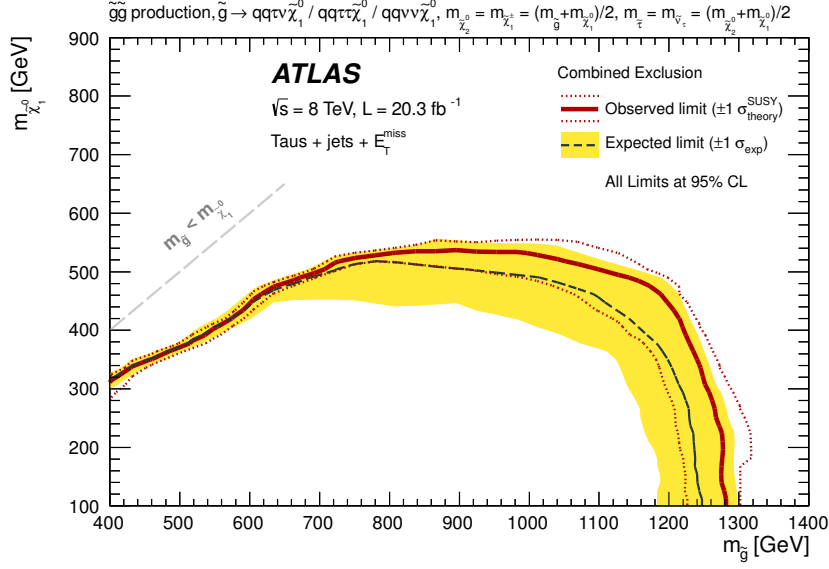


Figure 29: 95% CL exclusion limits in the $(m_{\tilde{g}}, m_{\tilde{\chi}_1^0})$ plane for a simplified model of gluino-pair production with two-step decay via staus. The solid red line and the dashed black line show respectively the observed and expected 95% CL exclusion limits.

11.2.4. Gluino decays via third-generation squarks

This section summarizes the exclusion limits placed in the various simplified models with gluino decays via third-generation squarks described in section 2.2.4.

The combined expected and observed exclusion limits for the gluino–off-shell–stop models are given in the $(m_{\tilde{g}}, m_{\tilde{\chi}_1^0})$ plane in figure 30, where a 100% branching ratio for the decay $\tilde{g} \rightarrow t\tilde{t}^*\tilde{\chi}_1^0$ via an off-shell stop is assumed. In the regions where $m_{\tilde{g}} < 2m_t + m_{\tilde{\chi}_1^0}$, the three-body decays ($\tilde{g} \rightarrow t\tilde{t}\tilde{\chi}_1^0$) are replaced by the more complex multi-body decays proceeding via off-shell top quarks and W bosons, as discussed in appendix A. The best sensitivity for this model is provided by the 0/1L3B and the SS/3L searches. In the regions of parameter space where the mass difference between the gluino and the lightest neutralino is small, the most sensitive search is the SS/3L, and the sensitivity is dominated by the SS/3L_SR3b signal region. In the regions with a large mass splitting between the gluino and the neutralino, where hard jets and large E_T^{miss} are expected, the sensitivity is dominated by the 0/1L3B_SR-0l-7j signal regions from the 0/1L3B search. For these models, gluino masses below about 1310 GeV are excluded for $m_{\tilde{\chi}_1^0} < 400$ GeV.

The exclusion limits for the gluino–stop simplified models are given in the $(m_{\tilde{g}}, m_{\tilde{t}_1})$ plane in figure 31. The \tilde{t}_1 is assumed to be the lightest squark while all other squarks are heavier than the gluino, and $m_{\tilde{g}} > m_{\tilde{t}_1} + m_t$ such that the branching ratio is 100% for $\tilde{g} \rightarrow \tilde{t}_1 t$ decays, and the top squark decays as $\tilde{t}_1 \rightarrow t\tilde{\chi}_1^0$. The 0/1L3B search provides the best sensitivity in these models, excluding gluino masses below 1220 GeV for stop masses up to 1000 GeV. Limits for the same class of simplified models, but assuming the $\tilde{t}_1 \rightarrow b\tilde{\chi}_1^\pm$ decay of the top squark, are also given in the $(m_{\tilde{g}}, m_{\tilde{t}_1})$ plane, and summarized in figure 32. The mass of the lightest neutralino in these models is set to 60 GeV and the mass of the chargino is assumed to be twice the mass of the neutralino. The chargino decays into a neutralino and a virtual W boson. The strongest limits are provided by the 0/1L3B search. Compared to the models where the top

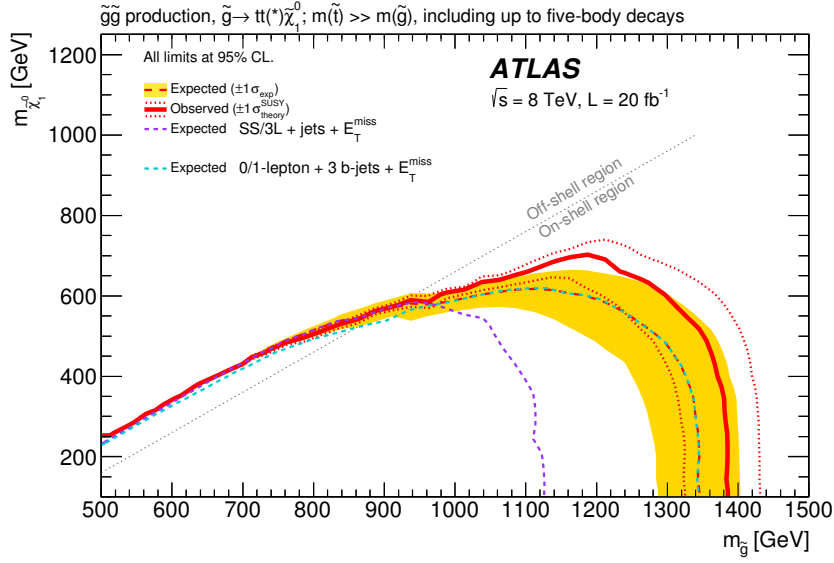


Figure 30: Exclusion limits in the $(m_{\tilde{g}}, m_{\tilde{\chi}_1^0})$ plane for the gluino–off-shell–stop simplified models in which the pair-produced gluinos decay via an off-shell stop, as $\tilde{g} \rightarrow t\tilde{\chi}_1^0$. In the region below the grey dashed line labelled “On-shell region”, $m_{\tilde{g}} > 2m_t + m_{\tilde{\chi}_1^0}$ and thus gluinos decay to two real top quarks. In the “Off-shell region”, $m_{\tilde{g}} < 2m_t + m_{\tilde{\chi}_1^0}$ and the decays of the gluino involve an off-shell top quark. Only four-body ($\tilde{g} \rightarrow tWb\tilde{\chi}_1^0$) and five-body ($\tilde{g} \rightarrow WbWb\tilde{\chi}_1^0$) decays are considered because for higher multiplicities the gluinos do not decay promptly. The solid red line and the dashed red line show respectively the combined observed and expected 95% CL exclusion limits. Expected limits from the individual analyses which contribute to the final combined limits are also shown for comparison.

squark decays via $\tilde{t}_1 \rightarrow t\tilde{\chi}_1^0$, presented in figure 31, the sensitivity in these models is lower for most of the parameter space where soft E_T^{miss} and jets are expected from the chargino decay $\tilde{\chi}_1^\pm \rightarrow W^*\tilde{\chi}_1^0$. Gluino masses below 1180 GeV are excluded for stop masses up to 1000 GeV in these models.

Another possible decay of the top squark, $\tilde{t}_1 \rightarrow c\tilde{\chi}_1^0$, is considered within the same class of simplified models, with the mass difference between the \tilde{t}_1 and the lightest neutralino fixed to 20 GeV. The (0+1)-lepton combination provides the best sensitivity in these models. The 1L(S,H) search is complementary to the 0L search in that the expected limit for the single-lepton search is able to cover higher top squark masses at intermediate gluino masses (e.g. 80 GeV higher at $m_{\tilde{g}} = 900$ GeV). The resulting exclusion limit is presented in the $(m_{\tilde{g}}, m_{\tilde{t}_1})$ plane in figure 33, and reaches gluino masses up to 1260 GeV.

A simplified model is also considered, in which the top squark decay, $\tilde{t}_1 \rightarrow sb$, involves R-parity and baryon number violation. The result is presented in the $(m_{\tilde{g}}, m_{\tilde{t}_1})$ plane in figure 34, where the best limit is obtained by the MULTJ search. Gluino masses below 880 GeV are excluded for top squark masses ranging from 400 GeV to 1000 GeV.

The sensitivity in the gluino–sbottom simplified models in which the branching ratio for $\tilde{g} \rightarrow \tilde{b}_1 b$ decays is 100% and the bottom squarks are assumed to decay exclusively via $\tilde{b}_1 \rightarrow b\tilde{\chi}_1^0$ is provided only by the 0/1L3B search [27] and the result is presented for completeness in figure 35. The search excludes gluino masses below 1200 GeV for sbottom masses up to about 1100 GeV.

The limits for the gluino–off-shell–sbottom simplified models, which assume 100% branching ratio for

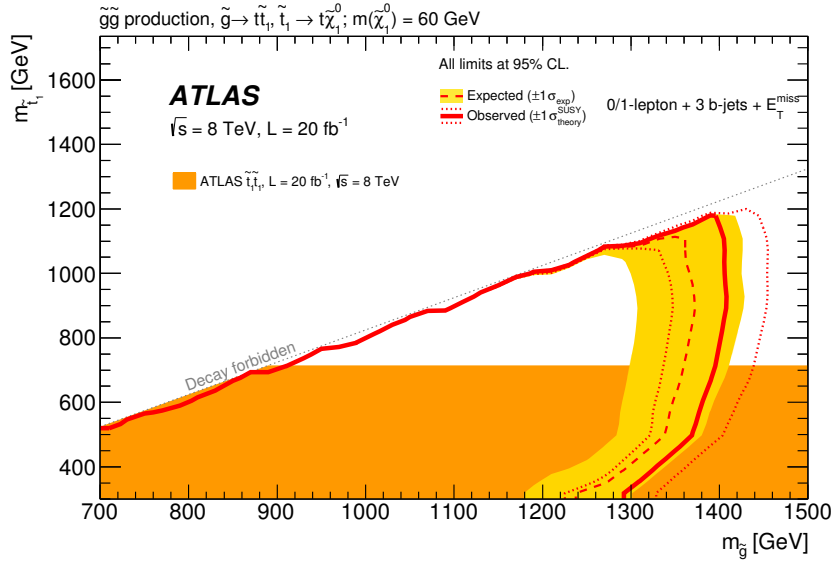


Figure 31: Exclusion limits in the $(m_{\tilde{g}}, m_{\tilde{t}_1})$ plane for the gluino–stop simplified models in which the top squarks are produced in the decay of pair-produced gluinos and decay via $\tilde{t}_1 \rightarrow t\tilde{\chi}_1^0$. The neutralino mass is set to 60 GeV. The solid red line and the dashed red line show respectively the combined observed and expected 95% CL exclusion limits. Also shown for reference is the limit from the ATLAS search for direct stop-pair production [18].

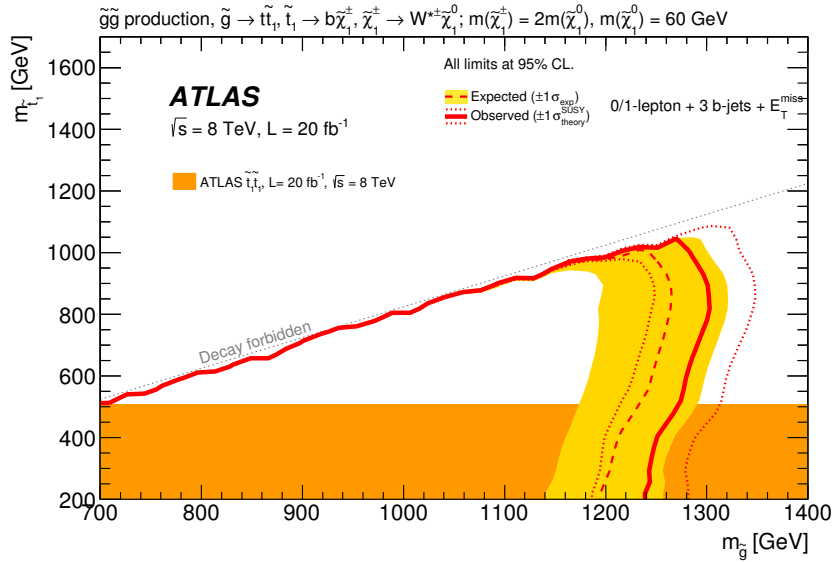


Figure 32: Exclusion limits in the $(m_{\tilde{g}}, m_{\tilde{t}_1})$ plane for the gluino–stop simplified models in which the top squarks are produced in the decay of pair-produced gluinos and decay via $\tilde{t}_1 \rightarrow b\tilde{\chi}_1^\pm$. The neutralino mass is set to 60 GeV and the mass of the chargino is assumed to be twice the mass of the neutralino. The solid red line and the dashed red line show respectively the combined observed and expected 95% CL exclusion limits. Also shown for reference is the limit from the ATLAS search for direct stop-pair production [18].

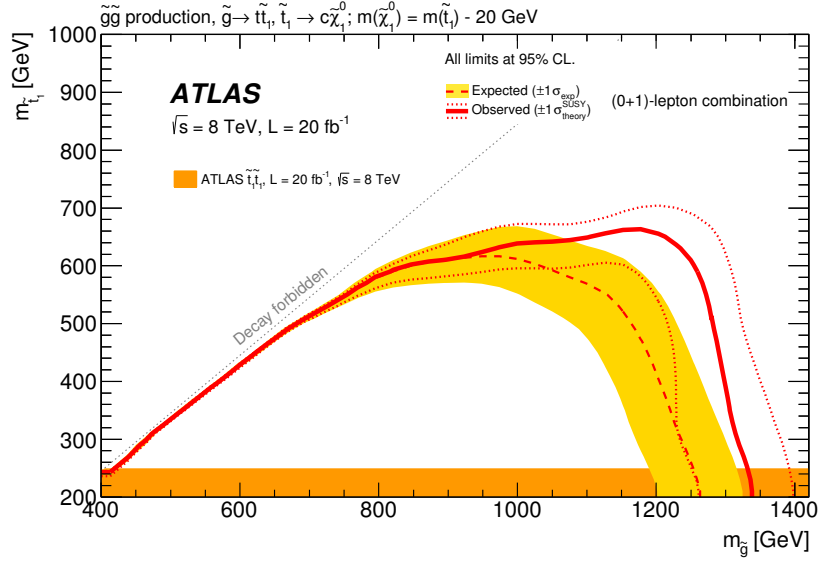


Figure 33: Exclusion limits in the $(m_{\tilde{g}}, m_{\tilde{t}_1})$ plane for the gluino–stop simplified models in which the top squarks are produced in the decay of pair-produced gluinos and decay via $\tilde{t}_1 \rightarrow c + \tilde{\chi}_1^0$. The mass difference between the \tilde{t}_1 and the lightest neutralino is fixed to 20 GeV. The solid red line and the dashed red line show respectively the combined observed and expected 95% CL exclusion limits. Also shown for reference is the limit from the ATLAS search for direct stop-pair production [18].

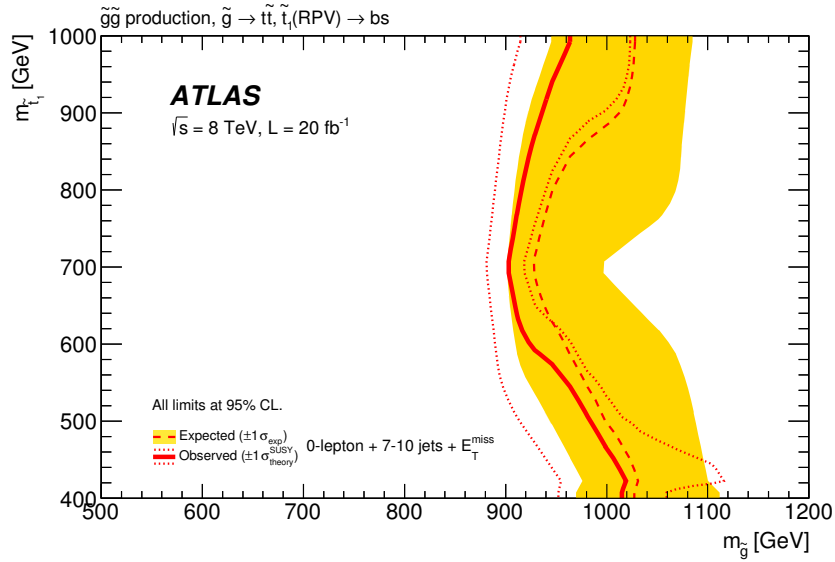


Figure 34: Exclusion limits in the $(m_{\tilde{g}}, m_{\tilde{t}_1})$ plane for the gluino–stop simplified models in which the top squarks are produced in the decay of pair-produced gluinos and decay via R-parity and baryon number violation $\tilde{t}_1 \rightarrow sb$. The solid red line and the dashed red line show respectively the combined observed and expected 95% CL exclusion limits. Expected limits from the individual analyses which contribute to the final combined limits are also shown for comparison.

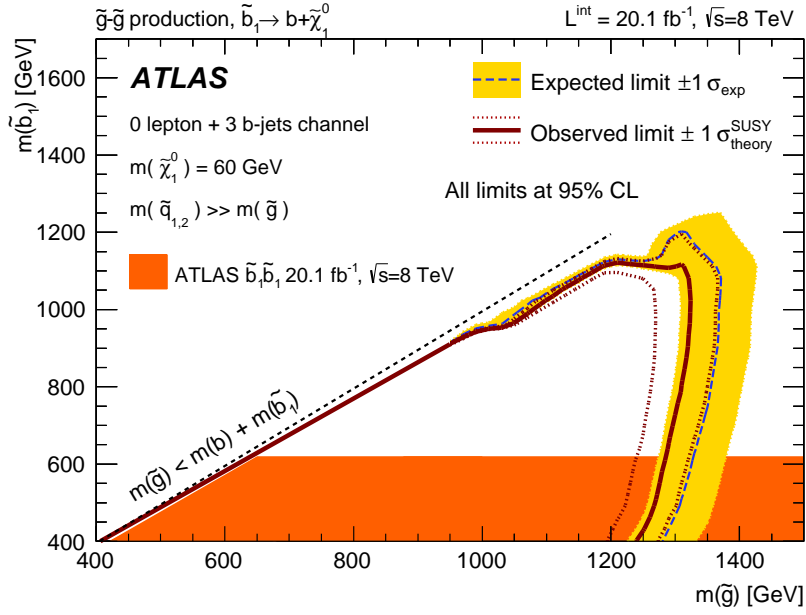


Figure 35: Exclusion limits in the $(m_{\tilde{g}}, m_{\tilde{b}_1})$ plane for the gluino–sbottom simplified models, taken from ref. [27]. Also shown for reference is the limit from the ATLAS search for direct sbottom-pair production [18].

the gluino three-body decay $\tilde{g} \rightarrow b\bar{b}\tilde{\chi}_1^0$ via an off-shell sbottom, are given in the $(m_{\tilde{g}}, m_{\tilde{\chi}_1^0})$ plane in figure 36. The best sensitivities are provided by two searches, the 0/1L3B and the 0L search. The former is the most sensitive search in regions of the parameter space with a large mass splitting between the gluino and the lightest neutralino, and the latter in regions with a small mass splitting where softer jets and smaller E_T^{miss} are expected in the final state. In these models, gluino masses below 1250 GeV are excluded for $m_{\tilde{\chi}_1^0} < 400$ GeV while neutralino masses below 600 GeV are excluded in the gluino mass range between 700 and 1200 GeV.

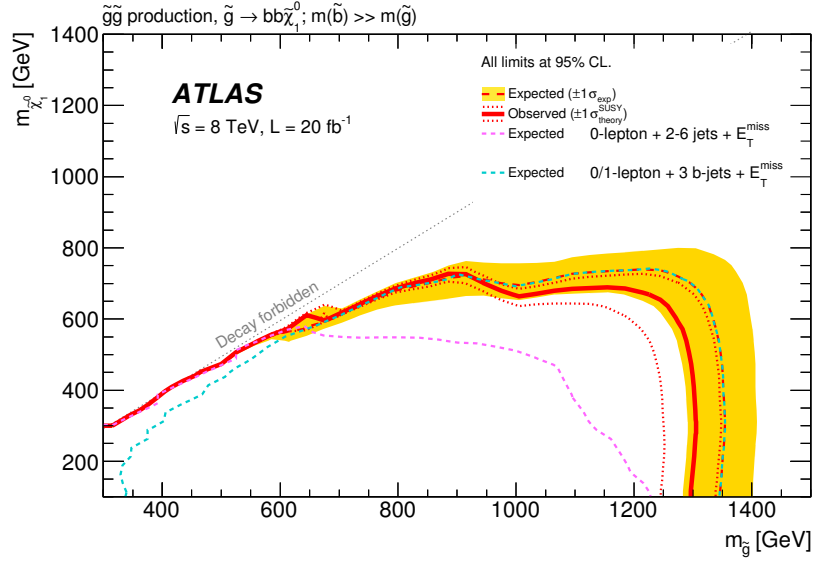


Figure 36: Exclusion limits in the $(m_{\tilde{g}}, m_{\tilde{\chi}_1^0})$ plane for the gluino–off-shell–bottom simplified models in which the pair-produced gluinos decay via an off-shell sbottom as $\tilde{g} \rightarrow b\tilde{b}\tilde{\chi}_1^0$. The solid red line and the dashed red line show respectively the combined observed and expected 95% CL exclusion limits. Expected limits from the individual analyses which contribute to the final combined limits are also shown for comparison.

The sensitivity in the gluino–off-shell–stop/sbottom simplified models in which gluinos decay via virtual stops or sbottoms is provided only by the 0/1L3B search [27]. Here the mass difference between the particles is set such that the gluino decays result in an effectively three-body final state ($b\tilde{t}\tilde{\chi}_1^0$). The exclusion limit is presented in figure 37 for completeness. For neutralino masses of 500 GeV, gluino masses are excluded between 750 and 1250 GeV.

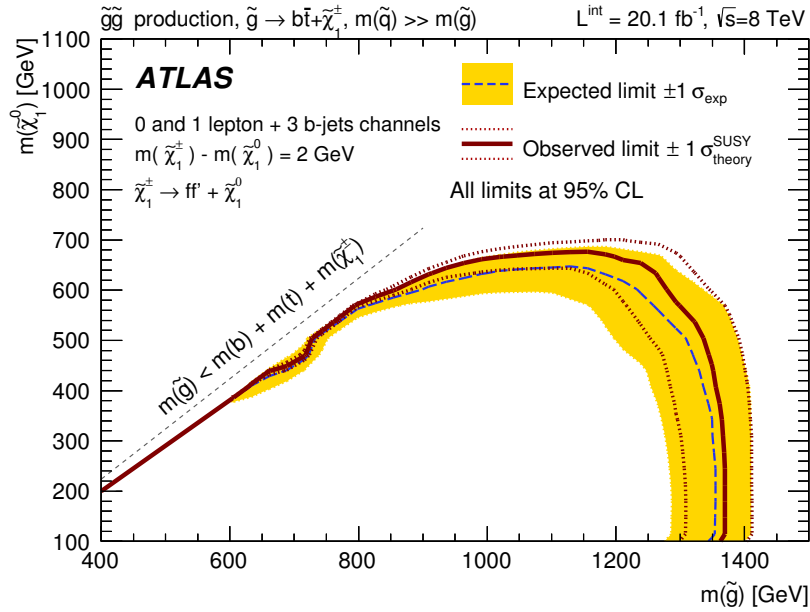


Figure 37: Exclusion limits in the $(m_{\tilde{g}}, m_{\tilde{\chi}_1^0})$ plane for the gluino–off-shell–stop/sbottom simplified models, taken from ref. [27].

12. Conclusions

A search for squarks and gluinos in inclusive final states containing high- p_T jets and missing transverse momentum, with or without leptons or b -jets, is presented. The data were recorded in 2012 by the ATLAS experiment with $\sqrt{s} = 8$ TeV proton–proton collisions at the Large Hadron Collider, with a total integrated luminosity up to 20.3 fb^{-1} . Earlier ATLAS searches have been extended and combined with new search techniques, thus improving the sensitivity for supersymmetric models. Good agreement is found with the predictions from SM processes. The data are therefore used to set exclusion limits for a variety of simplified and phenomenological SUSY models.

Limits in simplified models with gluinos and squarks of the first and second generations are derived for direct and one- or two-step decays of squarks and gluinos, and gluino decays via third-generation squarks. In all the considered simplified models that assume R-parity conservation, the limit on the gluino mass exceeds 1150 GeV at 95% CL, for an LSP mass smaller than 100 GeV. Additional limits are set in a phenomenological MSSM model used in the search for left-handed squarks, a minimal Supergravity/Constrained MSSM model, R-parity-violation scenarios, a minimal gauge-mediated supersymmetry breaking model, a natural gauge mediation model, a non-universal Higgs mass model with gaugino mediation and a minimal model of universal extra dimensions. These limits are either new or extend the region of parameter space excluded by previous searches with the ATLAS detector.

Acknowledgements

We thank CERN for the very successful operation of the LHC, as well as the support staff from our institutions without whom ATLAS could not be operated efficiently.

We acknowledge the support of ANPCyT, Argentina; YerPhI, Armenia; ARC, Australia; BMFWF and FWF, Austria; ANAS, Azerbaijan; SSTC, Belarus; CNPq and FAPESP, Brazil; NSERC, NRC and CFI, Canada; CERN; CONICYT, Chile; CAS, MOST and NSFC, China; COLCIENCIAS, Colombia; MSMT CR, MPO CR and VSC CR, Czech Republic; DNRF, DNSRC and Lundbeck Foundation, Denmark; EPLANET, ERC and NSRF, European Union; IN2P3-CNRS, CEA-DSM/IRFU, France; GNSF, Georgia; BMBF, DFG, HGF, MPG and AvH Foundation, Germany; GSRT and NSRF, Greece; RGC, Hong Kong SAR, China; ISF, MINERVA, GIF, I-CORE and Benoziyo Center, Israel; INFN, Italy; MEXT and JSPS, Japan; CNRST, Morocco; FOM and NWO, Netherlands; BRF and RCN, Norway; MNiSW and NCN, Poland; GRICES and FCT, Portugal; MNE/IFA, Romania; MES of Russia and NRC KI, Russian Federation; JINR; MSTD, Serbia; MSSR, Slovakia; ARRS and MIZŠ, Slovenia; DST/NRF, South Africa; MINECO, Spain; SRC and Wallenberg Foundation, Sweden; SER, SNSF and Cantons of Bern and Geneva, Switzerland; NSC, Taiwan; TAEK, Turkey; STFC, the Royal Society and Leverhulme Trust, United Kingdom; DOE and NSF, United States of America.

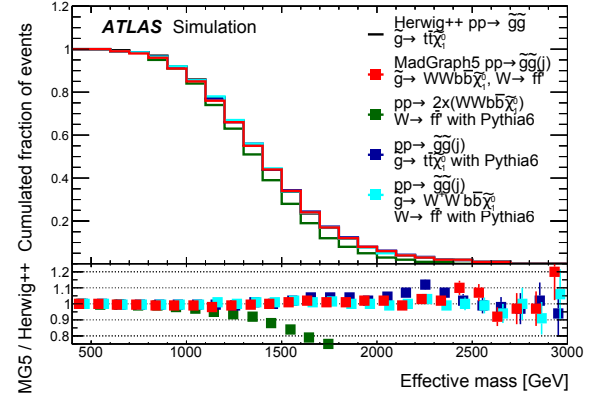
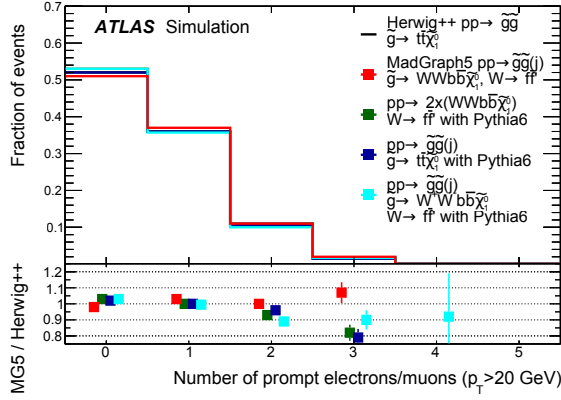
The crucial computing support from all WLCG partners is acknowledged gratefully, in particular from CERN and the ATLAS Tier-1 facilities at TRIUMF (Canada), NDGF (Denmark, Norway, Sweden), CC-IN2P3 (France), KIT/GridKA (Germany), INFN-CNAF (Italy), NL-T1 (Netherlands), PIC (Spain), ASGC (Taiwan), RAL (UK) and BNL (USA) and in the Tier-2 facilities worldwide.

A. Extension of the $\tilde{g} \rightarrow t\tilde{\chi}_1^0$ simplified model to include decays with off-shell top quarks

In this appendix, further details are provided about the extension of the gluino-mediated off-shell stop model $\tilde{g} \rightarrow t\tilde{\chi}_1^0$ to the region $m_t + m_W + m_b \leq m_{\tilde{g}} - m_{\tilde{\chi}_1^0} \leq 2m_t$, where three-body decays are replaced by more complex multi-body decays proceeding via off-shell top quarks and W bosons. This region is delimited by the kinematic boundaries corresponding to three- and four-body gluino decays. In principle, the extension could have been performed up to mass gaps as small as $m_{\tilde{g}} - m_{\tilde{\chi}_1^0} \geq 2m_b$, but it was found that for a 100% branching ratio hypothesis for the $\tilde{g} \rightarrow t\tilde{\chi}_1^0$ mode, mass gaps smaller than the four-body kinematic bound quickly lead to large gluino lifetimes, resulting in displaced gluino decays. This is verified even in the scenario leading to the smallest gluino lifetime ($m_{\tilde{t}_1} = m_{\tilde{g}}$, $\tilde{t}_1 = \tilde{t}_R$). Since the results of the various searches reported in this paper are all based on prompt objects, the expected sensitivity to these scenarios with small mass gaps is very small, and they are addressed by dedicated searches [157]. Therefore, the probed parameter space is limited to $m_{\tilde{g}} - m_{\tilde{\chi}_1^0} \geq m_t + m_W + m_b$.

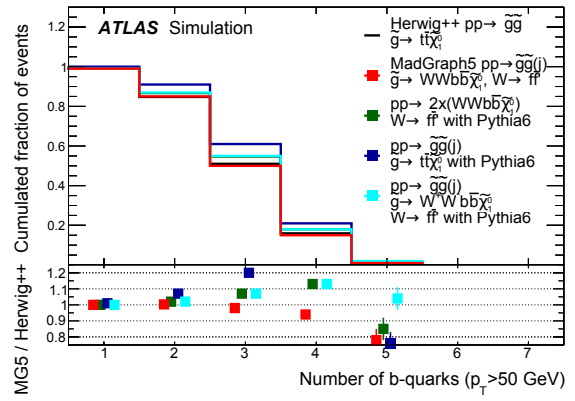
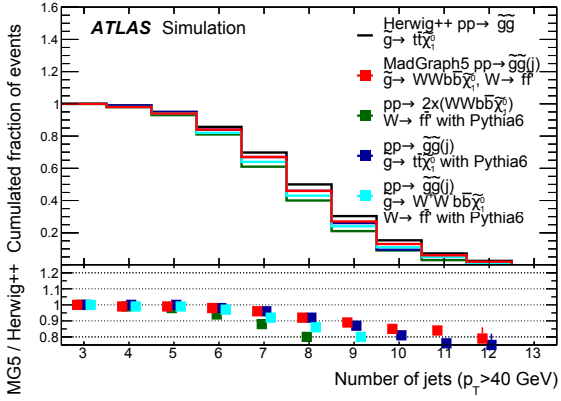
Despite the restriction of the model parameter space to regions where four-body gluino decays $\tilde{g} \rightarrow tWb\tilde{\chi}_1^0$ are always kinematically allowed, more complex decays (mainly five-body) can occur concurrently with a significant branching ratio, and even become dominant when the mass gap approaches its lower bound. Consideration of these alternative decay modes also sometimes leads to large differences in kinematic distributions of the decay products. For example, the b -quark in the decay $\tilde{g} \rightarrow tWb\tilde{\chi}_1^0$ becomes too soft for experimental detection when $m_{\tilde{g}} \approx m_t + m_W + m_b + m_{\tilde{\chi}_1^0}$, whereas it can still get sizeable momentum in the alternative decay $\tilde{g} \rightarrow WWbb\tilde{\chi}_1^0$. Since the most sensitive searches for this model rely on selections with at least three b -jets, one can see that the acceptance of these selections would vanish at the kinematic bound if considering only four-body decays, although it is not the case thanks to the alternative decay modes. To summarize, quantitative studies showed that it is important to consider at least the five-body decay as well in this region of the parameter space.

Finally, signal events were generated following a configuration defined and validated by comparing generator predictions for several observables in a region at low neutralino mass where only three-body decays contribute. The reference was provided by HERWIG++ (the generator used for the $m_{\tilde{g}} - m_{\tilde{\chi}_1^0} > 2m_t$ region of this scenario), characterized notably by the use of a matrix element amplitude for the gluino decay, and the preservation of spin correlation between the decay products. It was first observed that narrow-width approximations for the gluino decay compared poorly to the reference, hence imposing the need for decay amplitudes computed from matrix elements for the four- and five-body decays, and as a consequence the choice of the MADGRAPH generator. However, the computing requirements to obtain the amplitude associated with such a $2 \rightarrow 10(+1)$ hard process (with an extra parton) are too demanding. An approximation is used instead, consisting in the separate generation of pair-produced gluinos, and gluino decays into fermions $\tilde{g} \rightarrow f\bar{f}'f''\bar{f}'''bb\tilde{\chi}_1^0$. The two stages are then combined by boosting the gluino decay products according to the gluino's directions and momenta defined by the hard process, while preserving the gluino spin orientations. The use of the inclusive seven-body gluino decay, instead of the minimally required five-body decay, came at no additional computing cost and allowed, in particular, proper propagation of the various spin correlations along the gluino decay chain. This setup provided agreement with the reference at the level of 5%, for the shapes of various generator-level kinematic distributions (a few of which are presented in figure 38), as well as for fiducial acceptances of typical event selections used as signal regions in the relevant SUSY searches.



(a) Distribution of the number of prompt leptons (electrons and muons), $p_T > 20$ GeV, $|\eta| < 2.5$

(b) Cumulative distribution of the effective mass built from selected leptons, jets and non-interacting particles



(c) Cumulative distribution of the number of jets (anti- k , $R = 0.4$), $p_T > 40$ GeV, $|\eta| < 2.8$

(d) Cumulative distribution of the number of b -quarks, $p_T > 50$ GeV, $|\eta| < 2.5$

Figure 38: Validation of the MADGRAPH5+PYTHIA6 setup used to generate five-body gluino decays $\tilde{g} \rightarrow W^+W^-b\bar{b}\tilde{\chi}_1^0$: kinematic distributions obtained with the nominal configuration (red markers) are compared to the reference HERWIG++ sample (black), for a signal scenario featuring only three-body gluino decays $\tilde{g} \rightarrow t\tilde{\chi}_1^0$ ($m_{\tilde{g}} = 1$ TeV, $m_{\tilde{\chi}_1^0} = 100$ GeV). A few alternative (and simpler) generator configurations are also shown (other coloured markers), but they fail to reach a satisfactory level of agreement with the reference, for the typical signal region requirements (cf. SR3b in table 20). The distributions are built from the outgoing particles provided by the generators.

B. Summary of selection criteria

Tables 14–22 summarize the selection criteria for signal regions listed in table 5 which have been defined in previous ATLAS publications [20–27].

Requirement	Signal region		
	M1	M2	M3
Jets preselection	At most three jets with $p_T > 30$ GeV and $ \eta < 2.8$		
$p_T^{\text{jet}_1}$ [GeV] >	280	340	450
E_T^{miss} [GeV] >	220	340	450
$\Delta\phi(\text{jet}, \mathbf{E}_T^{\text{miss}}) >$	0.4		

Table 14: Selection criteria used to define the three signal regions in the search with at least one high- p_T jet and large missing transverse momentum (Monojet) [21]. The azimuthal separation $\Delta\phi(\text{jet}, \mathbf{E}_T^{\text{miss}})$ is calculated between the missing transverse momentum direction and each of the selected jets.

Requirement	Signal region					
	2jl	2jm	2jt	2jW	3j	4jW
E_T^{miss} [GeV] >	160					
p_T^{jet1} [GeV] >	130					
p_T^{jet2} [GeV] >	60					
p_T^{jet3} [GeV] >	–			60	40	
p_T^{jet4} [GeV] >	–				40	
$\Delta\phi(\text{jet}_{1,2,(3)}, \mathbf{E}_T^{\text{miss}})_{\text{min}}$ >	0.4					
$\Delta\phi(\text{jet}_{i>3}, \mathbf{E}_T^{\text{miss}})_{\text{min}}$ >	–				0.2	
W candidates	–		2($W \rightarrow j$)		–	($W \rightarrow j$) + ($W \rightarrow jj$)
$E_T^{\text{miss}} / \sqrt{H_T}$ [GeV ^{1/2}] >	8	15		–		
$E_T^{\text{miss}} / m_{\text{eff}}^{N_j}$ >	–			0.25	0.3	0.35
$m_{\text{eff}}^{\text{incl}}$ [GeV] >	800	1200	1600	1800	2200	1100

Requirement	Signal region								
	4jl-	4jl	4jm	4jt	5j	6jl	6jm	6jt	6jt+
E_T^{miss} [GeV] >	160								
p_T^{jet1} [GeV] >	130								
p_T^{jet2} [GeV] >	60								
p_T^{jet3} [GeV] >	60								
p_T^{jet4} [GeV] >	60								
p_T^{jet5} [GeV] >	–			60					
p_T^{jet6} [GeV] >	–				60				
$\Delta\phi(\text{jet}_{1,2,(3)}, \mathbf{E}_T^{\text{miss}})_{\text{min}}$ >	0.4								
$\Delta\phi(\text{jet}_{i>3}, \mathbf{E}_T^{\text{miss}})_{\text{min}}$ >	0.2								
$E_T^{\text{miss}} / \sqrt{H_T}$ [GeV ^{1/2}] >	10			–					
$E_T^{\text{miss}} / m_{\text{eff}}^{N_j}$ >	–		0.4	0.25	0.2		0.25	0.15	
$m_{\text{eff}}^{\text{incl}}$ [GeV] >	700	1000	1300	2200	1200	900	1200	1500	1700

Table 15: Selection criteria used to define the fifteen signal regions in the search with at least two to at least six jets, significant E_T^{miss} and the absence of isolated electrons or muons (0-lepton + 2–6 jets + E_T^{miss}) [20]. Each signal region is labelled with the inclusive jet multiplicity considered (‘2j’, ‘3j’, etc.) together with the degree of background rejection. The latter is denoted by labels ‘l-’ (‘very loose’), ‘l’ (‘loose’), ‘m’ (‘medium’), ‘t’ (‘tight’) and ‘t+’ (‘very tight’). The $E_T^{\text{miss}} / m_{\text{eff}}^{N_j}$ requirement in any N_j -jet channel uses a value of m_{eff} constructed from only the leading N_j jets ($m_{\text{eff}}^{N_j}$). The final $m_{\text{eff}}^{\text{incl}}$ selection, which is used to define the signal regions, includes all jets with $p_T > 40$ GeV. The variable H_T is defined as the scalar sum of the transverse momenta of all jets with $p_T > 40$ GeV. The azimuthal separation $\Delta\phi(\text{jet}, \mathbf{E}_T^{\text{miss}})_{\text{min}}$ is defined to be the smallest of the azimuthal separations between $\mathbf{E}_T^{\text{miss}}$ and the reconstructed jets. In SR 2jW and SR 4jW a requirement $60 \text{ GeV} < m(W_{\text{cand}}) < 100 \text{ GeV}$ is placed on the masses of candidate resolved or unresolved hadronically decaying W bosons. Candidate W bosons are reconstructed from single high-mass jets (unresolved candidates; $W \rightarrow j$ in the table) or from pairs of jets (resolved candidates; $W \rightarrow jj$ in the table).

Requirement	Signal regions in multi-jet + flavour stream														
	8j50			9j50			10j50			7j80			8j80		
$ \eta ^{\text{jet}} <$	2.0														
$p_T^{\text{jet}} [\text{GeV}] >$	50						80								
N_{jet}	= 8			= 9			≥ 10			= 7			≥ 8		
$N_{b\text{-jet}}$ ($p_T > 40 \text{ GeV}, \eta < 2.5$)	0	1	≥ 2	0	1	≥ 2	—	0	1	≥ 2	0	1	≥ 2		
$E_T^{\text{miss}} / \sqrt{H_T} [\text{GeV}^{1/2}] >$	4														

Requirement	Signal regions in multi-jet + M_J^Σ stream					
	8j50		9j50		10j50	
$ \eta ^{\text{jet}} <$	2.8					
$p_T^{\text{jet}} [\text{GeV}] >$	50					
N_{jet}	≥ 8		≥ 9		≥ 10	
$M_J^\Sigma [\text{GeV}]$	> 340 and > 420 for each case					
$E_T^{\text{miss}} / \sqrt{H_T} [\text{GeV}^{1/2}] >$	4					

Table 16: Selection criteria used to define the nineteen signal regions in the search with at least seven to at least ten jets, significant E_T^{miss} and the absence of isolated electrons or muons (0-lepton + 7–10 jets + E_T^{miss}) [22]. The four-momenta of the $R=0.4$ jets satisfying $p_T > 20 \text{ GeV}$ and $|\eta| < 2.8$ are used as inputs to a second iteration of the anti- k_r jet algorithm, this time using the larger distance parameter $R=1.0$. The resulting larger objects are denoted as composite jets. The selection variable M_J^Σ is then defined to be the sum of the masses of the composite jets: $M_J^\Sigma \equiv \sum_j m_j^{R=1.0}$, where the sum is over the composite jets that satisfy $p_T^{R=1.0} > 100 \text{ GeV}$ and $|\eta^{R=1.0}| < 1.5$. The variable H_T is defined as the scalar sum of p_T of all jets with $p_T > 40 \text{ GeV}$ and $|\eta| < 2.8$.

Requirement	Signal region			
	Single-bin (binned) soft single-lepton			Soft dimuon
	3-jet	5-jet	3-jet inclusive	2-jet
N_ℓ	1 electron or muon			2 muons
p_T^ℓ [GeV]	[7,25] for electron, [6,25] for muon			[6,25]
Lepton veto	No additional electron or muon with $p_T > 7$ GeV or 6 GeV, respectively			
$m_{\mu\mu}$ [GeV]	–	–	–	[15,60]
N_{jet}	[3,4]	≥ 5	≥ 3	≥ 2
p_T^{jet} [GeV] >	180, 25, 25	180, 25, 25, 25, 25	130, 100, 25	80, 25
$N_{b\text{-jet}}$	–	–	0	0
E_T^{miss} [GeV] >	400	300	180	
m_T [GeV] >	100		120	40
$E_T^{\text{miss}}/m_{\text{eff}}^{\text{incl}}$ >	0.3 (0.1)		0.1	0.3
$\Delta R_{\text{min}}(\text{jet}, \ell)$ >	1.0	–	–	1.0 (2 nd muon)
Binned variable	$(E_T^{\text{miss}}/m_{\text{eff}}^{\text{incl}}$ in 4 bins)			–
Bin width	(0.1, 4 th is inclusive)			–
Requirement	Signal region			
	Single-bin (binned) hard single-lepton			
	3-jet	5-jet	6-jet	
N_ℓ	1 electron or muon			
p_T^ℓ [GeV] >	25			
Lepton veto	$p_T^{2^{\text{nd}}\text{lepton}} < 10$ GeV			
N_{jet}	≥ 3	≥ 5	≥ 6	
p_T^{jet} [GeV] >	80, 80, 30	80, 50, 40, 40, 40	80, 50, 40, 40, 40, 40	
Jet veto	$(p_T^{5^{\text{th}}\text{jet}} < 40 \text{ GeV})$	$(p_T^{6^{\text{th}}\text{jet}} < 40 \text{ GeV})$	–	
E_T^{miss} [GeV] >	500 (300)	300	350 (250)	
m_T [GeV] >	150	200 (150)	150	
$E_T^{\text{miss}}/m_{\text{eff}}^{\text{excl}}$ >	0.3	–	–	
$m_{\text{eff}}^{\text{incl}}$ [GeV] >	1400 (800)		600	
Binned variable	$(m_{\text{eff}}^{\text{incl}}$ in 4 bins)		$(E_T^{\text{miss}}$ in 3 bins)	
Bin width	(200 GeV, 4 th is inclusive)		(100 GeV, 3 rd is inclusive)	

Table 17: Selection criteria used to define the signal regions in the search requiring at least one isolated lepton (1-lepton (soft+hard) + jets + E_T^{miss}) and in the search requiring two soft muons (2-leptons + jets + E_T^{miss}) [23]. For each jet multiplicity in the single-lepton channel, two sets of requirements are defined: one single-bin signal region optimized for discovery reach, which is also used to place limits on the visible cross-section, and one signal region which is binned in an appropriate variable in order to exploit the expected shape of the distribution of signal events when placing model-dependent limits. The requirements of the binned signal region are shown in parentheses when they differ from those of the single-bin signal region. The transverse mass (m_T) of the lepton (ℓ) and E_T^{miss} is defined as $m_T = \sqrt{2p_T^\ell E_T^{\text{miss}}(1 - \cos[\Delta\phi(\vec{\ell}, \vec{E}_T^{\text{miss}})])}$. The inclusive effective mass ($m_{\text{eff}}^{\text{inc}}$) is computed as the scalar sum of the p_T of the lepton(s), the jets and E_T^{miss} : $m_{\text{eff}}^{\text{inc}} = \sum_{i=1}^{N_\ell} p_{T,i}^\ell + \sum_{j=1}^{N_{\text{jet}}} p_{T,j} + E_T^{\text{miss}}$, where the index i identifies all the signal leptons and the index j all the signal jets in the event. The exclusive effective mass ($m_{\text{eff}}^{\text{excl}}$) is defined in a similar way to $m_{\text{eff}}^{\text{inc}}$, with the exception that only the three leading signal jets are considered. The minimum angular separation ΔR_{min} calculated between the signal lepton ℓ and all preselected jets is used to reduce the background coming from misidentified or non-prompt leptons in the soft-lepton signal region with three jets and in the soft dimuon signal region. In the latter case, the subleading signal muon is used to compute ΔR_{min} .

Requirement	Signal region			
	Single-bin (binned) hard dilepton			
	Low-multiplicity (≤ 2 -jet)		3-jet	
	$ee/\mu\mu$	$e\mu$	$ee/\mu\mu$	$e\mu$
N_ℓ	2, 2 of opposite sign or ≥ 2			
$p_T^\ell [\text{GeV}] >$	14, 10			
$N_{\ell\ell}$ with $81 < m_{\ell\ell} < 101$ GeV	0	–	0	–
N_{jet}	≤ 2		≥ 3	
$p_T^{\text{jet}} [\text{GeV}] >$	50, 50		50, 50, 50	
$N_{b\text{-jet}}$	0			
R	> 0.5		> 0.35	
$M'_R [\text{GeV}] >$	600 (400 in 8 bins)		800 (800 in 5 bins)	
M'_R bin width [GeV]	(100, the last is inclusive)			

Table 18: Selection criteria used to define the signal regions in the search requiring two hard leptons (2-leptons + jets + E_T^{miss}) [23]. For each jet multiplicity two sets of requirements are defined: one single-bin signal region optimized for discovery reach, which is also used to place limits on the visible cross-section, and one signal region which is binned in an appropriate variable in order to exploit the expected shape of the distribution of signal events when placing model-dependent limits. The requirements of the binned signal region are shown in parentheses when they differ from those of the single-bin signal region. Details of the construction of Razor variables M'_R and R can be found in the appendix C.1. In this case, mega-jets are constructed using the final-state jets and leptons.

Requirement	Signal region				
	SR-2j-bveto	SR-2j-btag	SR-4j-bveto	SR-4j-btag	SR-loose
$N_{\text{jet}} \geq$	≥ 2	≥ 2	≥ 4	≥ 4	(2, ≥ 3)
$N_{b\text{-jet}}$	= 0	≥ 1	= 0	≥ 1	–
$E_T^{\text{miss}} [\text{GeV}] >$	200	200	200	200	(150, 100)
$m_{\ell\ell} [\text{GeV}] \notin$	[80, 110]	[80, 110]	[80, 110]	[80, 110]	[80, 110]

Table 19: Selection criteria used to define the signal regions in the search requiring two same-flavour opposite-sign electrons or muons (2-leptons off-Z) [24]. If more than two leptons are present, the two with the largest values of p_T are selected. The leading lepton in the event must have $p_T > 25$ GeV and the subleading lepton is required to have $p_T > 20$ GeV. These two leptons are used to define the dilepton invariant mass, $m_{\ell\ell}$. In addition, one SR with the same requirements as those used in the CMS search [148], which reported an excess of events above the SM background with a significance of 2.6 standard deviations, is defined (SR-loose) for comparison purposes.

Requirement	Signal region				
	SR3b	SR0b	SR1b	SR3Low	SR3High
Leptons	SS or 3L	SS	SS	3L	3L
$N_{b\text{-jet}}$	≥ 3	=0	≥ 1	-	-
$N_{\text{jet}} \geq$	5	3	3	4	4
$E_{\text{T}}^{\text{miss}}$ [GeV]		> 150	> 150	$50 < E_{\text{T}}^{\text{miss}} < 150$	> 150
m_{T} [GeV] >	-	100	-	-	-
Veto	-	-	SR3b	Z boson, SR3b	SR3b
m_{eff} [GeV] >	350	400	700	400	400

Table 20: Selection criteria used to define the signal regions in the search with multiple jets, and either two leptons of the same electric charge (same-sign leptons) or at least three leptons (SS/3L + jets + $E_{\text{T}}^{\text{miss}}$) [25]. The effective mass (m_{eff}) is computed from all selected leptons and selected jets in event, as $m_{\text{eff}} = \sum_{i=1}^{N_{\ell}} p_{\text{T},i}^{\ell} + \sum_{j=1}^{N_{\text{jet}}} p_{\text{T},j} + E_{\text{T}}^{\text{miss}}$. The transverse mass (m_{T}) is computed from the highest- p_{T} lepton (ℓ_1) and $E_{\text{T}}^{\text{miss}}$ as $m_{\text{T}} = \sqrt{2p_{\text{T}}^{\ell_1} E_{\text{T}}^{\text{miss}} (1 - \cos[\Delta\phi(\ell_1, E_{\text{T}}^{\text{miss}})])}$.

Requirement	Signal region	
	1 τ Loose SR	1 τ Tight SR
Taus	$N_\tau^{\text{medium}} = 1$ $p_T > 30 \text{ GeV}$	
$\Delta\phi(\text{jet}_{1,2}, \mathbf{E}_T^{\text{miss}}) >$	0.4	
$\Delta\phi(\tau, \mathbf{E}_T^{\text{miss}}) >$	0.2	
$m_T^\tau [\text{GeV}] >$	140	
$E_T^{\text{miss}} [\text{GeV}] >$	200	300
$H_T [\text{GeV}] >$	800	1000

Requirement	Signal region			
	2 τ Inclusive SR	2 τ GMSB SR	2 τ nGM SR	2 τ bRPV SR
Taus	$N_\tau^{\text{loose}} \geq 2$ $p_T > 20 \text{ GeV}$			
$\Delta\phi(\text{jet}_{1,2}, \mathbf{E}_T^{\text{miss}}) \geq$	0.3			
$m_T^{\tau_1} + m_T^{\tau_2} [\text{GeV}] \geq$	150	250	250	150
$H_T^{2j} [\text{GeV}] >$	1000	1000	600	1000
$N_{\text{jet}} \geq$	-	4		

Requirement	Signal region			
	$\tau+\ell$ GMSB SR	$\tau+\ell$ nGM SR	$\tau+\ell$ bRPV SR	$\tau+\ell$ mSUGRA SR
Taus	$N_\tau^{\text{loose}} \geq 1$ $p_T > 20 \text{ GeV}$			
$N_\ell =$	1			
$m_T^\ell [\text{GeV}] >$	100			
$m_{\text{eff}} [\text{GeV}] >$	1700	-	1300	-
$E_T^{\text{miss}} [\text{GeV}] >$	-	350	-	300
$N_{\text{jet}} \geq$	-	3	4	3

Table 21: Selection criteria used to define the signal regions in the search requiring large missing transverse momentum, jets and at least one hadronically decaying tau lepton (taus + jets + E_T^{miss}) [26]. The transverse mass m_T^τ is formed from the E_T^{miss} and the p_T of the tau lepton in the 1 τ channel as: $m_T^\tau = \sqrt{2p_T^\tau E_T^{\text{miss}}(1 - \cos(\Delta\phi(\tau, \mathbf{E}_T^{\text{miss}})))}$. In addition, the variable $m_T^{\tau_1} + m_T^{\tau_2}$ is used as a discriminating variable in the 2 τ channel. The transverse mass m_T^ℓ is similarly formed from the E_T^{miss} and the p_T of the light leptons. The variable H_T is defined as the scalar sum of the transverse momenta of the tau, light lepton and jets ($p_T^{\text{jet}} > 30 \text{ GeV}$): $H_T = \sum_{i=1}^{N_\ell} p_T^\ell + \sum_{j=1}^{N_\tau} p_T^\tau + \sum_{k=1}^{N_{\text{jet}}} p_T^{\text{jet}}$. The variable H_T^{2j} is defined as the scalar sum of the transverse momenta of the tau and light lepton candidates, and the two jets with the largest transverse momenta in the event: $H_T^{2j} = \sum_{i=1}^{N_\ell} p_T^\ell + \sum_{j=1}^{N_\tau} p_T^\tau + \sum_{k=1,2} p_T^{\text{jet}_k}$. The effective mass (m_{eff}) is defined as $m_{\text{eff}} = H_T^{2j} + E_T^{\text{miss}}$.

Requirement	Signal region					
	SR-0 ℓ -4j-A	SR-0 ℓ -4j-B	SR-0 ℓ -4j-C*	SR-0 ℓ -7j-A	SR-0 ℓ -7j-B	SR-0 ℓ -7j-C
Baseline 0-lepton selection	lepton veto, $p_T^{\text{jet}_1} > 90$ GeV, $E_T^{\text{miss}} > 150$ GeV					
N jets (p_T [GeV]) \geq	4 (50)	4 (50)	4 (30)	7 (30)	7 (30)	7 (30)
E_T^{miss} [GeV] $>$	250	350	400	200	350	250
$m_{\text{eff}}^{\text{incl}}$ [GeV] $>$	-	-	-	1000	1000	1500
m_{eff}^{4j} [GeV] $>$	1300	1100	1100	-	-	-
$E_T^{\text{miss}}/\sqrt{H_T^{4j}}$ [$\sqrt{\text{GeV}}$] $>$	-	-	16	-	-	-

Requirement	Signal region		
	SR-1 ℓ -6j-A	SR-1 ℓ -6j-B	SR-1 ℓ -6j-C
Baseline 1-lepton selection	≥ 1 signal lepton (e, μ), $p_T^{\text{jet}_1} > 90$ GeV, $E_T^{\text{miss}} > 150$ GeV		
N jets (p_T [GeV]) \geq	6 (30)	6 (30)	6 (30)
E_T^{miss} [GeV] $>$	175	225	275
m_T [GeV] $>$	140	140	160
$m_{\text{eff}}^{\text{incl}}$ [GeV] $>$	700	800	900

Table 22: Selection criteria used to define the signal regions in the search that requires at least three jets tagged as b -jets, no or at least one lepton, jets and large missing transverse momentum (0/1-lepton + 3 b -jets + E_T^{miss}) [27]. The jet p_T threshold requirements are also applied to b -jets. The notation SR-0 ℓ -4j-C* means that the leading jet is required to fail the b -tagging requirements, in order to target the region close to the kinematic boundary in the gluino–sbottom simplified models. In the 0-lepton selection, the inclusive effective mass $m_{\text{eff}}^{\text{incl}}$ is defined as the scalar sum of the E_T^{miss} and the p_T of all jets with $p_T > 30$ GeV. In the 1-lepton selection the $m_{\text{eff}}^{\text{incl}}$ is defined as for the 0-lepton selection with the addition of the p_T of all selected leptons with $p_T > 20$ GeV. The exclusive effective mass (m_{eff}^{4j}) is defined as the scalar sum of the E_T^{miss} and the p_T of the four leading jets. The transverse mass (m_T) is computed from the leading lepton and the missing transverse momentum. The variable H_T^{4j} is defined as the scalar sum of the transverse momenta of the four leading jets.

C. 0-lepton Razor analysis details

Many kinematical variables have been used to search for SUSY at hadron colliders, typically making use of the expected heavy mass scale of the SUSY particles produced, and the missing transverse momentum originating from the LSP. The analysis described here searches for squarks in final states with high- p_T jets, missing transverse momentum and no electrons or muons, using the Razor variable set [19]. These variables provide longitudinal and transverse information about each event, contribute to the rejection of the background from the multi-jet processes that dominate hadronic collisions, and can be used as an approximation of the mass scale of the produced particles.

The basic analysis approach relies on the definition of statistically independent regions in the Razor variable phase space, R and M'_R , explained in details in the remainder of this section, that are rich in SUSY-like events, and other regions, each dominated by one SM background component. Following the strategy explained in section 6, the Monte Carlo expectations are normalized to the data in each background control region, and those normalization factors are then transferred to the MC prediction in the SUSY signal regions. The baseline object selection and event cleaning, as well as the choice of MC generators for SM background processes and the approach for calculating systematic uncertainties exactly follow those of the 0-lepton + 2–6 jets + E_T^{miss} (0L) search [20], and are not discussed here.

C.1. The Razor variables

The Razor variable set is designed to group together visible final-state particles associated with heavy produced sparticles, and in doing so contains information about the mass scale of the directly produced sparticles. The final-state jets are grouped into two hemispheres called “mega-jets”, where all visible objects from one side of the di-sparticle decay are collected together to create a single four-vector, representing the decay products of a single sparticle. The mega-jet construction involves iterating over all possible combinations of the four-vectors of the visible reconstructed objects, with the favoured combination being that which minimizes the sum of the squared masses of the mega-jet four-vectors. Using this mega-jet configuration, with some simplifying assumptions (e.g. symmetric sparticle production), the rest frame of the sparticles (the so-called “ R -frame” described in ref. [19]) can be reconstructed, and a characteristic mass M'_R can be defined in this frame:

$$M'_R = \sqrt{(j_{1,E} + j_{2,E})^2 - (j_{1,L} + j_{2,L})^2}, \quad (1)$$

where $j_{i,L}$ denotes the longitudinal momentum, and $j_{i,E}$ the energy in the R -frame, of the mega-jet i .

To help reduce the SM backgrounds, a second variable, M_T^R , is defined that includes information about the transverse quantities, including the total missing transverse momentum and its angular distance to the two mega-jets. In the di-sparticle decay there are two mega-jets, each with associated E_T^{miss} from the escaping LSPs. Assigning half of the missing transverse momentum per event to each of the LSPs, M_T^R is defined as

$$M_T^R = \sqrt{\frac{E_T^{\text{miss}}(j_{1,T} + j_{2,T}) - \mathbf{E}_T^{\text{miss}} \cdot (\mathbf{j}_{1,T} + \mathbf{j}_{2,T})}{2}}, \quad (2)$$

where $j_{i,T}$ denotes the transverse momentum of the mega-jet i . The variable M_T^R is designed such that for small values of E_T^{miss} , M_T^R is also small. If the multi-jet event were perfectly reconstructed then $E_T^{\text{miss}} = 0$ and M_T^R would also be zero, while in the case where a jet is mis-calibrated, the fake E_T^{miss} tends to align with one of the mega-jets (that are back-to-back), also creating small values of M_T^R . For SUSY-like events where the mega-jets tend not to be back-to-back, and their vector sum is opposite to the E_T^{miss} , the quantity M_T^R is large. The kinematic endpoint of M_T^R is the mass difference between the heavy and the light sparticles.

Finally, the razor variable is defined as:

$$R = \frac{M_T^R}{M'_R}. \quad (3)$$

For SUSY-like events, when the mass splitting between the heavier and light sparticles is large, M'_R peaks near the mass of the heavier sparticle and M_T^R has a kinematical endpoint at the mass of the heavier sparticle. For SM processes, R tends to have a low value, while it tends to have a broad distribution centred around 0.5 for SUSY-like events. Thus R can be used as a discriminant between signal and background.

C.2. Signal regions

The SUSY models targeted by this search are expected to have final states characterized by the presence of jets, missing transverse momentum, and no leptons. In the simplest case of squark-pair production with direct decays to quarks and neutralinos, there are at least two jets visible in the detector, so the baseline inclusive signal regions require at least two jets. This is also the minimum number of visible objects in the final state necessary to construct the Razor variables. Figure 39 shows the values of R and M'_R for two simplified model signal points, one with $m_{\tilde{q}} = 450$ GeV and $m_{\text{LSP}} = 400$ GeV, where the $\Delta m = 50$ GeV is small (referred to as small- Δm_{signal}) and the other with $m_{\tilde{q}} = 850$ GeV and $m_{\text{LSP}} = 100$ GeV, where the $\Delta m = 750$ GeV is large (referred to as large- Δm_{signal}), after requiring no leptons and at least two jets in the final state.

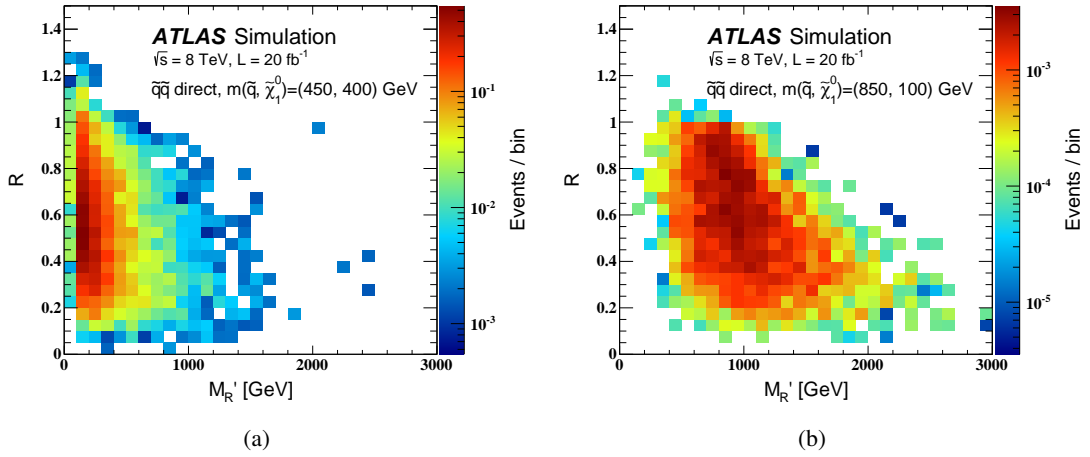


Figure 39: Distributions of the Razor variable R versus the characteristic mass in the R -frame M'_R for two points of the simplified model with squark-pair production assuming the direct decay of squarks, after requiring no leptons and at least two jets. Figure (a) shows the case where $m_{\tilde{q}} = 450$ GeV and $m_{LSP} = 400$ GeV, and (b) where $m_{\tilde{q}} = 850$ GeV and $m_{LSP} = 100$ GeV.

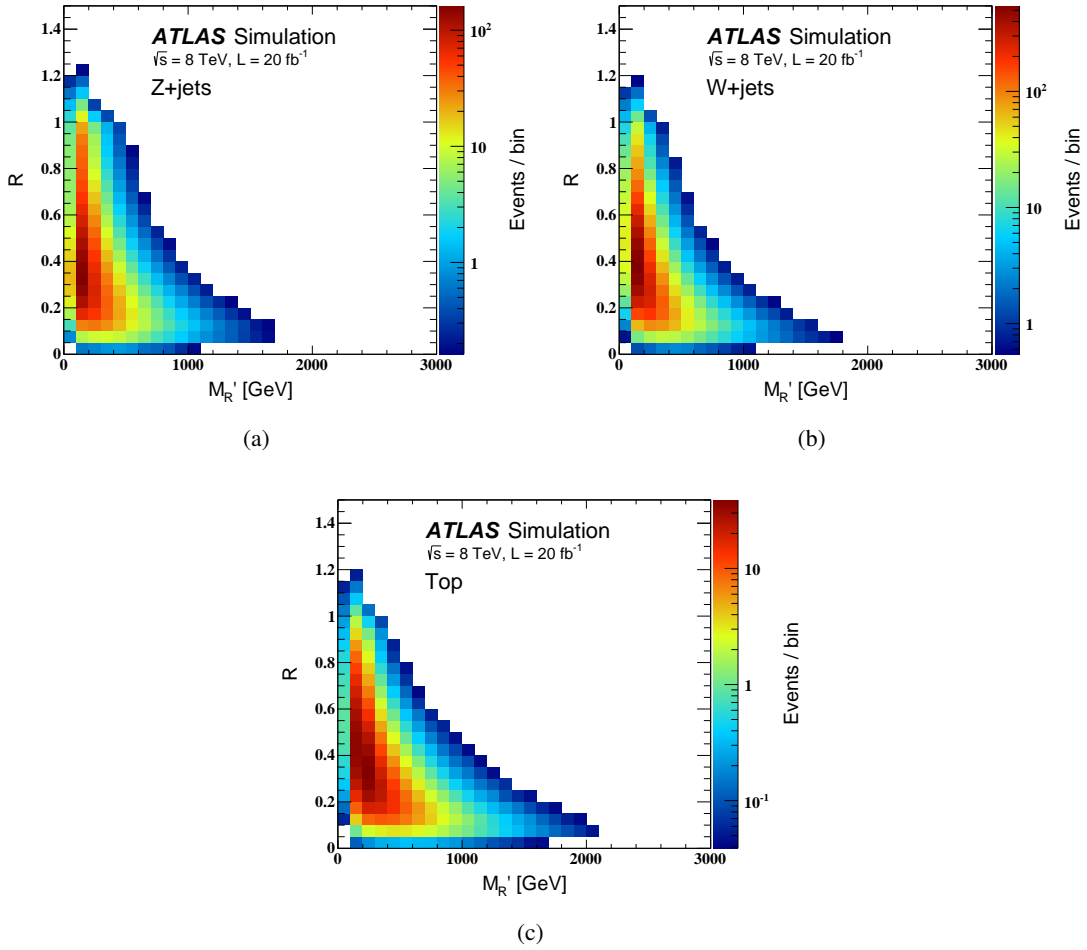


Figure 40: Distributions of the Razor variable R versus the characteristic mass in the R -frame M'_R for the dominant Standard Model backgrounds: (a) Z +jets, (b) W +jets and (c) $t\bar{t}$, after requiring no-leptons and at least two jets in the final state.

Since the variable M'_R is related to the mass difference between the squark and the neutralino, going from the small- Δm_{signal} to the large- Δm_{signal} , the events tend to populate higher M'_R regions. Extending this to all points of the model with squark-pair production followed by the direct decay of squarks, the average value of M'_R is approximately constant for a fixed mass splitting between the LSP and the squark, and increases with increasing Δm , while the average R -value tends to be around 0.5.

To select events for this search, the combination of two E_T^{miss} triggers, which are fully efficient in events having offline reconstructed $E_T^{\text{miss}} > 160$ GeV is used. Two signal regions which target different regions of the $(m_{\tilde{q}}, m_{\tilde{\chi}_1^0})$ plane are defined: SR_{loose} and SR_{tight} . Signal region SR_{loose} has a lower requirement on R and targets regions of the $(m_{\tilde{q}}, m_{\tilde{\chi}_1^0})$ plane with small mass splitting, which typically have softer visible objects. Signal region SR_{tight} was chosen to target high squark masses which typically contain harder visible objects. An overview of the selection criteria for these two signal regions is given in table 9.

C.3. Control and validation regions for SM background processes

The dominant SM background processes which contribute to the event counts in the signal regions are: Z +jets, W +jets, top quark pairs, and multiple jets. For each of these processes a dedicated control region is defined. The production of boson (W/Z) pairs in which at least one boson decays to charged leptons and/or neutrinos (referred to as ‘dibosons’ below), the single-top production, and the $t\bar{t}$ + W/Z boson production are small components of the total background and are estimated with MC simulated data.

Figure 40 shows the values of R and M'_R for the major SM backgrounds in this search. As previously discussed, the SM backgrounds tend to occupy regions with lower values of M'_R and R , which is taken into account while defining control regions for the main background processes. A summary of the selection criteria used to define the control and validation regions in this search is shown in table 23.

The largest potential background for a search with no leptons is expected to originate from the QCD-induced multi-jet event. However, the Razor variables were constructed to be able to distinguish this background from a SUSY-like signal, which minimizes the contribution of the multi-jet events after the SR event selection has been applied. To estimate the contribution of multi-jet background events in the final signal region selection, a data-driven technique [156], which applies a resolution function to well-measured multi-jet events in order to estimate the impact of jet energy mis-measurement and heavy-flavour semileptonic decays on E_T^{miss} and other variables, is used. Two dedicated control regions, $\text{CRQ}_{\text{loose}}$ and $\text{CRQ}_{\text{tight}}$, which use different selection criteria on R and $\Delta\phi(p_T^{j2}, E_T^{\text{miss}})$, correspond to the loose and tight signal regions respectively, and select samples of events with similar kinematics to the SR but enriched in multi-jet background events.

Since the QCD multi-jet background is significantly reduced by use of the Razor variables, the largest remaining backgrounds come from the production of W/Z bosons with additional jets and semileptonic $t\bar{t}$ decays, where the leptons can be mis-reconstructed as jets, non-prompt or be outside the lepton identification criteria. For each of these backgrounds a control region, rich in the respective process, is defined. The trigger requirements for these lepton-rich control regions follow those used by the corresponding control regions for the the 0L search [20]. The Razor variables are used to preselect a region which is dominated by the particular process. Following this preselection, to control the $t\bar{t}$ background, the control region CRT requires at least one jet tagged as a b -jet and exactly one electron or muon, while the W +jets control region, CRW, applies a veto on the presence of b -jets and requires exactly one electron or muon. In both cases the lepton is treated as a jet in the reconstruction of the Razor variables. This treatment of leptons as jets is motivated by the observation that $\sim 75\%$ of $W(\rightarrow \ell\nu)$ +jets and semileptonic $t\bar{t}$ events appearing in the SRs possess leptons which have fake jets, either through the misidentification of electrons or by the production of tau leptons decaying hadronically (identification of hadronic tau decays is not used in this analysis). The Z +jets control region, CRZ, is required to have exactly two opposite-sign same-flavour leptons. The Z +jets contribution to the signal region largely originates from Z decays to neutrinos. To mimic the behaviour of $Z \rightarrow \nu\nu$ in the control region, the two leptons have been treated as invisible and are used to re-calculate E_T^{miss} as $E_T^{\text{miss}'} = E_T^{\text{miss}} + p_T(\ell\ell)$ with the invariant mass of the leptons falling within a Z -mass window, $66 < m(\ell\ell) < 116$ GeV. The Razor variables are also calculated with this methodology where the leptons are treated as invisible objects.

To validate the normalization parameters extracted in the background control regions, validation regions VRZ , VRW , VRT , $\text{VRQ}_{\text{loose}}$ and $\text{VRQ}_{\text{tight}}$ for Z +jets, W +jets, $t\bar{t}$ and multi-jet backgrounds respectively, are defined (table 23). These validation regions are statistically independent from the signal and control regions previously defined, and are expected to have minimal contribution from any signal, if present.

Preselection			
Exactly two opposite-sign, same-flavour electrons or muons	Exactly one electron or muon	No leptons	No leptons
–	No b -jets	–	–
$66 < m(\ell\ell) < 116$ GeV	–	$p_T^{\text{jet}1,2} > 150$ GeV	$p_T^{\text{jet}1,2} > 200$ GeV
$E_T^{\text{miss}} = E_T^{\text{miss}} + p_T(\ell\ell)$	Treat lepton as a jet	–	–
0LRaz_CRZ	0LRaz_CRW	0LRaz_CRQ_loose	0LRaz_CRQ_tight
–	–	$\Delta\phi(p_T^{\text{jet}2}, E_T^{\text{miss}}) < 0.2$	$\Delta\phi(p_T^{\text{jet}2}, E_T^{\text{miss}}) < 0.2$
$0.3 < R < 0.55$	$0.3 < R < 0.55$	$0.35 < R < 0.45$	$0.5 < R < 0.55$
$M'_R > 800$ GeV	$M'_R > 800$ GeV	$M'_R > 1000$ GeV	$M'_R > 1000$ GeV
0LRaz_VRZ	0LRaz_VRW	0LRaz_VRQ_loose	0LRaz_VRQ_tight
–	–	$\Delta\phi(p_T^{\text{jet}2}, E_T^{\text{miss}}) < 0.4$	$\Delta\phi(p_T^{\text{jet}2}, E_T^{\text{miss}}) < 1.4$
$0.55 < R < 1.0$	$0.55 < R < 1.0$	$0.45 < R < 0.5$	$0.55 < R < 0.6$
$400 < M'_R < 1000$ GeV	$400 < M'_R < 1000$ GeV	$M'_R > 900$ GeV	$M'_R > 900$ GeV

Table 23: Overview of the selection criteria for the Z +jets, W +jets, semileptonic $t\bar{t}$ and multi-jet control regions (0LRaz_CRZ, 0LRaz_CRW, 0LRaz_CRZ and 0LRaz_CRQ_loose/tight respectively) and the corresponding validation regions (0LRaz_VRZ, 0LRaz_VRW, 0LRaz_VRT, 0LRaz_VRQ_loose/tight) used by the 0-lepton Razor analysis. Details of the construction of Razor variables M'_R and R can be found in the appendix C.1.

Following the definition of the control and validation regions, the backgrounds from Z +jets, W +jets, $t\bar{t}$ and multi-jet processes are estimated by using the background-only fit, as described in section 6. Figures 41 and 42 show the M'_R distributions for these control and validation regions after the fit. Good agreement is seen between the fitted and observed yields in all regions.

The Razor variable distributions, M'_R and R , for the SM backgrounds and a simplified model point with large- Δm_{signal} are shown in figure 43 for SR_{loose} and SR_{tight} .

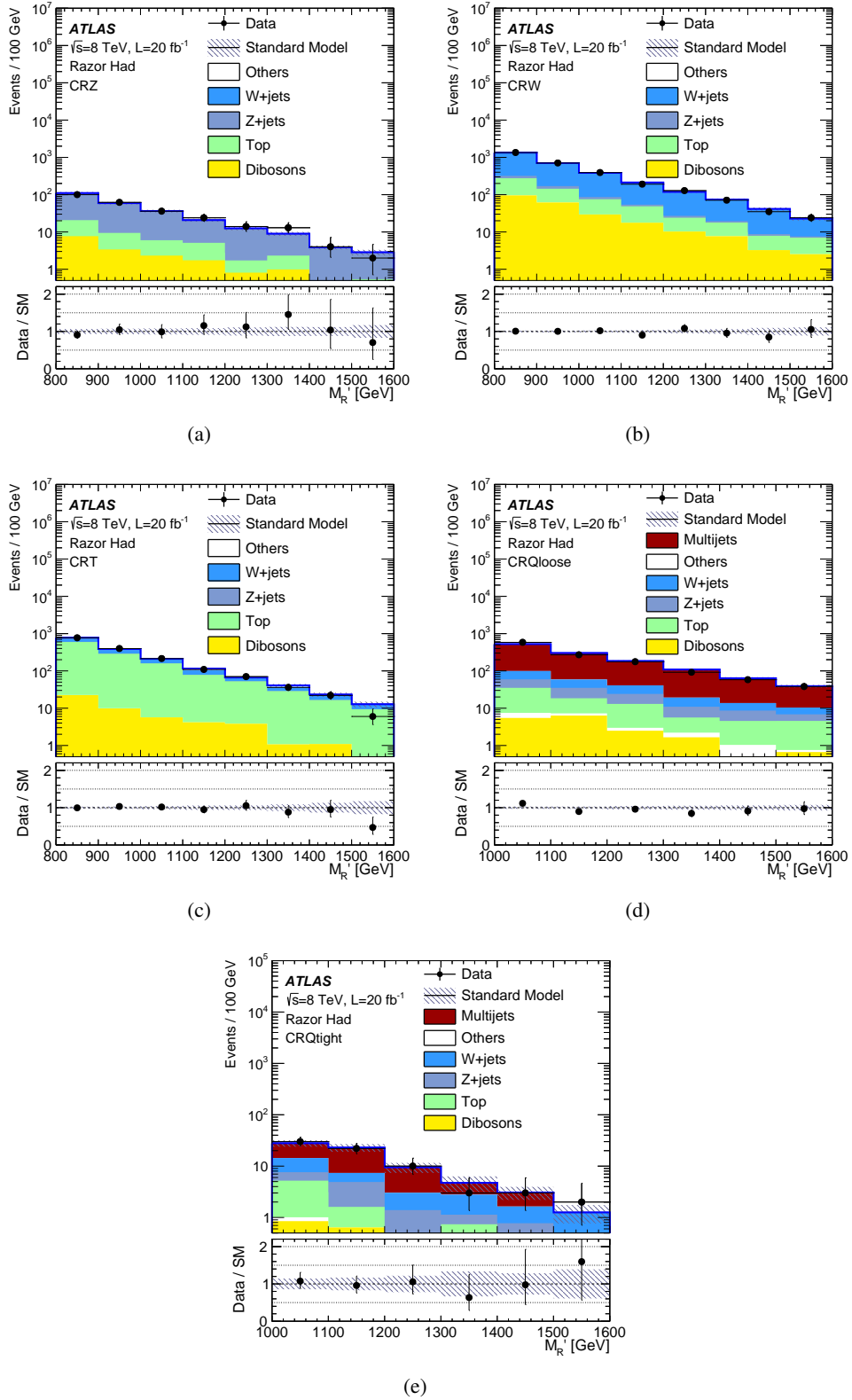


Figure 41: Observed M'_R distributions in control regions for (a) Z+jets, (b) W+jets, (c) $t\bar{t}$ and multi-jet backgrounds for (d) loose and (e) tight selection. The “Top” label includes all top-quark-related backgrounds ($t\bar{t}$, single top and $t\bar{t} + V$), while the “Others” includes the contributions of the jets misidentified as leptons or of non-prompt leptons, and the γ +jets background which is estimated with MC simulated data. All distributions are after the background-only fit has been performed.

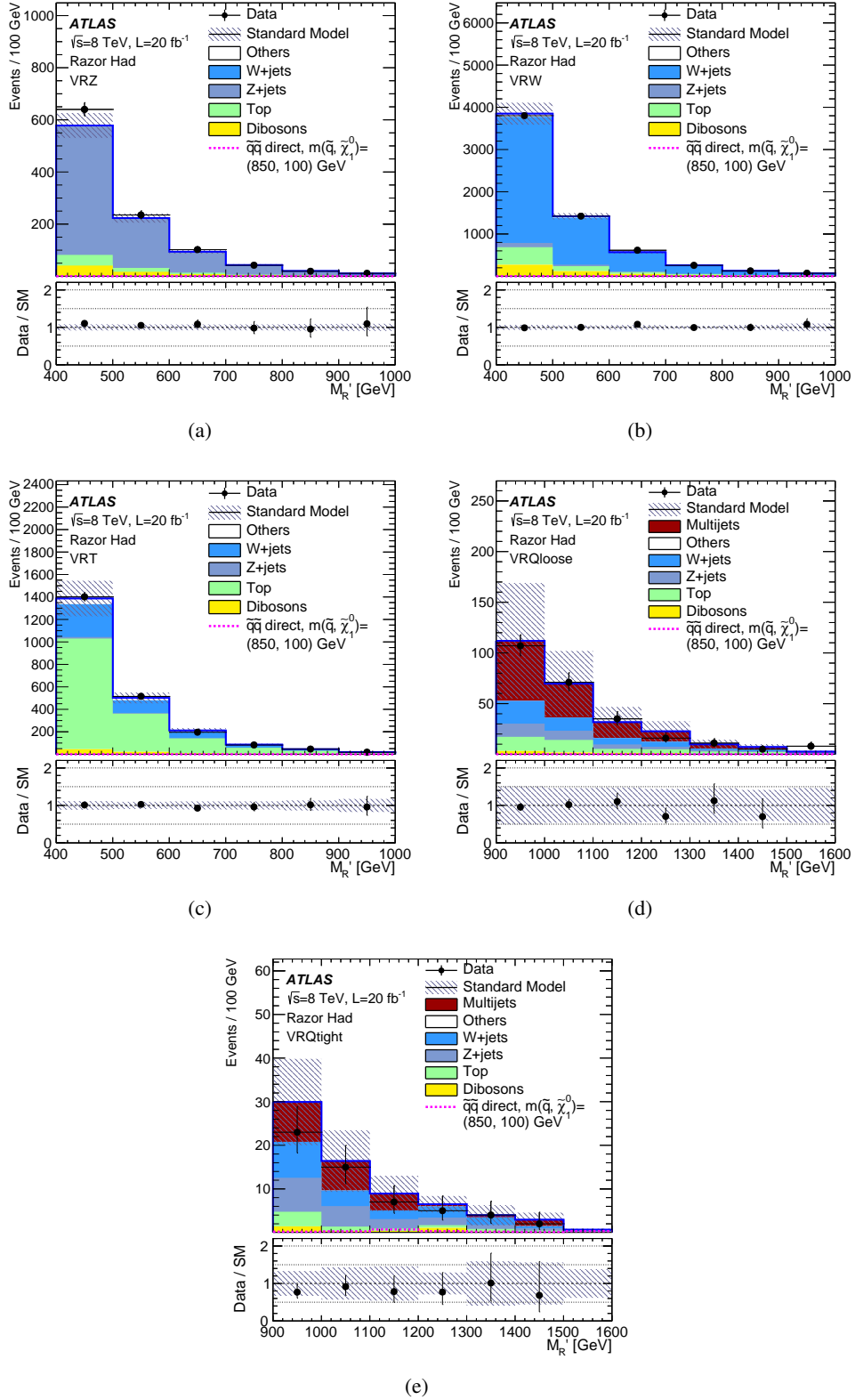


Figure 42: Observed M'_R distributions in validation regions for (a) Z+jets, (b) W+jets, (c) $t\bar{t}$ and multi-jet backgrounds for (d) loose and (e) tight selection. The “Top” label includes all top-quark-related backgrounds ($t\bar{t}$, single top and $t\bar{t} + V$), while the “Others” includes the contributions of the jets misidentified as leptons or of non-prompt leptons, and the γ +jets background which is estimated with MC simulated data. All distributions are after the background-only fit has been performed.

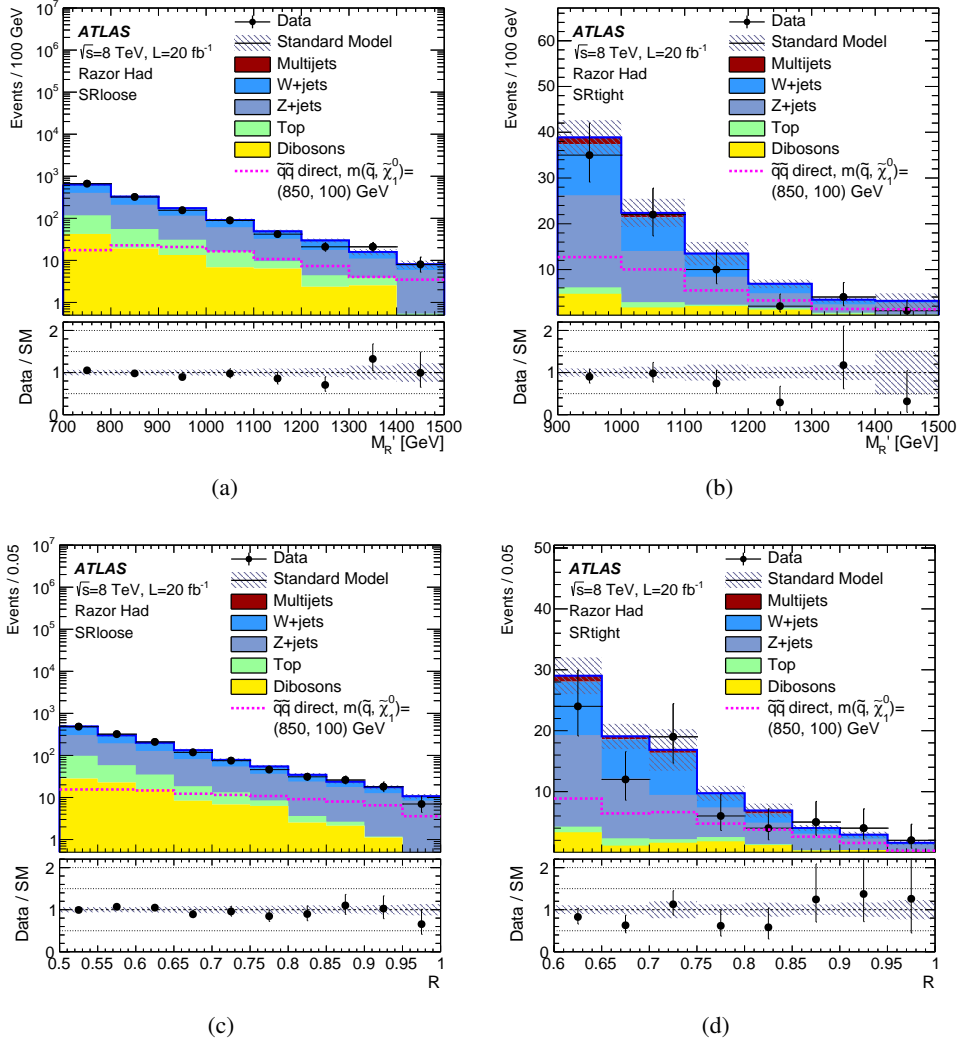


Figure 43: Observed (a, c) M'_R and (b, d) R distributions in (a, b) loose and (c, d) tight signal region selections listed in table 9. The “Top” label includes all top-quark-related backgrounds ($t\bar{t}$, single top and $t\bar{t} + V$). All distributions are after the background-only fit has been performed.

References

- [1] H. Miyazawa, ‘Baryon Number Changing Currents’, *Prog. Theor. Phys.* 36 (6) (1966) 1266, doi: [10.1143/PTP.36.1266](https://doi.org/10.1143/PTP.36.1266).
- [2] P. Ramond, ‘Dual Theory for Free Fermions’, *Phys. Rev. D* 3 (1971) 2415, doi: [10.1103/PhysRevD.3.2415](https://doi.org/10.1103/PhysRevD.3.2415).
- [3] Y. A. Golfand and E. P. Likhtman, ‘Extension of the Algebra of Poincare Group Generators and Violation of p Invariance’, *JETP Lett.* 13 (1971), [*Pisma Zh. Eksp. Teor. Fiz.* 13:452-455,1971] 323.
- [4] A. Neveu and J. H. Schwarz, ‘Factorizable dual model of pions’, *Nucl. Phys. B* 31 (1971) 86, doi: [10.1016/0550-3213\(71\)90448-2](https://doi.org/10.1016/0550-3213(71)90448-2).
- [5] A. Neveu and J. H. Schwarz, ‘Quark Model of Dual Pions’, *Phys. Rev. D* 4 (1971) 1109, doi: [10.1103/PhysRevD.4.1109](https://doi.org/10.1103/PhysRevD.4.1109).
- [6] J. Gervais and B. Sakita, ‘Field theory interpretation of supergauge in dual models’, *Nucl. Phys. B* 34 (1971) 632, doi: [10.1016/0550-3213\(71\)90351-8](https://doi.org/10.1016/0550-3213(71)90351-8).
- [7] D. V. Volkov and V. P. Akulov, ‘Is the Neutrino a Goldstone Particle?’, *Phys. Lett. B* 46 (1973) 109, doi: [10.1016/0370-2693\(73\)90490-5](https://doi.org/10.1016/0370-2693(73)90490-5).
- [8] J. Wess and B. Zumino, ‘A Lagrangian Model Invariant Under Supergauge Transformations’, *Phys. Lett. B* 49 (1974) 52, doi: [10.1016/0370-2693\(74\)90578-4](https://doi.org/10.1016/0370-2693(74)90578-4).
- [9] J. Wess and B. Zumino, ‘Supergauge Transformations in Four-Dimensions’, *Nucl. Phys. B* 70 (1974) 39, doi: [10.1016/0550-3213\(74\)90355-1](https://doi.org/10.1016/0550-3213(74)90355-1).
- [10] P. Fayet, ‘Supersymmetry and Weak, Electromagnetic and Strong Interactions’, *Phys. Lett. B* 64 (1976) 159, doi: [10.1016/0370-2693\(76\)90319-1](https://doi.org/10.1016/0370-2693(76)90319-1).
- [11] P. Fayet, ‘Spontaneously Broken Supersymmetric Theories of Weak, Electromagnetic and Strong Interactions’, *Phys. Lett. B* 69 (1977) 489, doi: [10.1016/0370-2693\(77\)90852-8](https://doi.org/10.1016/0370-2693(77)90852-8).
- [12] G. R. Farrar and P. Fayet, ‘Phenomenology of the Production, Decay, and Detection of New Hadronic States Associated with Supersymmetry’, *Phys. Lett. B* 76 (1978) 575, doi: [10.1016/0370-2693\(78\)90858-4](https://doi.org/10.1016/0370-2693(78)90858-4).
- [13] P. Fayet, ‘Relations Between the Masses of the Superpartners of Leptons and Quarks, the Goldstino Couplings and the Neutral Currents’, *Phys. Lett. B* 84 (1979) 416, doi: [10.1016/0370-2693\(79\)91229-2](https://doi.org/10.1016/0370-2693(79)91229-2).
- [14] L. Evans and P. Bryant, ‘LHC Machine’, *JINST* 3 (2008) S08001, doi: [10.1088/1748-0221/3/08/S08001](https://doi.org/10.1088/1748-0221/3/08/S08001).
- [15] S. Dimopoulos and H. Georgi, ‘Softly Broken Supersymmetry and SU(5)’, *Nucl. Phys. B* 193 (1981) 150, doi: [10.1016/0550-3213\(81\)90522-8](https://doi.org/10.1016/0550-3213(81)90522-8).
- [16] H. Goldberg, ‘Constraint on the photino mass from cosmology’, *Phys. Rev. Lett.* 50 (1983) 1419, doi: [10.1103/PhysRevLett.50.1419](https://doi.org/10.1103/PhysRevLett.50.1419).
- [17] ATLAS Collaboration, ‘The ATLAS Experiment at the CERN Large Hadron Collider’, *JINST* 3 (2008) S08003, doi: [10.1088/1748-0221/3/08/S08003](https://doi.org/10.1088/1748-0221/3/08/S08003).
- [18] ATLAS Collaboration, ‘ATLAS Run 1 searches for direct pair production of third-generation squarks at the Large Hadron Collider’, *Submitted to Eur. Phys. J. C* (2015), arXiv:[1506.08616](https://arxiv.org/abs/1506.08616) [[hep-ex](https://arxiv.org/abs/1506.08616)].

- [19] C. Rogan, ‘Kinematical variables towards new dynamics at the LHC’ (2010), arXiv:[1006.2727 \[hep-ph\]](#).
- [20] ATLAS Collaboration, ‘Search for squarks and gluinos with the ATLAS detector in final states with jets and missing transverse momentum using $\sqrt{s} = 8$ TeV proton–proton collision data’, *JHEP* 09 (2014) 176, doi: [10.1007/JHEP09\(2014\)176](#), arXiv:[1405.7875 \[hep-ex\]](#).
- [21] ATLAS Collaboration, ‘Search for Pair-Produced Third-Generation Squarks Decaying via Charm Quarks or in Compressed Supersymmetric Scenarios in pp Collisions at $\sqrt{s} = 8$ TeV with the ATLAS Detector’, *Phys. Rev. D* 90 (2014) 052008, doi: [10.1103/PhysRevD.90.052008](#), arXiv:[1407.0608 \[hep-ex\]](#).
- [22] ATLAS Collaboration, ‘Search for new phenomena in final states with large jet multiplicities and missing transverse momentum at $\sqrt{s}=8$ TeV proton-proton collisions using the ATLAS experiment’, *JHEP* 10 (2013) 130, doi: [10.1007/JHEP10\(2013\)130](#), [10.1007/JHEP01\(2014\)109](#), arXiv:[1308.1841 \[hep-ex\]](#).
- [23] ATLAS Collaboration, ‘Search for squarks and gluinos in events with isolated leptons, jets and missing transverse momentum at $\sqrt{s} = 8$ TeV with the ATLAS detector’, *JHEP* 04 (2015) 116, doi: [10.1007/JHEP04\(2015\)116](#), arXiv:[1501.03555 \[hep-ex\]](#).
- [24] ATLAS Collaboration, ‘Search for supersymmetry in events containing a same-flavour opposite-sign dilepton pair, jets, and large missing transverse momentum in $\sqrt{s} = 8$ TeV pp collisions with the ATLAS detector’, *Submitted to Eur. Phys. J. C* (2015), arXiv:[1503.03290 \[hep-ex\]](#).
- [25] ATLAS Collaboration, ‘Search for supersymmetry at $\sqrt{s}=8$ TeV in final states with jets and two same-sign leptons or three leptons with the ATLAS detector’, *JHEP* 06 (2014) 035, doi: [10.1007/JHEP06\(2014\)035](#), arXiv:[1404.2500 \[hep-ex\]](#).
- [26] ATLAS Collaboration, ‘Search for supersymmetry in events with large missing transverse momentum, jets, and at least one tau lepton in 20 fb^{-1} of $\sqrt{s} = 8$ TeV proton-proton collision data with the ATLAS detector’, *JHEP* 09 (2014) 103, doi: [10.1007/JHEP09\(2014\)103](#), arXiv:[1407.0603 \[hep-ex\]](#).
- [27] ATLAS Collaboration, ‘Search for strong production of supersymmetric particles in final states with missing transverse momentum and at least three b -jets at $\sqrt{s}= 8$ TeV proton-proton collisions with the ATLAS detector’, *JHEP* 10 (2014) 24, doi: [10.1007/JHEP10\(2014\)024](#), arXiv:[1407.0600 \[hep-ex\]](#).
- [28] P. Fayet and J. Iliopoulos, ‘Spontaneously Broken Supergauge Symmetries and Goldstone Spinors’, *Phys. Lett. B* 51 (1974) 461, doi: [10.1016/0370-2693\(74\)90310-4](#).
- [29] P. Fayet, ‘Supergauge Invariant Extension of the Higgs Mechanism and a Model for the electron and Its Neutrino’, *Nucl. Phys. B* 90 (1975) 104, doi: [10.1016/0550-3213\(75\)90636-7](#).
- [30] L. O’Raifeartaigh, ‘Spontaneous Symmetry Breaking for Chiral Scalar Superfields’, *Nucl. Phys. B* 96 (1975) 331, doi: [10.1016/0550-3213\(75\)90585-4](#).
- [31] A. H. Chamseddine, R. L. Arnowitt and P. Nath, ‘Locally Supersymmetric Grand Unification’, *Phys. Rev. Lett.* 49 (1982) 970, doi: [10.1103/PhysRevLett.49.970](#).
- [32] R. Barbieri, S. Ferrara and C. A. Savoy, ‘Gauge Models with Spontaneously Broken Local Supersymmetry’, *Phys. Lett. B* 119 (1982) 343, doi: [10.1016/0370-2693\(82\)90685-2](#).

- [33] L. E. Ibanez, ‘Locally Supersymmetric SU(5) Grand Unification’, *Phys. Lett. B* 118 (1982) 73, doi: [10.1016/0370-2693\(82\)90604-9](https://doi.org/10.1016/0370-2693(82)90604-9).
- [34] L. J. Hall, J. D. Lykken and S. Weinberg, ‘Supergravity as the Messenger of Supersymmetry Breaking’, *Phys. Rev. D* 27 (1983) 2359–2378, doi: [10.1103/PhysRevD.27.2359](https://doi.org/10.1103/PhysRevD.27.2359).
- [35] N. Ohta, ‘Grand unified theories based on local supersymmetry’, *Prog. Theor. Phys.* 70 (1983) 542, doi: [10.1143/PTP.70.542](https://doi.org/10.1143/PTP.70.542).
- [36] G. L. Kane et al., ‘Study of constrained minimal supersymmetry’, *Phys. Rev. D* 49 (1994) 6173, doi: [10.1103/PhysRevD.49.6173](https://doi.org/10.1103/PhysRevD.49.6173), arXiv:[9312272](https://arxiv.org/abs/9312272) [hep-ph].
- [37] M. Dine and W. Fischler, ‘A Phenomenological Model of Particle Physics Based on Supersymmetry’, *Phys. Lett. B* 110 (1982) 227, doi: [10.1016/0370-2693\(82\)91241-2](https://doi.org/10.1016/0370-2693(82)91241-2).
- [38] L. Alvarez-Gaume, M. Claudson and M. B. Wise, ‘Low-Energy Supersymmetry’, *Nucl. Phys. B* 207 (1982) 96, doi: [10.1016/0550-3213\(82\)90138-9](https://doi.org/10.1016/0550-3213(82)90138-9).
- [39] C. R. Nappi and B. A. Ovrut, ‘Supersymmetric Extension of the SU(3)×SU(2)×U(1) Model’, *Phys. Lett. B* 113 (1982) 175, doi: [10.1016/0370-2693\(82\)90418-X](https://doi.org/10.1016/0370-2693(82)90418-X).
- [40] M. Dine and A. E. Nelson, ‘Dynamical supersymmetry breaking at low-energies’, *Phys. Rev. D* 48 (1993) 1277, doi: [10.1103/PhysRevD.48.1277](https://doi.org/10.1103/PhysRevD.48.1277), arXiv:[9303230](https://arxiv.org/abs/9303230) [hep-ph].
- [41] M. Dine, A. E. Nelson and Y. Shirman, ‘Low-energy dynamical supersymmetry breaking simplified’, *Phys. Rev. D* 51 (1995) 1362, doi: [10.1103/PhysRevD.51.1362](https://doi.org/10.1103/PhysRevD.51.1362), arXiv:[9408384](https://arxiv.org/abs/9408384) [hep-ph].
- [42] M. Dine et al., ‘New tools for low-energy dynamical supersymmetry breaking’, *Phys. Rev. D* 53 (1996) 2658, doi: [10.1103/PhysRevD.53.2658](https://doi.org/10.1103/PhysRevD.53.2658), arXiv:[9507378](https://arxiv.org/abs/9507378) [hep-ph].
- [43] G. F. Giudice et al., ‘Gaugino mass without singlets’, *JHEP* 12 (1998) 027, doi: [10.1088/1126-6708/1998/12/027](https://doi.org/10.1088/1126-6708/1998/12/027), arXiv:[9810442](https://arxiv.org/abs/9810442) [hep-ph].
- [44] L. Randall and R. Sundrum, ‘Out of this world supersymmetry breaking’, *Nucl. Phys. B* 557 (1999) 79, doi: [10.1016/S0550-3213\(99\)00359-4](https://doi.org/10.1016/S0550-3213(99)00359-4), arXiv:[9810155](https://arxiv.org/abs/9810155) [hep-th].
- [45] J. Alwall, P. Schuster and N. Toro, ‘Simplified Models for a First Characterization of New Physics at the LHC’, *Phys. Rev. D* 79 (2009) 075020, doi: [10.1103/PhysRevD.79.075020](https://doi.org/10.1103/PhysRevD.79.075020), arXiv:[0810.3921](https://arxiv.org/abs/0810.3921) [hep-ph].
- [46] D. Alves et al., ‘Simplified Models for LHC New Physics Searches’, *J. Phys. G: Nucl. Part. Phys.* 39 (2012) 105005, doi: [10.1088/0954-3899/39/10/105005](https://doi.org/10.1088/0954-3899/39/10/105005), arXiv:[1105.2838](https://arxiv.org/abs/1105.2838) [hep-ph].
- [47] T. Appelquist, H.-C. Cheng and B. A. Dobrescu, ‘Bounds on Universal Extra Dimensions’, *Phys. Rev. D* 64 (2001) 35002, doi: [10.1103/PhysRevD.64.035002](https://doi.org/10.1103/PhysRevD.64.035002).
- [48] H.-C. Cheng, K. Matchev and M. Schmaltz, ‘Bosonic Supersymmetry? Getting Fooled at the LHC’, *Phys. Rev. D* 66 (2002) 56006, doi: [10.1103/PhysRevD.66.056006](https://doi.org/10.1103/PhysRevD.66.056006).
- [49] A. Djouadi et al., ‘The Minimal supersymmetric standard model: Group summary report’ (1998), arXiv:[9901246](https://arxiv.org/abs/9901246) [hep-ph].
- [50] C. F. Berger et al., ‘Supersymmetry Without Prejudice’, *JHEP* 02 (2009) 023, doi: [10.1088/1126-6708/2009/02/023](https://doi.org/10.1088/1126-6708/2009/02/023), arXiv:[0812.0980](https://arxiv.org/abs/0812.0980) [hep-ph].

- [51] M. W. Cahill-Rowley et al., ‘The New Look pMSSM with Neutralino and Gravitino LSPs’, *Eur. Phys. J. C* 72 (2012) 2156, doi: [10.1140/epjc/s10052-012-2156-1](https://doi.org/10.1140/epjc/s10052-012-2156-1), arXiv:[1206.4321](https://arxiv.org/abs/1206.4321) [hep-ph].
- [52] S. Roy and B. Mukhopadhyaya, ‘Some Implications of a Supersymmetric Model with R-Parity Breaking Bilinear Interactions’, *Phys. Rev. D* 55 (1997) 7020, doi: [10.1103/PhysRevD.55.7020](https://doi.org/10.1103/PhysRevD.55.7020).
- [53] J. Barnard et al., ‘Natural gauge mediation with a bino NLSP at the LHC’, *Phys. Rev. Lett.* 109 (2012) 241801, arXiv:[1208.6062](https://arxiv.org/abs/1208.6062) [hep-ph].
- [54] L. Covi and S. Kraml, ‘Collider signatures of gravitino dark matter with a sneutrino NLSP’, *JHEP* 08 (2007) 015, doi: [10.1088/1126-6708/2007/08/015](https://doi.org/10.1088/1126-6708/2007/08/015), arXiv:[0703130](https://arxiv.org/abs/0703130) [hep-ph].
- [55] G. D’Ambrosio et al., ‘Minimal Flavor Violation: An Effective Field Theory Approach’, *Nucl. Phys. B* 645 (2002) 155, doi: [10.1016/S0550-3213\(02\)00836-2](https://doi.org/10.1016/S0550-3213(02)00836-2), arXiv:[0207036](https://arxiv.org/abs/0207036) [hep-ph].
- [56] D. Carvalho, M. Gomez and J. Romao, ‘Charged Lepton Flavor Violation in Supersymmetry with Bilinear R-Parity Violation’, *Phys. Rev. D* 65 (2002) 093013, doi: [10.1103/PhysRevD.65.093013](https://doi.org/10.1103/PhysRevD.65.093013), arXiv:[0202054](https://arxiv.org/abs/0202054) [hep-ph].
- [57] Y. Grossman and S. Rakshit, ‘Neutrino masses in R-parity violating supersymmetric models’, *Phys. Rev. D* 69 (2004) 093002, doi: [10.1103/PhysRevD.69.093002](https://doi.org/10.1103/PhysRevD.69.093002), arXiv:[0311310](https://arxiv.org/abs/0311310) [hep-ph].
- [58] ATLAS Collaboration, ‘Search for supersymmetry with jets, missing transverse momentum and at least one hadronically decaying τ lepton in proton-proton collisions at $\sqrt{s} = 7$ TeV with the ATLAS detector’, *Phys. Lett. B* 714 (2012) 197, doi: [10.1016/j.physletb.2012.06.061](https://doi.org/10.1016/j.physletb.2012.06.061), arXiv:[1204.3852](https://arxiv.org/abs/1204.3852) [hep-ex].
- [59] ATLAS Collaboration, ‘Search for Events with Large Missing Transverse Momentum, Jets, and at least Two Tau Leptons in 7 TeV Proton-Proton Collision Data with the ATLAS Detector’, *Phys. Lett. B* 714 (2012) 180, doi: [10.1016/j.physletb.2012.06.055](https://doi.org/10.1016/j.physletb.2012.06.055), arXiv:[1203.6580](https://arxiv.org/abs/1203.6580) [hep-ex].
- [60] ATLAS Collaboration, ‘Further Search for Supersymmetry at $\sqrt{s} = 7$ TeV in Final States with Jets, Missing Transverse Momentum and Isolated Leptons with the ATLAS Detector’, *Phys. Rev. D* 86 (2012) 092002, doi: [10.1103/PhysRevD.86.092002](https://doi.org/10.1103/PhysRevD.86.092002), arXiv:[1208.4688](https://arxiv.org/abs/1208.4688) [hep-ex].
- [61] P. Meade, N. Seiberg and D. Shih, ‘General Gauge Mediation’, *Prog. Theor. Phys. Suppl.* 177 (2009) 143, arXiv:[0801.3278](https://arxiv.org/abs/0801.3278) [hep-ph].
- [62] M. Buican et al., ‘Exploring General Gauge Mediation’, *JHEP* 03 (2009) 016, doi: [10.1088/1126-6708/2009/03/016](https://doi.org/10.1088/1126-6708/2009/03/016), arXiv:[0812.3668](https://arxiv.org/abs/0812.3668) [hep-ph].
- [63] J. Barnard et al., ‘Natural Gauge Mediation with a Bino NLSP at the LHC’, *Phys. Rev. Lett.* 109 (2012) 241801, arXiv:[1208.6062](https://arxiv.org/abs/1208.6062) [hep-ph].
- [64] M. Asano et al., ‘Natural Supersymmetry at the LHC’, *JHEP* 12 (2010) 019, doi: [10.1007/JHEP12\(2010\)019](https://doi.org/10.1007/JHEP12(2010)019), arXiv:[1010.0692](https://arxiv.org/abs/1010.0692) [hep-ph].
- [65] M. Gabella, T. Gherghetta and J. Giedt, ‘A Gravity Dual and LHC Study of Single-Sector Supersymmetry Breaking’, *Phys. Rev. D* 76 (2007) 055001, doi: [10.1103/PhysRevD.76.055001](https://doi.org/10.1103/PhysRevD.76.055001), arXiv:[0704.3571](https://arxiv.org/abs/0704.3571) [hep-ph].

- [66] N. Craig, M. McCullough and J. Thaler, ‘Flavor Mediation Delivers Natural SUSY’, *JHEP* 06 (2012) 046, arXiv:[1203.1622 \[hep-ph\]](#).
- [67] T. J. LeCompte and S. P. Martin, ‘Large Hadron Collider Reach for Supersymmetric Models with Compressed Mass Spectra’, *Phys. Rev. D* 84 (2011) 015004, doi: [10.1103/PhysRevD.84.015004](#), arXiv:[1105.4304 \[hep-ph\]](#).
- [68] T. J. LeCompte and S. P. Martin, ‘Compressed supersymmetry after 1/fb at the Large Hadron Collider’, *Phys. Rev. D* 85 (2012) 035023, doi: [10.1103/PhysRevD.85.035023](#), arXiv:[1111.6897 \[hep-ph\]](#).
- [69] R. Mahbubani et al., ‘Light Nondegenerate Squarks at the LHC’, *Phys. Rev. Lett.* 110 (2013) 151804, doi: [10.1103/PhysRevLett.110.151804](#), arXiv:[1212.3328 \[hep-ph\]](#).
- [70] M. Toharia and J. D. Wells, ‘Gluino Decays with Heavier Scalar Superpartners’, *JHEP* 02 (2006) 015, doi: [10.1088/1126-6708/2006/02/015](#), arXiv:[0503175 \[hep-ph\]](#).
- [71] ATLAS Collaboration, ‘Performance of the ATLAS Trigger System in 2010’, *Eur. Phys. J. C* 72 (2012) 1849, doi: [10.1140/epjc/s10052-011-1849-1](#), arXiv:[1110.1530 \[hep-ex\]](#).
- [72] ATLAS Collaboration, ‘Improved Luminosity Determination in pp Collisions at $\sqrt{s} = 7$ TeV using the ATLAS detector at the LHC’, *Eur. Phys. J. C* 73 (2013) 2518, doi: [10.1140/epjc/s10052-013-2518-3](#), arXiv:[1302.4393 \[hep-ex\]](#).
- [73] ATLAS Collaboration, ‘Measurements of Top Quark Pair Relative Differential Cross-sections with ATLAS in pp Collisions at $\sqrt{s} = 7$ TeV’, *Eur. Phys. J. C* 73 (2013) 2261, doi: [10.1140/epjc/s10052-012-2261-1](#), arXiv:[1207.5644 \[hep-ex\]](#).
- [74] ATLAS Collaboration, ‘Measurements of Normalized Differential Cross Sections for $t\bar{t}$ Production in pp Collisions at $\sqrt{s} = 7$ TeV using the ATLAS Detector’, *Phys. Rev. D* 90 (2014) 072004, doi: [10.1103/PhysRevD.90.072004](#), arXiv:[1407.0371 \[hep-ex\]](#).
- [75] T. Gleisberg et al., ‘Event Generation with SHERPA 1.1’, *JHEP* 02 (2009) 007, doi: [10.1088/1126-6708/2009/02/007](#), arXiv:[0811.4622 \[hep-ph\]](#).
- [76] S. Catani et al., ‘Vector Boson Production at Hadron Colliders: A Fully Exclusive QCD Calculation at NNLO’, *Phys. Rev. Lett.* 103 (2009) 082001, doi: [10.1103/PhysRevLett.103.082001](#), arXiv:[0903.2120 \[hep-ph\]](#).
- [77] H.-L. Lai et al., ‘New Parton Distributions for Collider Physics’, *Phys. Rev. D* 82 (2010) 074024, doi: [10.1103/PhysRevD.82.074024](#), arXiv:[1007.2241 \[hep-ph\]](#).
- [78] K. Melnikov and F. Petriello, ‘Electroweak Gauge Boson Production at Hadron Colliders through $O(\alpha_S^2)$ ’, *Phys. Rev. D* 74 (2006) 114017, doi: [10.1103/PhysRevD.74.114017](#), arXiv:[0609070 \[hep-ph\]](#).
- [79] M. L. Mangano et al., ‘ALPGEN, a Generator for Hard Multiparton Processes in Hadronic Collisions’, *JHEP* 07 (2003) 001, doi: [doi:10.1088/1126-6708/2003/07/001](#), arXiv:[0206293 \[hep-ph\]](#).
- [80] ATLAS Collaboration, ‘New ATLAS Event Generator Tunes to 2010 Data’, *ATL-PHYS-PUB-2011-008* (2011), <http://cdsweb.cern.ch/record/1345343>.

- [81] J. Pumplin et al., ‘New Generation of Parton Distributions with Uncertainties from Global QCD Analysis’, *JHEP* 07 (2002) 012, doi: [10.1088/1126-6708/2002/07/012](https://doi.org/10.1088/1126-6708/2002/07/012), arXiv:[0201195](https://arxiv.org/abs/0201195) [[hep-ph](#)].
- [82] G. Corcella et al., ‘HERWIG 6.5: An Event Generator for Hadron Emission Reactions With Interfering Gluons (Including Supersymmetric Processes)’, *JHEP* 01 (2001) 010, doi: [10.1088/1126-6708/2001/01/010](https://doi.org/10.1088/1126-6708/2001/01/010), arXiv:[0011363](https://arxiv.org/abs/0011363) [[hep-ph](#)].
- [83] G Corcella et al., ‘HERWIG 6.5 release note’ (2002), arXiv:[0210213](https://arxiv.org/abs/0210213) [[hep-ph](#)].
- [84] J. Butterworth, J. R. Forshaw and M. Seymour, ‘Multiparton Interactions in Photoproduction at HERA’, *Z. Phys. C* 72 (1996) 637, doi: [10.1007/s002880050286](https://doi.org/10.1007/s002880050286), arXiv:[9601371](https://arxiv.org/abs/9601371) [[hep-ph](#)].
- [85] P. Nason, ‘A New Method for Combining NLO QCD with Shower Monte Carlo Algorithms’, *JHEP* 11 (2004) 040, doi: [10.1088/1126-6708/2004/11/040](https://doi.org/10.1088/1126-6708/2004/11/040), arXiv:[0409146](https://arxiv.org/abs/0409146) [[hep-ph](#)].
- [86] S. Frixione, P. Nason and C. Oleari, ‘Matching NLO QCD Computations with Parton Shower Simulations: the POWHEG Method’, *JHEP* 11 (2007) 070, doi: [10.1088/1126-6708/2007/11/070](https://doi.org/10.1088/1126-6708/2007/11/070), arXiv:[0709.2092](https://arxiv.org/abs/0709.2092) [[hep-ph](#)].
- [87] S. Alioli et al., ‘A General Framework for Implementing NLO Calculations in Shower Monte Carlo Programs: the POWHEG BOX’, *JHEP* 06 (2010) 043, doi: [10.1007/JHEP06\(2010\)043](https://doi.org/10.1007/JHEP06(2010)043), arXiv:[1002.2581](https://arxiv.org/abs/1002.2581) [[hep-ph](#)].
- [88] M. Czakon, P. Fiedler and A. Mitov, ‘Total Top-Quark Pair-Production Cross Section at Hadron Colliders Through $O(\alpha_s^4)$ ’, *Phys. Rev. Lett.* 110 (2013) 252004, doi: [10.1103/PhysRevLett.110.252004](https://doi.org/10.1103/PhysRevLett.110.252004), arXiv:[1303.6254](https://arxiv.org/abs/1303.6254) [[hep-ph](#)].
- [89] M. Czakon and A. Mitov, ‘Top++: A Program for the Calculation of the Top-Pair Cross-Section at Hadron Colliders’, *Comput. Phys. Commun.* 185 (2014) 2930, doi: [10.1016/j.cpc.2014.06.021](https://doi.org/10.1016/j.cpc.2014.06.021), arXiv:[1112.5675](https://arxiv.org/abs/1112.5675) [[hep-ph](#)].
- [90] T. Sjostrand, S. Mrenna and P. Z. Skands, ‘PYTHIA 6.4 Physics and Manual’, *JHEP* 05 (2006) 026, doi: [10.1088/1126-6708/2006/05/026](https://doi.org/10.1088/1126-6708/2006/05/026), arXiv:[0603175](https://arxiv.org/abs/0603175) [[hep-ph](#)].
- [91] B. Cooper et al., ‘Importance of a Consistent Choice of α_s in the Matching of AlpGen and Pythia’, *Eur. Phys. J. C* 72 (2012) 2078, doi: [10.1140/epjc/s10052-012-2078-y](https://doi.org/10.1140/epjc/s10052-012-2078-y), arXiv:[1109.5295](https://arxiv.org/abs/1109.5295) [[hep-ph](#)].
- [92] P. Z. Skands, ‘Tuning Monte Carlo Generators: The Perugia Tunes’, *Phys. Rev. D* 82 (2010) 074018, doi: [10.1103/PhysRevD.82.074018](https://doi.org/10.1103/PhysRevD.82.074018), arXiv:[1005.3457](https://arxiv.org/abs/1005.3457) [[hep-ph](#)].
- [93] B. P. Kersevan and E. Richter-Was, ‘The Monte Carlo event generator AcerMC versions 2.0 to 3.8 with interfaces to PYTHIA 6.4, HERWIG 6.5 and ARIADNE 4.1’, *Comput. Phys. Commun.* 184 (2013) 919–985, doi: [10.1016/j.cpc.2012.10.032](https://doi.org/10.1016/j.cpc.2012.10.032), arXiv:[0405247](https://arxiv.org/abs/0405247) [[hep-ph](#)].
- [94] N. Kidonakis, ‘Next-to-Next-to-Leading-Order Collinear and Soft Gluon Corrections for t-channel Single Top Quark Production’, *Phys. Rev. D* 83 (2011) 091503, doi: [10.1103/PhysRevD.83.091503](https://doi.org/10.1103/PhysRevD.83.091503), arXiv:[1103.2792](https://arxiv.org/abs/1103.2792) [[hep-ph](#)].
- [95] ATLAS Collaboration, ‘Further ATLAS tunes of PYTHIA 6 and Pythia 8’, *ATL-PHYS-PUB-2011-014* (2011), URL: <http://cds.cern.ch/record/1400677>.

- [96] S. Frixione and B. R. Webber, ‘Matching NLO QCD computations and parton shower simulations’, *JHEP* 06 (2002) 029, doi: [10.1088/1126-6708/2002/06/029](https://doi.org/10.1088/1126-6708/2002/06/029), arXiv:[0204244](https://arxiv.org/abs/0204244) [[hep-ph](#)].
- [97] S. Frixione, P. Nason and B. R. Webber, ‘Matching NLO QCD and Parton Showers in Heavy Flavour Production’, *JHEP* 08 (2003) 007, doi: [10.1088/1126-6708/2003/08/007](https://doi.org/10.1088/1126-6708/2003/08/007), arXiv:[0305252](https://arxiv.org/abs/0305252) [[hep-ph](#)].
- [98] N. Kidonakis, ‘NNLL Resummation for s-channel Single Top Quark Production’, *Phys. Rev. D* 81 (2010) 054028, doi: [10.1103/PhysRevD.81.054028](https://doi.org/10.1103/PhysRevD.81.054028), arXiv:[1001.5034](https://arxiv.org/abs/1001.5034) [[hep-ph](#)].
- [99] N. Kidonakis, ‘Two-Loop Soft Anomalous Dimensions for Single Top Quark Associated Production with a W^- or H^- ’, *Phys. Rev. D* 82 (2010) 054018, doi: [10.1103/PhysRevD.82.054018](https://doi.org/10.1103/PhysRevD.82.054018), arXiv:[1005.4451](https://arxiv.org/abs/1005.4451) [[hep-ph](#)].
- [100] J. Alwall et al., ‘MadGraph 5 : Going Beyond’, *JHEP* 06 (2011) 128, doi: [10.1007/JHEP06\(2011\)128](https://doi.org/10.1007/JHEP06(2011)128), arXiv:[1106.0522](https://arxiv.org/abs/1106.0522) [[hep-ph](#)].
- [101] A. Lazopoulos et al., ‘Next-to-Leading Order QCD Corrections to $t\bar{t}Z$ Production at the LHC’, *Phys. Lett. B* 666 (2008) 62, doi: [10.1016/j.physletb.2008.06.073](https://doi.org/10.1016/j.physletb.2008.06.073), arXiv:[0804.2220](https://arxiv.org/abs/0804.2220) [[hep-ph](#)].
- [102] M. Garzelli et al., ‘ $t\bar{t}W^\pm$ and $t\bar{t}Z$ Hadroproduction at NLO Accuracy in QCD with Parton Shower and Hadronization Effects’, *JHEP* 11 (2012) 056, doi: [10.1007/JHEP11\(2012\)056](https://doi.org/10.1007/JHEP11(2012)056), arXiv:[1208.2665](https://arxiv.org/abs/1208.2665) [[hep-ph](#)].
- [103] J. M. Campbell and R. K. Ellis, ‘ $t\bar{t}W^\pm$ Production and Decay at NLO’, *JHEP* 07 (2012) 052, doi: [10.1007/JHEP07\(2012\)052](https://doi.org/10.1007/JHEP07(2012)052), arXiv:[1204.5678](https://arxiv.org/abs/1204.5678) [[hep-ph](#)].
- [104] J. M. Campbell and R. K. Ellis, ‘An Update on Vector Boson Pair Production at Hadron Colliders’, *Phys. Rev. D* 60 (1999) 113006, doi: [10.1103/PhysRevD.60.113006](https://doi.org/10.1103/PhysRevD.60.113006), arXiv:[9905386](https://arxiv.org/abs/9905386) [[hep-ph](#)].
- [105] J. M. Campbell, R. K. Ellis and C. Williams, ‘Vector Boson Pair Production at the LHC’, *JHEP* 07 (2011) 018, doi: [10.1007/JHEP07\(2011\)018](https://doi.org/10.1007/JHEP07(2011)018), arXiv:[1105.0020](https://arxiv.org/abs/1105.0020) [[hep-ph](#)].
- [106] M. Bähr et al., ‘Herwig++ Physics and Manual’, *Eur. Phys. J. C* 58 (2008) 639, doi: [10.1140/epjc/s10052-008-0798-9](https://doi.org/10.1140/epjc/s10052-008-0798-9), arXiv:[0803.0883](https://arxiv.org/abs/0803.0883) [[hep-ph](#)].
- [107] M. L. Mangano et al., ‘Matching Matrix Elements and Shower Evolution for Top-Quark Production in Hadronic Collisions’, *JHEP* 01 (2007) 013, doi: [10.1088/1126-6708/2007/01/013](https://doi.org/10.1088/1126-6708/2007/01/013), arXiv:[0611129](https://arxiv.org/abs/0611129) [[hep-ph](#)].
- [108] S. Gieseke, C. Rohr and A. Siodmok, ‘Colour Reconnections in Herwig++’, *Eur. Phys. J. C* 72 (2012) 2225, doi: [10.1140/epjc/s10052-012-2225-5](https://doi.org/10.1140/epjc/s10052-012-2225-5), arXiv:[1206.0041](https://arxiv.org/abs/1206.0041) [[hep-ph](#)].
- [109] W. Beenakker et al., ‘Squark and Gluino Production at Hadron Colliders’, *Nucl. Phys. B* 492 (1997) 51, doi: [10.1016/S0550-3213\(97\)00084-9](https://doi.org/10.1016/S0550-3213(97)00084-9), arXiv:[9610490](https://arxiv.org/abs/9610490) [[hep-ph](#)].
- [110] A. Kulesza and L. Motyka, ‘Threshold Resummation for Squark-Antisquark and Gluino-Pair Production at the LHC’, *Phys. Rev. Lett.* 102 (2009) 111802, doi: [10.1103/PhysRevLett.102.111802](https://doi.org/10.1103/PhysRevLett.102.111802), arXiv:[0807.2405](https://arxiv.org/abs/0807.2405) [[hep-ph](#)].

- [111] A. Kulesza and L. Motyka, ‘Soft gluon resummation for the production of gluino-gluino and squark-antisquark pairs at the LHC’, *Phys. Rev. D* 80 (2009) 095004, doi: [10.1103/PhysRevD.80.095004](https://doi.org/10.1103/PhysRevD.80.095004), arXiv:[0905.4749](https://arxiv.org/abs/0905.4749) [hep-ph].
- [112] W. Beenakker et al., ‘Soft-Gluon Resummation for Squark and Gluino Hadroproduction’, *JHEP* 12 (2009) 041, doi: [10.1088/1126-6708/2009/12/041](https://doi.org/10.1088/1126-6708/2009/12/041), arXiv:[0909.4418](https://arxiv.org/abs/0909.4418) [hep-ph].
- [113] W. Beenakker et al., ‘Squark and gluino hadroproduction’, *Int. J. Mod. Phys. A* 26 (2011) 2637–2664, doi: [10.1142/S0217751X11053560](https://doi.org/10.1142/S0217751X11053560), arXiv:[1105.1110](https://arxiv.org/abs/1105.1110) [hep-ph].
- [114] M. Krämer et al., ‘Supersymmetry Production Cross Sections in pp Collisions at $\sqrt{s} = 7$ TeV’ (2012), arXiv:[1206.2892](https://arxiv.org/abs/1206.2892) [hep-ph].
- [115] A. Djouadi, M. Muhlleitner and M. Spira, ‘Decays of Supersymmetric Particles: The Program SUSY-HIT (SUSpect-SdecaY-Hdecay-INterface)’, *Acta Phys. Polon. B* 38 (2007) 635, arXiv:[0609292](https://arxiv.org/abs/0609292) [hep-ph].
- [116] M. Muhlleitner, A. Djouadi and Y. Mambrini, ‘SDECAY: A Fortran Code for the Decays of the Supersymmetric Particles in the MSSM’, *Comput. Phys. Commun.* 168 (2005) 46, doi: [10.1016/j.cpc.2005.01.012](https://doi.org/10.1016/j.cpc.2005.01.012), arXiv:[0311167](https://arxiv.org/abs/0311167) [hep-ph].
- [117] B. Allanach, ‘SOFTSUSY: a Program for Calculating Supersymmetric Spectra’, *Comput. Phys. Commun.* 143 (2002) 305, doi: [10.1016/S0010-4655\(01\)00460-X](https://doi.org/10.1016/S0010-4655(01)00460-X), arXiv:[0104145](https://arxiv.org/abs/0104145) [hep-ph].
- [118] S. Jadach et al., ‘The Tau Decay Library TAUOLA, Version 2.4’, *Comput. Phys. Commun.* 76 (1993) 361, doi: [10.1016/0010-4655\(93\)90061-G](https://doi.org/10.1016/0010-4655(93)90061-G).
- [119] P. Golonka et al., ‘The Tauola-Photos-F Environment for the TAUOLA and PHOTOS Packages, Release II’, *Comput. Phys. Commun.* 174 (2006) 818, arXiv:[0312240](https://arxiv.org/abs/0312240) [hep-ph].
- [120] ATLAS Collaboration, ‘The ATLAS Simulation Infrastructure’, *Eur. Phys. J. C* 70 (2010) 823, doi: [10.1140/epjc/s10052-010-1429-9](https://doi.org/10.1140/epjc/s10052-010-1429-9), arXiv:[1005.4568](https://arxiv.org/abs/1005.4568) [physics.ins-det].
- [121] S. Agostinelli et al., ‘GEANT4: A Simulation Toolkit’, *Nucl. Instrum. Meth. A* 506 (2003) 250, doi: [10.1016/S0168-9002\(03\)01368-8](https://doi.org/10.1016/S0168-9002(03)01368-8).
- [122] ATLAS Collaboration, ‘The Simulation Principle and Performance of the ATLAS Fast Calorimeter Simulation FastCaloSim’, *ATL-PHYS-PUB-2010-013* (2013), URL: <http://cds.cern.ch/record/1300517>.
- [123] A. Sherstnev and R. S. Thorne, ‘Parton Distributions for LO Generators’, *Eur. Phys. J. C* 55 (2008) 553, doi: [10.1140/epjc/s10052-008-0610-x](https://doi.org/10.1140/epjc/s10052-008-0610-x), arXiv:[0711.2473](https://arxiv.org/abs/0711.2473) [hep-ph].
- [124] M. Cacciari, G. P. Salam and G. Soyez, ‘The Anti- k_t Jet Clustering Algorithm’, *JHEP* 04 (2008) 063, doi: [10.1088/1126-6708/2008/04/063](https://doi.org/10.1088/1126-6708/2008/04/063), arXiv:[0802.1189](https://arxiv.org/abs/0802.1189) [hep-ph].
- [125] M. Cacciari and G. P. Salam, ‘Dispelling the N^3 Myth for the k_t Jet-Finder’, *Phys. Lett. B* 641 (2006) 57, doi: [10.1016/j.physletb.2006.08.037](https://doi.org/10.1016/j.physletb.2006.08.037), arXiv:[0512210](https://arxiv.org/abs/0512210) [hep-ph].
- [126] W. Lampl et al., ‘Calorimeter Clustering Algorithms: Description and Performance’, *ATL-LARG-PUB-2008-002* (2008), URL: <http://cdsweb.cern.ch/record/1099735>.

- [127] ATLAS Collaboration, ‘Jet Energy Measurement and its Systematic Uncertainty in Proton-Proton Collisions at $\sqrt{s} = 7$ TeV with the ATLAS Detector’, *Eur. Phys. J. C* 75.1 (2015) 17, doi: [10.1140/epjc/s10052-014-3190-y](https://doi.org/10.1140/epjc/s10052-014-3190-y), arXiv:[1406.0076](https://arxiv.org/abs/1406.0076) [hep-ex].
- [128] C. Issever, K. Borrás and D. Wegener, ‘An Improved Weighting Algorithm to Achieve Software Compensation in a Fine Grained LAr Calorimeter’, *Nucl. Instrum. Meth. A* 545 (2005) 803, doi: [10.1016/j.nima.2005.02.010](https://doi.org/10.1016/j.nima.2005.02.010), arXiv:[0408129](https://arxiv.org/abs/0408129) [physics].
- [129] M. Cacciari and G. P. Salam, ‘Pileup Subtraction using Jet Areas’, *Phys. Lett. B* 659 (2008) 119, doi: [10.1016/j.physletb.2007.09.077](https://doi.org/10.1016/j.physletb.2007.09.077), arXiv:[0707.1378](https://arxiv.org/abs/0707.1378) [hep-ph].
- [130] ATLAS Collaboration, ‘Pile-up subtraction and suppression for jets in ATLAS’, *ATLAS-CONF-2013-083* (2013), URL: <http://cdsweb.cern.ch/record/1570994>.
- [131] ATLAS Collaboration, ‘Jet Energy Scale and its Systematic Uncertainty in Proton-Proton Collisions at $\sqrt{s} = 7$ TeV with ATLAS 2011 Data’, *ATLAS-CONF-2013-004* (2013), URL: <http://cdsweb.cern.ch/record/1509552>.
- [132] ATLAS Collaboration, ‘Commissioning of the ATLAS High-Performance b -Tagging Algorithms in the 7 TeV Collision Data’, *ATLAS-CONF-2011-102* (2011), URL: <https://cds.cern.ch/record/1369219>.
- [133] ATLAS Collaboration, ‘Calibration of b -Tagging using Dileptonic Top Pair Events in a Combinatorial Likelihood Approach with the ATLAS Experiment’, *ATLAS-CONF-2014-004* (2014), URL: <http://cds.cern.ch/record/1664335>.
- [134] ATLAS Collaboration, ‘Calibration of the Performance of b -Tagging for c and Light-Flavour Jets in the 2012 ATLAS Data’, *ATLAS-CONF-2014-046* (2014), URL: <http://cds.cern.ch/record/1741020>.
- [135] ATLAS Collaboration, ‘Electron reconstruction and identification efficiency measurements with the ATLAS detector using the 2011 LHC proton-proton collision data’, *Eur. Phys. J. C* 74.7 (2014) 2941, doi: [10.1140/epjc/s10052-014-2941-0](https://doi.org/10.1140/epjc/s10052-014-2941-0), arXiv:[1404.2240](https://arxiv.org/abs/1404.2240) [hep-ex].
- [136] ATLAS Collaboration, ‘Measurements of the Photon Identification Efficiency with the ATLAS Detector using 4.9 fb^{-1} of pp Collision Data Collected in 2011’, *ATLAS-CONF-2012-123* (2012), URL: <https://cds.cern.ch/record/1473426>.
- [137] ATLAS Collaboration, ‘Muon Reconstruction Efficiency and Momentum Resolution of the ATLAS Experiment in Proton-Proton Collisions at $\sqrt{s} = 7$ TeV in 2010’, *Eur. Phys. J. C* 74.9 (2014) 3034, doi: [10.1140/epjc/s10052-014-3034-9](https://doi.org/10.1140/epjc/s10052-014-3034-9), arXiv:[1404.4562](https://arxiv.org/abs/1404.4562) [hep-ex].
- [138] ATLAS Collaboration, ‘Identification of Hadronic Decays of Tau Leptons in 2012 Data with the ATLAS Detector’, *ATLAS-CONF-2013-064* (2013), URL: <https://cdsweb.cern.ch/record/1562839>.
- [139] ATLAS Collaboration, ‘Determination of the Tau Energy Scale and the Associated Systematic Uncertainty in Proton-Proton Collisions at $\sqrt{s} = 8$ TeV with the ATLAS Detector at the LHC in 2012’, *ATLAS-CONF-2013-044* (2013), URL: <https://cdsweb.cern.ch/record/1544036>.

- [140] ATLAS Collaboration, ‘Performance of Missing Transverse Momentum Reconstruction in Proton-Proton Collisions at 7 TeV with ATLAS’, *Eur. Phys. J. C* 72 (2012) 1844, doi: [10.1140/epjc/s10052-011-1844-6](https://doi.org/10.1140/epjc/s10052-011-1844-6), arXiv:[1108.5602](https://arxiv.org/abs/1108.5602) [[hep-ex](#)].
- [141] ATLAS Collaboration, ‘Performance of Missing Transverse Momentum Reconstruction in ATLAS studied in Proton-Proton Collisions recorded in 2012 at 8 TeV’, *ATLAS-CONF-2013-082* (2013), URL: <https://cds.cern.ch/record/1570993>.
- [142] M. Baak et al., ‘HistFitter software framework for statistical data analysis’, *Eur. Phys. J. C* 75.4 (2015) 153, doi: [10.1140/epjc/s10052-015-3327-7](https://doi.org/10.1140/epjc/s10052-015-3327-7), arXiv:[1410.1280](https://arxiv.org/abs/1410.1280) [[hep-ex](#)].
- [143] A. L. Read, ‘Presentation of Search Results: The CL(s) Technique’, *J. Phys. G* 28 (2002) 2693, doi: [10.1088/0954-3899/28/10/313](https://doi.org/10.1088/0954-3899/28/10/313).
- [144] ATLAS Collaboration, ‘Search for Scalar Charm Quark Pair Production in pp Collisions at $\sqrt{s} = 8$ TeV with the ATLAS Detector’, *Phys. Rev. Lett.* 114.16 (2015) 161801, doi: [10.1103/PhysRevLett.114.161801](https://doi.org/10.1103/PhysRevLett.114.161801), arXiv:[1501.01325](https://arxiv.org/abs/1501.01325) [[hep-ex](#)].
- [145] M. Lisanti et al., ‘Study of LHC Searches for a Lepton and Many Jets’, *JHEP* 11 (2012) 081, doi: [10.1007/JHEP11\(2012\)081](https://doi.org/10.1007/JHEP11(2012)081), arXiv:[1107.5055](https://arxiv.org/abs/1107.5055) [[hep-ph](#)].
- [146] J. A. Evans et al., ‘Toward Full LHC Coverage of Natural Supersymmetry’, *JHEP* 07 (2014) 101, doi: [10.1007/JHEP07\(2014\)101](https://doi.org/10.1007/JHEP07(2014)101), arXiv:[1310.5758](https://arxiv.org/abs/1310.5758) [[hep-ph](#)].
- [147] I. Hinchliffe et al., ‘Precision SUSY measurements at CERN LHC’, *Phys. Rev. D* 55 (1997) 5520, doi: [10.1103/PhysRevD.55.5520](https://doi.org/10.1103/PhysRevD.55.5520), arXiv:[9610544](https://arxiv.org/abs/9610544) [[hep-ph](#)].
- [148] CMS Collaboration, ‘Search for physics beyond the standard model in events with two leptons, jets, and missing transverse momentum in pp collisions at $\sqrt{s} = 8$ TeV’, *JHEP* 04 (2015) 124, doi: [10.1007/JHEP04\(2015\)124](https://doi.org/10.1007/JHEP04(2015)124), arXiv:[1502.06031](https://arxiv.org/abs/1502.06031) [[hep-ex](#)].
- [149] R. Barbieri and G. Giudice, ‘Upper Bounds on Supersymmetric Particle Masses’, *Nucl. Phys. B* 306 (1988) 63, doi: [10.1016/0550-3213\(88\)90171-X](https://doi.org/10.1016/0550-3213(88)90171-X).
- [150] B. de Carlos and J. Casas, ‘One loop analysis of the electroweak breaking in supersymmetric models and the fine tuning problem’, *Phys. Lett. B* 309 (1993) 320, doi: [10.1016/0370-2693\(93\)90940-J](https://doi.org/10.1016/0370-2693(93)90940-J), arXiv:[9303291](https://arxiv.org/abs/9303291) [[hep-ph](#)].
- [151] J. R. Ellis et al., ‘Calculations of Neutralino-Stau Coannihilation Channels and the Cosmologically Relevant Region of MSSM Parameter Space’, *Astropart. Phys.* 13 (2000) 181, doi: [10.1016/S0927-6505\(99\)00104-8](https://doi.org/10.1016/S0927-6505(99)00104-8), arXiv:[9905481](https://arxiv.org/abs/9905481) [[hep-ph](#)].
- [152] D. Albornoz Vásquez, G. Bélanger and C. Boehm, ‘Revisiting Light Neutralino Scenarios in the MSSM’, *Phys. Rev. D* 84 (2011) 095015, doi: [10.1103/PhysRevD.84.095015](https://doi.org/10.1103/PhysRevD.84.095015), arXiv:[1108.1338](https://arxiv.org/abs/1108.1338) [[hep-ph](#)].
- [153] ATLAS Collaboration, ‘Single Hadron Response Measurement and Calorimeter Jet Energy Scale Uncertainty with the ATLAS Detector at the LHC’, *Eur. Phys. J. C* 73 (2013) 2305, doi: [10.1140/epjc/s10052-013-2305-1](https://doi.org/10.1140/epjc/s10052-013-2305-1), arXiv:[1203.1302](https://arxiv.org/abs/1203.1302) [[hep-ex](#)].
- [154] ATLAS Collaboration, ‘Jet Energy Resolution in Proton-Proton Collisions at $\sqrt{s} = 7$ TeV Recorded in 2010 with the ATLAS Detector’, *Eur. Phys. J. C* 73 (2013) 2306, doi: [10.1140/epjc/s10052-013-2306-0](https://doi.org/10.1140/epjc/s10052-013-2306-0), arXiv:[1210.6210](https://arxiv.org/abs/1210.6210) [[hep-ex](#)].
- [155] M. Botje et al., ‘The PDF4LHC Working Group Interim Recommendations’ (2011), arXiv:[1101.0538](https://arxiv.org/abs/1101.0538) [[hep-ph](#)].

- [156] ATLAS Collaboration, ‘Search for Squarks and Gluinos with the ATLAS Detector in Final States with Jets and Missing Transverse Momentum using 4.7 fb⁻¹ of $\sqrt{s} = 7$ TeV Proton-Proton Collision Data’, *Phys. Rev. D* 87 (2013) 012008, doi: [10.1103/PhysRevD.87.012008](https://doi.org/10.1103/PhysRevD.87.012008), arXiv:[1208.0949](https://arxiv.org/abs/1208.0949) [hep-ex].
- [157] ATLAS Collaboration, ‘Limits on Metastable Gluinos from ATLAS SUSY Searches at 8 TeV’, *ATLAS-CONF-2014-037* (2014), URL: <https://cds.cern.ch/record/1735199>.

The ATLAS Collaboration

G. Aad⁸⁵, B. Abbott¹¹³, J. Abdallah¹⁵¹, O. Abdinov¹¹, R. Aben¹⁰⁷, M. Abolins⁹⁰, O.S. AbouZeid¹⁵⁸, H. Abramowicz¹⁵³, H. Abreu¹⁵², R. Abreu¹¹⁶, Y. Abulaiti^{146a,146b}, B.S. Acharya^{164a,164b,a}, L. Adamczyk^{38a}, D.L. Adams²⁵, J. Adelman¹⁰⁸, S. Adomeit¹⁰⁰, T. Adye¹³¹, A.A. Affolder⁷⁴, T. Agatonovic-Jovin¹³, J. Agricola⁵⁴, J.A. Aguilar-Saavedra^{126a,126f}, S.P. Ahlen²², F. Ahmadov^{65,b}, G. Aielli^{133a,133b}, H. Akerstedt^{146a,146b}, T.P.A. Åkesson⁸¹, A.V. Akimov⁹⁶, G.L. Alberghi^{20a,20b}, J. Albert¹⁶⁹, S. Albrand⁵⁵, M.J. Alconada Verzini⁷¹, M. Aleksa³⁰, I.N. Aleksandrov⁶⁵, C. Alexa^{26a}, G. Alexander¹⁵³, T. Alexopoulos¹⁰, M. Alhroob¹¹³, G. Alimonti^{91a}, L. Alio⁸⁵, J. Alison³¹, S.P. Alkire³⁵, B.M.M. Allbrooke¹⁴⁹, P.P. Allport⁷⁴, A. Aloisio^{104a,104b}, A. Alonso³⁶, F. Alonso⁷¹, C. Alpigiani⁷⁶, A. Altheimer³⁵, B. Alvarez Gonzalez³⁰, D. Álvarez Piqueras¹⁶⁷, M.G. Alviggi^{104a,104b}, B.T. Amadio¹⁵, K. Amako⁶⁶, Y. Amaral Coutinho^{24a}, C. Amelung²³, D. Amidei⁸⁹, S.P. Amor Dos Santos^{126a,126c}, A. Amorim^{126a,126b}, S. Amoroso⁴⁸, N. Amram¹⁵³, G. Amundsen²³, C. Anastopoulos¹³⁹, L.S. Ancu⁴⁹, N. Andari¹⁰⁸, T. Andeen³⁵, C.F. Anders^{58b}, G. Anders³⁰, J.K. Anders⁷⁴, K.J. Anderson³¹, A. Andreazza^{91a,91b}, V. Andrei^{58a}, S. Angelidakis⁹, I. Angelozzi¹⁰⁷, P. Anger⁴⁴, A. Angerami³⁵, F. Anghinolfi³⁰, A.V. Anisenkov^{109,c}, N. Anjos¹², A. Annovi^{124a,124b}, M. Antonelli⁴⁷, A. Antonov⁹⁸, J. Antos^{144b}, F. Anulli^{132a}, M. Aoki⁶⁶, L. Aperio Bella¹⁸, G. Arabidze⁹⁰, Y. Arai⁶⁶, J.P. Araque^{126a}, A.T.H. Arce⁴⁵, F.A. Arduh⁷¹, J-F. Arguin⁹⁵, S. Argyropoulos⁴², M. Arik^{19a}, A.J. Armbruster³⁰, O. Arnaez³⁰, V. Arnal⁸², H. Arnold⁴⁸, M. Arratia²⁸, O. Arslan²¹, A. Artamonov⁹⁷, G. Artoni²³, S. Asai¹⁵⁵, N. Asbah⁴², A. Ashkenazi¹⁵³, B. Åsman^{146a,146b}, L. Asquith¹⁴⁹, K. Assamagan²⁵, R. Astalos^{144a}, M. Atkinson¹⁶⁵, N.B. Atlay¹⁴¹, K. Augsten¹²⁸, M. Aurousseau^{145b}, G. Avolio³⁰, B. Axen¹⁵, M.K. Ayoub¹¹⁷, G. Azuelos^{95,d}, M.A. Baak³⁰, A.E. Baas^{58a}, M.J. Baca¹⁸, C. Bacci^{134a,134b}, H. Bachacou¹³⁶, K. Bachas¹⁵⁴, M. Backes³⁰, M. Backhaus³⁰, P. Bagiachi^{132a,132b}, P. Bagnaia^{132a,132b}, Y. Bai^{33a}, T. Bain³⁵, J.T. Baines¹³¹, O.K. Baker¹⁷⁶, E.M. Baldin^{109,c}, P. Balek¹²⁹, T. Balestri¹⁴⁸, F. Balli⁸⁴, E. Banas³⁹, Sw. Banerjee¹⁷³, A.A.E. Bannoura¹⁷⁵, H.S. Bansil¹⁸, L. Barak³⁰, E.L. Barberio⁸⁸, D. Barberis^{50a,50b}, M. Barbero⁸⁵, T. Barillari¹⁰¹, M. Barisonzi^{164a,164b}, T. Barklow¹⁴³, N. Barlow²⁸, S.L. Barnes⁸⁴, B.M. Barnett¹³¹, R.M. Barnett¹⁵, Z. Barnovska⁵, A. Baroncelli^{134a}, G. Barone²³, A.J. Barr¹²⁰, F. Barreiro⁸², J. Barreiro Guimarães da Costa⁵⁷, R. Bartoldus¹⁴³, A.E. Barton⁷², P. Bartos^{144a}, A. Basalae¹²³, A. Bassalat¹¹⁷, A. Basye¹⁶⁵, R.L. Bates⁵³, S.J. Batista¹⁵⁸, J.R. Batley²⁸, M. Battaglia¹³⁷, M. Bauce^{132a,132b}, F. Bauer¹³⁶, H.S. Bawa^{143,e}, J.B. Beacham¹¹¹, M.D. Beattie⁷², T. Beau⁸⁰, P.H. Beauchemin¹⁶¹, R. Beccherle^{124a,124b}, P. Bechtel²¹, H.P. Beck^{17,f}, K. Becker¹²⁰, M. Becker⁸³, S. Becker¹⁰⁰, M. Beckingham¹⁷⁰, C. Becot¹¹⁷, A.J. Beddall^{19b}, A. Beddall^{19b}, V.A. Bednyakov⁶⁵, C.P. Bee¹⁴⁸, L.J. Beemster¹⁰⁷, T.A. Beermann¹⁷⁵, M. Begel²⁵, J.K. Behr¹²⁰, C. Belanger-Champagne⁸⁷, W.H. Bell⁴⁹, G. Bella¹⁵³, L. Bellagamba^{20a}, A. Bellerive²⁹, M. Bellomo⁸⁶, K. Belotskiy⁹⁸, O. Beltramello³⁰, O. Benary¹⁵³, D. Benchebkroun^{135a}, M. Bender¹⁰⁰, K. Bendtz^{146a,146b}, N. Benekos¹⁰, Y. Benhammou¹⁵³, E. Benhar Noccioli⁴⁹, J.A. Benitez Garcia^{159b}, D.P. Benjamin⁴⁵, J.R. Bensinger²³, S. Bentvelsen¹⁰⁷, L. Beresford¹²⁰, M. Beretta⁴⁷, D. Berge¹⁰⁷, E. Bergeas Kuutmann¹⁶⁶, N. Berger⁵, F. Berghaus¹⁶⁹, J. Beringer¹⁵, C. Bernard²², N.R. Bernard⁸⁶, C. Bernius¹¹⁰, F.U. Bernlochner²¹, T. Berry⁷⁷, P. Berta¹²⁹, C. Bertella⁸³, G. Bertoli^{146a,146b}, F. Bertolucci^{124a,124b}, C. Bertsche¹¹³, D. Bertsche¹¹³, M.I. Besana^{91a}, G.J. Besjes³⁶, O. Bessidskaia Bylund^{146a,146b}, M. Bessner⁴², N. Besson¹³⁶, C. Betancourt⁴⁸, S. Bethke¹⁰¹, A.J. Bevan⁷⁶, W. Bhimji¹⁵, R.M. Bianchi¹²⁵, L. Bianchini²³, M. Bianco³⁰, O. Biebel¹⁰⁰, D. Biedermann¹⁶, S.P. Bieniek⁷⁸, M. Biglietti^{134a}, J. Bilbao De Mendizabal⁴⁹, H. Bilokon⁴⁷, M. Bindi⁵⁴, S. Binet¹¹⁷, A. Bingul^{19b}, C. Bini^{132a,132b}, S. Biondi^{20a,20b}, C.W. Black¹⁵⁰, J.E. Black¹⁴³, K.M. Black²², D. Blackburn¹³⁸, R.E. Blair⁶, J.-B. Blanchard¹³⁶, J.E. Blanco⁷⁷, T. Blazek^{144a}, I. Bloch⁴², C. Blocker²³, W. Blum^{83,*}, U. Blumenschein⁵⁴, G.J. Bobbink¹⁰⁷, V.S. Bobrovnikov^{109,c}, S.S. Bocchetta⁸¹, A. Bocchi⁴⁵,

C. Bock¹⁰⁰, M. Boehler⁴⁸, J.A. Bogaerts³⁰, D. Bogavac¹³, A.G. Bogdanchikov¹⁰⁹, C. Bohm^{146a},
 V. Boisvert⁷⁷, T. Bold^{38a}, V. Boldea^{26a}, A.S. Boldyrev⁹⁹, M. Bomben⁸⁰, M. Bona⁷⁶, M. Boonekamp¹³⁶,
 A. Borisov¹³⁰, G. Borisso⁷², S. Borroni⁴², J. Bortfeldt¹⁰⁰, V. Bortolotto^{60a,60b,60c}, K. Bos¹⁰⁷,
 D. Boscherini^{20a}, M. Bosman¹², J. Boudreau¹²⁵, J. Bouffard², E.V. Bouhova-Thacker⁷²,
 D. Boumediene³⁴, C. Bourdarios¹¹⁷, N. Bousson¹¹⁴, A. Boveia³⁰, J. Boyd³⁰, I.R. Boyko⁶⁵, I. Bozic¹³,
 J. Bracinik¹⁸, A. Brandt⁸, G. Brandt⁵⁴, O. Brandt^{58a}, U. Bratzler¹⁵⁶, B. Brau⁸⁶, J.E. Brau¹¹⁶,
 H.M. Braun^{175,*}, S.F. Brazzale^{164a,164c}, W.D. Breaden Madden⁵³, K. Brendlinger¹²², A.J. Brennan⁸⁸,
 L. Brenner¹⁰⁷, R. Brenner¹⁶⁶, S. Bressler¹⁷², K. Bristow^{145c}, T.M. Bristow⁴⁶, D. Britton⁵³, D. Britzger⁴²,
 F.M. Brochu²⁸, I. Brock²¹, R. Brock⁹⁰, J. Bronner¹⁰¹, G. Brooijmans³⁵, T. Brooks⁷⁷, W.K. Brooks^{32b},
 J. Brosamer¹⁵, E. Brost¹¹⁶, J. Brown⁵⁵, P.A. Bruckman de Renstrom³⁹, D. Bruncko^{144b}, R. Bruneliere⁴⁸,
 A. Bruni^{20a}, G. Bruni^{20a}, M. Bruschi^{20a}, N. Bruscinò²¹, L. Bryngemark⁸¹, T. Buanes¹⁴, Q. Buat¹⁴²,
 P. Buchholz¹⁴¹, A.G. Buckley⁵³, S.I. Buda^{26a}, I.A. Budagov⁶⁵, F. Buehrer⁴⁸, L. Bugge¹¹⁹,
 M.K. Bugge¹¹⁹, O. Bulekov⁹⁸, D. Bullock⁸, H. Burckhart³⁰, S. Burdin⁷⁴, C.D. Burgard⁴⁸,
 B. Burghgrave¹⁰⁸, S. Burke¹³¹, I. Burmeister⁴³, E. Busato³⁴, D. Büscher⁴⁸, V. Büscher⁸³, P. Bussey⁵³,
 J.M. Butler²², A.I. Butt³, C.M. Buttar⁵³, J.M. Butterworth⁷⁸, P. Butti¹⁰⁷, W. Buttinger²⁵, A. Buzatu⁵³,
 A.R. Buzykaev^{109,c}, S. Cabrera Urbán¹⁶⁷, D. Caforio¹²⁸, V.M. Cairo^{37a,37b}, O. Cakir^{4a}, N. Calace⁴⁹,
 P. Calafiura¹⁵, A. Calandri¹³⁶, G. Calderini⁸⁰, P. Calfayan¹⁰⁰, L.P. Caloba^{24a}, D. Calvet³⁴, S. Calvet³⁴,
 R. Camacho Toro³¹, S. Camarda⁴², P. Camarri^{133a,133b}, D. Cameron¹¹⁹, R. Caminal Armadans¹⁶⁵,
 S. Campana³⁰, M. Campanelli⁷⁸, A. Campoverde¹⁴⁸, V. Canale^{104a,104b}, A. Canepa^{159a}, M. Cano Bret^{33e},
 J. Cantero⁸², R. Cantrill^{126a}, T. Cao⁴⁰, M.D.M. Capeans Garrido³⁰, I. Caprini^{26a}, M. Caprini^{26a},
 M. Capua^{37a,37b}, R. Caputo⁸³, R. Cardarelli^{133a}, F. Cardillo⁴⁸, T. Carli³⁰, G. Carlino^{104a},
 L. Carminati^{91a,91b}, S. Caron¹⁰⁶, E. Carquin^{32a}, G.D. Carrillo-Montoya³⁰, J.R. Carter²⁸,
 J. Carvalho^{126a,126c}, D. Casadei⁷⁸, M.P. Casado¹², M. Casolino¹², E. Castaneda-Miranda^{145b},
 A. Castelli¹⁰⁷, V. Castillo Gimenez¹⁶⁷, N.F. Castro^{126a,g}, P. Catastini⁵⁷, A. Catinaccio³⁰, J.R. Catmore¹¹⁹,
 A. Cattai³⁰, J. Caudron⁸³, V. Cavaliere¹⁶⁵, D. Cavalli^{91a}, M. Cavalli-Sforza¹², V. Cavasinni^{124a,124b},
 F. Ceradini^{134a,134b}, B.C. Cerio⁴⁵, K. Cerny¹²⁹, A.S. Cerqueira^{24b}, A. Cerri¹⁴⁹, L. Cerrito⁷⁶, F. Cerutti¹⁵,
 M. Cerv³⁰, A. Cervelli¹⁷, S.A. Cetin^{19c}, A. Chafaq^{135a}, D. Chakraborty¹⁰⁸, I. Chalupkova¹²⁹,
 P. Chang¹⁶⁵, J.D. Chapman²⁸, D.G. Charlton¹⁸, C.C. Chau¹⁵⁸, C.A. Chavez Barajas¹⁴⁹, S. Cheatham¹⁵²,
 A. Chegwidan⁹⁰, S. Chekanov⁶, S.V. Chekulaev^{159a}, G.A. Chelkov^{65,h}, M.A. Chelstowska⁸⁹,
 C. Chen⁶⁴, H. Chen²⁵, K. Chen¹⁴⁸, L. Chen^{33d,i}, S. Chen^{33c}, X. Chen^{33f}, Y. Chen⁶⁷, H.C. Cheng⁸⁹,
 Y. Cheng³¹, A. Cheplakov⁶⁵, E. Cheremushkina¹³⁰, R. Cherkaoui El Moursli^{135e}, V. Chernyatin^{25,*},
 E. Cheu⁷, L. Chevalier¹³⁶, V. Chiarella⁴⁷, G. Chiarelli^{124a,124b}, G. Chiodini^{73a}, A.S. Chisholm¹⁸,
 R.T. Chislett⁷⁸, A. Chitan^{26a}, M.V. Chizhov⁶⁵, K. Choi⁶¹, S. Chouridou⁹, B.K.B. Chow¹⁰⁰,
 V. Christodoulou⁷⁸, D. Chromek-Burckhart³⁰, J. Chudoba¹²⁷, A.J. Chuinard⁸⁷, J.J. Chwastowski³⁹,
 L. Chytka¹¹⁵, G. Ciapetti^{132a,132b}, A.K. Ciftci^{4a}, D. Cinca⁵³, V. Cindro⁷⁵, I.A. Cioara²¹, A. Ciocio¹⁵,
 Z.H. Citron¹⁷², M. Ciubancan^{26a}, A. Clark⁴⁹, B.L. Clark⁵⁷, P.J. Clark⁴⁶, R.N. Clarke¹⁵, W. Cleland¹²⁵,
 C. Clement^{146a,146b}, Y. Coadou⁸⁵, M. Cobal^{164a,164c}, A. Coccaro¹³⁸, J. Cochran⁶⁴, L. Coffey²³,
 J.G. Cogan¹⁴³, L. Colasurdo¹⁰⁶, B. Cole³⁵, S. Cole¹⁰⁸, A.P. Colijn¹⁰⁷, J. Collot⁵⁵, T. Colombo^{58c},
 G. Compostella¹⁰¹, P. Conde Muino^{126a,126b}, E. Coniavitis⁴⁸, S.H. Connell^{145b}, I.A. Connelly⁷⁷,
 S.M. Consonni^{91a,91b}, V. Consorti⁴⁸, S. Constantinescu^{26a}, C. Conta^{121a,121b}, G. Conti³⁰,
 F. Conventi^{104a,j}, M. Cooke¹⁵, B.D. Cooper⁷⁸, A.M. Cooper-Sarkar¹²⁰, T. Cornelissen¹⁷⁵, M. Corradi^{20a},
 F. Corriveau^{87,k}, A. Corso-Radu¹⁶³, A. Cortes-Gonzalez¹², G. Cortiana¹⁰¹, G. Costa^{91a}, M.J. Costa¹⁶⁷,
 D. Costanzo¹³⁹, D. Côte⁸, G. Cottin²⁸, G. Cowan⁷⁷, B.E. Cox⁸⁴, K. Cranmer¹¹⁰, G. Cree²⁹,
 S. Crépe-Renaudin⁵⁵, F. Crescioli⁸⁰, W.A. Cribbs^{146a,146b}, M. Crispin Ortuzar¹²⁰, M. Cristinziani²¹,
 V. Croft¹⁰⁶, G. Crosetti^{37a,37b}, T. Cuhadar Donszelmann¹³⁹, J. Cummings¹⁷⁶, M. Curatolo⁴⁷,
 C. Cuthbert¹⁵⁰, H. Cziri¹⁴¹, P. Czodrowski³, S. D'Auria⁵³, M. D'Onofrio⁷⁴,
 M.J. Da Cunha Sargedas De Sousa^{126a,126b}, C. Da Via⁸⁴, W. Dabrowski^{38a}, A. Dafinca¹²⁰, T. Dai⁸⁹,

O. Dale¹⁴, F. Dallaire⁹⁵, C. Dallapiccola⁸⁶, M. Dam³⁶, J.R. Dandoy³¹, N.P. Dang⁴⁸, A.C. Daniells¹⁸, M. Danninger¹⁶⁸, M. Dano Hoffmann¹³⁶, V. Dao⁴⁸, G. Darbo^{50a}, S. Darmora⁸, J. Dassoulas³, A. Dattagupta⁶¹, W. Davey²¹, C. David¹⁶⁹, T. Davidek¹²⁹, E. Davies^{120,l}, M. Davies¹⁵³, P. Davison⁷⁸, Y. Davygora^{58a}, E. Dawe⁸⁸, I. Dawson¹³⁹, R.K. Daya-Ishmukhametova⁸⁶, K. De⁸, R. de Asmundis^{104a}, A. De Benedetti¹¹³, S. De Castro^{20a,20b}, S. De Cecco⁸⁰, N. De Groot¹⁰⁶, P. de Jong¹⁰⁷, H. De la Torre⁸², F. De Lorenzi⁶⁴, L. De Nooij¹⁰⁷, D. De Pedis^{132a}, A. De Salvo^{132a}, U. De Sanctis¹⁴⁹, A. De Santo¹⁴⁹, J.B. De Vivie De Regie¹¹⁷, W.J. Dearnaley⁷², R. Debbe²⁵, C. Debenedetti¹³⁷, D.V. Dedovich⁶⁵, I. Deigaard¹⁰⁷, J. Del Peso⁸², T. Del Prete^{124a,124b}, D. Delgove¹¹⁷, F. Deliot¹³⁶, C.M. Delitzsch⁴⁹, M. Deliyergiyev⁷⁵, A. Dell'Acqua³⁰, L. Dell'Asta²², M. Dell'Orso^{124a,124b}, M. Della Pietra^{104a,j}, D. della Volpe⁴⁹, M. Delmastro⁵, P.A. Delsart⁵⁵, C. Deluca¹⁰⁷, D.A. DeMarco¹⁵⁸, S. Demers¹⁷⁶, M. Demichev⁶⁵, A. Demilly⁸⁰, S.P. Denisov¹³⁰, D. Derendarz³⁹, J.E. Derkaoui^{135d}, F. Derue⁸⁰, P. Dervan⁷⁴, K. Desch²¹, C. Deterre⁴², P.O. Deviveiros³⁰, A. Dewhurst¹³¹, S. Dhaliwal²³, A. Di Ciaccio^{133a,133b}, L. Di Ciaccio⁵, A. Di Domenico^{132a,132b}, C. Di Donato^{104a,104b}, A. Di Girolamo³⁰, B. Di Girolamo³⁰, A. Di Mattia¹⁵², B. Di Micco^{134a,134b}, R. Di Nardo⁴⁷, A. Di Simone⁴⁸, R. Di Sipio¹⁵⁸, D. Di Valentino²⁹, C. Diaconu⁸⁵, M. Diamond¹⁵⁸, F.A. Dias⁴⁶, M.A. Diaz^{32a}, E.B. Diehl⁸⁹, J. Dietrich¹⁶, S. Diglio⁸⁵, A. Dimitrievska¹³, J. Dingfelder²¹, P. Dita^{26a}, S. Dita^{26a}, F. Dittus³⁰, F. Djama⁸⁵, T. Djobava^{51b}, J.I. Djuvsland^{58a}, M.A.B. do Vale^{24c}, D. Dobos³⁰, M. Dobre^{26a}, C. Doglioni⁸¹, T. Dohmae¹⁵⁵, J. Dolejsi¹²⁹, Z. Dolezal¹²⁹, B.A. Dolgoshein^{98,*}, M. Donadelli^{24d}, S. Donati^{124a,124b}, P. Dondero^{121a,121b}, J. Donini³⁴, J. Dopke¹³¹, A. Doria^{104a}, M.T. Dova⁷¹, A.T. Doyle⁵³, E. Drechsler⁵⁴, M. Dris¹⁰, E. Dubreuil³⁴, E. Duchovni¹⁷², G. Duckeck¹⁰⁰, O.A. Ducu^{26a,85}, D. Duda¹⁰⁷, A. Dudarev³⁰, L. Duflot¹¹⁷, L. Duguid⁷⁷, M. Dührssen³⁰, M. Dunford^{58a}, H. Duran Yildiz^{4a}, M. Düren⁵², A. Durglishvili^{51b}, D. Duschinger⁴⁴, M. Dyndal^{38a}, C. Eckardt⁴², K.M. Ecker¹⁰¹, R.C. Edgar⁸⁹, W. Edson², N.C. Edwards⁴⁶, W. Ehrenfeld²¹, T. Eifert³⁰, G. Eigen¹⁴, K. Einsweiler¹⁵, T. Ekelof¹⁶⁶, M. El Kacimi^{135c}, M. Ellert¹⁶⁶, S. Elles⁵, F. Ellinghaus¹⁷⁵, A.A. Elliot¹⁶⁹, N. Ellis³⁰, J. Elmsheuser¹⁰⁰, M. Elsing³⁰, D. Emelianov¹³¹, Y. Enari¹⁵⁵, O.C. Endner⁸³, M. Endo¹¹⁸, J. Erdmann⁴³, A. Ereditato¹⁷, G. Ernis¹⁷⁵, J. Ernst², M. Ernst²⁵, S. Errede¹⁶⁵, E. Ertel⁸³, M. Escalier¹¹⁷, H. Esch⁴³, C. Escobar¹²⁵, B. Esposito⁴⁷, A.I. Etienne¹³⁶, E. Etzion¹⁵³, H. Evans⁶¹, A. Ezhilov¹²³, L. Fabbri^{20a,20b}, G. Facini³¹, R.M. Fakhruddinov¹³⁰, S. Falciano^{132a}, R.J. Falla⁷⁸, J. Faltova¹²⁹, Y. Fang^{33a}, M. Fanti^{91a,91b}, A. Farbin⁸, A. Farilla^{134a}, T. Farooque¹², S. Farrell¹⁵, S.M. Farrington¹⁷⁰, P. Farthouat³⁰, F. Fassi^{135e}, P. Fassnacht³⁰, D. Fassouliotis⁹, M. Fauci Giannelli⁷⁷, A. Favareto^{50a,50b}, L. Fayard¹¹⁷, P. Federic^{144a}, O.L. Fedin^{123,m}, W. Fedorko¹⁶⁸, S. Feigl³⁰, L. Felgioni⁸⁵, C. Feng^{33d}, E.J. Feng⁶, H. Feng⁸⁹, A.B. Fenyuk¹³⁰, L. Feremenga⁸, P. Fernandez Martinez¹⁶⁷, S. Fernandez Perez³⁰, J. Ferrando⁵³, A. Ferrari¹⁶⁶, P. Ferrari¹⁰⁷, R. Ferrari^{121a}, D.E. Ferreira de Lima⁵³, A. Ferrer¹⁶⁷, D. Ferrere⁴⁹, C. Ferretti⁸⁹, A. Ferretto Parodi^{50a,50b}, M. Fiascaris³¹, F. Fiedler⁸³, A. Filipčič⁷⁵, M. Filipuzzi⁴², F. Filthaut¹⁰⁶, M. Fincke-Keeler¹⁶⁹, K.D. Finelli¹⁵⁰, M.C.N. Fiolhais^{126a,126c}, L. Fiorini¹⁶⁷, A. Firan⁴⁰, A. Fischer², C. Fischer¹², J. Fischer¹⁷⁵, W.C. Fisher⁹⁰, E.A. Fitzgerald²³, N. Flaschel⁴², I. Fleck¹⁴¹, P. Fleischmann⁸⁹, S. Fleischmann¹⁷⁵, G.T. Fletcher¹³⁹, G. Fletcher⁷⁶, R.R.M. Fletcher¹²², T. Flick¹⁷⁵, A. Floderus⁸¹, L.R. Flores Castillo^{60a}, M.J. Flowerdew¹⁰¹, A. Formica¹³⁶, A. Forti⁸⁴, D. Fournier¹¹⁷, H. Fox⁷², S. Fracchia¹², P. Francavilla⁸⁰, M. Franchini^{20a,20b}, D. Francis³⁰, L. Franconi¹¹⁹, M. Franklin⁵⁷, M. Frate¹⁶³, M. Fraternali^{121a,121b}, D. Freeborn⁷⁸, S.T. French²⁸, F. Friedrich⁴⁴, D. Froidevaux³⁰, J.A. Frost¹²⁰, C. Fukunaga¹⁵⁶, E. Fullana Torregrosa⁸³, B.G. Fulsom¹⁴³, T. Fusayasu¹⁰², J. Fuster¹⁶⁷, C. Gabaldon⁵⁵, O. Gabizon¹⁷⁵, A. Gabrielli^{20a,20b}, A. Gabrielli^{132a,132b}, G.P. Gach^{38a}, S. Gadatsch³⁰, S. Gadomski⁴⁹, G. Gagliardi^{50a,50b}, P. Gagnon⁶¹, C. Galea¹⁰⁶, B. Galhardo^{126a,126c}, E.J. Gallas¹²⁰, B.J. Gallop¹³¹, P. Gallus¹²⁸, G. Galster³⁶, K.K. Gan¹¹¹, J. Gao^{33b,85}, Y. Gao⁴⁶, Y.S. Gao^{143,e}, F.M. Garay Walls⁴⁶, F. Garberson¹⁷⁶, C. García¹⁶⁷, J.E. García Navarro¹⁶⁷, M. Garcia-Sciveres¹⁵, R.W. Gardner³¹, N. Garelli¹⁴³, V. Garonne¹¹⁹, C. Gatti⁴⁷, A. Gaudiello^{50a,50b}, G. Gaudio^{121a}, B. Gaur¹⁴¹, L. Gauthier⁹⁵, P. Gauzzi^{132a,132b}, I.L. Gavrilenko⁹⁶, C. Gay¹⁶⁸, G. Gaycken²¹, E.N. Gazis¹⁰, P. Ge^{33d},

Z. Gecse¹⁶⁸, C.N.P. Gee¹³¹, Ch. Geich-Gimbel²¹, M.P. Geisler^{58a}, C. Gemme^{50a}, M.H. Genest⁵⁵, S. Gentile^{132a,132b}, M. George⁵⁴, S. George⁷⁷, D. Gerbaudo¹⁶³, A. Gershon¹⁵³, S. Ghasemi¹⁴¹, H. Ghazlane^{135b}, B. Giacobbe^{20a}, S. Giagu^{132a,132b}, V. Giangiobbe¹², P. Giannetti^{124a,124b}, B. Gibbard²⁵, S.M. Gibson⁷⁷, M. Gilchriese¹⁵, T.P.S. Gillam²⁸, D. Gillberg³⁰, G. Gilles³⁴, D.M. Gingrich^{3,d}, N. Giokaris⁹, M.P. Giordani^{164a,164c}, F.M. Giorgi^{20a}, F.M. Giorgi¹⁶, P.F. Giraud¹³⁶, P. Giromini⁴⁷, D. Giugni^{91a}, C. Giuliani⁴⁸, M. Giulini^{58b}, B.K. Gjelsten¹¹⁹, S. Gkaitatzis¹⁵⁴, I. Gkialas¹⁵⁴, E.L. Gkoukousis¹¹⁷, L.K. Gladilin⁹⁹, C. Glasman⁸², J. Glatzer³⁰, P.C.F. Glaysher⁴⁶, A. Glazov⁴², M. Goblirsch-Kolb¹⁰¹, J.R. Goddard⁷⁶, J. Godlewski³⁹, S. Goldfarb⁸⁹, T. Golling⁴⁹, D. Golubkov¹³⁰, A. Gomes^{126a,126b,126d}, R. Gonçalo^{126a}, J. Goncalves Pinto Firmino Da Costa¹³⁶, L. Gonella²¹, S. González de la Hoz¹⁶⁷, G. Gonzalez Parra¹², S. Gonzalez-Sevilla⁴⁹, L. Goossens³⁰, P.A. Gorbounov⁹⁷, H.A. Gordon²⁵, I. Gorelov¹⁰⁵, B. Gorini³⁰, E. Gorini^{73a,73b}, A. Gorišek⁷⁵, E. Gornicki³⁹, A.T. Goshaw⁴⁵, C. Gössling⁴³, M.I. Gostkin⁶⁵, D. Goujdami^{135c}, A.G. Goussiou¹³⁸, N. Govender^{145b}, E. Gozani¹⁵², H.M.X. Grabas¹³⁷, L. Graber⁵⁴, I. Grabowska-Bold^{38a}, P.O.J. Gradin¹⁶⁶, P. Grafström^{20a,20b}, K.-J. Grahn⁴², J. Gramling⁴⁹, E. Gramstad¹¹⁹, S. Grancagnolo¹⁶, V. Gratchev¹²³, H.M. Gray³⁰, E. Graziani^{134a}, Z.D. Greenwood^{79,n}, K. Gregersen⁷⁸, I.M. Gregor⁴², P. Grenier¹⁴³, J. Griffiths⁸, A.A. Grillo¹³⁷, K. Grimm⁷², S. Grinstein^{12,o}, Ph. Gris³⁴, J.-F. Grivaz¹¹⁷, J.P. Grohs⁴⁴, A. Grohsjean⁴², E. Gross¹⁷², J. Grosse-Knetter⁵⁴, G.C. Grossi⁷⁹, Z.J. Grout¹⁴⁹, L. Guan⁸⁹, J. Guenther¹²⁸, F. Guescini⁴⁹, D. Guest¹⁷⁶, O. Gueta¹⁵³, E. Guido^{50a,50b}, T. Guillemin¹¹⁷, S. Guindon², U. Gul⁵³, C. Gumpert⁴⁴, J. Guo^{33e}, Y. Guo^{33b}, S. Gupta¹²⁰, G. Gustavino^{132a,132b}, P. Gutierrez¹¹³, N.G. Gutierrez Ortiz⁷⁸, C. Gutschow⁴⁴, C. Guyot¹³⁶, C. Gwenlan¹²⁰, C.B. Gwilliam⁷⁴, A. Haas¹¹⁰, C. Haber¹⁵, H.K. Hadavand⁸, N. Haddad^{135e}, P. Haefner²¹, S. Hageböck²¹, Z. Hajduk³⁹, H. Hakobyan¹⁷⁷, M. Haleem⁴², J. Haley¹¹⁴, D. Hall¹²⁰, G. Halladjian⁹⁰, G.D. Hallowell⁸⁵, K. Hamacher¹⁷⁵, P. Hamal¹¹⁵, K. Hamano¹⁶⁹, A. Hamilton^{145a}, G.N. Hamity¹³⁹, P.G. Hamnett⁴², L. Han^{33b}, K. Hanagaki^{66,p}, K. Hanawa¹⁵⁵, M. Hance¹⁵, P. Hanke^{58a}, R. Hanna¹³⁶, J.B. Hansen³⁶, J.D. Hansen³⁶, M.C. Hansen²¹, P.H. Hansen³⁶, K. Hara¹⁶⁰, A.S. Hard¹⁷³, T. Harenberg¹⁷⁵, F. Hariri¹¹⁷, S. Harkusha⁹², R.D. Harrington⁴⁶, P.F. Harrison¹⁷⁰, F. Hartjes¹⁰⁷, M. Hasegawa⁶⁷, S. Hasegawa¹⁰³, Y. Hasegawa¹⁴⁰, A. Hasib¹¹³, S. Hassani¹³⁶, S. Haug¹⁷, R. Hauser⁹⁰, L. Hauswald⁴⁴, M. Havranek¹²⁷, C.M. Hawkes¹⁸, R.J. Hawkings³⁰, A.D. Hawkins⁸¹, T. Hayashi¹⁶⁰, D. Hayden⁹⁰, C.P. Hays¹²⁰, J.M. Hays⁷⁶, H.S. Hayward⁷⁴, S.J. Haywood¹³¹, S.J. Head¹⁸, T. Heck⁸³, V. Hedberg⁸¹, L. Heelan⁸, S. Heim¹²², T. Heim¹⁷⁵, B. Heinemann¹⁵, L. Heinrich¹¹⁰, J. Hejbal¹²⁷, L. Helary²², S. Hellman^{146a,146b}, D. Hellmich²¹, C. Hensens¹², J. Henderson¹²⁰, R.C.W. Henderson⁷², Y. Heng¹⁷³, C. Hengler⁴², A. Henrichs¹⁷⁶, A.M. Henriques Correia³⁰, S. Henrot-Versille¹¹⁷, G.H. Herbert¹⁶, Y. Hernández Jiménez¹⁶⁷, R. Herrberg-Schubert¹⁶, G. Herten⁴⁸, R. Hertenberger¹⁰⁰, L. Hervas³⁰, G.G. Hesketh⁷⁸, N.P. Hessey¹⁰⁷, J.W. Hetherly⁴⁰, R. Hickling⁷⁶, E. Higón-Rodríguez¹⁶⁷, E. Hill¹⁶⁹, J.C. Hill²⁸, K.H. Hiller⁴², S.J. Hillier¹⁸, I. Hinchliffe¹⁵, E. Hines¹²², R.R. Hinman¹⁵, M. Hirose¹⁵⁷, D. Hirschbuehl¹⁷⁵, J. Hobbs¹⁴⁸, N. Hod¹⁰⁷, M.C. Hodgkinson¹³⁹, P. Hodgson¹³⁹, A. Hoecker³⁰, M.R. Hoferkamp¹⁰⁵, F. Hoenig¹⁰⁰, M. Hohlfeld⁸³, D. Hohn²¹, T.R. Holmes¹⁵, M. Homann⁴³, T.M. Hong¹²⁵, L. Hooft van Huysduynen¹¹⁰, W.H. Hopkins¹¹⁶, Y. Horii¹⁰³, A.J. Horton¹⁴², J.-Y. Hostachy⁵⁵, S. Hou¹⁵¹, A. Hoummada^{135a}, J. Howard¹²⁰, J. Howarth⁴², M. Hrabovsky¹¹⁵, I. Hristova¹⁶, J. Hrivnac¹¹⁷, T. Hryn'ova⁵, A. Hrynevich⁹³, C. Hsu^{145c}, P.J. Hsu^{151,q}, S.-C. Hsu¹³⁸, D. Hu³⁵, Q. Hu^{33b}, X. Hu⁸⁹, Y. Huang⁴², Z. Hubacek¹²⁸, F. Hubaut⁸⁵, F. Huegging²¹, T.B. Huffman¹²⁰, E.W. Hughes³⁵, G. Hughes⁷², M. Huhtinen³⁰, T.A. Hülsing⁸³, N. Huseynov^{65,b}, J. Huston⁹⁰, J. Huth⁵⁷, G. Iacobucci⁴⁹, G. Iakovidis²⁵, I. Ibragimov¹⁴¹, L. Iconomidou-Fayard¹¹⁷, E. Ideal¹⁷⁶, Z. Idrissi^{135e}, P. Iengo³⁰, O. Igonkina¹⁰⁷, T. Iizawa¹⁷¹, Y. Ikegami⁶⁶, K. Ikematsu¹⁴¹, M. Ikeno⁶⁶, Y. Ilchenko^{31,r}, D. Iliadis¹⁵⁴, N. Ilic¹⁴³, T. Ince¹⁰¹, G. Introzzi^{121a,121b}, P. Ioannou⁹, M. Iodice^{134a}, K. Iordanidou³⁵, V. Ippolito⁵⁷, A. Irles Quiles¹⁶⁷, C. Isaksson¹⁶⁶, M. Ishino⁶⁸, M. Ishitsuka¹⁵⁷, R. Ishmukhametov¹¹¹, C. Issever¹²⁰, S. Istin^{19a}, J.M. Iturbe Ponce⁸⁴, R. Iuppa^{133a,133b}, J. Ivarsson⁸¹, W. Iwanski³⁹,

H. Iwasaki⁶⁶, J.M. Izen⁴¹, V. Izzo^{104a}, S. Jabbar³, B. Jackson¹²², M. Jackson⁷⁴, P. Jackson¹, M.R. Jaekel³⁰, V. Jain², K. Jakobs⁴⁸, S. Jakobsen³⁰, T. Jakoubek¹²⁷, J. Jakubek¹²⁸, D.O. Jamin¹¹⁴, D.K. Jana⁷⁹, E. Jansen⁷⁸, R. Jansky⁶², J. Janssen²¹, M. Janus⁵⁴, G. Jarlskog⁸¹, N. Javadov^{65,b}, T. Javůrek⁴⁸, L. Jeanty¹⁵, J. Jejelava^{51a,s}, G.-Y. Jeng¹⁵⁰, D. Jennens⁸⁸, P. Jenni^{48,t}, J. Jentzsch⁴³, C. Jeske¹⁷⁰, S. Jézéquel⁵, H. Ji¹⁷³, J. Jia¹⁴⁸, Y. Jiang^{33b}, S. Jiggins⁷⁸, J. Jimenez Pena¹⁶⁷, S. Jin^{33a}, A. Jinaru^{26a}, O. Jinnouchi¹⁵⁷, M.D. Joergensen³⁶, P. Johansson¹³⁹, K.A. Johns⁷, K. Jon-And^{146a,146b}, G. Jones¹⁷⁰, R.W.L. Jones⁷², T.J. Jones⁷⁴, J. Jongmanns^{58a}, P.M. Jorge^{126a,126b}, K.D. Joshi⁸⁴, J. Jovicevic^{159a}, X. Ju¹⁷³, C.A. Jung⁴³, P. Jussel⁶², A. Juste Rozas^{12,o}, M. Kaci¹⁶⁷, A. Kaczmarek³⁹, M. Kado¹¹⁷, H. Kagan¹¹¹, M. Kagan¹⁴³, S.J. Kahn⁸⁵, E. Kajomovitz⁴⁵, C.W. Kalderon¹²⁰, S. Kama⁴⁰, A. Kamenshchikov¹³⁰, N. Kanaya¹⁵⁵, S. Kaneti²⁸, V.A. Kantserov⁹⁸, J. Kanzaki⁶⁶, B. Kaplan¹¹⁰, L.S. Kaplan¹⁷³, A. Kapliy³¹, D. Kar^{145c}, K. Karakostas¹⁰, A. Karamaoun³, N. Karastathis^{10,107}, M.J. Kareem⁵⁴, E. Karentzos¹⁰, M. Karnevskiy⁸³, S.N. Karpov⁶⁵, Z.M. Karpova⁶⁵, K. Karthik¹¹⁰, V. Kartvelishvili⁷², A.N. Karyukhin¹³⁰, L. Kashif¹⁷³, R.D. Kass¹¹¹, A. Kastanas¹⁴, Y. Kataoka¹⁵⁵, C. Kato¹⁵⁵, A. Katre⁴⁹, J. Katzy⁴², K. Kawagoe⁷⁰, T. Kawamoto¹⁵⁵, G. Kawamura⁵⁴, S. Kazama¹⁵⁵, V.F. Kazanin^{109,c}, R. Keeler¹⁶⁹, R. Kehoe⁴⁰, J.S. Keller⁴², J.J. Kempster⁷⁷, H. Keoshkerian⁸⁴, O. Kepka¹²⁷, B.P. Kerševan⁷⁵, S. Kersten¹⁷⁵, R.A. Keyes⁸⁷, F. Khalil-zada¹¹, H. Khandanyan^{146a,146b}, A. Khanov¹¹⁴, A.G. Kharlamov^{109,c}, T.J. Khoo²⁸, V. Khovanskiy⁹⁷, E. Khramov⁶⁵, J. Khubua^{51b,u}, S. Kido⁶⁷, H.Y. Kim⁸, S.H. Kim¹⁶⁰, Y.K. Kim³¹, N. Kimura¹⁵⁴, O.M. Kind¹⁶, B.T. King⁷⁴, M. King¹⁶⁷, S.B. King¹⁶⁸, J. Kirk¹³¹, A.E. Kiryunin¹⁰¹, T. Kishimoto⁶⁷, D. Kisielewska^{38a}, F. Kiss⁴⁸, K. Kiuchi¹⁶⁰, O. Kivernyk¹³⁶, E. Kladiva^{144b}, M.H. Klein³⁵, M. Klein⁷⁴, U. Klein⁷⁴, K. Kleinknecht⁸³, P. Klimek^{146a,146b}, A. Klimentov²⁵, R. Klingenberg⁴³, J.A. Klinger¹³⁹, T. Klioutchnikova³⁰, E.-E. Kluge^{58a}, P. Kluit¹⁰⁷, S. Kluth¹⁰¹, J. Knapik³⁹, E. Kneringer⁶², E.B.F.G. Knoop⁸⁵, A. Knue⁵³, A. Kobayashi¹⁵⁵, D. Kobayashi¹⁵⁷, T. Kobayashi¹⁵⁵, M. Kobel⁴⁴, M. Kocian¹⁴³, P. Kodys¹²⁹, T. Koffas²⁹, E. Koffeman¹⁰⁷, L.A. Kogan¹²⁰, S. Kohlmann¹⁷⁵, Z. Kohout¹²⁸, T. Kohriki⁶⁶, T. Koi¹⁴³, H. Kolanoski¹⁶, I. Koletsou⁵, A.A. Komar^{96,*}, Y. Komori¹⁵⁵, T. Kondo⁶⁶, N. Kondrashova⁴², K. Köneke⁴⁸, A.C. König¹⁰⁶, T. Kono⁶⁶, R. Konoplich^{110,v}, N. Konstantinidis⁷⁸, R. Kopeliansky¹⁵², S. Koperny^{38a}, L. Köpke⁸³, A.K. Kopp⁴⁸, K. Korcyl³⁹, K. Kordas¹⁵⁴, A. Korn⁷⁸, A.A. Korol^{109,c}, I. Korolkov¹², E.V. Korolkova¹³⁹, O. Kortner¹⁰¹, S. Kortner¹⁰¹, T. Kosek¹²⁹, V.V. Kostyukhin²¹, V.M. Kotov⁶⁵, A. Kotwal⁴⁵, A. Kourkoumeli-Charalampidi¹⁵⁴, C. Kourkoumelis⁹, V. Kouskoura²⁵, A. Koutsman^{159a}, R. Kowalewski¹⁶⁹, T.Z. Kowalski^{38a}, W. Kozanecki¹³⁶, A.S. Kozhin¹³⁰, V.A. Kramarenko⁹⁹, G. Kramberger⁷⁵, D. Krasnopevtsev⁹⁸, M.W. Krasny⁸⁰, A. Krasznahorkay³⁰, J.K. Kraus²¹, A. Kravchenko²⁵, S. Kreiss¹¹⁰, M. Kretz^{58c}, J. Kretzschmar⁷⁴, K. Kreutzfeldt⁵², P. Krieger¹⁵⁸, K. Krizka³¹, K. Kroeninger⁴³, H. Kroha¹⁰¹, J. Kroll¹²², J. Kroseberg²¹, J. Krstic¹³, U. Kruchonak⁶⁵, H. Krüger²¹, N. Krumnack⁶⁴, A. Kruse¹⁷³, M.C. Kruse⁴⁵, M. Kruskal²², T. Kubota⁸⁸, H. Kucuk⁷⁸, S. Kудay^{4b}, S. Kuehn⁴⁸, A. Kugel^{58c}, F. Kuger¹⁷⁴, A. Kuhl¹³⁷, T. Kuhl⁴², V. Kukhtin⁶⁵, Y. Kulchitsky⁹², S. Kuleshov^{32b}, M. Kuna^{132a,132b}, T. Kunigo⁶⁸, A. Kupco¹²⁷, H. Kurashige⁶⁷, Y.A. Kurochkin⁹², V. Kus¹²⁷, E.S. Kuwertz¹⁶⁹, M. Kuze¹⁵⁷, J. Kvita¹¹⁵, T. Kwan¹⁶⁹, D. Kyriazopoulos¹³⁹, A. La Rosa¹³⁷, J.L. La Rosa Navarro^{24d}, L. La Rotonda^{37a,37b}, C. Lacasta¹⁶⁷, F. Lacava^{132a,132b}, J. Lacey²⁹, H. Lacker¹⁶, D. Lacour⁸⁰, V.R. Lacuesta¹⁶⁷, E. Ladygin⁶⁵, R. Lafaye⁵, B. Laforge⁸⁰, T. Lagouri¹⁷⁶, S. Lai⁵⁴, L. Lambourne⁷⁸, S. Lammers⁶¹, C.L. Lampen⁷, W. Lampl⁷, E. Lançon¹³⁶, U. Landgraf⁴⁸, M.P.J. Landon⁷⁶, V.S. Lang^{58a}, J.C. Lange¹², A.J. Lankford¹⁶³, F. Lanni²⁵, K. Lantzsch³⁰, A. Lanza^{121a}, S. Laplace⁸⁰, C. Lapoire³⁰, J.F. Laporte¹³⁶, T. Lari^{91a}, F. Lasagni Manghi^{20a,20b}, M. Lassnig³⁰, P. Laurelli⁴⁷, W. Lavrijsen¹⁵, A.T. Law¹³⁷, P. Laycock⁷⁴, T. Lazovich⁵⁷, O. Le Dortz⁸⁰, E. Le Guirriec⁸⁵, E. Le Menedeu¹², M. LeBlanc¹⁶⁹, T. LeCompte⁶, F. Ledroit-Guillon⁵⁵, C.A. Lee^{145b}, S.C. Lee¹⁵¹, L. Lee¹, G. Lefebvre⁸⁰, M. Lefebvre¹⁶⁹, F. Legger¹⁰⁰, C. Leggett¹⁵, A. Lehan⁷⁴, G. Lehmann Miotto³⁰, X. Lei⁷, W.A. Leight²⁹, A. Leisos^{154,w}, A.G. Leister¹⁷⁶, M.A.L. Leite^{24d}, R. Leitner¹²⁹, D. Lellouch¹⁷², B. Lemmer⁵⁴, K.J.C. Leney⁷⁸, T. Lenz²¹, B. Lenzi³⁰, R. Leone⁷, S. Leone^{124a,124b}, C. Leonidopoulos⁴⁶,

S. Leontsinis¹⁰, C. Leroy⁹⁵, C.G. Lester²⁸, M. Levchenko¹²³, J. Levêque⁵, D. Levin⁸⁹, L.J. Levinson¹⁷²,
 M. Levy¹⁸, A. Lewis¹²⁰, A.M. Leyko²¹, M. Leyton⁴¹, B. Li^{33b,x}, H. Li¹⁴⁸, H.L. Li³¹, L. Li⁴⁵, L. Li^{33e},
 S. Li⁴⁵, X. Li⁸⁴, Y. Li^{33c,y}, Z. Liang¹³⁷, H. Liao³⁴, B. Liberti^{133a}, A. Liblong¹⁵⁸, P. Lichard³⁰, K. Lie¹⁶⁵,
 J. Liebal²¹, W. Liebig¹⁴, C. Limbach²¹, A. Limosani¹⁵⁰, S.C. Lin^{151,z}, T.H. Lin⁸³, F. Linde¹⁰⁷,
 B.E. Lindquist¹⁴⁸, J.T. Linnemann⁹⁰, E. Lipeles¹²², A. Lipniacka¹⁴, M. Lisovyi^{58b}, T.M. Liss¹⁶⁵,
 D. Lissauer²⁵, A. Lister¹⁶⁸, A.M. Litke¹³⁷, B. Liu^{151,aa}, D. Liu¹⁵¹, H. Liu⁸⁹, J. Liu⁸⁵, J.B. Liu^{33b},
 K. Liu⁸⁵, L. Liu¹⁶⁵, M. Liu⁴⁵, M. Liu^{33b}, Y. Liu^{33b}, M. Livan^{121a,121b}, A. Lleres⁵⁵, J. Llorente Merino⁸²,
 S.L. Lloyd⁷⁶, F. Lo Sterzo¹⁵¹, E. Lobodzinska⁴², P. Loch⁷, W.S. Lockman¹³⁷, F.K. Loebinger⁸⁴,
 A.E. Loevschall-Jensen³⁶, A. Loginov¹⁷⁶, T. Lohse¹⁶, K. Lohwasser⁴², M. Lokajicek¹²⁷, B.A. Long²²,
 J.D. Long⁸⁹, R.E. Long⁷², K.A. Looper¹¹¹, L. Lopes^{126a}, D. Lopez Mateos⁵⁷, B. Lopez Paredes¹³⁹,
 I. Lopez Paz¹², J. Lorenz¹⁰⁰, N. Lorenzo Martinez⁶¹, M. Losada¹⁶², P. Loscutoff¹⁵, P.J. Lösel¹⁰⁰,
 X. Lou^{33a}, A. Lounis¹¹⁷, J. Love⁶, P.A. Love⁷², N. Lu⁸⁹, H.J. Lubatti¹³⁸, C. Luci^{132a,132b}, A. Lucotte⁵⁵,
 F. Luehring⁶¹, W. Lukas⁶², L. Luminari^{132a}, O. Lundberg^{146a,146b}, B. Lund-Jensen¹⁴⁷, D. Lynn²⁵,
 R. Lysak¹²⁷, E. Lytken⁸¹, H. Ma²⁵, L.L. Ma^{33d}, G. Maccarrone⁴⁷, A. Macchiolo¹⁰¹, C.M. Macdonald¹³⁹,
 B. Maček⁷⁵, J. Machado Miguens^{122,126b}, D. Macina³⁰, D. Madaffari⁸⁵, R. Madar³⁴, H.J. Maddocks⁷²,
 W.F. Mader⁴⁴, A. Madsen¹⁶⁶, J. Maeda⁶⁷, S. Maeland¹⁴, T. Maeno²⁵, A. Maevskiy⁹⁹, E. Magradze⁵⁴,
 K. Mahboubi⁴⁸, J. Mahlstedt¹⁰⁷, C. Maiani¹³⁶, C. Maidantchik^{24a}, A.A. Maier¹⁰¹, T. Maier¹⁰⁰,
 A. Maio^{126a,126b,126d}, S. Majewski¹¹⁶, Y. Makida⁶⁶, N. Makovec¹¹⁷, B. Malaescu⁸⁰, Pa. Malecki³⁹,
 V.P. Maleev¹²³, F. Malek⁵⁵, U. Mallik⁶³, D. Malon⁶, C. Malone¹⁴³, S. Maltezos¹⁰, V.M. Malyshev¹⁰⁹,
 S. Malyukov³⁰, J. Mamuzic⁴², G. Mancini⁴⁷, B. Mandelli³⁰, L. Mandelli^{91a}, I. Mandić⁷⁵,
 R. Mandrysch⁶³, J. Maneira^{126a,126b}, A. Manfredini¹⁰¹, L. Manhaes de Andrade Filho^{24b},
 J. Manjarres Ramos^{159b}, A. Mann¹⁰⁰, A. Manousakis-Katsikakis⁹, B. Mansoulie¹³⁶, R. Mantifel⁸⁷,
 M. Mantoani⁵⁴, L. Mapelli³⁰, L. March^{145c}, G. Marchiori⁸⁰, M. Marcisovsky¹²⁷, C.P. Marino¹⁶⁹,
 M. Marjanovic¹³, D.E. Marley⁸⁹, F. Marroquim^{24a}, S.P. Marsden⁸⁴, Z. Marshall¹⁵, L.F. Marti¹⁷,
 S. Marti-Garcia¹⁶⁷, B. Martin⁹⁰, T.A. Martin¹⁷⁰, V.J. Martin⁴⁶, B. Martin dit Latour¹⁴, M. Martinez^{12,o},
 S. Martin-Haugh¹³¹, V.S. Martoiu^{26a}, A.C. Martyniuk⁷⁸, M. Marx¹³⁸, F. Marzano^{132a}, A. Marzin³⁰,
 L. Masetti⁸³, T. Mashimo¹⁵⁵, R. Mashinistov⁹⁶, J. Masik⁸⁴, A.L. Maslennikov^{109,c}, I. Massa^{20a,20b},
 L. Massa^{20a,20b}, N. Massol⁵, P. Mastrandrea¹⁴⁸, A. Mastroberardino^{37a,37b}, T. Masubuchi¹⁵⁵,
 P. Mättig¹⁷⁵, J. Mattmann⁸³, J. Maurer^{26a}, S.J. Maxfield⁷⁴, D.A. Maximov^{109,c}, R. Mazini¹⁵¹,
 S.M. Mazza^{91a,91b}, L. Mazzaferro^{133a,133b}, G. Mc Goldrick¹⁵⁸, S.P. Mc Kee⁸⁹, A. McCarn⁸⁹,
 R.L. McCarthy¹⁴⁸, T.G. McCarthy²⁹, N.A. McCubbin¹³¹, K.W. McFarlane^{56,*}, J.A. McFayden⁷⁸,
 G. Mchedlidze⁵⁴, S.J. McMahon¹³¹, R.A. McPherson^{169,k}, M. Medinnis⁴², S. Meehan^{145a},
 S. Mehlhase¹⁰⁰, A. Mehta⁷⁴, K. Meier^{58a}, C. Meineck¹⁰⁰, B. Meirose⁴¹, B.R. Mellado Garcia^{145c},
 F. Meloni¹⁷, A. Mengarelli^{20a,20b}, S. Menke¹⁰¹, E. Meoni¹⁶¹, K.M. Mercurio⁵⁷, S. Mergelmeyer²¹,
 P. Mermod⁴⁹, L. Merola^{104a,104b}, C. Meroni^{91a}, F.S. Merritt³¹, A. Messina^{132a,132b}, J. Metcalfe²⁵,
 A.S. Mete¹⁶³, C. Meyer⁸³, C. Meyer¹²², J-P. Meyer¹³⁶, J. Meyer¹⁰⁷, H. Meyer Zu Theenhausen^{58a},
 R.P. Middleton¹³¹, S. Miglioranzzi^{164a,164c}, L. Mijović²¹, G. Mikenberg¹⁷², M. Mikestikova¹²⁷,
 M. Mikuž⁷⁵, M. Milesi⁸⁸, A. Milic³⁰, D.W. Miller³¹, C. Mills⁴⁶, A. Milov¹⁷², D.A. Milstead^{146a,146b},
 A.A. Minaenko¹³⁰, Y. Minami¹⁵⁵, I.A. Minashvili⁶⁵, A.I. Mincer¹¹⁰, B. Mindur^{38a}, M. Mineev⁶⁵,
 Y. Ming¹⁷³, L.M. Mir¹², T. Mitani¹⁷¹, J. Mitrevski¹⁰⁰, V.A. Mitsou¹⁶⁷, A. Miucci⁴⁹, P.S. Miyagawa¹³⁹,
 J.U. Mjörnmark⁸¹, T. Moa^{146a,146b}, K. Mochizuki⁸⁵, S. Mohapatra³⁵, W. Mohr⁴⁸, S. Molander^{146a,146b},
 R. Moles-Valls²¹, K. Mönig⁴², C. Monini⁵⁵, J. Monk³⁶, E. Monnier⁸⁵, J. Montejo Berlingen¹²,
 F. Monticelli⁷¹, S. Monzani^{132a,132b}, R.W. Moore³, N. Morange¹¹⁷, D. Moreno¹⁶², M. Moreno Llácer⁵⁴,
 P. Morettini^{50a}, D. Mori¹⁴², M. Morii⁵⁷, M. Morinaga¹⁵⁵, V. Morisbak¹¹⁹, S. Moritz⁸³, A.K. Morley¹⁵⁰,
 G. Mornacchi³⁰, J.D. Morris⁷⁶, S.S. Mortensen³⁶, A. Morton⁵³, L. Morvaj¹⁰³, M. Mosidze^{51b},
 J. Moss¹¹¹, K. Motohashi¹⁵⁷, R. Mout¹⁴³, E. Mountricha²⁵, S.V. Mouraviev^{96,*}, E.J.W. Moyses⁸⁶,
 S. Muanza⁸⁵, R.D. Mudd¹⁸, F. Mueller¹⁰¹, J. Mueller¹²⁵, R.S.P. Mueller¹⁰⁰, T. Mueller²⁸,

D. Muenstermann⁴⁹, P. Mullen⁵³, G.A. Mullier¹⁷, J.A. Murillo Quijada¹⁸, W.J. Murray^{170,131},
 H. Musheghyan⁵⁴, E. Musto¹⁵², A.G. Myagkov^{130,ab}, M. Myska¹²⁸, B.P. Nachman¹⁴³, O. Nackenhorst⁵⁴,
 J. Nadal⁵⁴, K. Nagai¹²⁰, R. Nagai¹⁵⁷, Y. Nagai⁸⁵, K. Nagano⁶⁶, A. Nagarkar¹¹¹, Y. Nagasaka⁵⁹,
 K. Nagata¹⁶⁰, M. Nagel¹⁰¹, E. Nagy⁸⁵, A.M. Nairz³⁰, Y. Nakahama³⁰, K. Nakamura⁶⁶, T. Nakamura¹⁵⁵,
 I. Nakano¹¹², H. Namasivayam⁴¹, R.F. Naranjo Garcia⁴², R. Narayan³¹, D.I. Narrias Villar^{58a},
 T. Naumann⁴², G. Navarro¹⁶², R. Nayyar⁷, H.A. Neal⁸⁹, P.Yu. Nechaeva⁹⁶, T.J. Neep⁸⁴, P.D. Nef¹⁴³,
 A. Negri^{121a,121b}, M. Negrini^{20a}, S. Nektarijevic¹⁰⁶, C. Nellist¹¹⁷, A. Nelson¹⁶³, S. Nemecek¹²⁷,
 P. Nemethy¹¹⁰, A.A. Nepomuceno^{24a}, M. Nessi^{30,ac}, M.S. Neubauer¹⁶⁵, M. Neumann¹⁷⁵,
 R.M. Neves¹¹⁰, P. Nevski²⁵, P.R. Newman¹⁸, D.H. Nguyen⁶, R.B. Nickerson¹²⁰, R. Nicolaidou¹³⁶,
 B. Nicquevert³⁰, J. Nielsen¹³⁷, N. Nikiforou³⁵, A. Nikiforov¹⁶, V. Nikolaenko^{130,ab}, I. Nikolic-Audit⁸⁰,
 K. Nikolopoulos¹⁸, J.K. Nilsen¹¹⁹, P. Nilsson²⁵, Y. Ninomiya¹⁵⁵, A. Nisati^{132a}, R. Nisius¹⁰¹, T. Nobe¹⁵⁵,
 M. Nomachi¹¹⁸, I. Nomidis²⁹, T. Nooney⁷⁶, S. Norberg¹¹³, M. Nordberg³⁰, O. Novgorodova⁴⁴,
 S. Nowak¹⁰¹, M. Nozaki⁶⁶, L. Nozka¹¹⁵, K. Ntekas¹⁰, G. Nunes Hanninger⁸⁸, T. Nunnemann¹⁰⁰,
 E. Nurse⁷⁸, F. Nuti⁸⁸, B.J. O'Brien⁴⁶, F. O'grady⁷, D.C. O'Neil¹⁴², V. O'Shea⁵³, F.G. Oakham^{29,d},
 H. Oberlack¹⁰¹, T. Obermann²¹, J. Ocariz⁸⁰, A. Ochi⁶⁷, I. Ochoa⁷⁸, J.P. Ochoa-Ricoux^{32a}, S. Oda⁷⁰,
 S. Odaka⁶⁶, H. Ogren⁶¹, A. Oh⁸⁴, S.H. Oh⁴⁵, C.C. Ohm¹⁵, H. Ohman¹⁶⁶, H. Oide³⁰, W. Okamura¹¹⁸,
 H. Okawa¹⁶⁰, Y. Okumura³¹, T. Okuyama⁶⁶, A. Olariu^{26a}, S.A. Olivares Pino⁴⁶, D. Oliveira Damazio²⁵,
 E. Oliver Garcia¹⁶⁷, A. Olszewski³⁹, J. Olszowska³⁹, A. Onofre^{126a,126e}, P.U.E. Onyisi^{31,r},
 C.J. Oram^{159a}, M.J. Oreglia³¹, Y. Oren¹⁵³, D. Orestano^{134a,134b}, N. Orlando¹⁵⁴, C. Oropeza Barrera⁵³,
 R.S. Orr¹⁵⁸, B. Osculati^{50a,50b}, R. Ospanov⁸⁴, G. Otero y Garzon²⁷, H. Otono⁷⁰, M. Ouchrif^{135d},
 F. Ould-Saada¹¹⁹, A. Ouraou¹³⁶, K.P. Oussoren¹⁰⁷, Q. Ouyang^{33a}, A. Ovcharova¹⁵, M. Owen⁵³,
 R.E. Owen¹⁸, V.E. Ozcan^{19a}, N. Ozturk⁸, K. Pachal¹⁴², A. Pacheco Pages¹², C. Padilla Aranda¹²,
 M. Pagáčová⁴⁸, S. Pagan Griso¹⁵, E. Paganis¹³⁹, F. Paige²⁵, P. Pais⁸⁶, K. Pajchel¹¹⁹, G. Palacino^{159b},
 S. Palestini³⁰, M. Palka^{38b}, D. Pallin³⁴, A. Palma^{126a,126b}, Y.B. Pan¹⁷³, E. Panagiotopoulou¹⁰,
 C.E. Pandini⁸⁰, J.G. Panduro Vazquez⁷⁷, P. Pani^{146a,146b}, S. Panitkin²⁵, D. Pantea^{26a}, L. Paolozzi⁴⁹,
 Th.D. Papadopoulou¹⁰, K. Papageorgiou¹⁵⁴, A. Paramonov⁶, D. Paredes Hernandez¹⁵⁴, M.A. Parker²⁸,
 K.A. Parker¹³⁹, F. Parodi^{50a,50b}, J.A. Parsons³⁵, U. Parzefall⁴⁸, E. Pasqualucci^{132a}, S. Passaggio^{50a},
 F. Pastore^{134a,134b,*}, Fr. Pastore⁷⁷, G. Pásztor²⁹, S. Patariaia¹⁷⁵, N.D. Patel¹⁵⁰, J.R. Pater⁸⁴, T. Pauly³⁰,
 J. Pearce¹⁶⁹, B. Pearson¹¹³, L.E. Pedersen³⁶, M. Pedersen¹¹⁹, S. Pedraza Lopez¹⁶⁷, R. Pedro^{126a,126b},
 S.V. Peleganchuk^{109,c}, D. Pelikan¹⁶⁶, O. Penc¹²⁷, C. Peng^{33a}, H. Peng^{33b}, B. Penning³¹, J. Penwell⁶¹,
 D.V. Perepelitsa²⁵, E. Perez Codina^{159a}, M.T. Pérez García-Están¹⁶⁷, L. Perini^{91a,91b}, H. Pernegger³⁰,
 S. Perrella^{104a,104b}, R. Peschke⁴², V.D. Peshekhonov⁶⁵, K. Peters³⁰, R.F.Y. Peters⁸⁴, B.A. Petersen³⁰,
 T.C. Petersen³⁶, E. Petit⁴², A. Petridis¹, C. Petridou¹⁵⁴, P. Petroff¹¹⁷, E. Petrolo^{132a}, F. Petrucci^{134a,134b},
 N.E. Pettersson¹⁵⁷, R. Pezoa^{32b}, P.W. Phillips¹³¹, G. Piacquadio¹⁴³, E. Pianori¹⁷⁰, A. Picazio⁴⁹,
 E. Piccaro⁷⁶, M. Piccinini^{20a,20b}, M.A. Pickering¹²⁰, R. Piegaia²⁷, D.T. Pignotti¹¹¹, J.E. Pilcher³¹,
 A.D. Pilkington⁸⁴, J. Pina^{126a,126b,126d}, M. Pinamonti^{164a,164c,ad}, J.L. Pinfeld³, A. Pingel³⁶, S. Pires⁸⁰,
 H. Pirumov⁴², M. Pitt¹⁷², C. Pizio^{91a,91b}, L. Plazak^{144a}, M.-A. Pleier²⁵, V. Pleskot¹²⁹, E. Plotnikova⁶⁵,
 P. Plucinski^{146a,146b}, D. Pluth⁶⁴, R. Poettgen^{146a,146b}, L. Poggioli¹¹⁷, D. Pohl²¹, G. Polesello^{121a},
 A. Poley⁴², A. Policicchio^{37a,37b}, R. Polifka¹⁵⁸, A. Polini^{20a}, C.S. Pollard⁵³, V. Polychronakos²⁵,
 K. Pommès³⁰, L. Pontecorvo^{132a}, B.G. Pope⁹⁰, G.A. Popeneciu^{26b}, D.S. Popovic¹³, A. Poppleton³⁰,
 S. Pospisil¹²⁸, K. Potamianos¹⁵, I.N. Potrap⁶⁵, C.J. Potter¹⁴⁹, C.T. Potter¹¹⁶, G. Poulard³⁰, J. Poveda³⁰,
 V. Pozdnyakov⁶⁵, P. Pralavorio⁸⁵, A. Pranko¹⁵, S. Prasad³⁰, S. Prell⁶⁴, D. Price⁸⁴, L.E. Price⁶,
 M. Primavera^{73a}, S. Prince⁸⁷, M. Proissl⁴⁶, K. Prokofiev^{60c}, F. Prokoshin^{32b}, E. Protopapadaki¹³⁶,
 S. Protopopescu²⁵, J. Proudfoot⁶, M. Przybycien^{38a}, E. Ptacek¹¹⁶, D. Puddu^{134a,134b}, E. Pueschel⁸⁶,
 D. Puldon¹⁴⁸, M. Purohit^{25,ae}, P. Puzo¹¹⁷, J. Qian⁸⁹, G. Qin⁵³, Y. Qin⁸⁴, A. Quadt⁵⁴, D.R. Quarrie¹⁵,
 W.B. Quayle^{164a,164b}, M. Queitsch-Maitland⁸⁴, D. Quilty⁵³, S. Raddum¹¹⁹, V. Radeka²⁵, V. Radescu⁴²,
 S.K. Radhakrishnan¹⁴⁸, P. Radloff¹¹⁶, P. Rados⁸⁸, F. Ragusa^{91a,91b}, G. Rahal¹⁷⁸, S. Rajagopalan²⁵,

M. Rammensee³⁰, C. Rangel-Smith¹⁶⁶, F. Rauscher¹⁰⁰, S. Rave⁸³, T. Ravenscroft⁵³, M. Raymond³⁰,
A.L. Read¹¹⁹, N.P. Readioff⁷⁴, D.M. Rebuzzi^{121a,121b}, A. Redelbach¹⁷⁴, G. Redlinger²⁵, R. Reece¹³⁷,
K. Reeves⁴¹, L. Rehnisch¹⁶, J. Reichert¹²², H. Reisin²⁷, M. Relich¹⁶³, C. Rembser³⁰, H. Ren^{33a},
A. Renaud¹¹⁷, M. Rescigno^{132a}, S. Resconi^{91a}, O.L. Rezanova^{109,c}, P. Reznicek¹²⁹, R. Rezvani⁹⁵,
R. Richter¹⁰¹, S. Richter⁷⁸, E. Richter-Was^{38b}, O. Ricken²¹, M. Ridel⁸⁰, P. Rieck¹⁶, C.J. Riegel¹⁷⁵,
J. Rieger⁵⁴, M. Rijssenbeek¹⁴⁸, A. Rimoldi^{121a,121b}, L. Rinaldi^{20a}, B. Ristić⁴⁹, E. Ritsch³⁰, I. Riu¹²,
F. Rizatdinova¹¹⁴, E. Rizvi⁷⁶, S.H. Robertson^{87,k}, A. Robichaud-Veronneau⁸⁷, D. Robinson²⁸,
J.E.M. Robinson⁴², A. Robson⁵³, C. Roda^{124a,124b}, S. Roe³⁰, O. Røhne¹¹⁹, S. Rolli¹⁶¹, A. Romaniouk⁹⁸,
M. Romano^{20a,20b}, S.M. Romano Saez³⁴, E. Romero Adam¹⁶⁷, N. Rompotis¹³⁸, M. Ronzani⁴⁸,
L. Roos⁸⁰, E. Ros¹⁶⁷, S. Rosati^{132a}, K. Rosbach⁴⁸, P. Rose¹³⁷, P.L. Rosendahl¹⁴, O. Rosenthal¹⁴¹,
V. Rossetti^{146a,146b}, E. Rossi^{104a,104b}, L.P. Rossi^{50a}, J.H.N. Rosten²⁸, R. Rosten¹³⁸, M. Rotaru^{26a},
I. Roth¹⁷², J. Rothberg¹³⁸, D. Rousseau¹¹⁷, C.R. Royon¹³⁶, A. Rozanov⁸⁵, Y. Rozen¹⁵², X. Ruan^{145c},
F. Rubbo¹⁴³, I. Rubinskiy⁴², V.I. Rud⁹⁹, C. Rudolph⁴⁴, M.S. Rudolph¹⁵⁸, F. Rühr⁴⁸, A. Ruiz-Martinez³⁰,
Z. Rurikova⁴⁸, N.A. Rusakovich⁶⁵, A. Ruschke¹⁰⁰, H.L. Russell¹³⁸, J.P. Rutherford⁷, N. Ruthmann⁴⁸,
Y.F. Ryabov¹²³, M. Rybar¹⁶⁵, G. Rybkin¹¹⁷, N.C. Ryder¹²⁰, A.F. Saavedra¹⁵⁰, G. Sabato¹⁰⁷,
S. Sacerdoti²⁷, A. Saddique³, H.F.W. Sadrozinski¹³⁷, R. Sadykov⁶⁵, F. Safai Tehrani^{132a},
M. Sahinsoy^{58a}, M. Saimpert¹³⁶, T. Saito¹⁵⁵, H. Sakamoto¹⁵⁵, Y. Sakurai¹⁷¹, G. Salamanna^{134a,134b},
A. Salamon^{133a}, J.E. Salazar Loyola^{32b}, M. Saleem¹¹³, D. Salek¹⁰⁷, P.H. Sales De Bruin¹³⁸,
D. Salihagic¹⁰¹, A. Salnikov¹⁴³, J. Salt¹⁶⁷, D. Salvatore^{37a,37b}, F. Salvatore¹⁴⁹, A. Salvucci^{60a},
A. Salzburger³⁰, D. Sammel⁴⁸, D. Sampsonidis¹⁵⁴, A. Sanchez^{104a,104b}, J. Sánchez¹⁶⁷,
V. Sanchez Martinez¹⁶⁷, H. Sandaker¹¹⁹, R.L. Sandbach⁷⁶, H.G. Sander⁸³, M.P. Sanders¹⁰⁰,
M. Sandhoff¹⁷⁵, C. Sandoval¹⁶², R. Sandstroem¹⁰¹, D.P.C. Sankey¹³¹, M. Sannino^{50a,50b}, A. Sansoni⁴⁷,
C. Santoni³⁴, R. Santonico^{133a,133b}, H. Santos^{126a}, I. Santoyo Castillo¹⁴⁹, K. Sapp¹²⁵, A. Saponov⁶⁵,
J.G. Saraiva^{126a,126d}, B. Sarrazin²¹, O. Sasaki⁶⁶, Y. Sasaki¹⁵⁵, K. Sato¹⁶⁰, G. Sauvage^{5,*}, E. Sauvan⁵,
G. Savage⁷⁷, P. Savard^{158,d}, C. Sawyer¹³¹, L. Sawyer^{79,n}, J. Saxon³¹, C. Sbarra^{20a}, A. Sbrizzi^{20a,20b},
T. Scanlon⁷⁸, D.A. Scannicchio¹⁶³, M. Scarcella¹⁵⁰, V. Scarfone^{37a,37b}, J. Schaarschmidt¹⁷²,
P. Schacht¹⁰¹, D. Schaefer³⁰, R. Schaefer⁴², J. Schaeffer⁸³, S. Schaepe²¹, S. Schaetzel^{58b}, U. Schäfer⁸³,
A.C. Schaffer¹¹⁷, D. Schaile¹⁰⁰, R.D. Schamberger¹⁴⁸, V. Scharf^{58a}, V.A. Schegelsky¹²³, D. Scheirich¹²⁹,
M. Schernau¹⁶³, C. Schiavi^{50a,50b}, C. Schillo⁴⁸, M. Schioppa^{37a,37b}, S. Schlenker³⁰, E. Schmidt⁴⁸,
K. Schmieden³⁰, C. Schmitt⁸³, S. Schmitt^{58b}, S. Schmitt⁴², B. Schneider^{159a}, Y.J. Schnellbach⁷⁴,
U. Schnoor⁴⁴, L. Schoeffel¹³⁶, A. Schoening^{58b}, B.D. Schoenrock⁹⁰, E. Schopf²¹,
A.L.S. Schorlemmer⁵⁴, M. Schott⁸³, D. Schouten^{159a}, J. Schovancova⁸, S. Schramm⁴⁹, M. Schreyer¹⁷⁴,
C. Schroeder⁸³, N. Schuh⁸³, M.J. Schultens²¹, H.-C. Schultz-Coulon^{58a}, H. Schulz¹⁶, M. Schumacher⁴⁸,
B.A. Schumm¹³⁷, Ph. Schune¹³⁶, C. Schwanenberger⁸⁴, A. Schwartzman¹⁴³, T.A. Schwarz⁸⁹,
Ph. Schwegler¹⁰¹, H. Schweiger⁸⁴, Ph. Schwemling¹³⁶, R. Schwienhorst⁹⁰, J. Schwindling¹³⁶,
T. Schwindt²¹, F.G. Sciaccia¹⁷, E. Scifo¹¹⁷, G. Sciolla²³, F. Scuri^{124a,124b}, F. Scutti²¹, J. Searcy⁸⁹,
G. Sedov⁴², E. Sedykh¹²³, P. Seema²¹, S.C. Seidel¹⁰⁵, A. Seiden¹³⁷, F. Seifert¹²⁸, J.M. Seixas^{24a},
G. Sekhniaidze^{104a}, K. Sekhon⁸⁹, S.J. Sekula⁴⁰, D.M. Seliverstov^{123,*}, N. Semprini-Cesari^{20a,20b},
C. Serfon³⁰, L. Serin¹¹⁷, L. Serkin^{164a,164b}, T. Serre⁸⁵, M. Sessa^{134a,134b}, R. Seuster^{159a}, H. Severini¹¹³,
T. Sfiligoi⁷⁵, F. Sforza³⁰, A. Sfyrla³⁰, E. Shabalina⁵⁴, M. Shamim¹¹⁶, L.Y. Shan^{33a}, R. Shang¹⁶⁵,
J.T. Shank²², M. Shapiro¹⁵, P.B. Shatalov⁹⁷, K. Shaw^{164a,164b}, S.M. Shaw⁸⁴, A. Shcherbakova^{146a,146b},
C.Y. Shehu¹⁴⁹, P. Sherwood⁷⁸, L. Shi^{151,af}, S. Shimizu⁶⁷, C.O. Shimmin¹⁶³, M. Shimojima¹⁰²,
M. Shiyakova⁶⁵, A. Shmeleva⁹⁶, D. Shoaleh Saadi⁹⁵, M.J. Shochet³¹, S. Shojaii^{91a,91b}, S. Shrestha¹¹¹,
E. Shulga⁹⁸, M.A. Shupe⁷, S. Shushkevich⁴², P. Sicho¹²⁷, P.E. Sidebo¹⁴⁷, O. Sidiropoulou¹⁷⁴,
D. Sidorov¹¹⁴, A. Sidoti^{20a,20b}, F. Siegert⁴⁴, Dj. Sijacki¹³, J. Silva^{126a,126d}, Y. Silver¹⁵³,
S.B. Silverstein^{146a}, V. Simak¹²⁸, O. Simard⁵, Lj. Simic¹³, S. Simion¹¹⁷, E. Simioni⁸³, B. Simmons⁷⁸,
D. Simon³⁴, R. Simoniello^{91a,91b}, P. Sinervo¹⁵⁸, N.B. Sinev¹¹⁶, M. Sioli^{20a,20b}, G. Siragusa¹⁷⁴,

A.N. Sisakyan^{65,*}, S.Yu. Sivoklov⁹⁹, J. Sjölin^{146a,146b}, T.B. Sjurson¹⁴, M.B. Skinner⁷²,
 H.P. Skottowe⁵⁷, P. Skubic¹¹³, M. Slater¹⁸, T. Slavicek¹²⁸, M. Slawinska¹⁰⁷, K. Sliwa¹⁶¹,
 V. Smakhtin¹⁷², B.H. Smart⁴⁶, L. Smestad¹⁴, S.Yu. Smirnov⁹⁸, Y. Smirnov⁹⁸, L.N. Smirnova^{99,ag},
 O. Smirnova⁸¹, M.N.K. Smith³⁵, R.W. Smith³⁵, M. Smizanska⁷², K. Smolek¹²⁸, A.A. Snesarev⁹⁶,
 G. Snidero⁷⁶, S. Snyder²⁵, R. Sobie^{169,k}, F. Socher⁴⁴, A. Soffer¹⁵³, D.A. Soh^{151,af}, C.A. Solans³⁰,
 M. Solar¹²⁸, J. Solc¹²⁸, E.Yu. Soldatov⁹⁸, U. Soldevila¹⁶⁷, A.A. Solodkov¹³⁰, A. Soloshenko⁶⁵,
 O.V. Solovyanov¹³⁰, V. Solovyev¹²³, P. Sommer⁴⁸, H.Y. Song^{33b}, N. Soni¹, A. Sood¹⁵, A. Sopczak¹²⁸,
 B. Sopko¹²⁸, V. Sopko¹²⁸, V. Sorin¹², D. Sosa^{58b}, M. Sosebee⁸, C.L. Sotiropoulou^{124a,124b},
 R. Soualah^{164a,164c}, A.M. Soukharev^{109,c}, D. South⁴², B.C. Sowden⁷⁷, S. Spagnolo^{73a,73b},
 M. Spalla^{124a,124b}, F. Spanò⁷⁷, W.R. Spearman⁵⁷, D. Sperlich¹⁶, F. Spettel¹⁰¹, R. Spighi^{20a}, G. Spigo³⁰,
 L.A. Spiller⁸⁸, M. Spousta¹²⁹, T. Spreitzer¹⁵⁸, R.D. St. Denis^{53,*}, S. Staerz⁴⁴, J. Stahlman¹²²,
 R. Stamen^{58a}, S. Stamm¹⁶, E. Stanecka³⁹, C. Stanescu^{134a}, M. Stanescu-Bellu⁴², M.M. Stanitzki⁴²,
 S. Stapnes¹¹⁹, E.A. Starchenko¹³⁰, J. Stark⁵⁵, P. Staroba¹²⁷, P. Starovoitov^{58a}, R. Staszewski³⁹,
 P. Stavina^{144a,*}, P. Steinberg²⁵, B. Stelzer¹⁴², H.J. Stelzer³⁰, O. Stelzer-Chilton^{159a}, H. Stenzel⁵²,
 G.A. Stewart⁵³, J.A. Stillings²¹, M.C. Stockton⁸⁷, M. Stoebe⁸⁷, G. Stoicea^{26a}, P. Stolte⁵⁴, S. Stonjek¹⁰¹,
 A.R. Stradling⁸, A. Straessner⁴⁴, M.E. Stramaglia¹⁷, J. Strandberg¹⁴⁷, S. Strandberg^{146a,146b},
 A. Strandlie¹¹⁹, E. Strauss¹⁴³, M. Strauss¹¹³, P. Strizenc^{144b}, R. Ströhmer¹⁷⁴, D.M. Strom¹¹⁶,
 R. Stroynowski⁴⁰, A. Strubig¹⁰⁶, S.A. Stucci¹⁷, B. Stugu¹⁴, N.A. Styles⁴², D. Su¹⁴³, J. Su¹²⁵,
 R. Subramaniam⁷⁹, A. Succurro¹², Y. Sugaya¹¹⁸, C. Suhr¹⁰⁸, M. Suk¹²⁸, V.V. Sulin⁹⁶, S. Sultansoy^{4c},
 T. Sumida⁶⁸, S. Sun⁵⁷, X. Sun^{33a}, J.E. Sundermann⁴⁸, K. Suruliz¹⁴⁹, G. Susinno^{37a,37b}, M.R. Sutton¹⁴⁹,
 S. Suzuki⁶⁶, M. Svatos¹²⁷, M. Swiatlowski¹⁴³, I. Sykora^{144a}, T. Sykora¹²⁹, D. Ta⁹⁰, C. Taccini^{134a,134b},
 K. Tackmann⁴², J. Taenzer¹⁵⁸, A. Taffard¹⁶³, R. Tafirout^{159a}, N. Taiblum¹⁵³, H. Takai²⁵, R. Takashima⁶⁹,
 H. Takeda⁶⁷, T. Takeshita¹⁴⁰, Y. Takubo⁶⁶, M. Talby⁸⁵, A.A. Talyshev^{109,c}, J.Y.C. Tam¹⁷⁴, K.G. Tan⁸⁸,
 J. Tanaka¹⁵⁵, R. Tanaka¹¹⁷, S. Tanaka⁶⁶, B.B. Tannenwald¹¹¹, N. Tannoury²¹, S. Tapprogge⁸³,
 S. Tarem¹⁵², F. Tarrade²⁹, G.F. Tartarelli^{91a}, P. Tas¹²⁹, M. Tasevsky¹²⁷, T. Tashiro⁶⁸, E. Tassi^{37a,37b},
 A. Tavares Delgado^{126a,126b}, Y. Tayalati^{135d}, F.E. Taylor⁹⁴, G.N. Taylor⁸⁸, W. Taylor^{159b},
 F.A. Teischinger³⁰, M. Teixeira Dias Castanheira⁷⁶, P. Teixeira-Dias⁷⁷, K.K. Temming⁴⁸, D. Temple¹⁴²,
 H. Ten Kate³⁰, P.K. Teng¹⁵¹, J.J. Teoh¹¹⁸, F. Tepel¹⁷⁵, S. Terada⁶⁶, K. Terashi¹⁵⁵, J. Terron⁸², S. Terzo¹⁰¹,
 M. Testa⁴⁷, R.J. Teuscher^{158,k}, T. Theveneaux-Pelzer³⁴, J.P. Thomas¹⁸, J. Thomas-Wilsker⁷⁷,
 E.N. Thompson³⁵, P.D. Thompson¹⁸, R.J. Thompson⁸⁴, A.S. Thompson⁵³, L.A. Thomsen¹⁷⁶,
 E. Thomson¹²², M. Thomson²⁸, R.P. Thun^{89,*}, M.J. Tibbetts¹⁵, R.E. Ticse Torres⁸⁵,
 V.O. Tikhomirov^{96,ah}, Yu.A. Tikhonov^{109,c}, S. Timoshenko⁹⁸, E. Tiouchichine⁸⁵, P. Tipton¹⁷⁶,
 S. Tisserant⁸⁵, K. Todome¹⁵⁷, T. Todorov⁵, S. Todorova-Nova¹²⁹, J. Tojo⁷⁰, S. Tokár^{144a},
 K. Tokushuku⁶⁶, K. Tollefson⁹⁰, E. Tolley⁵⁷, L. Tomlinson⁸⁴, M. Tomoto¹⁰³, L. Tompkins^{143,ai},
 K. Toms¹⁰⁵, E. Torrence¹¹⁶, H. Torres¹⁴², E. Torró Pastor¹³⁸, J. Toth^{85,aj}, F. Touchard⁸⁵, D.R. Tovey¹³⁹,
 T. Trefzger¹⁷⁴, L. Tremblet³⁰, A. Tricoli³⁰, I.M. Trigger^{159a}, S. Trincaz-Duvoid⁸⁰, M.F. Tripania¹²,
 W. Trischuk¹⁵⁸, B. Trocmé⁵⁵, C. Troncon^{91a}, M. Trotter-McDonald¹⁵, M. Trovatelli¹⁶⁹, P. True⁹⁰,
 L. Truong^{164a,164c}, M. Trzebinski³⁹, A. Trzupek³⁹, C. Tsarouchas³⁰, J.C-L. Tseng¹²⁰, P.V. Tsiareshka⁹²,
 D. Tsionou¹⁵⁴, G. Tsipolitis¹⁰, N. Tsirintanis⁹, S. Tsiskaridze¹², V. Tsiskaridze⁴⁸, E.G. Tskhadadze^{51a},
 I.I. Tsukerman⁹⁷, V. Tsulaia¹⁵, S. Tsuno⁶⁶, D. Tsybychev¹⁴⁸, A. Tudorache^{26a}, V. Tudorache^{26a},
 A.N. Tuna¹²², S.A. Tupputi^{20a,20b}, S. Turchikhin^{99,ag}, D. Turecek¹²⁸, R. Turra^{91a,91b}, A.J. Turvey⁴⁰,
 P.M. Tuts³⁵, A. Tykhonov⁴⁹, M. Tylmad^{146a,146b}, M. Tyndel¹³¹, I. Ueda¹⁵⁵, R. Ueno²⁹,
 M. Ughetto^{146a,146b}, M. Ugland¹⁴, F. Ukegawa¹⁶⁰, G. Unal³⁰, A. Undrus²⁵, G. Unel¹⁶³, F.C. Ungaro⁴⁸,
 Y. Unno⁶⁶, C. Unverdorben¹⁰⁰, J. Urban^{144b}, P. Urquijo⁸⁸, P. Urrejola⁸³, G. Usai⁸, A. Usanova⁶²,
 L. Vacavant⁸⁵, V. Vacek¹²⁸, B. Vachon⁸⁷, C. Valderanis⁸³, N. Valencic¹⁰⁷, S. Valentini^{20a,20b},
 A. Valero¹⁶⁷, L. Valery¹², S. Valkar¹²⁹, E. Valladolid Gallego¹⁶⁷, S. Vallecorsa⁴⁹, J.A. Valls Ferrer¹⁶⁷,
 W. Van Den Wollenberg¹⁰⁷, P.C. Van Der Deijl¹⁰⁷, R. van der Geer¹⁰⁷, H. van der Graaf¹⁰⁷,

N. van Eldik¹⁵², P. van Gemmeren⁶, J. Van Nieuwkoop¹⁴², I. van Vulpen¹⁰⁷, M.C. van Woerden³⁰, M. Vanadia^{132a,132b}, W. Vandelli³⁰, R. Vanguri¹²², A. Vaniachine⁶, F. Vannucci⁸⁰, G. Vardanyan¹⁷⁷, R. Vari^{132a}, E.W. Varnes⁷, T. Varol⁴⁰, D. Varouchas⁸⁰, A. Vartapetian⁸, K.E. Varvell¹⁵⁰, F. Vazeille³⁴, T. Vazquez Schroeder⁸⁷, J. Veatch⁷, L.M. Veloce¹⁵⁸, F. Veloso^{126a,126c}, T. Velz²¹, S. Veneziano^{132a}, A. Ventura^{73a,73b}, D. Ventura⁸⁶, M. Venturi¹⁶⁹, N. Venturi¹⁵⁸, A. Venturini²³, V. Vercesi^{121a}, M. Verducci^{132a,132b}, W. Verkerke¹⁰⁷, J.C. Vermeulen¹⁰⁷, A. Vest⁴⁴, M.C. Vetterli^{142,d}, O. Viazlo⁸¹, I. Vichou¹⁶⁵, T. Vickey¹³⁹, O.E. Vickey Boeriu¹³⁹, G.H.A. Viehhauser¹²⁰, S. Viel¹⁵, R. Vigne⁶², M. Villa^{20a,20b}, M. Villaplana Perez^{91a,91b}, E. Vilucchi⁴⁷, M.G. Vincter²⁹, V.B. Vinogradov⁶⁵, I. Vivarelli¹⁴⁹, F. Vives Vaque³, S. Vlachos¹⁰, D. Vladoiu¹⁰⁰, M. Vlasak¹²⁸, M. Vogel^{32a}, P. Vokac¹²⁸, G. Volpi^{124a,124b}, M. Volpi⁸⁸, H. von der Schmitt¹⁰¹, H. von Radziewski⁴⁸, E. von Toerne²¹, V. Vorobel¹²⁹, K. Vorobev⁹⁸, M. Vos¹⁶⁷, R. Voss³⁰, J.H. Vosseveld⁷⁴, N. Vranjes¹³, M. Vranjes Milosavljevic¹³, V. Vrba¹²⁷, M. Vreeswijk¹⁰⁷, R. Vuillermet³⁰, I. Vukotic³¹, Z. Vykydal¹²⁸, P. Wagner²¹, W. Wagner¹⁷⁵, H. Wahlberg⁷¹, S. Wahrmund⁴⁴, J. Wakabayashi¹⁰³, J. Walder⁷², R. Walker¹⁰⁰, W. Walkowiak¹⁴¹, C. Wang¹⁵¹, F. Wang¹⁷³, H. Wang¹⁵, H. Wang⁴⁰, J. Wang⁴², J. Wang^{33a}, K. Wang⁸⁷, R. Wang⁶, S.M. Wang¹⁵¹, T. Wang²¹, T. Wang³⁵, X. Wang¹⁷⁶, C. Wanotayaroj¹¹⁶, A. Warburton⁸⁷, C.P. Ward²⁸, D.R. Wardrope⁷⁸, A. Washbrook⁴⁶, C. Wasicki⁴², P.M. Watkins¹⁸, A.T. Watson¹⁸, I.J. Watson¹⁵⁰, M.F. Watson¹⁸, G. Watts¹³⁸, S. Watts⁸⁴, B.M. Waugh⁷⁸, S. Webb⁸⁴, M.S. Weber¹⁷, S.W. Weber¹⁷⁴, J.S. Webster³¹, A.R. Weidberg¹²⁰, B. Weinert⁶¹, J. Weingarten⁵⁴, C. Weiser⁴⁸, H. Weits¹⁰⁷, P.S. Wells³⁰, T. Wenaus²⁵, T. Wengler³⁰, S. Wenig³⁰, N. Vermes²¹, M. Werner⁴⁸, P. Werner³⁰, M. Wessels^{58a}, J. Wetter¹⁶¹, K. Whalen¹¹⁶, A.M. Wharton⁷², A. White⁸, M.J. White¹, R. White^{32b}, S. White^{124a,124b}, D. Whiteson¹⁶³, F.J. Wickens¹³¹, W. Wiedenmann¹⁷³, M. Wielers¹³¹, P. Wienemann²¹, C. Wiglesworth³⁶, L.A.M. Wiik-Fuchs²¹, A. Wildauer¹⁰¹, H.G. Wilkens³⁰, H.H. Williams¹²², S. Williams¹⁰⁷, C. Willis⁹⁰, S. Willocq⁸⁶, A. Wilson⁸⁹, J.A. Wilson¹⁸, I. Wingerter-Seez⁵, F. Winklmeier¹¹⁶, B.T. Winter²¹, M. Wittgen¹⁴³, J. Wittkowski¹⁰⁰, S.J. Wollstadt⁸³, M.W. Wolter³⁹, H. Wolters^{126a,126c}, B.K. Wosiek³⁹, J. Wotschack³⁰, M.J. Woudstra⁸⁴, K.W. Wozniak³⁹, M. Wu⁵⁵, M. Wu³¹, S.L. Wu¹⁷³, X. Wu⁴⁹, Y. Wu⁸⁹, T.R. Wyatt⁸⁴, B.M. Wynne⁴⁶, S. Xella³⁶, D. Xu^{33a}, L. Xu^{33b,ak}, B. Yabsley¹⁵⁰, S. Yacoob^{145a}, R. Yakabe⁶⁷, M. Yamada⁶⁶, D. Yamaguchi¹⁵⁷, Y. Yamaguchi¹¹⁸, A. Yamamoto⁶⁶, S. Yamamoto¹⁵⁵, T. Yamanaka¹⁵⁵, K. Yamauchi¹⁰³, Y. Yamazaki⁶⁷, Z. Yan²², H. Yang^{33e}, H. Yang¹⁷³, Y. Yang¹⁵¹, W-M. Yao¹⁵, Y. Yasu⁶⁶, E. Yatsenko⁵, K.H. Yau Wong²¹, J. Ye⁴⁰, S. Ye²⁵, I. Yeletsikh⁶⁵, A.L. Yen⁵⁷, E. Yildirim⁴², K. Yorita¹⁷¹, R. Yoshida⁶, K. Yoshihara¹²², C. Young¹⁴³, C.J.S. Young³⁰, S. Youssef²², D.R. Yu¹⁵, J. Yu⁸, J.M. Yu⁸⁹, J. Yu¹¹⁴, L. Yuan⁶⁷, S.P.Y. Yuen²¹, A. Yurkewicz¹⁰⁸, I. Yusuff^{28,al}, B. Zabinski³⁹, R. Zaidan⁶³, A.M. Zaitsev^{130,ab}, J. Zalieckas¹⁴, A. Zaman¹⁴⁸, S. Zambito⁵⁷, L. Zanello^{132a,132b}, D. Zanzi⁸⁸, C. Zeitnitz¹⁷⁵, M. Zeman¹²⁸, A. Zemla^{38a}, Q. Zeng¹⁴³, K. Zengel²³, O. Zenin¹³⁰, T. Ženiš^{144a}, D. Zerwas¹¹⁷, D. Zhang⁸⁹, F. Zhang¹⁷³, H. Zhang^{33c}, J. Zhang⁶, L. Zhang⁴⁸, R. Zhang^{33b}, X. Zhang^{33d}, Z. Zhang¹¹⁷, X. Zhao⁴⁰, Y. Zhao^{33d,117}, Z. Zhao^{33b}, A. Zhemchugov⁶⁵, J. Zhong¹²⁰, B. Zhou⁸⁹, C. Zhou⁴⁵, L. Zhou³⁵, L. Zhou⁴⁰, N. Zhou^{33f}, C.G. Zhu^{33d}, H. Zhu^{33a}, J. Zhu⁸⁹, Y. Zhu^{33b}, X. Zhuang^{33a}, K. Zhukov⁹⁶, A. Zibell¹⁷⁴, D. Zieminska⁶¹, N.I. Zimine⁶⁵, C. Zimmermann⁸³, S. Zimmermann⁴⁸, Z. Zinonos⁵⁴, M. Zinser⁸³, M. Ziolkowski¹⁴¹, L. Živković¹³, G. Zobernig¹⁷³, A. Zoccoli^{20a,20b}, M. zur Nedden¹⁶, G. Zurzolo^{104a,104b}, L. Zwalinski³⁰.

¹ Department of Physics, University of Adelaide, Adelaide, Australia

² Physics Department, SUNY Albany, Albany NY, United States of America

³ Department of Physics, University of Alberta, Edmonton AB, Canada

⁴ (a) Department of Physics, Ankara University, Ankara; (b) Istanbul Aydin University, Istanbul; (c)

Division of Physics, TOBB University of Economics and Technology, Ankara, Turkey

⁵ LAPP, CNRS/IN2P3 and Université Savoie Mont Blanc, Annecy-le-Vieux, France

⁶ High Energy Physics Division, Argonne National Laboratory, Argonne IL, United States of America

- ⁷ Department of Physics, University of Arizona, Tucson AZ, United States of America
- ⁸ Department of Physics, The University of Texas at Arlington, Arlington TX, United States of America
- ⁹ Physics Department, University of Athens, Athens, Greece
- ¹⁰ Physics Department, National Technical University of Athens, Zografou, Greece
- ¹¹ Institute of Physics, Azerbaijan Academy of Sciences, Baku, Azerbaijan
- ¹² Institut de Física d'Altes Energies and Departament de Física de la Universitat Autònoma de Barcelona, Barcelona, Spain
- ¹³ Institute of Physics, University of Belgrade, Belgrade, Serbia
- ¹⁴ Department for Physics and Technology, University of Bergen, Bergen, Norway
- ¹⁵ Physics Division, Lawrence Berkeley National Laboratory and University of California, Berkeley CA, United States of America
- ¹⁶ Department of Physics, Humboldt University, Berlin, Germany
- ¹⁷ Albert Einstein Center for Fundamental Physics and Laboratory for High Energy Physics, University of Bern, Bern, Switzerland
- ¹⁸ School of Physics and Astronomy, University of Birmingham, Birmingham, United Kingdom
- ¹⁹ ^(a) Department of Physics, Bogazici University, Istanbul; ^(b) Department of Physics Engineering, Gaziantep University, Gaziantep; ^(c) Department of Physics, Dogus University, Istanbul, Turkey
- ²⁰ ^(a) INFN Sezione di Bologna; ^(b) Dipartimento di Fisica e Astronomia, Università di Bologna, Bologna, Italy
- ²¹ Physikalisches Institut, University of Bonn, Bonn, Germany
- ²² Department of Physics, Boston University, Boston MA, United States of America
- ²³ Department of Physics, Brandeis University, Waltham MA, United States of America
- ²⁴ ^(a) Universidade Federal do Rio De Janeiro COPPE/EE/IF, Rio de Janeiro; ^(b) Electrical Circuits Department, Federal University of Juiz de Fora (UFJF), Juiz de Fora; ^(c) Federal University of Sao Joao del Rei (UFSJ), Sao Joao del Rei; ^(d) Instituto de Fisica, Universidade de Sao Paulo, Sao Paulo, Brazil
- ²⁵ Physics Department, Brookhaven National Laboratory, Upton NY, United States of America
- ²⁶ ^(a) National Institute of Physics and Nuclear Engineering, Bucharest; ^(b) National Institute for Research and Development of Isotopic and Molecular Technologies, Physics Department, Cluj Napoca; ^(c) University Politehnica Bucharest, Bucharest; ^(d) West University in Timisoara, Timisoara, Romania
- ²⁷ Departamento de Física, Universidad de Buenos Aires, Buenos Aires, Argentina
- ²⁸ Cavendish Laboratory, University of Cambridge, Cambridge, United Kingdom
- ²⁹ Department of Physics, Carleton University, Ottawa ON, Canada
- ³⁰ CERN, Geneva, Switzerland
- ³¹ Enrico Fermi Institute, University of Chicago, Chicago IL, United States of America
- ³² ^(a) Departamento de Física, Pontificia Universidad Católica de Chile, Santiago; ^(b) Departamento de Física, Universidad Técnica Federico Santa María, Valparaíso, Chile
- ³³ ^(a) Institute of High Energy Physics, Chinese Academy of Sciences, Beijing; ^(b) Department of Modern Physics, University of Science and Technology of China, Anhui; ^(c) Department of Physics, Nanjing University, Jiangsu; ^(d) School of Physics, Shandong University, Shandong; ^(e) Department of Physics and Astronomy, Shanghai Key Laboratory for Particle Physics and Cosmology, Shanghai Jiao Tong University, Shanghai; ^(f) Physics Department, Tsinghua University, Beijing 100084, China
- ³⁴ Laboratoire de Physique Corpusculaire, Clermont Université and Université Blaise Pascal and CNRS/IN2P3, Clermont-Ferrand, France
- ³⁵ Nevis Laboratory, Columbia University, Irvington NY, United States of America
- ³⁶ Niels Bohr Institute, University of Copenhagen, Kobenhavn, Denmark
- ³⁷ ^(a) INFN Gruppo Collegato di Cosenza, Laboratori Nazionali di Frascati; ^(b) Dipartimento di Fisica, Università della Calabria, Rende, Italy

- 38 ^(a) AGH University of Science and Technology, Faculty of Physics and Applied Computer Science, Krakow; ^(b) Marian Smoluchowski Institute of Physics, Jagiellonian University, Krakow, Poland
- 39 Institute of Nuclear Physics Polish Academy of Sciences, Krakow, Poland
- 40 Physics Department, Southern Methodist University, Dallas TX, United States of America
- 41 Physics Department, University of Texas at Dallas, Richardson TX, United States of America
- 42 DESY, Hamburg and Zeuthen, Germany
- 43 Institut für Experimentelle Physik IV, Technische Universität Dortmund, Dortmund, Germany
- 44 Institut für Kern- und Teilchenphysik, Technische Universität Dresden, Dresden, Germany
- 45 Department of Physics, Duke University, Durham NC, United States of America
- 46 SUPA - School of Physics and Astronomy, University of Edinburgh, Edinburgh, United Kingdom
- 47 INFN Laboratori Nazionali di Frascati, Frascati, Italy
- 48 Fakultät für Mathematik und Physik, Albert-Ludwigs-Universität, Freiburg, Germany
- 49 Section de Physique, Université de Genève, Geneva, Switzerland
- 50 ^(a) INFN Sezione di Genova; ^(b) Dipartimento di Fisica, Università di Genova, Genova, Italy
- 51 ^(a) E. Andronikashvili Institute of Physics, Iv. Javakhishvili Tbilisi State University, Tbilisi; ^(b) High Energy Physics Institute, Tbilisi State University, Tbilisi, Georgia
- 52 II Physikalisches Institut, Justus-Liebig-Universität Giessen, Giessen, Germany
- 53 SUPA - School of Physics and Astronomy, University of Glasgow, Glasgow, United Kingdom
- 54 II Physikalisches Institut, Georg-August-Universität, Göttingen, Germany
- 55 Laboratoire de Physique Subatomique et de Cosmologie, Université Grenoble-Alpes, CNRS/IN2P3, Grenoble, France
- 56 Department of Physics, Hampton University, Hampton VA, United States of America
- 57 Laboratory for Particle Physics and Cosmology, Harvard University, Cambridge MA, United States of America
- 58 ^(a) Kirchhoff-Institut für Physik, Ruprecht-Karls-Universität Heidelberg, Heidelberg; ^(b) Physikalisches Institut, Ruprecht-Karls-Universität Heidelberg, Heidelberg; ^(c) ZITI Institut für technische Informatik, Ruprecht-Karls-Universität Heidelberg, Mannheim, Germany
- 59 Faculty of Applied Information Science, Hiroshima Institute of Technology, Hiroshima, Japan
- 60 ^(a) Department of Physics, The Chinese University of Hong Kong, Shatin, N.T., Hong Kong; ^(b) Department of Physics, The University of Hong Kong, Hong Kong; ^(c) Department of Physics, The Hong Kong University of Science and Technology, Clear Water Bay, Kowloon, Hong Kong, China
- 61 Department of Physics, Indiana University, Bloomington IN, United States of America
- 62 Institut für Astro- und Teilchenphysik, Leopold-Franzens-Universität, Innsbruck, Austria
- 63 University of Iowa, Iowa City IA, United States of America
- 64 Department of Physics and Astronomy, Iowa State University, Ames IA, United States of America
- 65 Joint Institute for Nuclear Research, JINR Dubna, Dubna, Russia
- 66 KEK, High Energy Accelerator Research Organization, Tsukuba, Japan
- 67 Graduate School of Science, Kobe University, Kobe, Japan
- 68 Faculty of Science, Kyoto University, Kyoto, Japan
- 69 Kyoto University of Education, Kyoto, Japan
- 70 Department of Physics, Kyushu University, Fukuoka, Japan
- 71 Instituto de Física La Plata, Universidad Nacional de La Plata and CONICET, La Plata, Argentina
- 72 Physics Department, Lancaster University, Lancaster, United Kingdom
- 73 ^(a) INFN Sezione di Lecce; ^(b) Dipartimento di Matematica e Fisica, Università del Salento, Lecce, Italy
- 74 Oliver Lodge Laboratory, University of Liverpool, Liverpool, United Kingdom
- 75 Department of Physics, Jožef Stefan Institute and University of Ljubljana, Ljubljana, Slovenia

- ⁷⁶ School of Physics and Astronomy, Queen Mary University of London, London, United Kingdom
- ⁷⁷ Department of Physics, Royal Holloway University of London, Surrey, United Kingdom
- ⁷⁸ Department of Physics and Astronomy, University College London, London, United Kingdom
- ⁷⁹ Louisiana Tech University, Ruston LA, United States of America
- ⁸⁰ Laboratoire de Physique Nucléaire et de Hautes Energies, UPMC and Université Paris-Diderot and CNRS/IN2P3, Paris, France
- ⁸¹ Fysiska institutionen, Lunds universitet, Lund, Sweden
- ⁸² Departamento de Física Teórica C-15, Universidad Autónoma de Madrid, Madrid, Spain
- ⁸³ Institut für Physik, Universität Mainz, Mainz, Germany
- ⁸⁴ School of Physics and Astronomy, University of Manchester, Manchester, United Kingdom
- ⁸⁵ CPPM, Aix-Marseille Université and CNRS/IN2P3, Marseille, France
- ⁸⁶ Department of Physics, University of Massachusetts, Amherst MA, United States of America
- ⁸⁷ Department of Physics, McGill University, Montreal QC, Canada
- ⁸⁸ School of Physics, University of Melbourne, Victoria, Australia
- ⁸⁹ Department of Physics, The University of Michigan, Ann Arbor MI, United States of America
- ⁹⁰ Department of Physics and Astronomy, Michigan State University, East Lansing MI, United States of America
- ⁹¹ ^(a) INFN Sezione di Milano; ^(b) Dipartimento di Fisica, Università di Milano, Milano, Italy
- ⁹² B.I. Stepanov Institute of Physics, National Academy of Sciences of Belarus, Minsk, Republic of Belarus
- ⁹³ National Scientific and Educational Centre for Particle and High Energy Physics, Minsk, Republic of Belarus
- ⁹⁴ Department of Physics, Massachusetts Institute of Technology, Cambridge MA, United States of America
- ⁹⁵ Group of Particle Physics, University of Montreal, Montreal QC, Canada
- ⁹⁶ P.N. Lebedev Institute of Physics, Academy of Sciences, Moscow, Russia
- ⁹⁷ Institute for Theoretical and Experimental Physics (ITEP), Moscow, Russia
- ⁹⁸ National Research Nuclear University MEPhI, Moscow, Russia
- ⁹⁹ D.V. Skobel'syn Institute of Nuclear Physics, M.V. Lomonosov Moscow State University, Moscow, Russia
- ¹⁰⁰ Fakultät für Physik, Ludwig-Maximilians-Universität München, München, Germany
- ¹⁰¹ Max-Planck-Institut für Physik (Werner-Heisenberg-Institut), München, Germany
- ¹⁰² Nagasaki Institute of Applied Science, Nagasaki, Japan
- ¹⁰³ Graduate School of Science and Kobayashi-Maskawa Institute, Nagoya University, Nagoya, Japan
- ¹⁰⁴ ^(a) INFN Sezione di Napoli; ^(b) Dipartimento di Fisica, Università di Napoli, Napoli, Italy
- ¹⁰⁵ Department of Physics and Astronomy, University of New Mexico, Albuquerque NM, United States of America
- ¹⁰⁶ Institute for Mathematics, Astrophysics and Particle Physics, Radboud University Nijmegen/Nikhef, Nijmegen, Netherlands
- ¹⁰⁷ Nikhef National Institute for Subatomic Physics and University of Amsterdam, Amsterdam, Netherlands
- ¹⁰⁸ Department of Physics, Northern Illinois University, DeKalb IL, United States of America
- ¹⁰⁹ Budker Institute of Nuclear Physics, SB RAS, Novosibirsk, Russia
- ¹¹⁰ Department of Physics, New York University, New York NY, United States of America
- ¹¹¹ Ohio State University, Columbus OH, United States of America
- ¹¹² Faculty of Science, Okayama University, Okayama, Japan
- ¹¹³ Homer L. Dodge Department of Physics and Astronomy, University of Oklahoma, Norman OK,

United States of America

¹¹⁴ Department of Physics, Oklahoma State University, Stillwater OK, United States of America

¹¹⁵ Palacký University, RCPTM, Olomouc, Czech Republic

¹¹⁶ Center for High Energy Physics, University of Oregon, Eugene OR, United States of America

¹¹⁷ LAL, Université Paris-Sud and CNRS/IN2P3, Orsay, France

¹¹⁸ Graduate School of Science, Osaka University, Osaka, Japan

¹¹⁹ Department of Physics, University of Oslo, Oslo, Norway

¹²⁰ Department of Physics, Oxford University, Oxford, United Kingdom

¹²¹ ^(a) INFN Sezione di Pavia; ^(b) Dipartimento di Fisica, Università di Pavia, Pavia, Italy

¹²² Department of Physics, University of Pennsylvania, Philadelphia PA, United States of America

¹²³ National Research Centre "Kurchatov Institute" B.P.Konstantinov Petersburg Nuclear Physics Institute, St. Petersburg, Russia

¹²⁴ ^(a) INFN Sezione di Pisa; ^(b) Dipartimento di Fisica E. Fermi, Università di Pisa, Pisa, Italy

¹²⁵ Department of Physics and Astronomy, University of Pittsburgh, Pittsburgh PA, United States of America

¹²⁶ ^(a) Laboratório de Instrumentação e Física Experimental de Partículas - LIP, Lisboa; ^(b) Faculdade de Ciências, Universidade de Lisboa, Lisboa; ^(c) Department of Physics, University of Coimbra, Coimbra; ^(d) Centro de Física Nuclear da Universidade de Lisboa, Lisboa; ^(e) Departamento de Física, Universidade do Minho, Braga; ^(f) Departamento de Física Teórica y del Cosmos and CAFPE, Universidad de Granada, Granada (Spain); ^(g) Dep Física and CEFITEC of Faculdade de Ciências e Tecnologia, Universidade Nova de Lisboa, Caparica, Portugal

¹²⁷ Institute of Physics, Academy of Sciences of the Czech Republic, Praha, Czech Republic

¹²⁸ Czech Technical University in Prague, Praha, Czech Republic

¹²⁹ Faculty of Mathematics and Physics, Charles University in Prague, Praha, Czech Republic

¹³⁰ State Research Center Institute for High Energy Physics, Protvino, Russia

¹³¹ Particle Physics Department, Rutherford Appleton Laboratory, Didcot, United Kingdom

¹³² ^(a) INFN Sezione di Roma; ^(b) Dipartimento di Fisica, Sapienza Università di Roma, Roma, Italy

¹³³ ^(a) INFN Sezione di Roma Tor Vergata; ^(b) Dipartimento di Fisica, Università di Roma Tor Vergata, Roma, Italy

¹³⁴ ^(a) INFN Sezione di Roma Tre; ^(b) Dipartimento di Matematica e Fisica, Università Roma Tre, Roma, Italy

¹³⁵ ^(a) Faculté des Sciences Ain Chock, Réseau Universitaire de Physique des Hautes Energies - Université Hassan II, Casablanca; ^(b) Centre National de l'Énergie des Sciences Techniques Nucleaires, Rabat; ^(c) Faculté des Sciences Semlalia, Université Cadi Ayyad, LPHEA-Marrakech; ^(d) Faculté des Sciences, Université Mohamed Premier and LPTPM, Oujda; ^(e) Faculté des sciences, Université Mohammed V-Agdal, Rabat, Morocco

¹³⁶ DSM/IRFU (Institut de Recherches sur les Lois Fondamentales de l'Univers), CEA Saclay (Commissariat à l'Énergie Atomique et aux Énergies Alternatives), Gif-sur-Yvette, France

¹³⁷ Santa Cruz Institute for Particle Physics, University of California Santa Cruz, Santa Cruz CA, United States of America

¹³⁸ Department of Physics, University of Washington, Seattle WA, United States of America

¹³⁹ Department of Physics and Astronomy, University of Sheffield, Sheffield, United Kingdom

¹⁴⁰ Department of Physics, Shinshu University, Nagano, Japan

¹⁴¹ Fachbereich Physik, Universität Siegen, Siegen, Germany

¹⁴² Department of Physics, Simon Fraser University, Burnaby BC, Canada

¹⁴³ SLAC National Accelerator Laboratory, Stanford CA, United States of America

¹⁴⁴ ^(a) Faculty of Mathematics, Physics & Informatics, Comenius University, Bratislava; ^(b) Department

of Subnuclear Physics, Institute of Experimental Physics of the Slovak Academy of Sciences, Kosice, Slovak Republic

¹⁴⁵ ^(a) Department of Physics, University of Cape Town, Cape Town; ^(b) Department of Physics, University of Johannesburg, Johannesburg; ^(c) School of Physics, University of the Witwatersrand, Johannesburg, South Africa

¹⁴⁶ ^(a) Department of Physics, Stockholm University; ^(b) The Oskar Klein Centre, Stockholm, Sweden

¹⁴⁷ Physics Department, Royal Institute of Technology, Stockholm, Sweden

¹⁴⁸ Departments of Physics & Astronomy and Chemistry, Stony Brook University, Stony Brook NY, United States of America

¹⁴⁹ Department of Physics and Astronomy, University of Sussex, Brighton, United Kingdom

¹⁵⁰ School of Physics, University of Sydney, Sydney, Australia

¹⁵¹ Institute of Physics, Academia Sinica, Taipei, Taiwan

¹⁵² Department of Physics, Technion: Israel Institute of Technology, Haifa, Israel

¹⁵³ Raymond and Beverly Sackler School of Physics and Astronomy, Tel Aviv University, Tel Aviv, Israel

¹⁵⁴ Department of Physics, Aristotle University of Thessaloniki, Thessaloniki, Greece

¹⁵⁵ International Center for Elementary Particle Physics and Department of Physics, The University of Tokyo, Tokyo, Japan

¹⁵⁶ Graduate School of Science and Technology, Tokyo Metropolitan University, Tokyo, Japan

¹⁵⁷ Department of Physics, Tokyo Institute of Technology, Tokyo, Japan

¹⁵⁸ Department of Physics, University of Toronto, Toronto ON, Canada

¹⁵⁹ ^(a) TRIUMF, Vancouver BC; ^(b) Department of Physics and Astronomy, York University, Toronto ON, Canada

¹⁶⁰ Faculty of Pure and Applied Sciences, University of Tsukuba, Tsukuba, Japan

¹⁶¹ Department of Physics and Astronomy, Tufts University, Medford MA, United States of America

¹⁶² Centro de Investigaciones, Universidad Antonio Narino, Bogota, Colombia

¹⁶³ Department of Physics and Astronomy, University of California Irvine, Irvine CA, United States of America

¹⁶⁴ ^(a) INFN Gruppo Collegato di Udine, Sezione di Trieste, Udine; ^(b) ICTP, Trieste; ^(c) Dipartimento di Chimica, Fisica e Ambiente, Università di Udine, Udine, Italy

¹⁶⁵ Department of Physics, University of Illinois, Urbana IL, United States of America

¹⁶⁶ Department of Physics and Astronomy, University of Uppsala, Uppsala, Sweden

¹⁶⁷ Instituto de Física Corpuscular (IFIC) and Departamento de Física Atómica, Molecular y Nuclear and Departamento de Ingeniería Electrónica and Instituto de Microelectrónica de Barcelona (IMB-CNM), University of Valencia and CSIC, Valencia, Spain

¹⁶⁸ Department of Physics, University of British Columbia, Vancouver BC, Canada

¹⁶⁹ Department of Physics and Astronomy, University of Victoria, Victoria BC, Canada

¹⁷⁰ Department of Physics, University of Warwick, Coventry, United Kingdom

¹⁷¹ Waseda University, Tokyo, Japan

¹⁷² Department of Particle Physics, The Weizmann Institute of Science, Rehovot, Israel

¹⁷³ Department of Physics, University of Wisconsin, Madison WI, United States of America

¹⁷⁴ Fakultät für Physik und Astronomie, Julius-Maximilians-Universität, Würzburg, Germany

¹⁷⁵ Fachbereich C Physik, Bergische Universität Wuppertal, Wuppertal, Germany

¹⁷⁶ Department of Physics, Yale University, New Haven CT, United States of America

¹⁷⁷ Yerevan Physics Institute, Yerevan, Armenia

¹⁷⁸ Centre de Calcul de l'Institut National de Physique Nucléaire et de Physique des Particules (IN2P3), Villeurbanne, France

- ^a Also at Department of Physics, King's College London, London, United Kingdom
- ^b Also at Institute of Physics, Azerbaijan Academy of Sciences, Baku, Azerbaijan
- ^c Also at Novosibirsk State University, Novosibirsk, Russia
- ^d Also at TRIUMF, Vancouver BC, Canada
- ^e Also at Department of Physics, California State University, Fresno CA, United States of America
- ^f Also at Department of Physics, University of Fribourg, Fribourg, Switzerland
- ^g Also at Departamento de Fisica e Astronomia, Faculdade de Ciencias, Universidade do Porto, Portugal
- ^h Also at Tomsk State University, Tomsk, Russia
- ⁱ Also at CPPM, Aix-Marseille Université and CNRS/IN2P3, Marseille, France
- ^j Also at Università di Napoli Parthenope, Napoli, Italy
- ^k Also at Institute of Particle Physics (IPP), Canada
- ^l Also at Particle Physics Department, Rutherford Appleton Laboratory, Didcot, United Kingdom
- ^m Also at Department of Physics, St. Petersburg State Polytechnical University, St. Petersburg, Russia
- ⁿ Also at Louisiana Tech University, Ruston LA, United States of America
- ^o Also at Institutio Catalana de Recerca i Estudis Avancats, ICREA, Barcelona, Spain
- ^p Also at Graduate School of Science, Osaka University, Osaka, Japan
- ^q Also at Department of Physics, National Tsing Hua University, Taiwan
- ^r Also at Department of Physics, The University of Texas at Austin, Austin TX, United States of America
- ^s Also at Institute of Theoretical Physics, Ilia State University, Tbilisi, Georgia
- ^t Also at CERN, Geneva, Switzerland
- ^u Also at Georgian Technical University (GTU), Tbilisi, Georgia
- ^v Also at Manhattan College, New York NY, United States of America
- ^w Also at Hellenic Open University, Patras, Greece
- ^x Also at Institute of Physics, Academia Sinica, Taipei, Taiwan
- ^y Also at LAL, Université Paris-Sud and CNRS/IN2P3, Orsay, France
- ^z Also at Academia Sinica Grid Computing, Institute of Physics, Academia Sinica, Taipei, Taiwan
- ^{aa} Also at School of Physics, Shandong University, Shandong, China
- ^{ab} Also at Moscow Institute of Physics and Technology State University, Dolgoprudny, Russia
- ^{ac} Also at Section de Physique, Université de Genève, Geneva, Switzerland
- ^{ad} Also at International School for Advanced Studies (SISSA), Trieste, Italy
- ^{ae} Also at Department of Physics and Astronomy, University of South Carolina, Columbia SC, United States of America
- ^{af} Also at School of Physics and Engineering, Sun Yat-sen University, Guangzhou, China
- ^{ag} Also at Faculty of Physics, M.V.Lomonosov Moscow State University, Moscow, Russia
- ^{ah} Also at National Research Nuclear University MEPhI, Moscow, Russia
- ^{ai} Also at Department of Physics, Stanford University, Stanford CA, United States of America
- ^{aj} Also at Institute for Particle and Nuclear Physics, Wigner Research Centre for Physics, Budapest, Hungary
- ^{ak} Also at Department of Physics, The University of Michigan, Ann Arbor MI, United States of America
- ^{al} Also at University of Malaya, Department of Physics, Kuala Lumpur, Malaysia
- * Deceased